WESTERN SYDNEY
UNIVERSITY

INVESTIGATING THE ROLE OF RETINOBLASTOMA-BINDING PROTEIN 9 IN HUMAN PLURIPOTENT STEM CELLS AND EMBRYONIC DEVELOPMENT

Seakcheng Lim (BMedSci, Hons)

A thesis submitted in fulfilment of the requirements for the degree of

Doctor of Philosophy

School of Medicine, Western Sydney University, Australia

2016

Supervisor: Dr. Michael O'Connor

Co-Supervisor: Prof. Jens Coorssen

Statement of Authentication

I hereby, declare that this thesis contains no material that has been accepted for the award of any other degree or diploma and that, to the best of my knowledge and belief, this thesis contains no material previously published or written by another person, except where due reference has been made in the text of this thesis.

[redacted]

Seakcheng Lim

September, 2016

Acknowledgements

I would like to first thank my supervisor Dr. Michael O'Connor for being the best mentor. I am forever grateful for all the time and patience you have invested in helping me learn to be a better researcher and a better person. Thank you for your continued advice, encouragement, support, and guidance over the past few years and most of all thank you for putting up with me!

I would like to thank Professor Jens Coorssen for your advice and support during my project, and for allowing me to use your lab where I have learnt so much. I would also like to thank everyone who has helped me during my project. I would like to thank Ashleigh for all of your help and support in the zebrafish lab. Also I would like to say a big thank you to my uni mum Sindy for being so caring and helpful whenever I needed some advice.

Thank you to my best friends Kads, Rania and Mel. You guys always know how to make me laugh. Thanks Kads for always being there for me at any time, for being my ride or die. Rania thanks for always checking in on me and making sure I'm ok and that I have cake. Mel thanks for putting up with me all day every day and for 11am lunches. I would also like to thank Carol, Arlene, Mel, and Katie for your friendship and chocolates you always leave at my desk

I would like to thank my family for being so supportive of me and whatever I chose to do. A big thanks to my cousins Vyja, Mauri and Aunties for always taking care of me and feeding me – I cannot thank you enough because I can't cook. I would like to thank Elizabeth and Richie for all your support and help when I need you. I would like to thank my grandparents for teaching me how to be caring and to work through anything. And finally, the biggest thanks go to my parents, who have made sure I can be the best person I can be. Thank you for all your support, love and care.

Table of Contents

List of Tables

List of Figures

List of Abbreviations

.CLS	Geocoding classification file
.GCT	Gene cluster text format
1-DE	1-Dimensional electrophoresis
A	Absent
Ab	Antibody
ABPP	Activity based protein profiling
AP	Alkaline Phosphatase
bp	Base pair
BrdU	Bromodeoxyuridine
BSA	Bovine Serum Albumin
CBB	Coomassie Brilliant Blue
cDNA	Complementary DNA
CFC	Colony Forming Cells
CH_3CN	Acetonitrile
CHAPS	3-[(3-Cholamidopropyl)dimethylammonio]-1-propanesulfonate
DAVID	Database for Annotation, Visualisation and Integrated Discovery
DEAF1	Deformed epidermal autoregulatory factor-1

dH_2O	Distilled water
DMEM	Dulbecco's Modified Eagles Medium
DMSO	Dimethyl sulfoxide
DNA	Deoxyribonucleic acid
dpf	Days post-fertilisation
DTT	Dithiothreitol
E3	Embryo maintenance medium
EDTA	Ethylenediaminetetraacetic acid
EdU	5-ethynyl-2'-deoxyuridine
EGTA	Ethylene glycol tetraacetic acid
ESCs	Embryonic stem cells
EtOH	Ethanol
FACS	Fluorescence Activated Cell Sorting
FBS	Fetal Bovine Serum
FDR	False discovery rate
FITC-H	Fluorescein isothiocyanate-Height
FSC-A	Forward Scatter-Area
FSC-H	Forward Scatter-Height

g	G-force
GO	Gene ontology
GOI	Gene of interest
H & E	Haematoxylin and Eosin
H_2O	Water
HAc	Acetic Acid
hESCs	Human embryonic stem cells
hiPSCs	Human induced pluripotent stem cells
hpf	Hours post fertilization
hPSCs	Human pluripotent stem cells
ICM	Inner Cell Mass
IgG	Immunoglobulin G
IgM	Immunoglobulin M
iPS	Induced Pluripotent Stem
iPSC	Induced Pluripotent Stem Cell
IVF	*In vitro* fertilisation
K	One thousand
kb	Kilo base

kDa	Kilodalton
M	Molar
MeOH	Methanol
mESCs	Mouse embryonic stem cells
mg	Milligram
miRNA	microRNA
mL	Millilitre
ML114	[1-(1,3-thiazol-2-yl)ethylideneamino] cyclohexanecarboxylate
mm	Millimetre
mM	Millimolar
MOs	Morpholino oligonucleotides
mRNA	Messenger RNA
MW	Molecular Weight
MWCO	Molecular Weight Cut Off
NFYA	Nuclear transcription factor Y subunit A
NH_4HCO_3	Ammonium Hydrogen Carbonate
nm	nanometre
ng	nanogram

P	Present
p	p-value
p53	Tumor protein 53
PASTAA	Predicting Associated Transcription Factors from Annotated Affinities
PBS	Phosphate Buffered Saline
PBST	Phosphate Buffered Saline in TWEEN20
PCR	Polymerase Chain Reaction
PFA	Paraformaldehyde
PI	Protease Inhibitor
PMSF	Phenylmethanesulfonylfluoride
PSCs	Pluripotent stem cells
PVDF	Polyvinylidene difluoride
PVP40	Polyvinylpyrrolidone 40
qPCR	Quantitative PCR
RB	Retinoblastoma protein
RBBP9	Retinoblastoma-Binding Protein 9
RNA	Ribonucleic Acid

RNase	Ribonuclease
ROCK	Rho- associated kinase
ROI	Region of Interest
RT-PCR	Reverse transcription polymerase chain reaction
SDS	Sodium Dodecyl Sulfate
Ser75	Active serine site of RBBP9
SH	Serine hydrolase
siRNA	small interfering RNA
SSC-A	Side Scatter – Area
SSEA	Stage specific embryonic antigen
TAB	Tübingen/AB
TBS	Tris Buffered Saline
TGF-β	Transforming Growth Factor-Beta
tif	Tagged image file format
V	Volts
v	Version
v/v	Volume per volume
W	Watts

w/v Weight per volume

µA Microamps

µM Micromolar

µm Micrometer

µS Micro-Siemens

Abstract

Many intricate networks are required to work together to regulate two defining characteristics of human pluripotent stem cells (hPSCs): the capacity to self-renew, and the potential to produce (through differentiation processes) any cell type of the body. The discovery of PSCs has provided an invaluable tool for investigating fundamental aspects of developmental biology, drug discovery, disease modelling, and tissue-replacement therapies. Master regulators of pluripotency have been identified in PSCs including OCT4, NANOG, and SOX2. However, the molecular events that drive self-renewal and differentiation currently are not completely understood. Previous results from our group identified the retinoblastoma (RB)-binding protein 9 (RBBP9) as a novel pluripotency regulator. Small interfering RNA (siRNA)-mediated loss of RBBP9 protein in hPSCs decreased expression of pluripotency and cell cycle genes, and increased expression of neurogenesis genes. RBBP9 is reported to have two potential mechanisms of action: the ability to i) bind RB protein and influence the RB/E2F pathway, and ii) serine hydrolase (SH) activity. To investigate the relative contribution of these two activities to hPSC maintenance and embryonic development *in vitro* and *in vivo*, we compared the responses of hPSCs and zebrafish treated with a recently identified selective chemical inhibitor of RBBP9 SH activity (ML114), to those treated with either RBBP9 siRNA or *rbbp9* morpholino.

Data presented in this thesis show the requirement of RBBP9, including RBBP9 SH activity, in hPSC maintenance *in vitro*, and possibly its requirement in early embryogenesis *in vivo*. In *Chapter 2*, selective loss of RBBP9 SH activity was investigated in hPSCs *via* ML114. This treatment resulted in the decoupling of hPSC self-renewal from differentiation,

as seen by a significant reduction in hPSC proliferation without any observable decrease in pluripotency marker expression or morphological change. *Chapter 3* then investigated effectors which could potentially be responsible for this unusual decoupling effect. Promoter analyses identified the Nuclear transcription factor Y subunit A (NFYA) as a highly-ranked candidate effector of RBBP9 SH activity through analyses of gene expression changes arising from ML114 treatment of hPSCs. The up-regulation of NFYA was hypothesised to mediate the changes in cell proliferation seen whilst maintaining pluripotency in hPSCs. *Chapter 4* began to explore the impacts of RBBP9 and its activities *in vivo*. Rbbp9 is expressed in a large range of zebrafish tissues, and the data presented here is consistent with the idea that Rbbp9 and its activities are required for zebrafish embryogenesis. However, the complexity of the observed phenotypes suggests that toxicity might be an alternate explanation of the data.

Further investigation into the role of RBBP9 activities during hPSC generation, maintenance and differentiation, as well as the early stages of embryonic development, is required to better understand the mechanisms behind developmental abnormalities resulting from Rbbp9 losses. A better understanding of RBBP9 activities and its role throughout embryonic development *in vitro* and *in vivo* will help us better understand the molecular networks required to: maintain hPSCs; generate hPSCs *via* somatic reprograming; and also drive or facilitate normal embryogenesis and cancer progression.

CHAPTER 1: General Introduction

1.1. Retinoblastoma-binding protein 9: a putative regulator of pluripotency.

The retinoblastoma (RB) binding protein 9 (RBBP9) has been shown to be expressed in human pluripotent stem cells (hPSCs), and in a large number of cells throughout embryonic development such as the eye, heart, brain and digestive tract (Bastian et al., 2008). RBBP9 has also been found expressed in a range of human cancer cells (Shields et al., 2010, Woitach et al., 1998). Despite its broad expression, little is known of the roles RBBP9 plays in normal development or cancer progression. The few published studies of RBBP9 suggest it might control cell cycle progression either by regulating the activity of RB protein (which itself regulates E2F transcription factors whose activity is critical for cell proliferation) (Woitach et al., 1998) or by acting as a serine hydrolase (SH) (Shields et al., 2010) on as yet undefined target proteins.

In a study aimed at better understanding the molecular circuitry of hPSC maintenance, O'Connor and colleagues (2011) identified RBBP9 as a novel pluripotency regulator. This study showed small interfering RNA (siRNA)-mediated loss of RBBP9 expression in hPSCs resulted in a specific loss of pluripotent cells (as detected by the colony forming cell assay), decreased *FOXD3* expression, decreased cell cycle gene expression, and increased expression of neural differentiation genes. These data suggested that RBBP9 plays a role in maintaining molecular networks required for pluripotency. However, decreased RBBP9 protein expression in this study *via* siRNA did not enable determination of the relative contribution of RB-binding activity and/or SH activity to hPSC maintenance. More detailed analysis of the role of RBBP9 in hPSCs and during development could provide important information on how pluripotent cells are generated/maintained, and how normal development and cancers progress.

1.2. Models of embryonic development.

1.2.1. Human pluripotent stem cells.

The discovery of PSCs has unlocked a new generation of cells which possess unique properties such as the ability to self-renew indefinitely, and to differentiate into all cells of the body (Martin, 1981, Thomson et al., 1998). These properties, unique to PSCs such as human embryonic stem cells (hESCs) and human induced pluripotent stem cells (hiPSCs) amongst others, have made these cells an invaluable tool for investigating fundamental aspects of developmental biology, drug discovery, disease modelling and cell therapies (Park et al., 2008, Takahashi et al., 2007b, Yu et al., 2007, Reubinoff et al., 2000, Thomson et al., 1998) (Figure 1.1). hESCs share similarities with mouse embryonic stem cells (mESCs), however differences between these two embryonic cell types are known to exist (Hanna et al., 2010). It has been shown that hESCs are more equivalent to mouse epiblast stem cells, which represents a later stage of development than mESCs (Tesar et al., 2007). By expanding our understanding of the molecular events that drive self-renewal and differentiation, including the molecular networks regulated by RBBP9, it is anticipated that the potential benefits offered by hPSCs will become closer to reality.

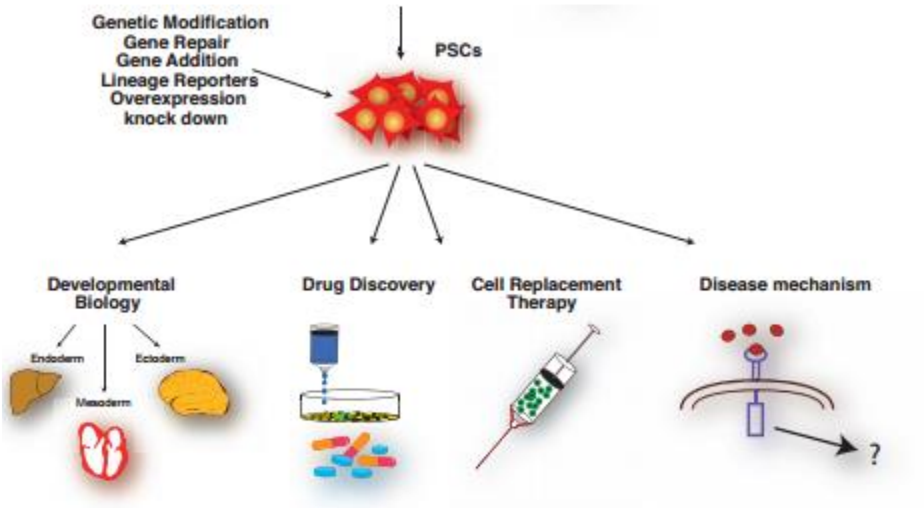

Figure 1.1 The origin and cell fate of hESCs. hESCs are obtained from the ICM of surplus IVF blastocysts, and hiPSCs are obtained from reprogrammed somatic cells. Once hPSC lines are generated they can be maintained in culture for long periods, or differentiated into cell types derived from the endoderm, mesoderm, and ectoderm. hPSCs open doors for drug discovery, cell replacement therapies, and investigations into disease mechanisms. Adapted from (Irion et al., 2008).

1.2.1.1. Origin of hESCs.

hESCs are derived from the inner cell mass (ICM) obtained from pre-implantation human blastocysts approximately 6-7 days post fertilisation (Mitalipova et al., 2003, Reubinoff et al., 2000, Thomson et al., 1998). Blastocysts are composed of two cell types which are responsible for different cell fates. The outer layer of the blastocyst consists of: i) the trophoectoderm layer which is essential for generating the placenta and extra-embryonic yolk sac; and ii) the ICM (Fleming, 1987, Gardner and Rossant, 1979, Adjaye et al., 2005). For hESC derivation, the trophoectoderm layer is typically removed from surplus blastocysts donated from IVF programs after informed consent (Cowan et al., 2004, Heins et al., 2004). The ICM is then placed in cell culture and propagated. With appropriate conditions, the cells that grow out into the culture dish can be maintained in an undifferentiated state in long term cultures (Thomson et al., 1998, Amit et al., 2000, Ludwig et al., 2006), or be induced to follow differentiation programs that appear to mimic aspects of normal embryonic development (Schuldiner et al., 2000). Examples of differentiated cells that can be generated include derivatives of: i) the endoderm, such as the stomach lining, gastrointestinal tract, and epithelium and glands of the lungs; ii) the mesoderm, such as muscle, bone, and blood; and iii) ectodermal derivatives, such as epidermal and neural tissues (Thomson et al., 1998, Shamblott et al., 1998, Amit et al., 2000, Itskovitz-Eldor et al., 2000, Heins et al., 2004). The capacity of hPSCs to self-renew and differentiate into any cell type has been correlated with specific phenotypic and/or functional markers that have been shown to provide reliable assays for pluripotency. These assays include detection of alkaline phosphatase (AP) activity, assessment of 'pluripotency antigen' expression such as the stage specific embryonic antigens as well asTRA-1-60 and TRA-1-81 (O'Connor et al., 2008, Lensch et al., 2007, Thomson et al., 1995, Draper et al., 2002), and also teratoma formation.

1.2.1.2 Core regulatory factors controlling pluripotency in hESCs.

The regulation of self-renewal within hPSCs is inadequately understood at present. Current knowledge suggests that certain transcription factors act as molecular switches to either activate or repress specific gene expression programs which ultimately determine the overall fate of each cell. The transcription factors OCT4 (i.e., POU5F1), NANOG, and SOX2 are amongst the most highly studied pluripotency factors and have been shown to be key regulators of hPSC maintenance (Boyer et al., 2005, Loh et al., 2006, Masui et al., 2007, Niwa et al., 2000, Rodda et al., 2005, Xu et al., 2008).

1.2.1.2.1. OCT4.

The homeodomain protein OCT4 is a transcription factor encoded by the gene *POU5F1* (Boyer et al., 2005, Niwa et al., 2000, Rodda et al., 2005, Xu et al., 2008). Studies in mESCs have shown that imbalanced expression of Oct4 results in differentiation of mESCs and hESCs into different cell lineages (Hay et al., 2004, Hough et al., 2006, Nichols et al., 1998, Niwa et al., 1998). Decreased Oct4 expression results in the failure to maintain pluripotency and has been shown to stimulate differentiation into trophoectoderm and endoderm lineages (Hay et al., 2004, Nichols et al., 1998). Interestingly, over-expression of Oct4 can initiate differentiation into primitive mesoderm and ectoderm in mESCs (Niwa et al., 2000) (Figure 1.2). In hESCs increased expression of OCT4 in hESCs results in differentiation towards endodermal and mesodermal lineages, whereas decreased expression results in endodermal differentiation (Rodriguez et al., 2007). Together, these studies demonstrate a requirement for tight regulation of OCT4 expression levels within a specific range in order to maintain pluripotency, indicating that OCT4 is a master regulator of pluripotency.

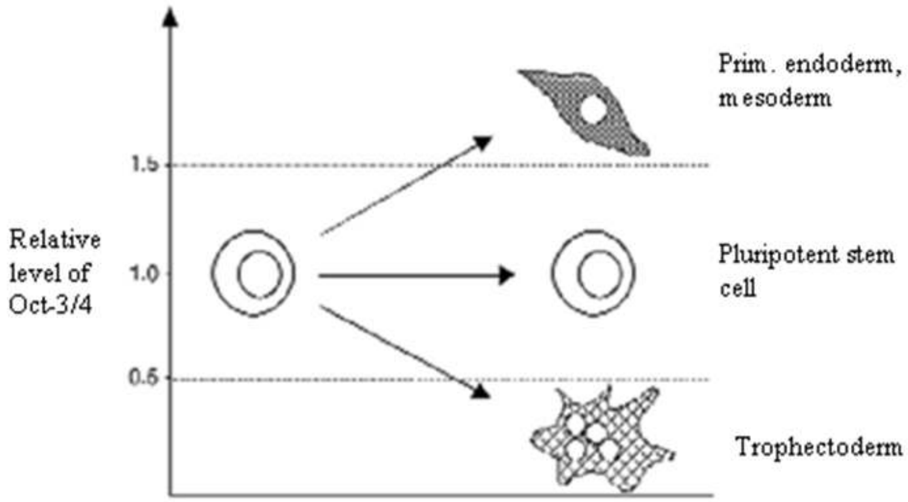

Figure 1.2 Relative expression levels of Oct4 control the pluripotent state. High levels of Oct4 expression induce ESC differentiation into primitive endoderm and mesoderm. Low levels of Oct4 expression induce formation of trophoectoderm. Controlled levels of Oct4 expression between these two extremes allow the cell to remain pluripotent (Niwa et al., 2000).

1.2.1.2.2. NANOG.

Another highly studied regulator of pluripotency is Nanog, a member of the homeobox family of DNA binding factors. Nanog has been shown to play a key role in the maintenance of pluripotency in mESCs and hESCs (Hart et al., 2004). *Nanog* was first identified as a regulator of pluripotency in mouse embryos, where mRNA transcripts were detected within the ICM of the blastocyst that were lost with differentiation into trophoectoderm. *Nanog* expression was also enriched in multiple pluripotent cell lines such as embryonic stem, embryonic germ, and embryonic carcinoma cells, however not detected in adult tissues (Chambers et al., 2003, Mitsui et al., 2003)**.** Loss of both Nanog gene and protein expression was shown to induce differentiation into extra-embryonic lineages in both mESCs and hESCs (Chambers et al., 2007, Hatano et al., 2005, Hough et al., 2006, Hyslop et al., 2005, Ivanova et al., 2006, Lin et al., 2005, Pan and Pei, 2005, Xu et al., 2008). Concomitantly, stable expression of *NANOG* in hESCs has been shown to repress the differentiation of hESCs into extra-embryonic endoderm derivatives (Masui et al., 2007). Together, these findings demonstrate NANOG is key to the maintenance of pluripotency within hESCs.

1.2.1.2.3. SOX2.

SOX2 is also an essential element of pluripotency as loss of *Sox2* has been shown to affect self-renewal and result in differentiation (Avilion et al., 2003, Masui et al., 2007, Ivanova et al., 2006). SOX2 is thought to function by maintaining expression of OCT4 and, similar to OCT4, SOX2 expression needs to be maintained within specific limits to maintain pluripotency and avoid differentiation (Kopp et al., 2008, Masui et al., 2007). Over-expression of Sox2 protein has been associated with neural differentiation in mESCs, where up-regulation of Sox2 was found to down-regulate several developmentally regulated genes including *Nanog* (Kopp et al., 2008). In addition, studies in hESCs have shown that loss of *SOX2* expression results in differentiation into trophoectoderm-like cells (Fong et al., 2008, Wang et al., 2012). Together, these studies show Sox2 acts as a key molecular switch to aid in the regulation of other genes that are critically required for maintaining self-renewal or differentiation or PSCs.

1.2.1.2.4. FOXD3.

The transcription factor FOXD3 is highly expressed in hESCs and has been shown to be essential for maintaining pluripotency within early mouse embryos (Guo et al., 2002, Liu and Labosky, 2008). In mouse embryos, *Foxd3* was shown to contribute to the establishment of an epiblast-like state (a pluripotent state which is thought to be equivalent to hESCs), due to the dramatic loss of cells within mouse epiblasts as a result of *Foxd3* loss of function (Hanna et al., 2002). Additionally, *Foxd3* expression was shown to lead to a slight up-regulation of known regulators of pluripotency *Oct4, Sox2, Nanog, Esrrb, Tbx3, Klf4,* and *C-myc*. This change suggests that *Foxd3* may act downstream or in parallel to these pluripotency factors to regulate self-renewal and induce stem-cell like properties (Liu and Labosky, 2008). This up-regulation of *Foxd3* in the maintenance of self-renewal in ESCs indicates that *Foxd3* may act as a gatekeeper by preventing pluripotent cells from undergoing inappropriate differentiation (Hanna et al., 2002, Liu and Labosky, 2008, Zhu et al., 2014) (Figure 1.3). *FOXD3* has also been shown to act as a transcriptional repressor that blocks mesodermal differentiation from occurring (Steiner et al., 2006). The proposed mechanisms of action for *Foxd3* as either a

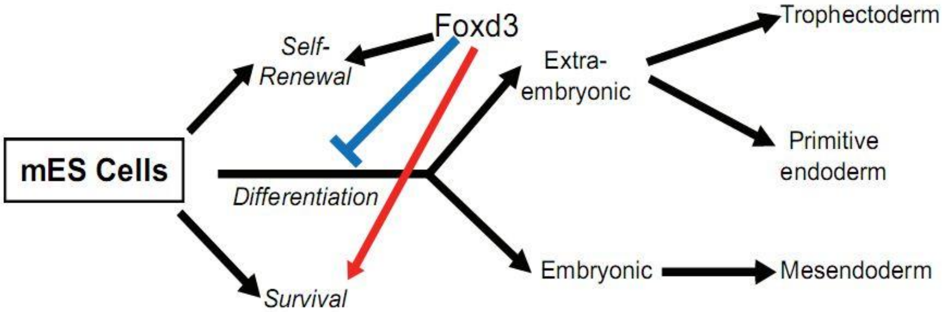

Figure 1.3 Model of Foxd3 functions in mESCs. The expression of Foxd3 appears to repress differentiation within mESCs. This repression allows mESCs to retain self-renewal potential, thus allowing ESCs to survive in a pluripotent state (Liu and Labosky, 2008).

repressor or activator could indicate a role for *Foxd3* as a convergent point for multiple pathways within pluripotent cells (Liu and Labosky, 2008).

1.1.1.3. Regulation of pluripotency in hESCs.

Regulation and integration of the above transcription factors into pluripotency networks is tightly controlled in order to maintain self-renewal and pluripotent differentiation capacity. Alterations to the expression of key pluripotency regulators and the associated genes they regulate results in differentiation or even cell death (Hanna et al., 2002). Studies have identified strong interaction between core regulators of pluripotency in ESCs. For example, OCT4, NANOG, and SOX2 have been shown to contribute to ESC pluripotency through a positive feedback loop whereby they each regulate the expression of each other (Boyer et al., 2005, Chen et al., 2008, Cole et al., 2008, Kim et al., 2008, Kuroda et al., 2005). OCT4, NANOG and SOX2 were identified to co-occupy promoters of at least 353 genes in hESCs and were shown to work together to form an interconnected auto-regulatory feedback loop to control and maintain embryonic stem cell transcriptional circuitry, and to repress genes essential for embryonic development (Boyer et al., 2005) (Figure 1.4).

The activity of Oct4 and Sox2 has been shown to be linked, with Sox2 found to play a large role in assembling key target regulatory elements of Oct4 to maintain ESC self-renewal (Avilion et al., 2003, Chambers et al., 2003, Mitsui et al., 2003). Targeted loss of Sox2 was found to replicate differentiation events seen with loss of Oct4 expression in ESCs (Masui et al., 2007, Niwa et al., 2000). Additionally, a positive feedback loop has been identified between Oct4, Nanog, and Sox2 interactions. In order to maintain a pluripotent state within embryonic stem cells, Nanog has been shown to promote the expression of Oct3/4 and Sox2, which are also required for transcriptional regulation of Nanog gene expression (Boyer et al., 2005, Kuroda et al., 2005, Loh et al., 2006, Wang et al., 2006).

As described above, tight regulation of Oct4, Nanog and Sox2 expression is required for ESCs to remain in an undifferentiated state (Chambers et al., 2003, Mitsui et al., 2003, Niwa et al., 2000). Interestingly, Foxd3 was shown to act as a transcriptional activator through its binding interactions with Oct4, which in turn activates osteopontin enhancers expressed in hESCs (Guo et al., 2002). An immunoprecipitation study has also shown Oct4 can interact with the DNA-binding domain of Foxd3, suggesting Oct4 might regulate Foxd3 transcriptional activity. Overexpression of Oct4 has also been shown to repress both Nanog, and Oct4 expression, ultimately resulting in differentiation of ESCs. However, Foxd3 can function as a positive activator of Nanog in ESCs, overcoming repression induced by Oct4 and therefore resulting in retention of pluripotent ESCs (Pan et al., 2006). This study suggested that the negative feedback loop created from the interactions of Foxd3, Nanog, and Oct4 leads to an interdependent network of transcription factors as part of the complex regulation involved in ESC pluripotency (Figure 1.5). This proposed model may function in a similar manner to the OCT4/NANOG/SOX2 transcriptional regulatory network proposed by Boyer and colleagues (Boyer et al., 2005). More recent studies have also shown that FOXD3 simultaneously acts as a transcriptional activator and repressor to maintain pluripotency in ESCs (Krishnakumar et al., 2016). In this context it is interesting to note that RBBP9 expression is required for maintenance of pluripotency, and that loss of RBBP9 in hESCs rapidly led to a significant reduction in FOXD3 expression.

1.1.1.4. Consequences of pluripotency networks.

The auto-regulatory feedback loop responsible for regulating pluripotency within embryonic stem cells is thought to be advantageous as it could reduce the cellular response time to environmental stimuli. This would allow the pluripotent cells *in vivo* to respond appropriately to developmental cues as well as increasing the stability of gene expression (Alon, 2007). This auto-regulatory feedback loop would be compromised if the expression of the above transcription factors were to be altered, thus resulting in either loss of pluripotency or priming for loss of pluripotency. Together, appropriate regulation of expression of these core pluripotency regulators is required to repress differentiation and retain pluripotency, although the full mechanisms controlling how they act, including pathways regulated by RBBP9, are not known.

Accompanying these core regulatory pluripotency factors are many other known or suspected factors that are though to contribute to long term maintenance of ESCs. For example Klf4, c-myc, Stat3, Sall4, β-catenin, Esrrb and RBBP9 have all been found to contribute to the maintenance of ESCs (Li et al., 2005, Cartwright et al., 2005, Matsuda et al., 1999, Niwa et al., 1998, Wu et al., 2006, Zhang et al., 2006, Loh et al., 2006, Qiu et al., 2010, Richards et al., 2004, Sperger et al., 2003, O'Connor et al., 2011). The requirement for at least some of these pluripotent factors in the maintenance of ESCs across species is variable, as shown by known discrepancies between hESCs and mESCs. For example in hESCs the requirement of STAT3 is not critical in maintenance of self-renewal (Daheron et al., 2004, Humphrey et al., 2004). Nevertheless, these studies show that pluripotent factors other than the quartet of OCT4, SOX2, NANOG and FOXD3 help sustain the transcriptional regulatory network required for the regulation of pluripotency and self-renewal.

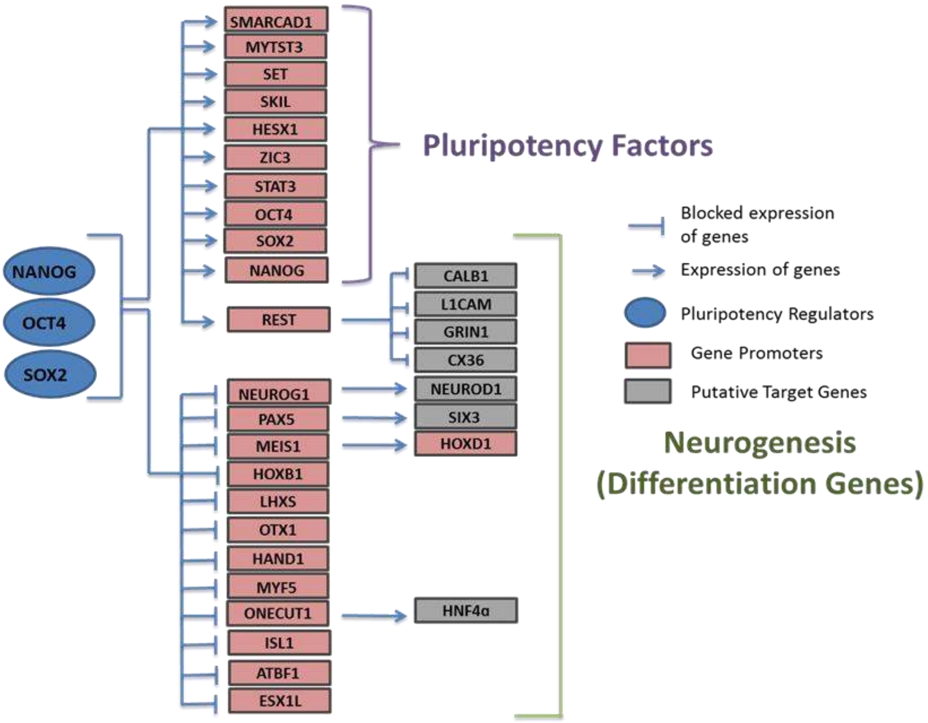

Figure 1.4 A core transcriptional regulatory network model for maintenance of pluripotency. In this model OCT4, NANOG, SOX2 co-occupy a range of mutual target genes to either promote or repress expression of the target genes. Adapted from (Boyer et al., 2005).

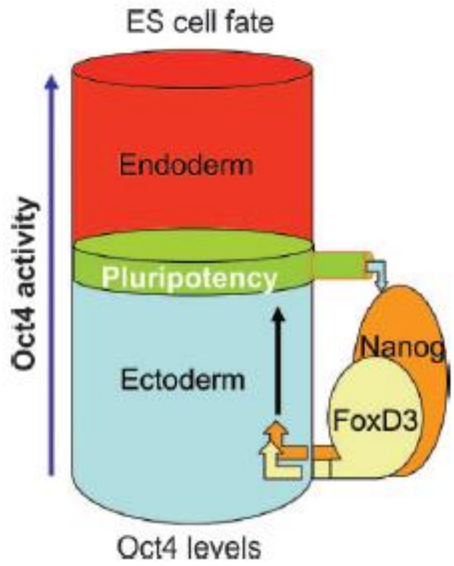

Figure 1.5 Proposed model for Foxd3-Nanog-Oct4 negative feedback loop. This model proposes the interaction of Foxd3 with Nanog to ensure the optimal expression of Nanog in PSCs and ultimately aid in obtaining the appropriate level of Oct4 expression needed to maintain pluripotency (Pan et al., 2006).

1.1.2. hiPSCs: advancements in cell reprogramming and disease modelling.

The identification of *Oct4, Nanog* and *Sox*2 as key pluripotency regulators, as well as other pluripotency regulators such as Klf4 and Lin28, led to ground-breaking pluripotency factor over-expression experiments that identified approaches to reprogramming somatic cells to a pluripotent state. This process generates disease-specific and/or patient-specific mouse (m) iPSCs and hiPSCs (Park et al., 2008, Takahashi et al., 2007b, Takahashi and Yamanaka, 2006, Yu et al., 2007). These iPSCs have become an invaluable tool for modelling normal develop and diseases, and potentially also providing patient-specific cells for transplantation.

Two general reprogramming gene cocktails have been established, consisting of the original miPSC and hiPSC reprogramming cocktail of *Oct4/Sox2/Klf4* (+/- *c-myc*), and an alternate cocktail of *Oct4/Nanog/Sox2/Lin28* (Park et al., 2008, Takahashi et al., 2007b, Takahashi and Yamanaka, 2006, Yu et al., 2007). The original reprogramming cocktail was derived from a list of 24 genes selected based on i) their high expression in ESCs (Takahashi and Yamanaka, 2006), and ii) the finding that nuclei transplanted from a somatic cell to an oocyte could be reprogrammed back to a pluripotent state (Gurdon, 1962). Re-expression of these 'reprogramming genes' in somatic cells is typically achieved using retro-viral vectors (Takahashi et al., 2014). The resulting iPSCs possess the ability to be integrated into organisms when transplanted into embryos (only ethically possible with miPSCs), and also to generate teratomas containing derivatives of endoderm, mesoderm and ectoderm when transplanted typically into immunocompromised mice (Lensch et al., 2007, Thomson et al., 1998) (Figure 1.6). Reprogramming gene cocktails originally contained the oncogene *c-myc*, however, in 2007 Takahashi and colleagues demonstrated reprogramming can occur in the absence of *c-myc*, and in doing so reduced the tumorigenicity of the reprogrammed cells (Takahashi et al., 2007a).

Originally, hiPSC production required the use of viruses to re-introduce expression of pluripotency genes, resulting in viral integration within the genome of the reprogrammed cells. Due to the simplicity of this method it is often still used today. To avoid this viral integration a number of groups have investigated reprogramming methods that either excise the integrated viral DNA, or that do not require viruses to insert cDNA into the genome such as the *piggyBac* transposon approach (Jia et al., 2010, Narsinh et al., 2011, Okita et al., 2008, Stadtfeld et al., 2008, Woltjen et al., 2009). Unfortunately these methods tend to result in a significant decrease in iPSC formation (Takahashi et al., 2007b). In an attempt to overcome this issue, small molecules have been tested to both increase reprogramming efficiency, and decrease the number of genes required for the reprogramming cocktail. For instance Huangfu and colleagues identified that the addition of valporic acid (a histone deacetylase inhibitor) increased the efficiency for human fibroblast reprogramming (Huangfu et al., 2008). Nevertheless, significant time and effort is still required to generate hiPSCs. Efforts are therefore being made to better understand the molecular mechanisms of pluripotency and the reprogramming process, so the time and expense of this technology can be sufficiently reduced to make it feasible for the investigation for patient specific stem cell-based transplantation therapies.

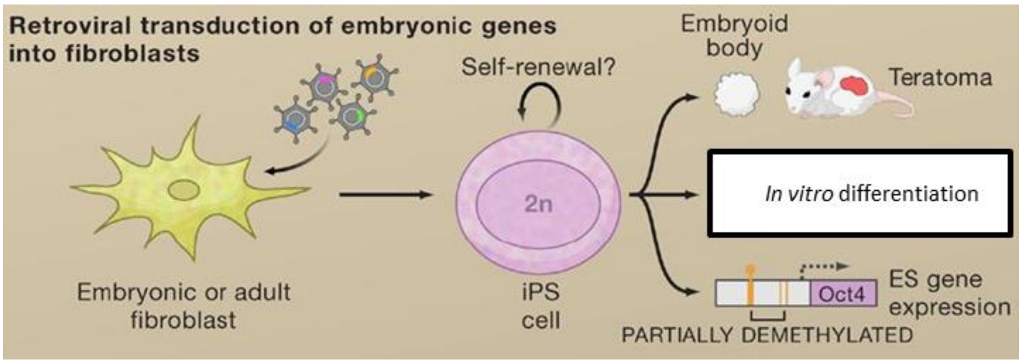

Figure 1.6 Reprogramming of differentiated somatic cells using retroviral transduction. A schematic of iPSC generation and downstream analyses. Once expression of the exogenous pluripotency factors has been achieved (e.g., *via* retroviral transduction), re-organisation of the genome occurs to re-activate expression of the endogenous pluripotency genes. As a result, an iPSC is generated that can be maintained indefinitely in culture, or induced to differentiate, e.g., *via* teratoma formation. Adapted from (Rodolfa and Eggan, 2006).

Various studies have suggested that hiPSCs and hESCs are almost identical in terms of morphology, pluripotency antigen expression, and gene expression profiles (Takahashi et al., 2007b, Chin et al., 2009). However, subtle differences have been seen and it is not yet clear how significant these are (i.e., whether they significantly change the properties of iPSCs compared to ESCs). One concern is the potential for mutations to arise during the reprogramming process that then lead to the potential for tumors in any transplanted hiPSC-derived cells. Indeed, the first ever hiPSC-based clinical trial (that aimed to treat macular degeneration with patient-specific retinal pigment epithelial cells) was recently put on hold due to mutations found in the cells prior to transplantation (Scudellari, 2016). In addition to using hESCs and hiPSCs as models of development, a clearer understanding of the molecular mechanisms that govern pluripotent cells is a high priority for the field to enable continued improvements to reprogramming technology.

1.1.3. Zebrafish as an *in vivo* model of embryonic development.

1.1.3.1. Unique properties of zebrafish embryogenesis.

Zebrafish (*Danio rerio*) have been increasing in popularity as an *in vivo* model for embryonic development (Kimmel et al., 1995, Chen et al., 2015a, Chen et al., 2015b, Zou et al., 2015, Behra et al., 2004, Ekker and Larson, 2001, Langheinrich et al., 2002, Parng et al., 2002, Robles et al., 2011). Compared to other animal models, zebrafish models possess unique properties making them ideal for studying the early stages of embryonic development. Zebrafish embryos are fertilised and continue to develop rapidly outside the mother's body, with hatching within three to four days. In addition to this, developmental changes can easily be tracked as zebrafish embryos are optically transparent, thus allowing simple microscopic visualisation of clearly defined, stage-specific phenotypes of zebrafish embryos (Kimmel et al., 1995, Streisinger et al., 1981). Zebrafish are able to produce large numbers of fertilised embryos (approximately 200-300) at any one time, making them ideal candidates for high throughput screens. This also results in relatively low cost maintenance compared to other animal models (e.g., mice) (Parng, 2005, Parng et al., 2004).

1.1.3.2. Molecular similarities of zebrafish and hPSC models.

Developmental and molecular similarities are present between hPSCs and zebrafish. As described above, hPSCs express high levels of the core pluripotency regulator *OCT4* (Boyer et al., 2005, Masui et al., 2007, Niwa et al., 2000). Similarly, high levels of *oct4* have been detected in early blastomeres of zebrafish embryos (Kotkamp et al., 2014, Robles et al., 2011) which are equivalent to the ICM from which hESCs are derived (Mitalipova et al., 2003, Reubinoff et al., 2000, Thomson et al., 1998). Not surprisingly, zebrafish PSCs have been successfully generated from zebrafish embryos (Fan et al., 2004, Ghosh and Collodi, 1994) approximately 2.25 hours post fertilisation (hpf) (blastula stage) and 5.5 hpf (gastrula stage) (Kimmel et al., 1995). Cells derived from zebrafish embryos between the blastula and gastrula stages have the potential to generate a variety of cell lineages (Kimmel and Warga, 1986) similarly to hPSCs (Thomson et al., 1998). These similarities between zebrafish and hPSCs make zebrafish ideal candidates for *in vivo* modelling of general embryonic development.

In 2013, sequencing of the zebrafish genome was completed and revealed a significant (~70%) genetic similarity between zebrafish and humans (Howe et al., 2013) (Figure 1.7). Earlier studies identified thousands of mutants in early zebrafish development through genetic screens (Amsterdam et al., 1999, Driever et al., 1996, Haffter et al., 1996). Similarities observed between human and zebrafish genomes enable the use of zebrafish to model developmental phenotypes and offer the potential to provide a greater understanding of factors which control specification of cell types and organ systems relevant to some human diseases. Despite obvious physiological differences apparent between humans and zebrafish, the availability of screens to select for developmental mutants coupled with the complete sequencing of the zebrafish genome is advantageous. This provides the opportunity for a greater understanding of cell and biological processes behind disease phenotypes at specific early developmental time points which are difficult to obtain using other animal models.

1.1.3.3. Morpholino oligonucleotides: A gene knockdown approach in vertebrate development.

Zebrafish have been utilised in many gene knockdown studies due to the unique developmental properties they possess. The identification of antisense morpholino oligonucleotides (MOs) provided a tool for transient gene knockdown in animal models by developmental biologists since its first identification in 2000 (Heasman et al., 2000, Ekker and Larson, 2001, Nasevicius and Ekker, 2000). MOs are chemically modified synthetic oligonucleotides composed of chains of approximately 25 subunits, and are highly similar to DNA and RNA oligonucleotides. MOs have a modification where a morpholine ring replaces the ribose ring, allowing MOs to still undergo Watson-Crick base pairing (Summerton and Weller, 1997) (Figure 1.8 B).

First generation antisense MOs were developed as DNA oligonucleotides between 18-22 subunits in length (Summerton and Bartlett, 1978, Zamecnik and Stephenson, 1978) (Figure 1.8 A). These MOs were designed to form RNA-DNA hybrids with target mRNA to then act as a substrate where the target mRNA could be degraded by RNase H (Cazenave et al., 1989). However, it was later shown that these DNA oligonucleotides were not ideal in developmental studies due to non-specific toxic side effects. Also, the knockdown effect was temporary due to degraded mRNA transcripts being replenished with new transcription (Woolf et al., 1990).

To overcome these limitations, MOs were re-developed as DNA analogs to block mRNA translation. Re-design of MO structure offered greater advantages over conventional oligonucleotides, including greater stability. Rather than inhibiting protein translation through RNAse H-mediated degradation of the mRNA (Cazenave et al., 1989), the redesigned MOs specifically target the initiation codon of the target mRNA, inhibiting translation of mRNA both *in vitro* and *in vivo* without the need for RNAse H (Summerton, 1999). These MOs can only block translation when designed to be complementary to the 5' leader sequences, or designed to the first 25 bases 3' to the AUG translational start site (where it is hypothesised ribosomes are inhibited from binding). Generally, MOs are designed to be the exact antisense match against the region surrounding the first translated ATG to successfully block translation (Figure 1.8 C). This MO redesign also decreased the likelihood of toxicity and non-specific binding with other components of the cell as they do not have a negatively charged backbone, unlike previous oligonucleotide structures. These translation blocking MOs can be injected into zebrafish embryos at the 1-2 cell stage to determine the role of particular genes during development (Nasevicius and Ekker, 2000, Draper et al., 2001).

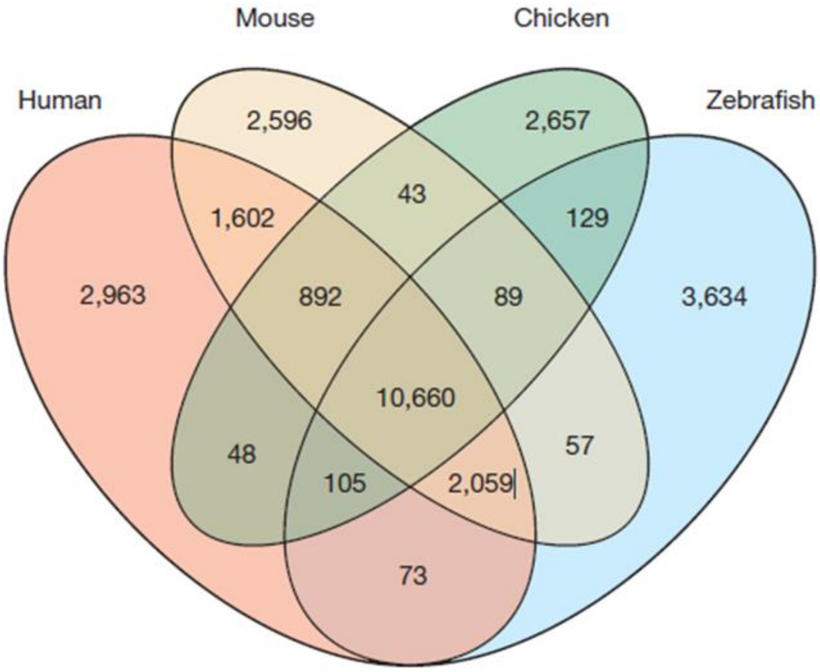

Figure 1.7 Genome comparisons between *in vivo* developmental models. Shows orthologue genes shared between human, mouse, chicken, and zebrafish (Howe et al., 2013).

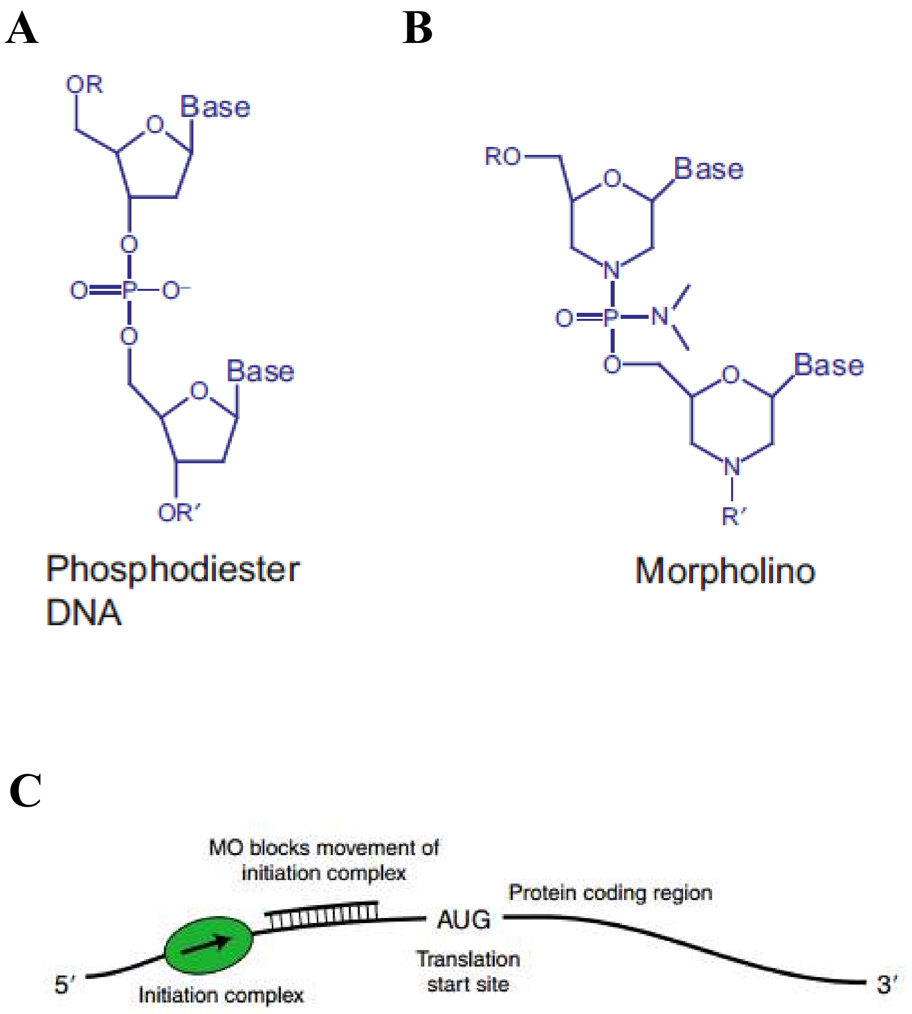

Figure 1.8 MO structure. Structures of MOs where; **A)** shows the structure of phosphodiester DNA oligonucleotide, and **B)** shows the structure of the widely used MO, where R' represent continuation of the oligomer chain in the 5' or 3' direction (Corey and Abrams, 2001). **C)** Representative diagram of mRNA inhibition *via* MO, where the MO is targeted to a sequence 5' of the translation start site and inhibits the initiation complex from completing mRNA translation (Eisen and Smith, 2008).

1.1.3.4. Effectiveness of MO mediated gene knockdown.

To minimise the potential for off-target effects arising from MOs, a range of controls are routinely implemented (Robu et al., 2007, Eisen and Smith, 2008, Kok et al., 2015, Stainier et al., 2015). A key control is the co-injection of MO targeting p53 together with the MO targeting the gene of interest. This is done to determine whether any phenotype seen as a result of the test MO is due to activation of the p53 pathway - if the phenotype remains even in the presence of the p53 MO then the effect is most likely due to specific loss of expression of the target gene (Robu et al., 2007). Thus MO technology provides a useful tool for investigating the role of particular genes of interest during embryonic development in a way that both parallels and complements hPSC technology.

1.2. Role of the RB/E2F pathway in cell cycle regulation.

Appropriate regulation of cell cycle progression, self-renewal of stem cells and cell differentiation are key aspects of normal and cancer development. These processes are regulated by many networks, one of those being controlled by interaction between the RB and E2F transcription factors (Woitach et al., 1998). The highly studied RB protein has been identified as a negative regulator of cell proliferation when hypo-phosphorylated; as a result RB is a key tumor suppressor that acts at the 'G_1 checkpoint' that regulates progression into the S (i.e., DNA synthesis) phase of the cell cycle (Woitach et al., 1998, Boyer et al., 1996). By binding and sequestering E2F transcription factors, Rb inhibits transcription of E2F target genes that are required for cell cycle progression by forming a repressor domain in G_1/G_0 (Boyer et al., 1996). Absence of hypo-phosphorylated Rb is thought to contribute to high proliferation rates observed in ESCs (Savatier et al., 1994, Fluckiger et al., 2006). Phosphorylation of RB was found to inactivate the protein, and this event was shown to reinstate E2F transcriptional activity (Chellappan et al., 1991, Vandel et al., 2001). A crucial balance of RB and E2F expression is required within hESCs to maintain the optimal balance necessary between cell proliferation and survival (Conklin et al., 2012). In the context of pluripotency in hESCs, it has been shown that accumulation of hypo-phosphorylated RB in G_1 of the cell cycle coincides with loss of hESC markers such as OCT4, and also with hESC differentiation (Filipczyk et al., 2007). RB activity can also be regulated by RB-binding proteins. Importantly, loss of control of the RB-mediated G1 checkpoint is a key step in cancer formation.

As mentioned above, RBBP9 has been shown to bind to RB in both non-pluripotent cells and in hPSCs (O'Connor et al., 2011, Woitach et al., 1998). Moreover, siRNA-mediated knockdown of RBBP9 resulted in loss of pluripotent cells, decreased expression of cell cycle and some pluripotency genes, as well as increased expression of neurogenesis genes (O'Connor et al., 2011). However, the relative contribution of RBBP9's RB-binding and SH activities to hPSC maintenance remains unknown. Further investigation of the RB-binding and SH activities of RBBP9 in hPSCs could therefore yield valuable new information on cell proliferation and differentiation relevant to both hPSCs and cancer.

1.3. Proposed activities of RBBP9: RB-binding and SH activity.

1.3.1. Identification of RBBP9 SH activity.

The first identification of RBBP9 demonstrated it to be able to bind RB protein and thus release active E2F1 transcription factors. Consistent with this, overexpression of RBBP9 promoted cell proliferation by overcoming growth inhibitory effects. These data suggested that RBBP9 might be involved in oncogenic transformation. Since then, RBBP9 transcripts have been detected throughout normal development and also in a range of cancer cells (Woitach et al., 1998). As mentioned above, RBBP9 has also been shown to bind RB in hPSCs and to be required for maintenance of hPSCs (O'Connor et al., 2011). However, RBBP9 has also been suggested to be a SH (Shields et al., 2010, Vorobiev et al., 2012). Notably, SHs are central effectors of the proliferative, invasive, and migratory properties of tumours. Studies have shown SH transcript and protein levels are elevated in many cancer cell lines such as human breast and melanoma and primary tumours (Jessani et al., 2002, Chiang et al., 2006). Additionally, serine proteases have been implicated in Drosophila gastrulation, with loss of function due to mutations of serine proteases resulting in incomplete neural development during early embryogenesis (Han et al., 2000). Also, the serine protease Furin has been shown to be essential for the formation of key tissues derived from endoderm, mesoderm and ectoderm. Disruption of this enzymatic activity was shown to result in malformation of epiblast derivatives such as the primitive heart, gut, and extraembryonic mesoderm (Constam and Robertson, 2000, Roebroek et al., 1998).

DNA sequence analysis shows that RBBP9 contains GXSXG residues that suggest a putative SH nucleophilic serine. These residues are conserved across RBBP9 orthologs in human, mouse and zebrafish sequences amongst other species, suggesting an evolutionarilyimportant function for these residues (Figure 1.9) (Shields et al., 2010, Vorobiev et al., 2009). Elucidation of the crystal structure of human RBBP9 revealed an α/β fold common to SHs. Within this domain lies serine 75 (Ser75) and other amino acids of the putative RBBP9 SH catalytic triad (His165-Ser75-Asp138), suggesting an enzymatic role for RBBP9 (Vorobiev et al., 2009, Ollis et al., 1992) (Figure 1.10).

1.3.2. RBBP9 SH activity in cancer.

A study by Shields and colleagues identified for the first time SH activity in RBBP9, and its specific involvement in pancreatic cancer progression (Shields et al., 2010). Over-expression of normal RBBP9 promoted cellular proliferation in human pancreatic carcinoma cells, with over-expression of a mutant and catalytically inactive version of RBBP9 resulting in decreased proliferation. Fortuitously, a highly selective inhibitor of RBBP9 SH activity called [1-(1,3-thiazol-2-yl)ethylideneamino] cyclohexanecarboxylate (or ML114), was recently reported (Bachovchin et al., 2010b). Activity-based protein profiling (ABPP) was used to test RBBP9 SH activity against a library of putative chemical SH inhibitors. This analysis showed that only ML114 was able to specifically and selectively inactivate RBBP9 SH activity by modifying the active site (Ser75). Furthermore, Bachovchin and colleagues also showed that this inhibitor acts by covalently modifying the active site Ser75, whist simultaneously releasing a soluble fragment during RBBP9-mediated hydrolysis (Bachovchin et al., 2010b) (Figure 1.11). The identification of this highly selective chemical inhibitor of RBBP9 SH activity offers a useful tool to further define the relative contributions of RB-binding and SH activities in both pluripotent cells and in development. The information gained through such studies will be relevant to our understanding of how pluripotent cells are maintained and

		GxSxG/A	
Homo sapiens	61-	TELHCDEKTIIIGHSSGAIAAMRYAETHRV	-90
Macaca mulatta	61-	TELHCDEKTIIIGHSSGAIAAMRYAETHRV	-90
Mus musculus	61-	TELHCDEKTIIIGHSSGAIAAMRYAETHQV	-90
Rattus norvegicus	61-	TELHCDEKTIIIGHSSGAIAAMRYAETHQV	-90
Monodelphis domestica	115-	SEFHCDEKTIIIGHSSGAIAAMRYAETHRV	-144
Bos taurus	61-	MELHCDEETIIIGHSSGAIAAMRYAETHRV	-90
Xenopus Laevis	65-	SELGCDDKTIIIGHSSGAAAAMRFAETHK	-93
Canis familiaris	18-	TELHCDEKTVIIGHSSGAIAAMRYAETHRV	-47
Danio rerio	60-	KDLKCDEETLIIGHSSGAAAAMRYAETHK	-88
Arabidopsis thaliana	70-	SLGSDDDKVILVAHSMGGISASLAADIFPS	-99
Acinetobacter sp.	53-	VQQLEQPVQIVAHSFGCLTTLAALEQHPQ	-81

Figure 1.9 Primary sequence alignment of RBBP9 orthologues shows a conserved GXSXG motif common to SHs. Alignment of RBBP9 amino acid sequences shows a conserved serine residue within a GXSXG motif across a variety of species including Homo sapiens, Mus musculus, Danio rerio and others. This motif is known from analysis of confirmed SHs to contain the active site serine (Shields et al., 2010).

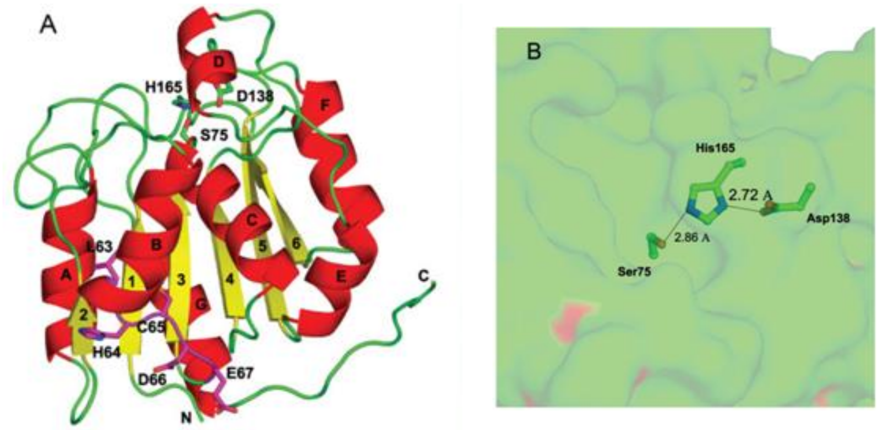

Figure 1.10 Crystal structure of RBBP9 identified a putative SH catalytic triad. A) Ribbon structure of RBBP9. The secondary structure of RBBP9 is depicted as red for α-helixes, yellow for β-strands and green for connecting loops. **B)** Space-filling model shows Ser75 is the predicted active serine of RBBP9 (Vorobiev et al., 2009).

A B C

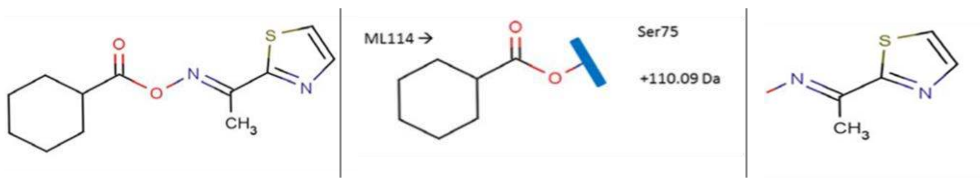

Figure 1.11 The RBBP9 SH inhibitor ML114. A) Chemical structure of ML114. **B)** Hydrolysis of ML114 by RBBP9 Ser75 leads to covalent modification of Ser75, resulting in an increased mass of +110.09 Da. **C)** The soluble ML114 fragment released upon ML114 hydrolysis by RBBP9 SH activity. Adapted from (Bachovchin et al., 2010b).

possibly generated, and also to our understanding of development and/or progression of cancer

1.4. Hypothesis and Aims.

1.4.1. Hypothesis.

That targeted loss of RBBP9 SH activity within hPSCs and zebrafish embryos will identify candidate molecular networks regulated by the two putative RBBP9 activities. These data will then provide new leads for future investigations aimed at improving the efficiency of somatic cell reprogramming and/or better understanding cancer cell behaviour.

1.4.2. Aims.

The work undertaken for this thesis therefore aimed to:

1) Investigate the consequences of chemically-mediated inhibition of RBBP9 SH activity in hPSCs.
2) Identify putative effectors of RBBP9 SH activity in hPSCs.
3) Investigate the consequences of chemically-mediated inhibition of RBBP9 SH activity during early development *in vivo* using zebrafish embryos.

CHAPTER 2: RBBP9 SH inhibitor ML114 decouples hPSC proliferation and differentiation

2.1. INTRODUCTION

Analysis of published gene expression data shows RBBP9 is expressed in hPSCs, and in a range of human cancer cells, as well as during developmental time points of different species such as rats and zebrafish (Bastian et al., 2008, Hirst et al., 2007, O'Connor et al., 2011, Woitach et al., 1998, Vorobiev et al., 2009). Despite this very broad expression little is known of the roles RBBP9 plays in normal development or cancer progression. The few published RBBP9 studies available have suggested RBBP9 has two different activities: i) the ability to bind RB protein and regulate the activity of the RB/E2F cell cycle pathway (Woitach et al., 1998), and ii) the ability to act as a SH on as yet undefined target proteins (Shields et al., 2010).

The RB-binding activity of RBBP9 was first described in 1998 when it was shown to displace E2F1 from RB/E2F1complexes, thus allowing expression of cell cycle-related genes. This interaction has been shown to occur through interactions of a LXCXE RB-binding motif; a base-pair change of leucine to glutamine of the LXCXE RB-binding motif abolishes the ability of RBBP9 to bind to RB and displace E2F1 (Woitach et al., 1998). More recently, RBBP9 SH activity was first suspected by sequence similarity. It has been suggested that RBBP9 belongs to the Domain of unknown function (DUF1234) superfamily of serine proteases (Vorobiev et al., 2009). Comparison of protein sequences identified a conserved serine residue hypothesised to be the putative nucleophilic serine (Ser75) within a GXSXG motif (Shields et al., 2010, Vorobiev et al., 2009). This motif is contained within known SHs such as seprase, a serine protease expressed in human malignant melanoma cells (Aoyama and Chen, 1990, Goldstein et al., 1997). Overexpression of the catalytically inactive mutant RBBP-S75A in human carcinoma cells demonstrated that loss of RBBP9 SH activity led to a decrease in cell proliferation (Shields et al., 2010). More recently, high throughput screening for inhibitors of enzymes with poorly characterised biochemical activity identified a potent and specific chemical inhibitor of RBBP9 SH activity (Bachovchin et al., 2010b). This chemical, ML114, has an IC_{50} of 0.63 μM on cell-free recombinant RBBP9. At 20 μM to 100 μM ML114 is capable of blocking the SH activity of recombinant RBBP9 in human embryonic kidney 293T (HEK) cells, or RBBP9 doped into mouse brain membrane proteome. The selectivity of ML114 is shown by its IC_{50} for 30 other serine hydrolases being >100 μM. ML114 also showed low cytotoxicity, with its CC_{50} being >100 μM in HEK cells (Bachovchin et al., 2010a).

To date, only one study has investigated the activity of endogenously-expressed RBBP9 (O'Connor et al., 2011). In this study, RBBP9 RNA and protein expression was shown in a range of hPSCs including human embryonic stem cells, human induced pluripotent stem cells, and human embryonal carcinoma cells. Co-immunoprecipitation showed RBBP9 interacts with RB protein in hPSCs. siRNA-mediated knockdown of endogenous RBBP9 protein (i.e., loss of both RB-binding and SH activities) resulted in: i) decreased population growth rate; ii) decreased expression of cell cycle genes; iii) decreased expression of some pluripotency genes; and iv) increased expression of genes involved in neurogenesis. While this study demonstrated a requirement for RBBP9 in hPSC maintenance, the use of siRNA did not allow the identification of the relative contributions of RB-binding and SH activity to be established.

To obtain insights into the relative importance of RBBP9 SH activity to hPSC maintenance, the present study used ML114 to identify the consequences of inhibiting only RBBP9 SH activity in hPSCs. The findings showed that ML114-mediated loss of RBBP9 SH activity partially phenocopied the published effects of siRNA-mediated loss of RBBP9 protein (O'Connor et al., 2011) though with a key difference. ML114 treatment of hPSCs resulted in reduced population growth rate and altered cell proliferation patterns, but with retention of pluripotency markers and teratoma-forming ability. These data suggest that ML114 decouples initiation of hPSC differentiation from inhibition of hPSC proliferation - an unusual, though not unprecedented, phenomena. Further investigation and clarification of RBBP9 and its activities will enable a greater understanding of its role in the maintenance of hPSCs, in development, and in progression of cancer.

2.2. METHODS

2.2.1. General reagents and consumables.

Reagents used for cell culture including mTeSR1™, Dispase and Trypan Blue were acquired from StemCell Technologies (Melbourne, Australia). Reagents used in cell harvesting and antibody staining, including TryPLE™ Express, Dulbecco's Modified Eagles Medium (DMEM), and Dulbecco's Phosphate Buffered Saline (PBS), were acquired from Thermo Fisher Scientific (Scoresby, Australia) unless stated otherwise. Matrigel used to coat tissue culture plates for cell adherence was acquired from Corning, Falcon-Discovery Labware (Clayton, Australia). All tissue culture plates (6-well, 96-well, 35 mm and 60 mm) and pipette tips used for general cell culture were acquired from Interpath Services (Heidelberg West, Australia). All consumables used for electrophoresis, including acrylamide, tris-glycine, and sodium dodecyl sulfate (SDS) buffer were of electrophoresis grade or higher quality and were obtained from Ameresco Inc. distributed by Astral Scientific Pty Ltd., Sydney, Australia.

2.2.2. General equipment.

2.2.2.1. General cell culture.

All cell culture was conducted within a Gelaire BH-EN 2000 D Series Class II Biological Safety Cabinet (Seven Hills, Australia). All surfaces were disinfected using isopropanol both prior to and upon completion of use. All cell cultures were incubated in a Heracell 150 CO_2 incubator at 37 °C, 5% CO_2 (Thermo Fisher Scientific). All non-sterile pipette tips, tubes and glassware were sterilised by autoclaving at 121 °C for 20 minutes with a 5 minute drying time using a benchtop Tuttnauer 3150EL autoclave (Tuttnauer, Breda, Netherlands) prior to cell culture use. All waste cell culture media was disinfected with bleach prior to disposal. Used pipette tips, tissue culture plates and tubes were sterilised using a Getinge HS 6610 AM-2 autoclave (Getinge AB, Getinge, Sweden).

2.2.2.2. Light microscopy.

Prior to routine tissue culture (including daily medium changes), all cultures were visually inspected for any differentiation or abnormalities using an Olympus CKX41 inverted microscope and accompanying digital camera (Olympus, Macquarie Park, Australia). Light microscopy images were captured using the imaging software Q Capture Pro v6 (Q Imaging, Brisbane, Australia).

2.2.2.3. Centrifugation.

All centrifugation with volumes higher than 1.5 mL was conducted using a Beckman and Coulter Allegra® X-15R Centrifuge (Gladesville, Australia). All centrifugation with volumes lower than 1.5 mL was conducted using a Beckman and Coulter Microfuge® 22R Centrifuge or QikSpin Personal Microfuge (Edwards Instrument Co., Narellan, Australia).

2.2.2.4. Storage of samples.

All protein and RNA samples were stored at -80 ℃ in an ultra-low temperature freezer (Thermo Fisher Scientific).

2.2.3. General cell culture.

The hPSC line used in this study was the CA1 human embryonic stem cell line. hPSCs were obtained from Prof. Andras Nagy of The University of Toronto, Canada (Adewumi et al., 2007) and seeded either as aggregates or single cells. Use of hPSCs complied with national guidelines with oversight by Western Sydney University Human Research Committee (approval H10950) and Biosafety and Radiation Committee (approval B8022 and B10355). All hPSCs were cultured using the defined, feeder cell-free medium mTeSR1™ (Ludwig et al., 2006) and the extracellular matrix product Matrigel (0.08 mg/mL Matrigel in DMEM) to aid cell attachment. The tissue culture plates were coated with Matrigel for a minimum time of 30 minutes at room temperature. Prior to seeding of cells the Matrigel was removed, leaving a coating for cell attachment.

2.2.3.1. Aggregate cell seeding.

Confluent hPSCs were passaged every 7 days using previously optimised hPSC culture conditions (O'Connor et al., 2008). hPSCs were first washed with 1 X PBS, and were incubated in 1 X Dispase (3 minutes at 37 °C, 5% CO_2). Dispase was removed and hPSCs were washed with 1X PBS. Following this, DMEM was added and hPSCs were harvested using a cell scraper and collected, followed by a 1 X PBS wash to collect any residual hPSCs remaining on the tissue culture dish. hPSCs were then centrifuged (300 × *g*, 5 minutes), supernatant was removed and the pellet was resuspended with mTesR1™ by gentle trituration. A clump count was performed by adding 5 µL of triturated hPSCs to 20 µL of 1 X PBS to create a 1/5 dilution; clumps were then counted using a light microscope. The average concentration of clumps was calculated and the desired number of clumps then seeded into Matrigel-coated tissue culture plates with mTeSR1™ and incubated (37 °C, 5% CO_2) until required.

2.2.3.2. Single-cell seeding and ML114 treatment conditions.

Confluent hPSC cultures were washed with 1 X PBS, then incubated in TrypLE™ to generate single cells (7 minutes at 37 °C, 5% CO_2). Single cells were collected and the culture dishes washed with 1 X PBS to collect remaining hPSCs. Supernatant was removed and the cell pellet was resuspended with mTesR1™ with 10 µM Rho-Kinase Inhibitor (ROCK inhibitor, Ri) (Merk, Kilsyth, Australia). A single cell count was performed by adding 10 µL of the single cell mixture to 40 µL of 0.4% (w/v) Trypan blue to create a 1/5 dilution for each cell sample in a well of a 96-well tissue culture plate. The mixture of cell sample and Trypan Blue was then placed into a hemocytometer (Bright-Line; Hausser Scientific, Pennsylvania, USA) and a cell count was performed using a light microscope. Two counts on the same sample were performed, counting live (unstained) cells present within the neubauer grid of the hemocytometer (the frequency of dead - i.e., stained - cells was also determined). This count was then averaged and divided by 0.1 μL (the volume of cells contained on the hemocytometer), and multiplied by 5 (for the dilution factor used). This enabled determination of the total cell number present within each sample. The desired number of single cells were then seeded into a Matrigel-coated tissue culture dish with mTesR1™ and 10 μM of Ri and incubated (37 °C, 5% CO_2). The mTeSR1™ medium was replaced the following day without Ri and both control and ML114 treatments were added after this time-point. For ML114-based experiments, cells were treated either with 0.25% DMSO (Sigma Aldrich, Castle Hill, Australia) as a vehicle-only control, the ML114 soluble fragment (Key Organics) made up in 0.25% DMSO as an additional control, or the RBBP9 SH inhibitor ML114 (Key Organics, Cornwall, UK) made up in 0.25% DMSO (Figure 1.11). Unless otherwise stated, treatments were added 72 hours after cell seeding to ensure maximal cell yield of treated hPSCs for downstream assays. In all cases, final DMSO concentration was 0.25%.

2.2.4. ML114 dose response using hPSCs plated as single cells.

hPSCs were plated (see section 2.2.3.2), and treatment was added 24 hours after initial cell seeding. Each well of the 6-well tissue culture plate was treated with different doses of ML114 (5, 50, and 100 μM) for 7 days of culture. Colonies present within the tissue culture dish were counted with a light microscope 1, 2, and 5 days after treatment. Colony numbers were averaged and all 0 μM bars were set to 100% to compare the changes in magnitude due to ML114 treatment. A student's t-Test verified statistical significance of the data.

2.2.5. hPSC post-ML114 recovery treatment.

Treated hPSCs were harvested at day 7 of treatment and re-seeded into optimal hPSC maintenance conditions and maintained *via* standard passaging for up to 12 weeks. Cells counts were recorded at each passage prior to hPSC re-seeding.

2.2.6. Colony forming cell (CFC) assay.

Treated hPSCs were assessed using the alkaline phosphatase (AP) CFC assay (O'Connor et al., 2008). The CFC assay was performed using reagents obtained from the Alkaline Phosphatase (AP) Leukocyte kit (Sigma Aldrich) with adjustments to the protocol as follows: hPSCs were cultured (see section 2.2.4) and at the appropriate time point culture media was removed and cells were washed with PBS and fixed with AP fixative (25 mL Citrate Solution, 65 mL Acetone and 8 mL 37% Formaldehyde) for 30 seconds. The fixative was then removed and the cells washed with PBS. Sufficient AP stain was made for each 35 mm tissue culture to be analysed by adding 22 µL/well of Sodium Nitrate solution to 22 µL/well of FBB-Alkaline Solution. This was allowed to sit for 2 minutes before1 mL/well of distilled water (dH_2O) and 22 µL/well of Napthol AS-BI Alkaline Solution was added. Each well was then stained with 1 mL of AP stain for 15 minutes in the dark before being washed with PBS. Fresh PBS was added for storage purposes and to maintain the integrity of stains for analysis.

2.2.6.1. CFC analysis.

Representative light micrographs of AP-stained colonies were captured using the Olympus CKX41 inverted microscope/camera and Q Capture Pro v6. The cell number per colony was determined by approximating the plate area occupied by each colony. These sizes were based on the estimated average colony diameters as well as the assumption that each undifferentiated hESC colony had an approximate diameter of 30 μM after fixation. To determine the diameter of the colonies, the average length of the longest colony axis was estimated as well as the colony axis length that was perpendicular to this. The diameter of colonies was estimated using a linear (mm) graph paper printed on a transparent sheet then placed on an inverted microscope (O'Connor et al., 2011).

2.2.7. Flow cytometry analysis.

Cells were harvested as single cells (see section 2.2.3.2) and cell counts performed to ensure appropriate numbers were used for analysis. The cells were then centrifuged (300 × *g*, 5 minutes), the supernatant removed, and the residual supernatant used to re-suspend the cell pellet. Cells were fixed in 100 μL of 2% para-formaldehyde and placed on ice for 15 minutes. After incubation 1 mL of PBS was added to the suspension before centrifugation (300 × *g*, 5 minutes). The supernatant was removed and the pellet re-suspended in 10% fetal bovine serum (FBS) in PBS. The cell suspension was kept on ice during all subsequent antibody staining procedures.

2.2.7.1 Extracellular and Intracellular Antigen Staining.

Extracellular staining for the antigens TRA-1-60 and TRA-1-81 used 1×10^5 cells, and intracellular staining for the antigen OCT4 used 2×10^5 cells. Samples for extracellular staining were placed in the QikSpin microfuge (2000 × *g*, 1 minute), after which the supernatant was removed and the cell pellet re-suspended in 10% FBS in PBS then placed on ice. Samples designated for intracellular staining were centrifuged using the QikSpin Microfuge (2000 × *g*, 1 minute), the supernatant was removed and the cells re-suspended in 500 µL of 0.1% Saponin permeabilisation buffer (100 mg Saponin, 100 mL PBS and 10% bovine serum albumin, BSA) for 15 minutes on ice. The intracellular staining samples were then placed in the QikSpin microfuge (2000 × *g*, 1 minute), after which 400 µL of supernatant was removed from each sample.

To each tube test sample, 1 µL of titrated primary antibody was added to the cells, i.e. 2 µg/µL anti- TRA-1-60 and 2 µg/µL anti-TRA-1-81 antibodies (Abcam, Cambridge, UK); and 0.25 µg/µL anti-OCT4 antibody (BD Biosciences). All samples stained with primary antibody were placed on ice for 20 minutes then washed with 1 mL of 10% FBS in PBS for extracellular stained samples and 1 mL of 0.1% Saponin/10% FBS in PBS for intracellular stained samples. Samples were centrifuged using a QikSpin microfuge (2000 × *g*, 1 minute) followed by removal of 1 mL of supernatant. All samples were stained with 1 µL of 1 in 10 diluted secondary antibody for 20 minutes on ice (control samples were stained with secondary antibody without primary antibody). The secondary antibody used for extracellular samples was Alexa Fluor-488 anti-mouse IgM secondary antibody (Thermo Fisher Scientific), and Alexa Fluor-488 anti-mouse IgG antibody (Thermo Fisher Scientific) was used for intracellular staining. After incubation, 1 mL of 10% FBS in PBS was added to the extracellular staining samples and 1 mL of 0.1% Saponin/10% FBS in PBS was added to the intracellular samples. All samples were centrifuged in the QikSpin microfuge (2000 × *g*, 1 minute), followed by the removal of 1 mL supernatant. Sample volumes were adjusted to 300 µL with either 10% FBS in PBS for extracellular samples or 0.1% Saponin/10% FBS in PBS for intracellular samples. The samples were then kept on ice until analysis.

2.2.7.2. Flow cytometry data acquisition and analysis.

The antibody-stained samples were analysed using a MACSQuant® Analyser Flow Cytometer (Miltenyi Biotec, North Ryde, Australia). During flow cytometry data acquisition, cells were visualized using the following parameters:

1) Plot 1: Forward scatter-area (FSC-A) vs. side scatter-area (SSC-A) plot. Cells within this plot were then gated to define the main cell population.
2) Plot 2: The main cell population was gated using FSC-A vs. FSC-height (FSC-H) to ensure that only single cells were subsequently analyzed.
3) Plot 3: The fluorescence detector most suited to the emission and excitation profiles of the secondary antibody fluorophores was used to detect secondary antibody fluorescence

Appropriate instrument settings were configured by analyzing control stained samples (i.e. secondary antibody only), and setting a gating control to capture 99.9% of these stained cells as negative events (Figure 2.1 A). Test (primary and secondary antibody) stained samples were then analysed using the gating control obtained previously, and the number of positive events were recorded Figures 2.1 B-C). Biological replicates for each sample were then recorded and averaged, with comparisons made using the student's t-Test.

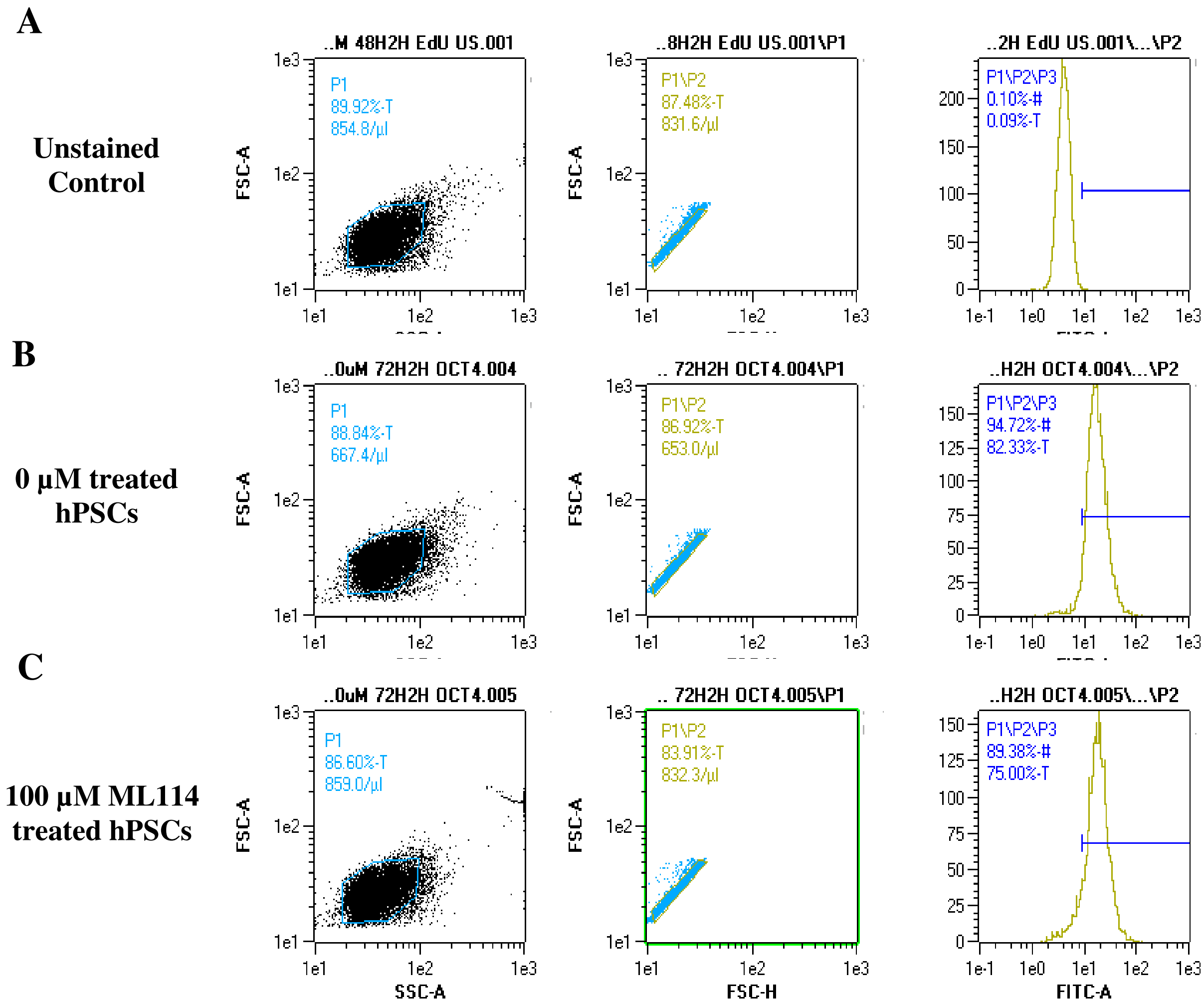

Figure 2.1 Flow cytometry data acquisition. Representative flow cytometry plots used for data acquisition and analysis for: **A)** unstained control samples. **B)** 0 µM control-treated hPSCs and **C)** 100 µM ML114-treated hPSCs.

2.2.8. Cell proliferation assay.

hPSCs were treated with DMSO and ML114 as previously described (see section 2.3.2). Prior to confluency (generally after 5 days of treatment) 10 µM of EdU label (Thermo Fisher Scientific) was added to the cell culture for 2 and 6 hours of incubation. Following this, cells were then harvested as a single cell suspension as previously described (see section 2.3.2) and 1×10^6 cells were collected from each condition and fixed with 4% para–formaldehyde in PBS for 15 minutes on ice in the dark. Samples were then washed with 1% BSA in PBS, centrifuged ($300 \times g$, 1 minute), and supernatant removed. The cell pellet was then processed using the Click-iT EdU detection kit (Thermo Fisher Scientific) as per the manufacturer's instructions. The EdU labelled samples were then analysed *via* flow cytometry as described in 2.2.6.2, however, plot 3 was adjusted to detect PI and Alexa Fluor 647 within the samples. The plot parameters were set at FL6-A (to detect Alexa Fluor 647 positive events) and FL4-A (to detect PI positive events as a negative control). Populations of cells present in each phase of the cell cycle were measured by dividing Plot 3 into quadrants that clearly separated each phase of the cell cycle. The values within each quadrant were recorded for each biological replicate and averaged, with comparisons made using the student's t-Test.

2.2.9. Teratoma and karyoptyping analyses.

hPSCs were treated with 100 µM ML114 in 0.25% DMSO for 7 days. The cells were then harvested and re-seeded as single cell suspensions in mTeSR1™ and passaged for a further 11 weeks. Teratoma formation was performed externally by the StemCore Facility, University of Queensland, with histological analysis via an expert pathologist. Karyotyping (i.e. G-banding) was also performed by the StemCore Facility.

2.3. RESULTS

2.3.1. ML114 reduces population growth rates.

To investigate whether RBBP9 SH activity is required for the maintenance of pluripotency, hSPCs were cultured with the highly selective chemical inhibitor of RBBP9 SH activity, ML114 (Bachovchin et al., 2010b). A dose-response curve was established to find the effective concentration of ML114 in hPSCs (Figure 2.2 A), comparing vehicle control (0.25% DMSO) with various concentrations of ML114 up to 100 μM - the highest reported concentration enabling inhibition with minimal cell death due to toxicity (Bachovchin et al., 2010b). This dose response study showed that all concentrations of ML114 tested (i.e., 5-100 μM) significantly reduced hPSC population growth rate after 7 days of culture compared to control treatment (Figure 2.2 B), with the greatest effect seen with the highest concentrations. These data suggest that ML114 treatment decreased hPSC proliferation and/or induced hPSC death. hPSCs were also cultured with ML114 fragment to test whether the effect of ML114 on hPSC number was due to the presence of the ML114 fragment released after RBBP9 SH activity (Figure 2.2 A). Notably, the hPSC yield was not significantly reduced by treatment with ML114 soluble fragment even when the fragment was used at 100 μM (Figure. 2.2 B; $p = 0.124$).

2.3.2. Exposure to ML114 does not induce hPSC differentiation.

As inhibition of hPSC proliferation has been correlated with hPSC differentiation (O'Connor et al., 2011, Becker et al., 2006, Calder et al., 2013), a number of pluripotency assays were performed to investigate whether ML114 treatment induced differentiation in addition to its effect on hPSC population growth rate. These assays included the CFC assay and flow cytometric analysis for known pluripotency-associated antigens.

The AP-based CFC assay showed a decrease in colony number within the initial 24 hours (Figure 2.3 A), suggesting that ML114 might impair hPSC attachment and/or cause cell death within the initial cell-seeding phase of the assay. A small decrease was noted in colony number within each treatment over the 5 days (day 1 vs day 5; approximately 3-fold for control treatment and 16-fold for 100 µM-treated hPSCs). However, comparison of control- and 100 µM consistently showed a much higher fold change (75-fold change at day 5), indicating that inhibitor had a larger effect than the DMSO in the treatment. Consistent with the population growth rate data described above, the ML114-treated colonies were much smaller than the control-treated colonies - suggesting that ML114 decreased cell proliferation and/or caused cell death (Figure 2.3 B). At the end of the assay the colonies derived from all ML114 treatments remained AP positive, suggesting they remained pluripotent (Figure 2.3 B). Overall, increasing concentrations of ML114 decreased both the CFC frequency and size of colonies (Figure 2.4).

Next, control- and ML114-treated hPSCs were assessed *via* flow cytometry to look for changes in expression of the pluripotency antigens OCT4, TRA-1-60, and TRA-1-81. This analysis showed detection of equally high levels of all 3 pluripotency-associated antigens in both control- and ML114-treated hPSCs even after 7 days of treatment with 100 µM of ML114, with no statistically significant difference between each treatment (Figure 2.5).

2.3.3. ML114 slows hPSC proliferation.

To test whether the reduced hPSC population growth rate and reduced CFC colony growth rate that resulted from ML114 treatment were due to changes in the cell cycle, both control-

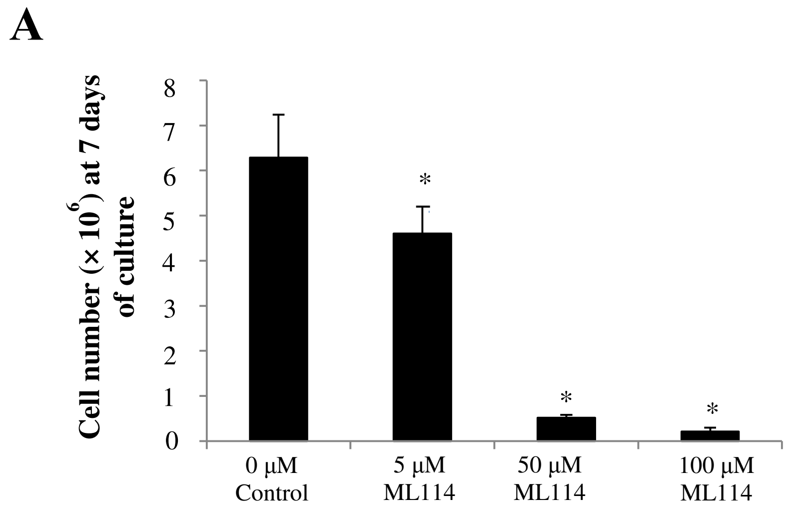

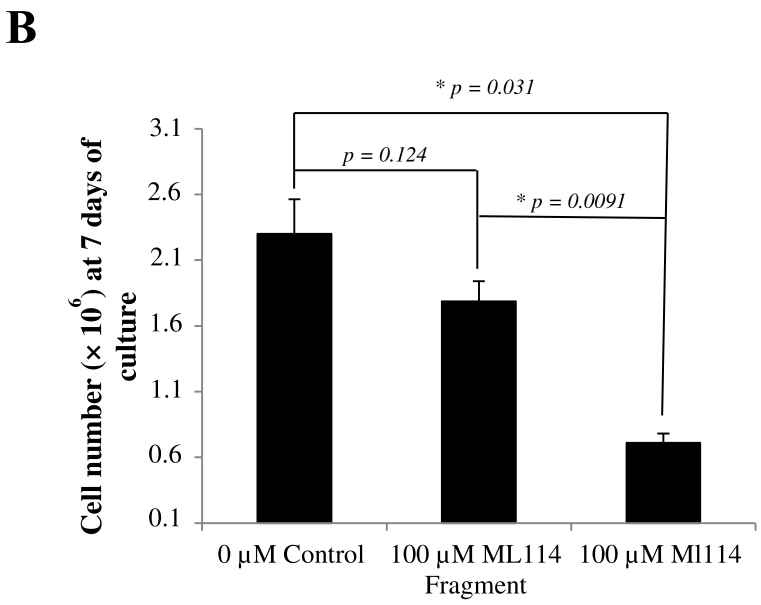

Figure 2.2 ML114 reduces hPSC population growth rate. A) Dose response showing all concentrations of ML114 used decrease hPSC growth rate after 7 days of treatment, with greater effects seen with concentrations. (n = 3; * p < 0.05). **B)** hPSC population size is significantly reduced after 7 days of ML114 treatment, with no significant changes in hPSC population size when treated with ML114 soluble fragment. (n = 3).

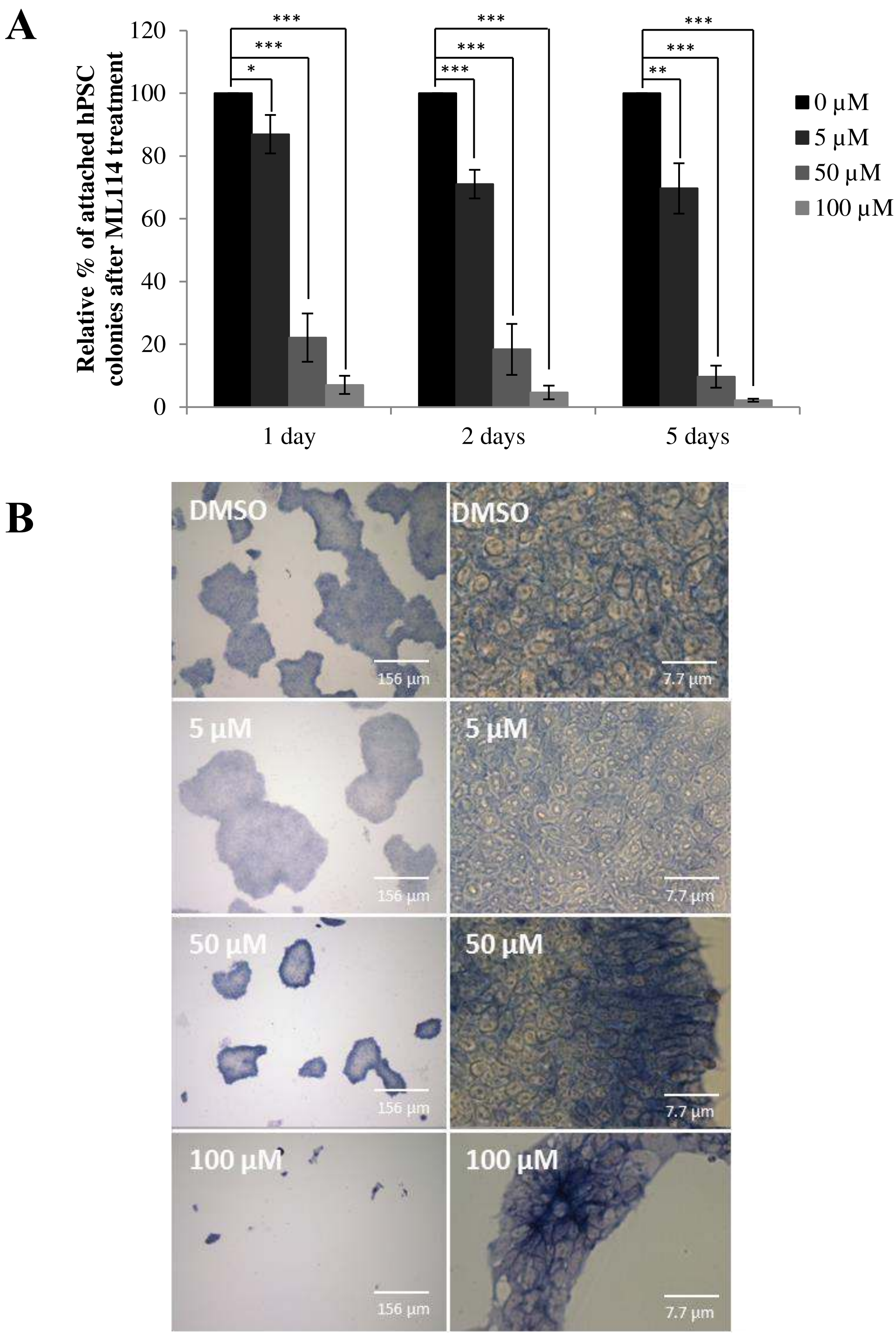

Figure 2.3 hPSC colony survival after ML114 treatment. A) Colonies that remain attached after ML114 treatment were counted 1, 2, and 5 days post ML114 treatment. The initial reduction in hPSC colony number by day 1 remained relatively stable throughout the duration of culture. (n = 5; * p = 0.05, ** p = 0.001, *** p = 0.0001). **B)** CFC assay data showing CFC colony size decreases with increasing ML114 concentration, but that AP expression is maintained at all ML114 concentrations tested. (n = 5).

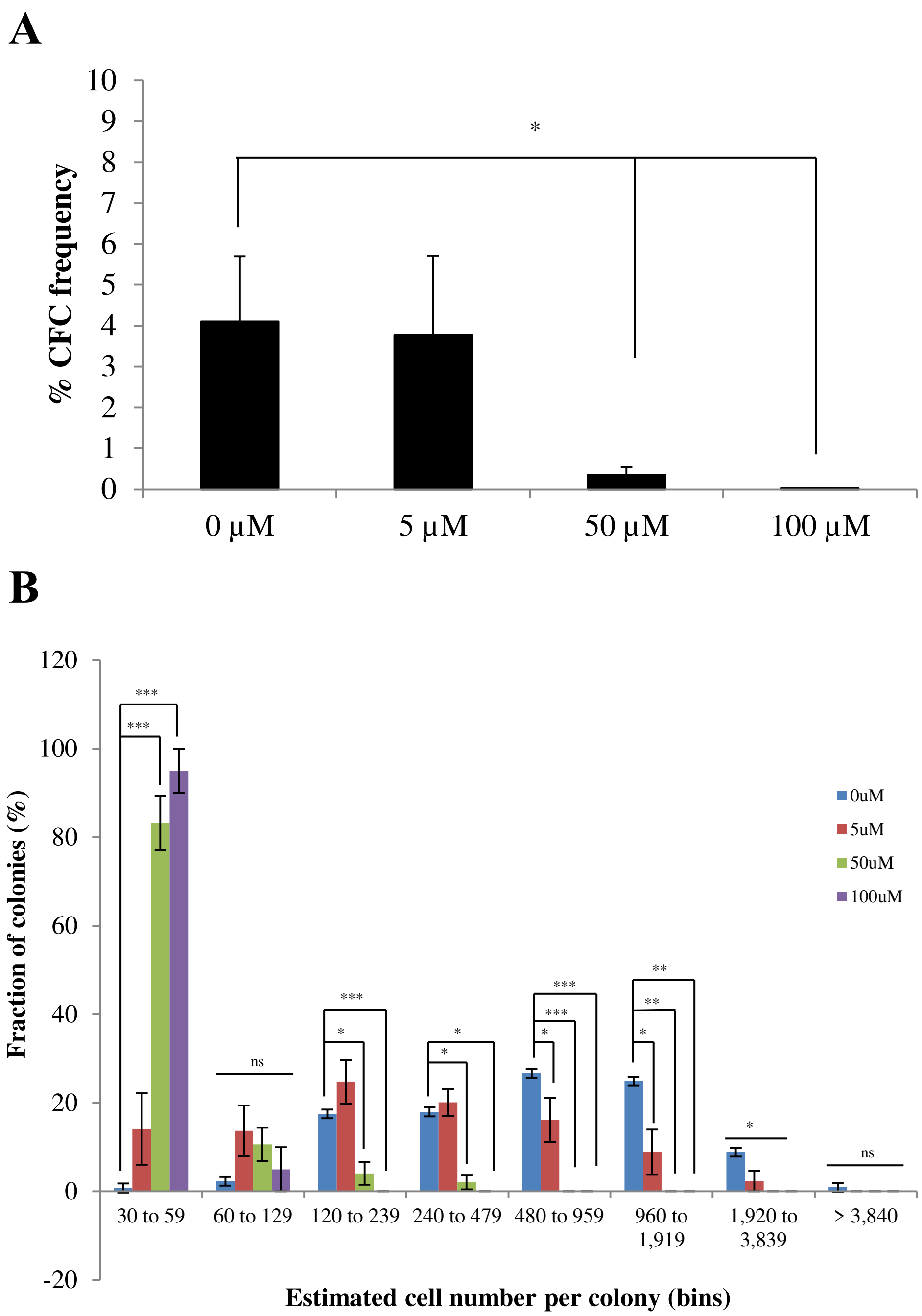

Figure 2.4 ML114 treatment decreases CFC frequency and colony size. CFC assay data showing that: **A)** increasing concentrations of ML114, reduce CFC colony frequency; and **B)** increasing concentrations of ML114 reduce CFC colony size, as shown by the reduction in cell number estimated within each CFC colony. (n = 5; * p = 0.05, ** p = 0.001, *** p = 0.0001)

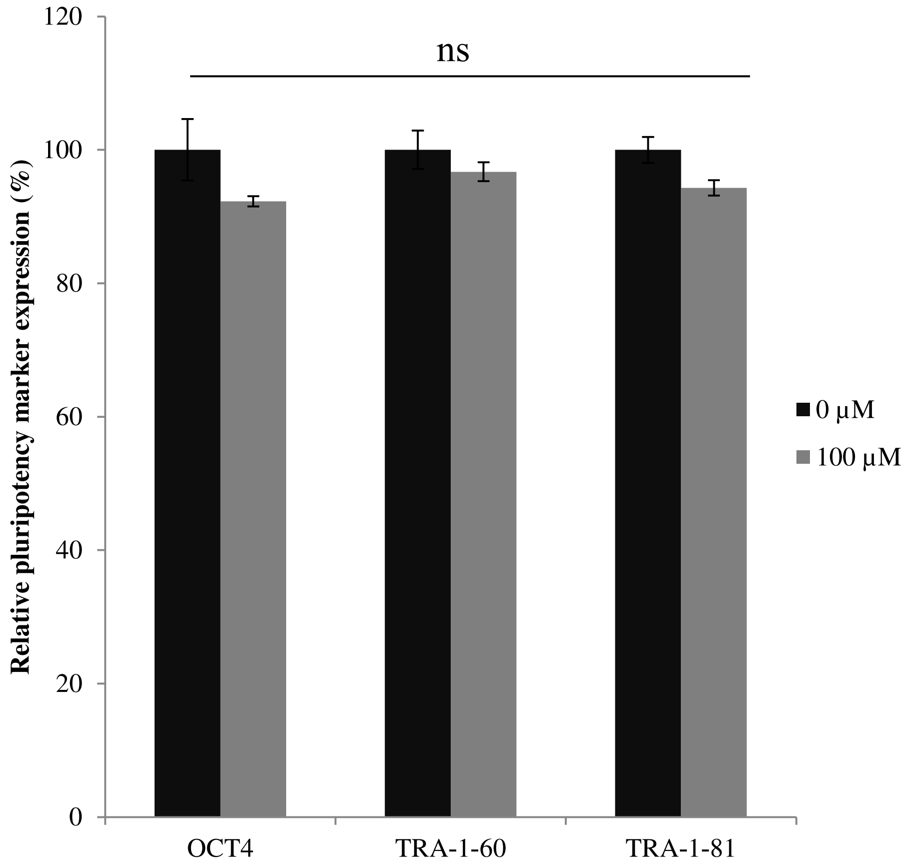

Figure 2.5 ML114-treated hPSCs retain high expression of pluripotency associated antigens. Flow cytometry revealed control- and ML114-treated hPSCs express similarly high levels of pluripotency associated antigens OCT4, TRA-1-60, and TRA-1-81 with no significant differences in expression levels. (n = 3; OCT4 * p = 0.16, TRA-1-60 * p = 0.35, and TRA-1-81 * p = 0.26).

and ML114-treated cells were assessed *via* the EdU cell proliferation assay. This analysis showed a significantly larger number of ML114-treated hPSCs remained in G_0/G_1, while fewer hPSCs had progressed to S-phase and G_2/M compared to control-treated hPSCs (Figure 2.6 A). After 2 hours of EdU exposure approximately 55% of control-treated hPSCs had entered S-phase (Figure 2.6 A). In contrast, it took 6 hours for the same percentage of hPSCs to enter S-phase after ML114 treatment (Figure 2.6 B). These data suggest that ML114-treated hPSCs progressed through the cell cycle approximately three times slower than the control-treated hPSCs.

2.3.4. ML114 effects are not permanent.

To test whether the effects of ML114 treatment were permanent or reversible, hPSCs were subject to either control- or ML114-treatment for 7 days, and then re-seeded into optimal hPSC maintenance conditions without further ML114 treatment for 7 weeks. Consistent with earlier findings, these data showed that ML114 treatment resulted in a dramatic and statistically-significant reduction in cell number as a result of the initial 7 day treatment period relative to the control treatment. However, after removal of ML114, the hPSC population growth rate of the ML114-treated cultures increased, becoming indistinguishable from that of the control cultures within approximately 2 weeks (Figure 2.7 A). In addition, the CFC assay showed that the colony size and colony/cell morphology from both control- and ML114-treated cells were identical after 7 weeks of culture in optimal hPSC maintenance conditions (Figure 2.7 B).

A teratoma assay was then performed to assess whether the hPSCs previously treated with ML114 retained functional pluripotency, i.e., the ability to form derivatives of all 3 germ layers of the body. This analysis showed that hPSCs previously treated with ML114 for 1 week before expansion in standard pluripotency-maintenance conditions retained the ability to form teratomas containing cell types representative of endoderm, mesoderm, and ectoderm (Figure 2.8). A karyotyping assay was also performed to investigate whether the hPSCs previously treated with ML114 had developed significant chromosomal damage. These data indicated that both the control- and ML114-treated hPSCs had normal karyotypes (Figure 2.9).

2.4. DISCUSSION

Various studies have implicated RBBP9 in normal development (O'Connor et al., 2011, Woitach et al., 1998), and progression of cancer (Shields et al., 2010, Woitach et al., 1998). These studies have suggested two possible mechanisms of RBBP9 activity: i) the ability to bind RB protein and regulate the activity of the RB/E2F cell cycle pathway (Woitach et al., 1998), and ii) the ability to act as a SH (Shields et al., 2010). RBBP9 has been shown to be required for maintenance of hPSCs (O'Connor et al., 2011). RBBP9 protein is expressed in hPSCs, and siRNA-mediated loss of RBBP9 protein results in decreased CFC frequency, decreased expression of pluripotency and cell cycle genes, and increased expression of genes involved in neurogenesis (O'Connor et al., 2011). However, the mechanism(s) by which it controls cell behaviour in hPSCs is currently unknown.

A

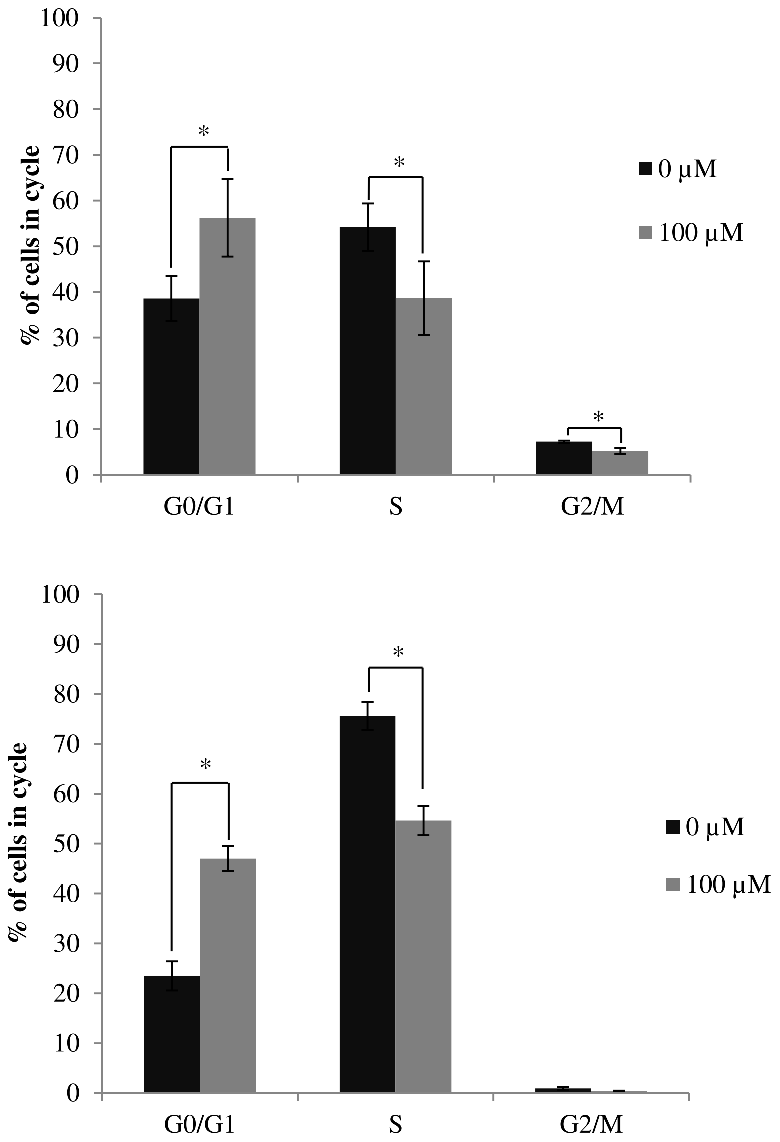

Figure 2.6 ML114 slows hPSC progression through the cell cycle. EdU-based flow cytometry assessment of cell distribution across different phases of the cell cycle for control- and ML114-treated hPSCs after **A)** 2 hours, and **B)** 6 hours of EdU exposure. Comparison of the data shows it took 2 hours EdU exposure for ~55% of control-treated hPSCs to enter S-phase (**A**), whereas it took 6 hours EdU exposure for 55% of hPSCs treated with 100 μM ML114 to enter S-phase (**B**). (n = 4; * p < 0.05).

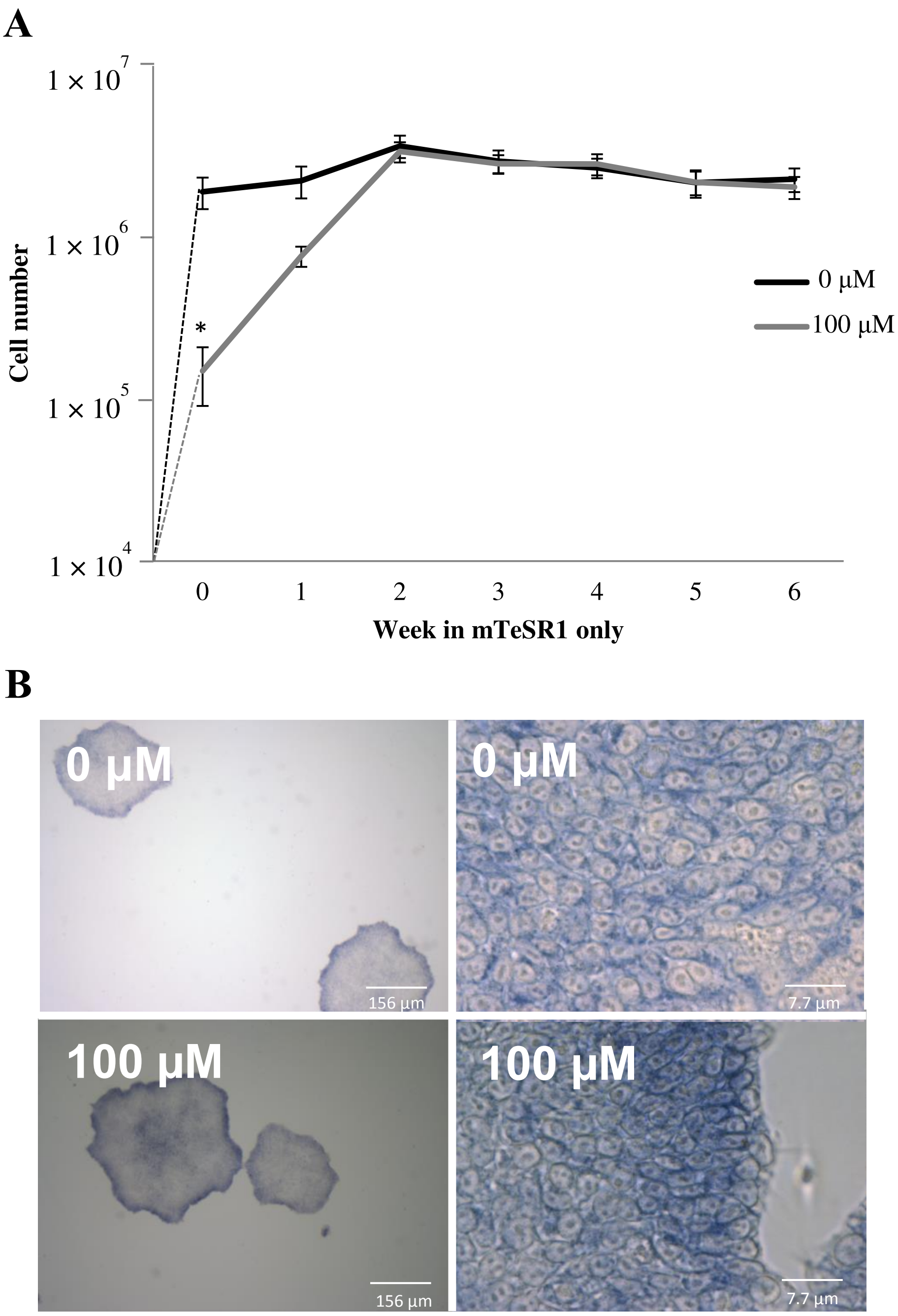

Figure 2.7 The effects of ML114 are not permanent once removed from hPSC culture. A) ML114 treatment of hESCs results in significantly fewer cells after 7 days. However, after removal of ML114 treatment followed by 7 weeks culture in optimal hPSC maintenance conditions, the population growth rate increased to be indistinguishable from the control-treated cells. ($n = 4$; $*p < 0.05$). **B)** hESCs previously treated with ML114 display identical cell morphology, colony size and AP staining as control-treated hESCs.

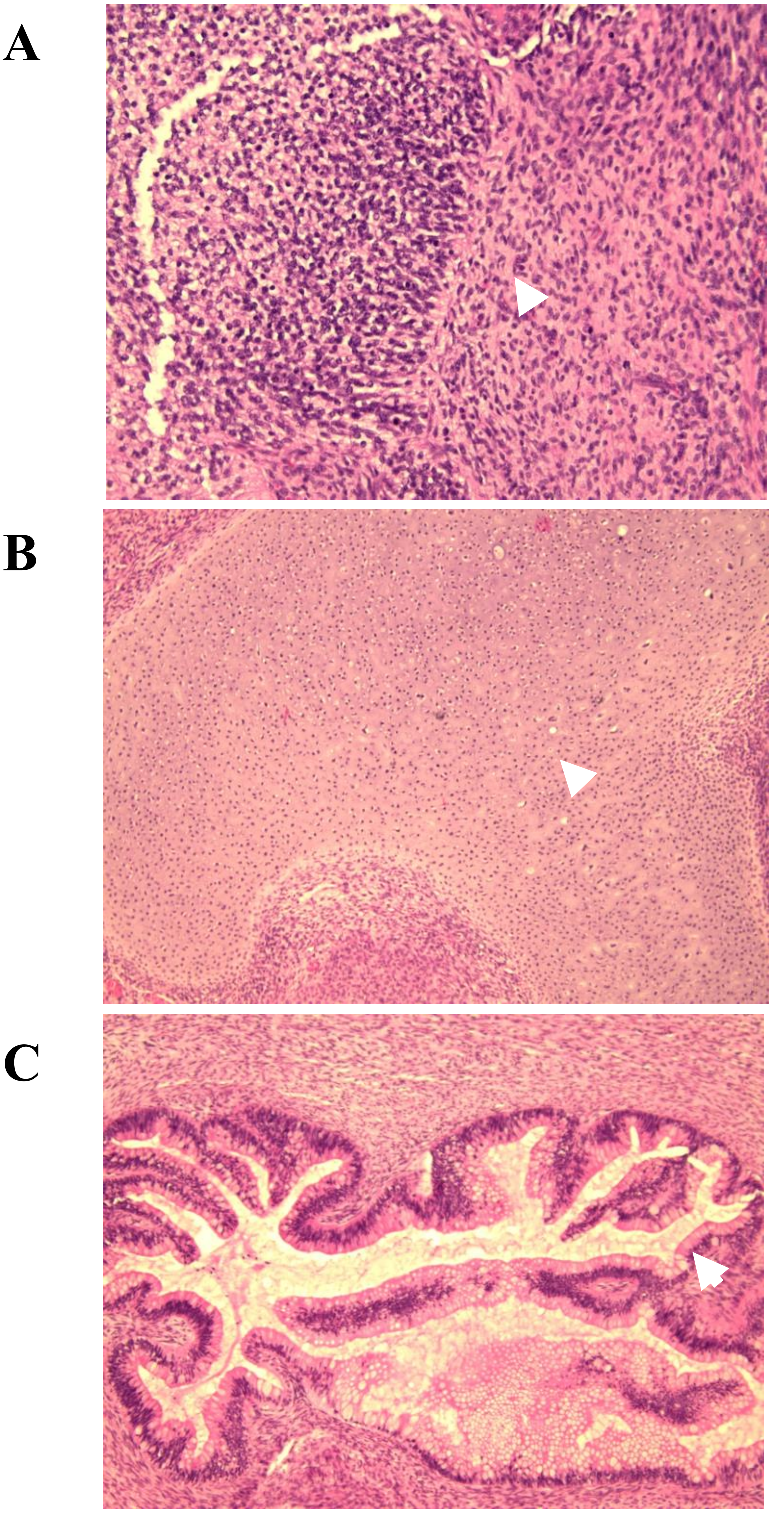

Figure 2.8 hPSCs treated with ML114 retain teratoma-forming ability. Histological analysis of teratomas derived from hPSCs treated for 7 days with 100 mM ML114, and then cultured re-seeded in mTeSR1 for an additional 11 weeks. All 3 germ layers are present in the teratomas including: A) ectoderm (e.g. neuroepithelium, arrow head); B) mesoderm (e.g. stroma; cartilage, arrowhead; and smooth muscle); and C) endoderm (e.g. glandular epithelium, arrow head).

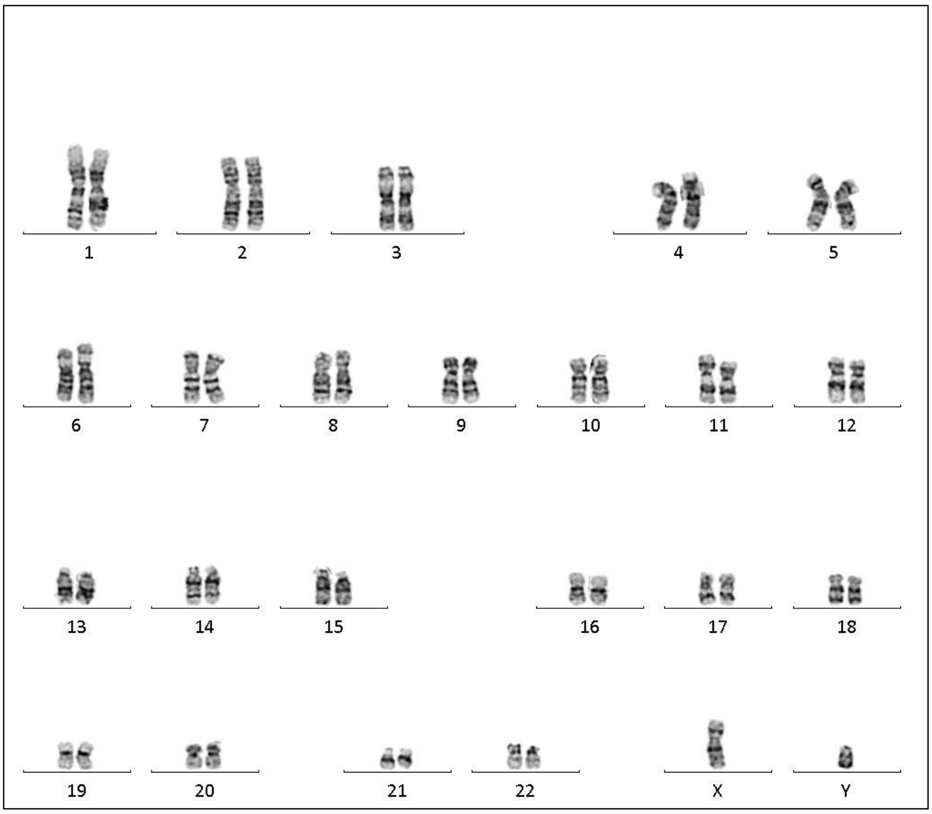

Figure 2.9 G-banding analysis of hPSCs revealed ML114 does not induce large-scale DNA rearrangements. Karyotype data shows hPSCs exposed to 100 µM ML114, followed by a further 11 weeks of culture in hPSC maintenance conditions, do not possess abnormal chromosomes at a resolution of 400 bands per haploid set.

2.4.1. Use of ML114 decouples hPSC proliferation from differentiation.

In the present study, loss of RBBP9 SH activity was investigated using ML114, the newly identified and selective chemical inhibitor of RBBP9 SH activity. Upon cleavage by RBBP9, a fragment of ML114 has been shown to covalently bind to the catalytically active Ser75 of RBBP9 and thus inhibit RBBP9 activity, while the remaining RBBP9 fragment is released. In complex cell and protein assays, ML114 inhibits RBBP9 at concentrations between 20 and 100 μM – concentrations at which it does not affect the activity of 30 other serine proteases. ML114 is also reported to have very low cytotoxicity up to at least 100 μM (Bachovchin et al., 2010a). In this chapter it was shown that ML114, but not its soluble cleavage product, decreased hPSC growth rate regardless of whether the hPSCs were passaged as aggregates or plated as single cells in the CFC assay. Some effect on hPSC attachment and/or cell death was evident from the CFC assay, and an apoptosis assay such as the TUNEL assay could be used to distinguish whether the effects of ML114 resulted in apoptosis or prohibited a high frequency of cell attachment (Watanabe et al., 2007). However from the work presented here it was clear that ML114 had an inhibitory effect on hPSC proliferation by: i) decreasing the population and CFC colony growth rates; ii) increasing the number of hPSCs in G_0/G_1; and iii) decreasing the number of cells in $S/G_2/M$ (equating to a 3-fold decrease in progression through the cell cycle). After removal of ML114 the cells were shown to recover their growth rate, consistent with newly transcribed/translated RBBP9 replenished the RBBP9 covalently inactivated by ML114 treatment.

Data from the CFC assay, flow cytometry analyses and teratoma assay all indicated that ML114-treatment did not induce differentiation. Interestingly, literature reports show that addition of potent differentiation agents such as retinoic acid result in significant changes in cell morphology within 5 days of treatment, as well as a large reduction in CFC frequency (~80 fold) and a significant decrease in expression of pluripotency markers such as OCT4 (~5 fold) in that same timeframe (Bain et al., 1996, Schuldiner et al., 2000, O'Connor et al., 2008). In comparison, ML114-treated hPSCs did not show morphological changes during the 7 days of treatment, and retained cells which expressed equally high levels of pluripotency-associated antigens as control-treated cells. While the size and number of CFC-derived colonies were reduced by ML114 treatment, the cells still had typical hPSC morphology and AP activity suggesting retention of a pluripotent phenotype. The pluripotent potential of the ML114-treated hPSCs was supported by the teratoma-forming ability of hPSCs previously treated with 100 μM ML114. These data suggest that the 7 day ML114 treatment did not induce differentiation, although it is still possible that subtle differentiation events might be initiated that need a longer ML114 treatment to manifest themselves. Genomic expression of both early differentiation and pluripotency marker levels could be assessed during the 7 day ML114 treatment to determine whether longer exposure to ML114 during and beyond 7 days would drive hPSCs towards differentiation. Alternatively, agents such as retinoic acid can be used to induce differentiation of hPSCs, such as the embryonal carcinoma cell line NTeraD2 and induced PSC line iPSC65, during ML114 treatment (O'Connor et al., 2008). This would determine whether selective loss of RBBP9 SH activity has the capacity to accelerate, delay or have no effect on differentiation of hPSCs and reprogramming. Overall, the hPSC growth rate, cell cycle and pluripotency assay data indicate that in ML114-treated hPSCs inhibition of proliferation does not lead to and is not coupled with initiation of hPSC differentiation.

2.4.2. Evidence for coupling of proliferation and differentiation in pluripotent cells.

Numerous studies of pluripotent cells have suggested that differentiation of pluripotent cells is coupled with decreased proliferation (Becker et al., 2006, O'Connor et al., 2011, Calder et al., 2013, Singh et al., 2013, Savatier et al., 1996). Rapid transition from G_1 phase to S-phase has been used as an indicator of pluripotency, where cells undergoing differentiation were found to accumulate in the G_1 phase of the cell cycle with fewer cells present in S-phase (Becker et al., 2006, Calder et al., 2013, Pauklin and Vallier, 2013). Furthermore, treatment with the differentiation agent retinoic acid in embryonal carcinoma cells for 2-4 hours was enough time to lengthen G_1 phase of the cell cycle and rapidly induce differentiation (Mummery et al., 1987, Berg and McBurney, 1990).

More recently though, a number of studies have suggested that hPSC proliferation and differentiation can be decoupled, and that decreased hPSC proliferation does not always determine their differentiation. For example, *E2F2* is a gene that encodes a transcription factor with important functions in control of embryonic development, differentiation, proliferation, and apoptosis (Muller and Helin, 2000). Knockdown of E2F2 expression in hESCs led to a reduction in proliferation, reduced numbers of CFCs, and an accumulation of cells in G_1. Yet these same cells maintained expression of pluripotency markers and also the ability to form differentiating embryoid bodies (Suzuki et al., 2014). Similarly, depletion of the protein arginine methyltransferase 5 enzyme, PRMT5, was found to decrease hPSC proliferation, to increase the number of hPSCs in G_0/G_1, and reduce the number of cells in G_2M (Gkountela et al., 2014). However, this decrease in hPSC proliferation did not affect expression of pluripotency markers such as OCT4, NANOG, TRA-1-60, and SSEA4, nor did it remove the capacity for multi-lineage differentiation in embryoid bodies. In light of these studies, the observed decoupling of hPSC proliferation and differentiation is consistent with an emerging understanding of hPSC biology. Notably, the effectors involved in this de-coupling of hPSC differentiation and proliferation due to ML114 treatment are currently unknown.

2.4.3. ML114 slows down progression of hPSCs through the cell cycle.

Proliferation of pancreatic cancer cells has been shown to be mediated by RBBP9 SH activity (Shields et al., 2010). Overexpression of wildtype RBBP9, but not the enzymatically inactive S75A mutant RBBP9, was able to overcome the anti-proliferative effects of TGF-β on pancreatic cancer cells in vitro. Interestingly, TGF-β signalling is known to regulate PSC proliferation. For example, specific inhibition of TGF-β signalling in mESCs results in a significant decrease of cell proliferation, but does not affect pluripotency (Ogawa et al., 2007). Other studies have shown TGF-β signalling to be a major contributor to the maintenance of pluripotency in hPSCs. TGF-β signalling has been shown to enable expression of master regulators of pluripotency such as OCT4, NANOG, and SOX2, while supressing expression of BMP4, a known inducer of differentiation (James et al., 2005, Vallier et al., 2009, Wei et al., 2005, Xu et al., 2008, Greber et al., 2007). Further investigating the impact of RBBP9 SH activity and TGF-β signalling in hPSCs might provide a molecular framework for understanding how both pluripotent cells and cancer cells regulate proliferative signalling.

In summary, the data presented in this chapter has shown ML114 treatment of hPSCs (at concentrations known to have low cytotoxicity and high specificity for RBBP9 SH) results in the de-coupling of cellular proliferation from pluripotency, thereby indicating RBBP9 SH activity is required for hPSC proliferation. These data also show that inhibition of RBBP9 SH activity does not completely phenocopy the effects of siRNA-mediated RBBP9 protein loss in hPSCs (O'Connor et al., 2011). In turn, this suggests that both the SH and RB-binding/E2F regulating activities of RBBP9 are required for hPSC proliferation, and that RBBP9-mediated regulation of the RB/E2F pathway is also involved in regulating differentiation towards the neural lineage. This later conclusion is consistent with the known role for RB/E2F in neurogenesis in mouse models (Callaghan et al., 1999, Ghanem et al., 2012). Further analyses to identify potential effectors of RBBP9 SH activity could help decipher the molecular pathways through which RBBP9 SH inhibition regulates hPSC proliferation. Understanding these mechanisms will give insights into the role of RBBP9 in hPSC maintenance and differentiation, tissue development, and progression of numerous cancers.

CHAPTER 3: Identification of putative effectors of RBBP9 SH activity

3.1. INTRODUCTION

The originally identified mechanism of action for RBBP9 involved regulation of cell cycle progression through its interactions with RB. This led to the hypothesis that RBBP9 was involved in various cancers and tumours such as colorectal adenocarcinoma, lymphoblastic leukaemia, lung carcinoma, and melanoma cell lines (Woitach et al., 1998). RBBP9 has been implicated in the progression of pancreatic cancers through its poorly described role as a SH (Shields et al., 2010). More recently, our group has identified RBBP9 as a putative regulator of pluripotency in hPSCs. siRNA-mediated loss of RBBP9 protein resulted in decreased CFCs, cell cycle and pluripotency gene expression, with an increase in expression of genes involved in neurogenesis (O'Connor et al., 2011). However, this study did not determine whether these changes resulted from the loss of RB/RBBP9-binding interactions and/or the loss of SH activity. Moreover, the effectors of RBBP9 SH activity are currently unknown. Thus investigation that define the effectors of RBBP9 SH activity will enable further understanding of the role of RBBP9 in maintenance in hPSCs, tissue-specific stem cells and in the progression of various cancers.

The data presented in Chapter 2 shows that ML114 treatment of hPSCs resulted in a significant reduction in population growth rate, reduced frequency and size of CFCs, decreased progression through the cell cycle, and decoupling of differentiation from reduced proliferation. In the study described here, a bioinformatics approach was taken to identify candidate RBBP9 SH effectors in hPSCs. Gene expression profiles generated from control- and ML114-treated hPSCs described in the previous chapter were compared. This data was also compared with previously published gene expression profiles from hPSCs treated with

RBBP9 siRNA. Gene ontology (GO) analyses were then used to identify gene categories affected by ML114-induced loss of RBBP9 SH activity. Subsequent promoter analyses were used to predict putative effectors of RBBP9 SH activity, with PCR and Western blotting used to further investigate two predicted RBBP9 effectors, Nuclear transcription factor Y subunit A (NFYA) and Deformed epidermal auto-regulatory factor-1 (DEAF1).

3.2. METHODS

3.2.1. Treatment of hPSCs with ML114.

Refer to (Chapter 2 sections; 2.2.1, 2.2.2, and 2.2.3) for general reagents and consumables, general equipment, and general cell culture. CA1 hESCs were treated with 0.25% DMSO, and 100 μM ML114 chemical inhibitor 72 h post initial cell seeding and cultured for a further 7 days.

3.2.2. Reverse-Transcription Polymerase Chain Reaction (RT-PCR).

3.2.2.1. RNA harvest.

After treatment 1×10^6 hPSCs were collected as a single cell suspension with TryPLE, centrifuged at $300 \times g$ for 5 minutes and the supernatant removed. RNA was extracted and purified using the Bioline Isolate II RNA purification kit as per the manufacturer's instructions (Bioline, Eveleigh, Australia). The concentration and purity of RNA samples was assessed using triplicate A_{260}/A_{280} absorbance readings *via* an Implen nanophotometer (Implen, München, Germany). RNA was stored at – 80 °C for downstream applications.

3.2.2.2. cDNA synthesis via reverse transcription.

Each RNA sample was analysed using a combination of 3 cDNA reactions: i) RNA with Reverse Transcriptase (+RT); ii) RNA without Reverse Transcriptase (-RT) to test for genomic contamination; and iii) a non-template control (NTC) without RNA to test for DNA contamination of PCR reagents. For cDNA production, 500 ng of purified RNA, 2 µL of 25 µg random hexamer primers (Bioline) and RNase/DNase free water for a final volume of 15 µL were mixed briefly with a QikSpin personal centrifuge (2000 × *g*, 1 minute). Samples were placed in the Mastercycler™ (70 °C, 5 minutes), then 6 µL of 5 X Reverse Transcriptase (RT) buffer, 1.5 µL 10 mM dNTPs, 1.5 µL U/µL RNase inhibitor and 6 µL RNase/DNase free water were added to a final volume of 15 µL. To the +RT and NTC samples, 0.4 µL of 200 U/µL Bioscript enzyme (Bioline) was added. Samples were mixed briefly with a QikSpin personal centrifuge (2000 × *g*, 1 minute) before being placed in the Mastercycler ™ for cDNA production using the following cycles: cycle 1 (42 °C, 60 minutes), and cycle 2 (70 °C, 10 minutes).

3.2.2.3. Primer design.

Forward and reverse primers for specific genes were designed using the Primer3Plus web page (http://www.bioinformatics.nl/cgi-bin/primer3plus/primer3plus.cgi). Exon sequences for specific genes of interest were obtained using the Ensembl genome browser (http://asia.ensembl.org/index.html) noting known splice variants or mutations. Sequences covering the 3’ end of an exon to the 5’ end of the next exon were copied into Primer3Plus and primer design initiated using 60 °C melting temperature and 80-200 base amplicon length. The specificity of output primers was assessed by searching the sequences against the entire known human genome and transcriptome using the National Centre of Biotechnology Information BLAST nucleotide web page (https://blast.ncbi.nlm.nih.gov/Blast.cgi?PAGE_TYPE=BlastSearch). Primers were considered unique if they generated a high BLAST score coupled with a low expect (E) value. Primers were synthesised by GeneWorks (Table 3.1) (Thebarton, Australia).

Table 3.1 hPSC primer sequences (5' to 3')		
Gene	**Forward primer sequence**	**Reverse primer sequence**
NFYA	GCACGGAGTGTACCTCACAG	TGCTGTATACTGCTCCATGGTC
GAPDH	ATTGCCCTCAACGACCACT	ATGAGGTCCACCACCCTGT

3.2.2.4. PCR amplification of mRNA transcripts.

Each PCR primer was tested with trial PCR reactions at temperatures ranging between 55-60 °C. Each PCR reaction consisted of 5 µL 5 X Go-Taq flexi PCR buffer, 1.5 µL 25 mM $MgCl_2$, 1 µL 10 mM dNTPs, 2 µL 12.5 µM forward and reverse primers, 14 µL RNase/DNase free water, 0.5 µL Go-Taq flexi buffer, and 1 µL of cDNA (+RT, -RT, and NTC). Samples were placed into the Mastercycler® using the test temperatures for cDNA amplification starting at 60 °C. Each PCR reaction consisted of 3 steps: denaturation (95 °C, 5 minutes and 30 seconds); annealing of primers to cDNA (55-60 °C, 20 seconds); and extension (72 °C, 2 minutes and 30 seconds). PCR products were assessed via gel electrophoresis using 2% agarose gels containing 5 µL of 10, 000 X Gel Red Nucleic Acid (Bioline) and a 100 bp DNA ladder (4 µL of 50 µg/µL). Electrophoresis was performed at 100 V, 300 mA, and 50 W for 40 minutes. Gels were imaged using a Gel Dock Transilumminator (Fisher Biotec, Wembley, Australia) and E-box software.

3.2.3. Quantitative PCR (qPCR).

qPCR was performed in triplicate using the optimal primer temperatures identified as described above. The RT-PCR efficiency of each primer was determined using a standard curve for all primers for all genes of interest (GOI), including the housekeeping gene *GAPDH*. Primer pairs were kept if their amplification efficiency was between 90%-110%. RT-PCR reaction mixture consisted of 5 µL of SYBR® Green PCR Master Mix (Thermo Fisher Scientific), 1 µL of 12.5 µM forward and reverse primer mixture, and 4 µL of sample cDNA (+RT, -RT, and NTC). Triplicates technical replicates were performed per test sample in a flat top low profile 96-well plate (Scientific Specialties, Inc., California, USA). Plates were centrifuged (1,000 × *g*, 1 minute) and RT-PCR performed using an Mx3005P qPCR system (Aligent Technologies, Sydney, Australia), MxPro software, a polymerase activation cycle (50 °C, 2 minutes) followed by 40 cycles of: denaturation (95 °C, 5 minutes and 30 seconds); annealing of primers to target sequences (optimal temperature identified between 55-60 °C, 20 seconds); and extension (72 °C, 2 minutes and 30 seconds) Triplicate cycle threshold (Ct) values for each primer/sample set were averaged and the quantification (Q) value obtained based on:

$$Q\ value = Efficiency\ of\ Gene\ of\ Interest\ (GOI)^{(Sample\ 1\text{-}Sample\ 2\ Ct\ values)}.$$

The Q value of the GOI was then normalised against the Q value of the housekeeping gene *GAPDH*.

$$\frac{Q\ GOI}{Q\ Housekeeping\ gene}$$

A students t-Test was then performed to determine whether the change seen in gene expression levels were statistically-significant (i.e., $p < 0.05$).

3.2.4. Affymetrix gene expression profiling.

3.2.2.1. Sample preparation for Affymetrix analysis.

Affymetrix profiling was performed on 6 samples (3 × DMSO control-treated and 3 × 100 µM ML114 treated hPSCs), with each sample harvested after 7 days of treatment.

3.2.4.2. RNA extraction, purification, and quantification for Affymetrix analyses.

Treated hPSCs were harvested at confluency for RNA, purified, and then quantified (see section 3.2.2.1). Following this, separate samples containing 500 ng of purified RNA were analysed using HuGene-1.0-st-v1 arrays (Affymetrix, Santa Clara, CA, USA) at the Ramaciotti Centre for Gene Function Analysis (University of New South Wales, Sydney, Australia) as per manufacturer's instructions. Analysis of Affymetrix profiling data was performed using the GenePattern software suite (Reich et al., 2006) as described below.

3.2.4.3 Identifying present and absent calls in microarray data.

As a method of validation, Affymetrix gene expression profiling data was analysed to identify which transcripts were present (P) or absent (A) across all 3 Affymetrix profiling arrays for each treatment. Transcripts were considered for further analysis if they were found present across all 3 Affymetrix profiling arrays for their respective treatments (i.e., '3P'). After identifying 3P genes, a .RES file containing unique identifiers relating to particular transcripts was used to generate P and A calls *via* the GenePattern module 'AffySTExpressionFileCreator'. Transcript identifiers from the sample array data were then sorted based on 3P and 3A calls for each transcript using the 'Sort' function embedded within Microsoft Excel. Once genes in both treatments were identified as 3P, they were saved in a Microsoft Excel document for future reference.

3.2.4.4. Identifying statistically significant gene expression differences between control- and ML114-treatments.

Affymetrix microarray data was initially analysed using the GenePattern module 'NormalizeAffymetrixST', together with a .CLS file which defined the treatment type and order for each Affymetrix sample to be analysed. This generated a .GCT file which described the expression dataset of control- and ML114-treated hPSCs. An additional pre-processing step was performed to identify interesting trends present within Affymetrix data, such as differential expression between DMSO-control, and ML114-treatment, as well as remove platform noise and transcripts whose probe did not emit a signal. The .GCT and .CLS files were input into to a log-base 2 filter to further increase signal-to-noise, thus creating the pre-processed .GCT file. In this step, up- and down-regulated genes were brought to the same scale and allowed the identification of gene expression signatures unique to ML114 treatment. This pre-processed output was input into the 'ComparativeMarkerSelection' module of GenePattern, and results were viewed and extracted using the 'ComparativeMarkerSelectionViewer' module.

In order to identify candidate genes statistically significantly up-regulated by ML114 treatment, the 'ComparativeMarkerSelectionViewer' data was partitioned to identify transcripts with differential expression *p* values <0.05 and associated false discovery rate values (FDR-value) <0.05. The FDR-value was included as a consideration for statistical-significance to reduce the probability of a false-positive result due to random chance that can occur with analysis of large datasets. Once transcripts were classed as statistically-significantly affected by ML114 treatment, they were then compared against the corresponding 3P list from 3.2.4.1 to generate a high confidence list of genes affected by ML114 treatment. This guaranteed that the transcripts found statistically-significantly differentially expressed by ML114 treatment were expressed in all 3 Affymetrix profiling arrays for either the control- or ML114-treated samples. This final gene list was used for downstream analyses. As a number of genes had multiple Affymetrix probes due to different potential gene transcripts, genes were considered expressed if at least 1 transcript probe was identified as 3P in either control- or ML114-treated samples.

3.2.5. Gene Ontology (GO) analysis.

Genes whose expression was statistically-significantly affected by ML114 treatment were input into the Database for Annotation, Visualisation and Integrated Discovery (DAVID) online bioinformatics database suite (https://david.ncifcrf.gov/). Selected genes were uploaded into the ‘Functional Annotation Tool’ as ‘Official Gene Symbols’. The GO terms of genes categorised under ‘Homo sapiens’ were selected for further analysis. The GO term category of level 5 or higher was used for the Biological processes category to provide a useful balance between breadth and specificity of the output GO term groupings. Selection of GO terms within this category with stringent parameters (*kappa* statistics based on score distribution of all human genes to reported human protein-protein interaction pairs, and $p < 0.05$) enabled broad GO class identifications in order to understand biological roles of selected genes and gene products (Huang et al., 2007).

3.2.6. Promotor analyses.

Putative transcription factor binding sites common to genes affected by ML114 treatment were identified using the PASTAA (Predicting associated transcription factors from annotated affinities) online suite (Roider et al., 2009). The list of unique ENSEMBL identifiers for genes affected by ML114-treatment were obtained using the DAVID webpage were input into the PASTAA online suite. Proximal promoter analyses (i.e. +400 base pairs (bp) either side of the transcription start sites) and distal analyses (i.e. -10,000 kilo bases (kb) upstream from the transcription start sites) were performed. Candidate regulator transcription factors motifs were identified by having a reported PASTAA p value < 0.05.

3.2.7. Gene expression comparisons between hPSCs treated with ML114 and RBBP9 siRNA.

To identify genes expressed by hPSCs and commonly affected by ML114 treatment and RBBP9 siRNA, Affymetrix datasets produced in Chapter 2 (for ML114) or previously published by our group (for RBBP9 siRNA) were processed in the same way as described above (see sections 3.2.4.2 and 3.2.4.3). Gene lists which were found significantly affected by loss of RBBP9 activities were compared using the following equation in Microsoft Excel:

=IF(ISNA(VLOOKUP(*LIST*,*LIST2*!A:A,1,FALSE)),'NO','YES')

This formula identified genes which were commonly up-regulated by the loss of both RBBP9 activities. Gene ontology and promoter analyses were performed as described above (see sections 3.2.5 and 3.2).

3.2.8. Proteomics.

3.2.8.1. Protein collection.

Treated hPSCs were harvested as a single cell suspension (see section 2.2.3.2), centrifuged (300 × *g*, 5 minutes), the supernatant removed and the cell pellet resuspended in 500 µL of lysis buffer (25 mM Tris, 150 mM NaCl, 1 mM EDTA, 1 mM EGTA, 1% Triton-X 100, 1 mM Na Vanadate, 1 mM PMSF, 5 µg Aprotinin, 1 X Protease inhibitor (PI), pH 7.4). Samples were incubated on ice for 5 minutes with occasional vortexing, then centrifuged (300 × g, 5 minutes, 4 °C), and the supernatant collected. Samples underwent a urea exchange purification and concentration step using a 3,000 Da molecular weight cut-off filter (Merck Millipore, Bayswater, Australia) and three consecutive wash steps using 1 mL exchange buffer (4 M urea, 1 X protease inhibitors) and centrifugation (4,000 × *g*, 20 minutes, 4 °C). Sample protein concentration was quantified against a BSA standard using the EZQ® protein quantification kit (Molecular probes, Oregon, USA). To a clean filter paper, 2 µL aliquots of all protein standards and samples were blotted in triplicate and allowed to air dry. The blot was then fixed with 100% MeOH for 5 minutes and allowed to air dry. The blot was then stained with EZQ protein stain for 30 minutes with agitation, whilst protected from light. All proceeding steps were consequently performed in the dark. Following this, the blot was de-stained with 3 × 25 second washes using 10% MeOH/7% HAc. The blot was then imaged using the LAS-4000 imager (Fuji Film, Brookvale, Australia) using densitrometry and quantification analysis *via* Multi Gauge v3.0 software (Fuji Film).

3.2.8.2. 1-Dimensional electrophoresis (1-DE) and Western Blotting.

For each sample, 25 µg of isolated protein was diluted 1:1 with 1-D sample buffer containing 2% SDS, 25 mM Tris pH 8.8, 12.5 mM Dithiothretretiol (DTT), and 5% glycerol. Prior to electrophoresis samples were heated at 100 °C for 5 minutes, cooled to room temperature, and loaded into 12 % Mini Protean® TGX, long shelf life pre-cast gels (Bio-Rad Laboratories, Gladesville, Australia). Electrophoresis was carried out using 150 V during initial migration through the stacking gel, and then protein separation using 90 V at 4 °C. Gels were either stained for total protein or analysed via Western Blotting. For total protein staining, gels were fixed with 10% MeOH/7%HAc and stained with Neuhoff Coomassie stain (0.1% CBB-G250, 2% Phosphoric acid, 10% Ammonium sulfate, and 20% MeOH) for 20 hours. Gels were de-stained with 5 × 5 minute washes of 0.5 M NaCl. Gels and imaged using a FLA-9000 imager (Fuji Film). For Western blotting proteins were transferred from the 1-DE gel onto a 0.2 µM pore-size polyvinylidene difluoride (PVDF) membrane (Merck Millipore) that had been pre-soaked in western transfer buffer (25 mM Tris, 192 mM Glycine, 20% MeOH, 0.025% SDS). Electro-blotting of the PVDF membrane was carried out at 120 V at 4 °C for 1 hour using a Mini Trans-Blot® Cell apparatus (Bio-Rad Laboratories). After transfer, the membrane was placed in blocking buffer (1 X PBS, 0.1% Tween-20, 1% PVP40, 5% skim milk) for 1 hour at room temperature. The blocked membrane then underwent 2 × 15 minute washes with 0.1% PBST (1 X PBS, 0.1% Tween-20) before being exposed to a 1/500 dilution of antibody. Antibodies used were: anti-DEAF-1 monoclonal antibody (Sapphire Bioscience, Redfern, Australia); anti-NFYA monoclonal antibody (Sapphire Bioscience); and anti-GAPDH polyclonal antibody (Sapphire Bioscience). Membranes were incubated with their respective antibodies overnight at 4 °C, with constant agitation. The following day, the membrane underwent 2 × 15 minute washes with 0.1% PBST before being treated with a 1/2,500 dilution of peroxidase-conjugated goat anti-mouse IgG antibody (Sigma Aldrich) for membranes treated with DEAF1 primary antibody, or peroxidase-conjugated goat anti-rabbit IgG antibody (Sigma Aldrich) for membranes treated with NFYA and GAPDH primary antibodies. Membranes were incubated in secondary antibody for 1 hour at room temperature with constant agitation. The membrane then underwent 2 × 15 minute washes with 0.1% PBST followed by 1 × 15 minute wash with 1 X PBS. The membrane was then exposed to 1 mL of the Luminata Cresendo Western HRP Substrate (Merck Millipore) for 1 minute in the dark and imaged using a LAS-4000 (Fuji Film) and Multi-Gauge v3.0 software (Fuji Film). Entire western blot images were imported into Adobe Photoshop to visualise bands for analysis with ImageJ software. Arbitrary units obtained from bands of predicted size for proteins of interest were normalised against those of the housekeeping protein GAPDH. Statistical-significance was determined with a paired one-tail student's t-Test.

3.3. RESULTS

3.3.1. ML114-mediated loss of RBBP9 SH activity alters hPSC gene expression.

To begin investigating the molecular consequences of ML114-mediated RBBP9 SH inhibition, Affymetrix gene expression analysis was performed on DMSO- and ML114-treated hPSCs. This analysis revealed 2208 genes that were significantly up-regulated with ML114 treatment and expressed in all 3 ML114-treated samples (Figure 3.1 A, B), based on a p value < 0.002 and false-discovery rate of 0.021. Comparison of these 2208 genes with published gene expression data from RBBP9 siRNA-treated hPSCs (O'Connor et al., 2011) identified 152 genes commonly up-regulated by loss of both RBBP9 activities (Figure 3.1 C).

3.3.2. ML114 up-regulates genes involved in protein modification processes.

Gene ontology (GO) analysis of the 2208 genes up-regulated by ML114 identified ‘protein modification processes’ as the only significantly enriched GO term after testing for the likelihood of false-positive discoveries due to the size of the dataset (Table 3.2). As shown in Tables 3.3 to 3.5, this GO term category included genes involved in regulating: i) the cell cycle; ii) proteolysis; and iii) apoptosis. Notably, a number of these genes altered by ML114 treatment are known targets of transcription factors involved in regulation of proliferation and PSC maintenance. For example, *CDC25C, CCNB2,* and *SOX9* are targets of *NFYA* (Manni et al., 2001, Shi et al., 2015) (Appendix 1).

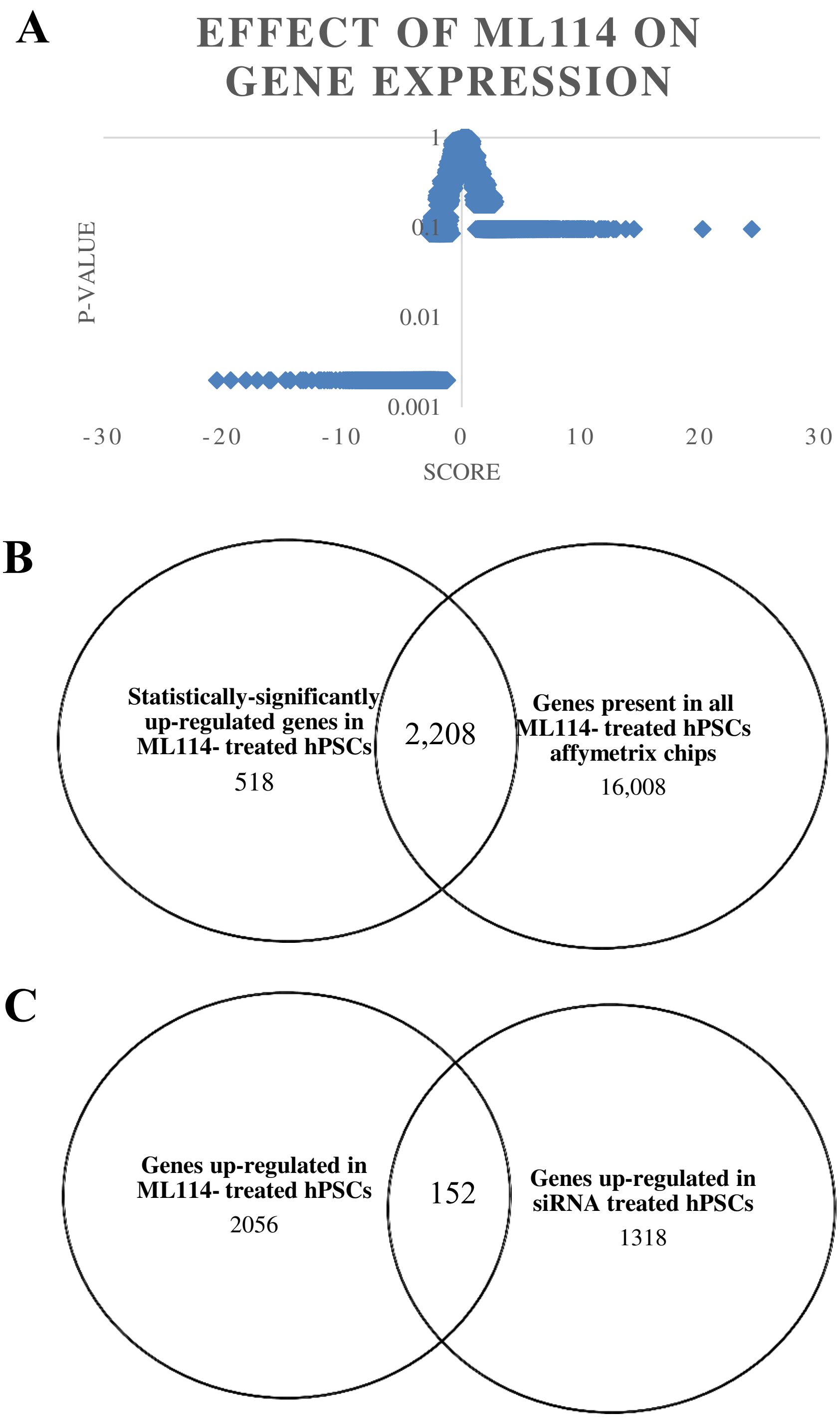

Figure 3.1 Affymetrix analysis revealed an up-regulation of genes in hPSCs treated with ML114. A) Affymetrix comparison of DMSO- control and ML114-treated hPSCs revealed a significant up-regulation of 2,726 genes in hPSCs treated with ML114. B) Identification of 2,208 genes affected by ML114 treatment in hPSCs were shown in all 3 Affymetrix profiling arrays. C) Comparison of genes show 152 genes significantly up-regulated by ML114 mediated loss of RBBP9 SH activity, and siRNA mediated loss of RBBP9 protein.

Table 3.2 Top 30 Biological Process (level 5) GO terms enriched by genes up-regulated in ML114-treated hPSCs	*p*-value	Benjamini
protein modification process	**1.20E-05**	**2.50E-02**
hexose metabolic process	1.30E-04	1.30E-01
regulation of Wnt receptor signaling pathway	3.10E-04	2.00E-01
endoderm development	3.60E-04	1.70E-01
formation of primary germ layer	9.60E-04	3.40E-01
lipid modification	1.20E-03	3.40E-01
glucose metabolic process	1.30E-03	2.70E-01
Wnt receptor signaling pathway	1.30E-03	3.00E-01
fatty acid catabolic process	1.30E-03	3.30E-01
protein transport	1.40E-03	2.70E-01
intracellular signaling cascade	1.50E-03	2.60E-01
protein import into peroxisome matrix	2.60E-03	3.70E-01
fatty acid oxidation	2.70E-03	3.40E-01
lipid oxidation	2.70E-03	3.40E-01
regulation of small GTPase mediated signal transduction	2.70E-03	3.60E-01
gastrulation	3.60E-03	4.00E-01
peroxisomal transport	3.80E-03	4.00E-01
tissue morphogenesis	4.70E-03	4.50E-01
positive regulation of RNA metabolic process	5.00E-03	4.50E-01
epithelial tube morphogenesis	5.80E-03	4.80E-01
positive regulation of transcription, DNA-dependent	5.90E-03	4.70E-01
mesoderm morphogenesis	7.10E-03	5.20E-01
hippocampus development	7.80E-03	5.30E-01
cellular lipid catabolic process	8.40E-03	5.40E-01
cellular protein metabolic process	8.60E-03	5.40E-01
carboxylic acid catabolic process	1.00E-02	5.80E-01
pallium development	1.00E-02	5.80E-01
anterior/posterior pattern formation	1.10E-02	5.80E-01
development of secondary sexual characteristics	1.10E-02	5.90E-01
embryonic placenta development	1.30E-02	6.20E-01

Table 3.3 Genes affected by ML114-treatment are involved in the 'regulation of cell cycle process'	
HECTD3	HECT domain containing E3 ubiquitin protein ligase 3
APBB1	Amyloid beta precursor protein binding family B member 1
CAMK2D	Calcium/calmodulin-dependent protein kinase II delta
CDC25C	Cell division cycle 25 homolog C (S. pombe) [Gorilla gorilla]
CDC7	Cell cycle division 7
HERC2	HECT and RLD domain containing E3 ubiquitin protein ligase 2
PRKCQ	Protein kinase C theta
ATM	ATM serine/threonine kinase
TGFA	Transforming growth factor alpha
TGFB1	Transforming growth factor 1

Table 3.4 Genes affected by ML114-treatment are involved in 'proteolysis'	
ATG10	Auophagy related 10
ATG7	Autophagy related 7
BAP1	BRCA1 associated protein 1
DZIP3	DAZ interacting zinc finger protein 3
FBXL5	F-box and leucine-rich repeat protein 5
FBXO11	F-box protein 11
FBXO25	F-box protein 25
FBXO4	F-box protein 4
HERC2	HECT and RLD domain containing E3 ubiquitin protein ligase 2
HERC3	HECT domain containing E3 ubiquitin protein ligase 3
HECW2	HECT, C2 and WW domain containing E3 ubiquitin protein ligase 2
KEL	Kell blood group, metallo-endopeptidase
MYSM1	Myb-like, SWIRM and MPN domains 1
PCNP	PEST proteolytic signal containing nuclear protein
SENP7	SUMO1/sentrin specific peptidase 7
UEVLD	UEV and lactate/malate dehydrogenase domains
CHFR	Checkpoint with forkhead and ring finger domains,E3 ubiquitin protein ligase
C3	Complement component 3
DDB1	Damage specific DNA binding protein 1
HERC2	HECT and RLD domain containing E3 ubiquitin protein ligase 2
HECTD3	HECT domain containing E3 ubiquitin protein ligase 3
HERC6	HECT and RLD domain containing E3 ubiquitin ligase family member 6
HGF	Hepatocyte growth factor
HDAC6	Histone deacetylase 6
LNX1	Ligand of numb-protein X 1, E3 ubiquitin protein ligase
MAPK1	Mitogen-activated protein kinase 1
PRKCQ	Protein kinase C theta
RING1	Ring finger protein 1
RNF14	Ring finger protein 14
RNF19A	Ring finger protein 19A
UBE3B	Ubiquitin protein ligase E3B
USP20	Ubiquitin specific peptidase 20
UBE2H	Ubiquitin conjugating enzyme E2H
UBA1	Ubiquitin like modifier activating enzyme 1

Table 3.5 Genes affected by ML114-treatment are involved in the 'regulation of apoptosis'	
FASTK	Fas activated serine/threonine kinase
STRADB	STE20-related kinase adaptor beta
B4GALT1	UDP-Gal:betaGlcNAc beta 1,4- galactosyltransferase, polypeptide 1
ACVR1C	Activin A receptor type IC
APP	Amyloid beta precursor protein
APBB1	Amyloid beta precursor protein binding family B member 1
ABL1	ABL proto-oncogene 1, non-receptor tyrosine kinase
CCL2	chemokine (C-C motif) ligand 2
CDK5	cyclin-dependent kinase 5
ERCC6	excision repair cross-complementation group 6
GRM4	glutamate receptor, metabotropic 4
GSK3B	glycogen synthase kinase 3 beta
HGF	Hepatocyte growth factor
HDAC3	Histone deacetylase 3
HDAC6	Histone deacetylase 6
ING4	Inhibitor of growth family member 4
LCK	LCK proto-oncogene, Src family tyrosine kinase for
MAPK1	Mitogen-activated protein kinase 1
PIK3CA	phosphatidylinositol-4,5-bisphosphate 3-kinase catalytic subunit alpha
PRLR	prolactin receptor
CHEK2	Checkpoint kinase 2
PPP2R1A	protein phosphatase 2 regulatory subunit A, alpha
STK17B	Serine/threonine kinase 17b
STAT5A	Signal transducer and activator of transcription 5A
ATM	ATM serine/threonine kinase
TGFB1	Transforming growth factor 1
TGFB2	Transforming growth factor 2

3.3.2. NFYA is a predicted effector of RBBP9 SH activity.

Promoter analyses were used to identify transcription factor binding motifs common to genes whose expression was altered by ML114 treatment, as a way of identifying candidate transcription factors responsible for the gene expression changes caused by ML114. Two separate promoter analyses were performed: i) a distal analysis interrogated a region extending 10 kb upstream from the transcription start site of each genes promoter, and ii) a proximal analysis interrogated a region situated ± 400 bp either side of the transcription start site for each gene affected by ML114 treatment. Using this approach a number of transcription factors were found to be highly ranked predicted regulators of the genes up-regulated by ML114 treatment in both the proximal and distal analyses (Tables 3.6 and 3.7). This included ELF-1 and SP1, previously implicated in tumorigenesis and cell cycle regulation (Gerloff et al., 2011, Davie et al., 2008, Chuang et al., 2009), with SP1 also implicated in regulation of NANOG expression in murine embryonic carcinoma cells (Wu and Yao, 2006). Interestingly NFYA and DEAF1 were identified as the top, or close to top, predicted transcriptional regulators of the ML114-affected genes in both the proximal and distal analyses. These two transcription factors have been implicated in proliferation, PSC maintenance, and early embryo development (Bhattacharya et al., 2003, Dolfini et al., 2012, Gu et al., 2010, Manni et al., 2001). Similar promoter analyses of the genes commonly affected by both ML114 treatment and RBBP9 siRNA also predicted DEAF1 and NFYA (through its alternate name CBF_01) as putative candidate regulators of RBBP9 activities (Tables 3.8 and 3.9).

To test whether NFYA and DEAF1 might be effectors of RBBP9 SH activity, a variety of gene and protein expression analyses were performed. A small fold change in transcripts was observed (less than 2-fold change), with fold change increases ranging from 24.7% to 0.05%. Firstly, analysis of Affymetrix gene expression data showed a small but significant increase in *NFYA* transcript levels (fold change = 1.005218, p = 0.001996), but no significant changes with *DEAF1* expression (fold change = 1.000845, p = 0.469062) between DMSO- and ML114-treated hPSCs. Additional analysis *via* qPCR revealed no difference in *NFYA* transcript levels resulting from ML114 treatment (Figure 3.2 A). Western blotting was then used to determine whether NFYA and/or DEAF1 protein might be targets of RBBP9 SH activity. Analysis of hPSCs treated with DMSO, 100 μM ML114 soluble fragment, or 100 μM ML114 showed DEAF1 protein expression in all three conditions, with no significant difference in expression between the different treatments (Figure 3.2 A-D). In contrast, NFYA protein expression increased by ~50% in the ML114-treated cells relative to GAPDH expression, p = 0.04 (Figure 3.3 B-D).

3.4. DISCUSSION

The molecular networks regulated by RBBP9 SH activity are currently unknown, but are of significant interest given the demonstrated roles RBBP9 plays in hPSC maintenance and proliferation of cancer cells (O'Connor et al., 2011, Woitach et al., 1998, Shields et al., 2010). In an attempt to identify effectors of RBBP9 SH activity, this chapter used a variety of complementary approaches including gene expression profiling, promoter analyses and Western blotting.

Table 3.6 Proximal analysis using PASTAA: Top 20 predicted regulators of genes up-regulated in hPSCs treated with ML114.

Candidate mediators of genes affected by ML114 (Proximal Analysis ± 400 bp)			
Matrix	*Transcription Factor*	*Association Score*	*P-Value*
ARNT_02	Arnt	10.876	0.00E+00
STRA13_01	Stra13	9.882	0.00E+00
NFY_01	**N/A**	**7.035**	**5.00E-06**
TFIII_Q6	Tfii-i	6.654	1.70E-05
MAZR_01	Mazr	6.294	4.20E-05
NFKAPPAB65_01	Rela	6.156	5.40E-05
USF_Q6	Usf1 , Usf2a	6.139	5.40E-05
MZF1_01	Mzf-1	6.09	6.70E-05
DEAF1_01	**Deaf-1**	**5.999**	**8.00E-05**
USF_Q6_01	Usf-1 , Usf1	5.802	1.27E-04
ATF1_Q6	Atf-1	5.652	1.63E-04
NERF_Q2	Nerf-1a	5.422	2.79E-04
DEAF1_02	**Deaf-1**	**5.354**	**3.16E-04**
MTF1_Q4	Mtf-1	5.266	3.98E-04
MOVOB_01	Movo-b	5.161	4.91E-04
EGR2_01	Egr-2	5.155	4.94E-04
CETS1P54_03	C-ets-1	4.928	8.23E-04
NRF2_01	N/A	4.768	1.17E-03
ARNT_01	Arnt	4.584	1.72E-03
EGR3_01	Egr-3	4.565	1.80E-03
YY1_Q6_02	Yy1	4.563	1.80E-03

Table 3.7 Distal analysis using PASTAA: Top 20 predicted regulators of genes up-regulated in hPSCs treated with ML114.

Candidate mediators of genes affected by ML114 (Distal Analysis - 10 kb)			
Matrix	*Transcription Factor*	*Association Score*	*P-Value*
NFY_01	**N/A**	**4.681**	**1.37E-03**
ETS_Q4	**Erf , Elf-1**	**4.194**	**3.76E-03**
NFKAPPAB50_01	N/A	4.147	4.05E-03
PR_02	N/A	4.059	4.91E-03
NFY_Q6	**Cbf-a , Cbf-b**	**3.616**	**1.21E-02**
SZF11_01	N/A	3.597	1.26E-02
NFY_Q6_01	**Cbf-a , Cbf-b**	**3.515**	**1.47E-02**
DEAF1_02	**Deaf-1**	**3.393**	**1.88E-02**
NFY_C	**Cbf-a , Cbf-b**	**3.314**	**2.15E-02**
CRX_Q4	Crx , Rx	3.311	2.17E-02
ETS2_B	C-ets-1 , C-ets-2	3.293	2.27E-02
MAZR_01	Mazr	3.288	2.34E-02
OCT1_01	Pou2f1 , Pou2f1a	3.19	2.82E-02
E2F_Q4_01	Dp-1 , E2f-1	3.149	3.07E-02
CDP_02	Cutl1	3.037	3.71E-02
CLOX_01	Cutl	3.037	3.71E-02
YY1_02	Yy1	3.014	3.98E-02
HNF4_Q6_02	Hnf-4 , Hnf-4alpha	2.98	4.20E-02
HSF1_Q6	Hsf1 , Hsf1long	2.898	4.81E-02

Table 3.8 Proximal analysis using PASTAA: Top 20 predicted regulators of genes up-regulated in hPSCs treated with both ML114- and RBB9 siRNA.

Candidate mediators of genes affected by loss of both RBBP9 activities (Proximal Analysis ± 400 bp)			
Matrix	*Transcription Factor*	*Association Score*	*P-Value*
LBP1_Q6	N/A	5.55	1.12E-04
PAX4_03	Pax-4a	4.392	1.32E-03
MAZR_01	Mazr	4.348	1.43E-03
HEN1_01	N/A	4.133	2.10E-03
PAX9_B	Pax-9a	4.133	2.10E-03
ETF_Q6	N/A	4.132	2.10E-03
HEB_Q6	Heb	3.898	3.45E-03
E2_Q6	N/A	3.806	4.25E-03
AP4_Q6_01	Ap-4	3.804	4.25E-03
GC_01	N/A	3.556	7.05E-03
DEAF1_01	**Deaf-1**	**3.535**	**7.34E-03**
SP1_Q4_01	**Sp1 , Sp2**	**3.468**	**8.12E-03**
SP1_Q6	**Sp1**	**3.468**	**8.12E-03**
SP1_Q6_01	**Sp1 , Sp3**	**3.468**	**8.12E-03**
PAX5_01	Pax-5	3.425	9.26E-03
SP1_01	**Sp1**	**3.357**	**1.03E-02**
MYB_Q6	C-myb	3.352	1.03E-02
GATA1_01	Gata-1	3.349	1.03E-02
E2_01	N/A	3.259	1.25E-02
CHCH_01	Chch	3.126	1.62E-02

Table 3.9 Distal analysis using PASTAA: Top 20 predicted regulators of genes up-regulated in hPSCs treated with both ML114- and RBB9 siRNA.

Candidate mediators of genes affected by loss of both RBBP9 activities (Distal Analysis - 10 kb)			
Matrix	*Transcription Factor*	*Association Score*	*P-Value*
POU1F1_Q6	Pou1f1 , Pou1f1a	4.809	5.41E-04
YY1_02	Yy1	3.697	5.30E-03
AHR_01	Ahr	3.413	9.58E-03
PU1_Q6	Pu.1	3.365	1.01E-02
LXR_DR4_Q3	N/A	3.153	1.55E-02
CDP_02	Cutl1	3.061	1.83E-02
GATA3_03	Gata-3	3.043	1.92E-02
NFKAPPAB50_01	N/A	3.017	2.07E-02
STAT3_02	Stat3	2.99	2.20E-02
ROAZ_01	Roaz	2.967	2.27E-02
COUP_DR1_Q6	Coup-tf1 , Coup-tf2	2.931	2.41E-02
GATA1_02	Gata-1	2.893	2.59E-02
NFE2_01	Nf-e2	2.799	3.09E-02
OLF1_01	Olf-1	2.772	3.23E-02
HFH4_01	Foxf1 , Foxj1	2.75	3.34E-02
LYF1_01	N/A	2.748	3.35E-02
E2_Q6	N/A	2.72	3.67E-02
NFMUE1_Q6	N/A	2.699	3.83E-02
PBX1_02	Pbx1a	2.646	4.14E-02
CBF_01	**N/A**	**2.645**	**4.14E-02**

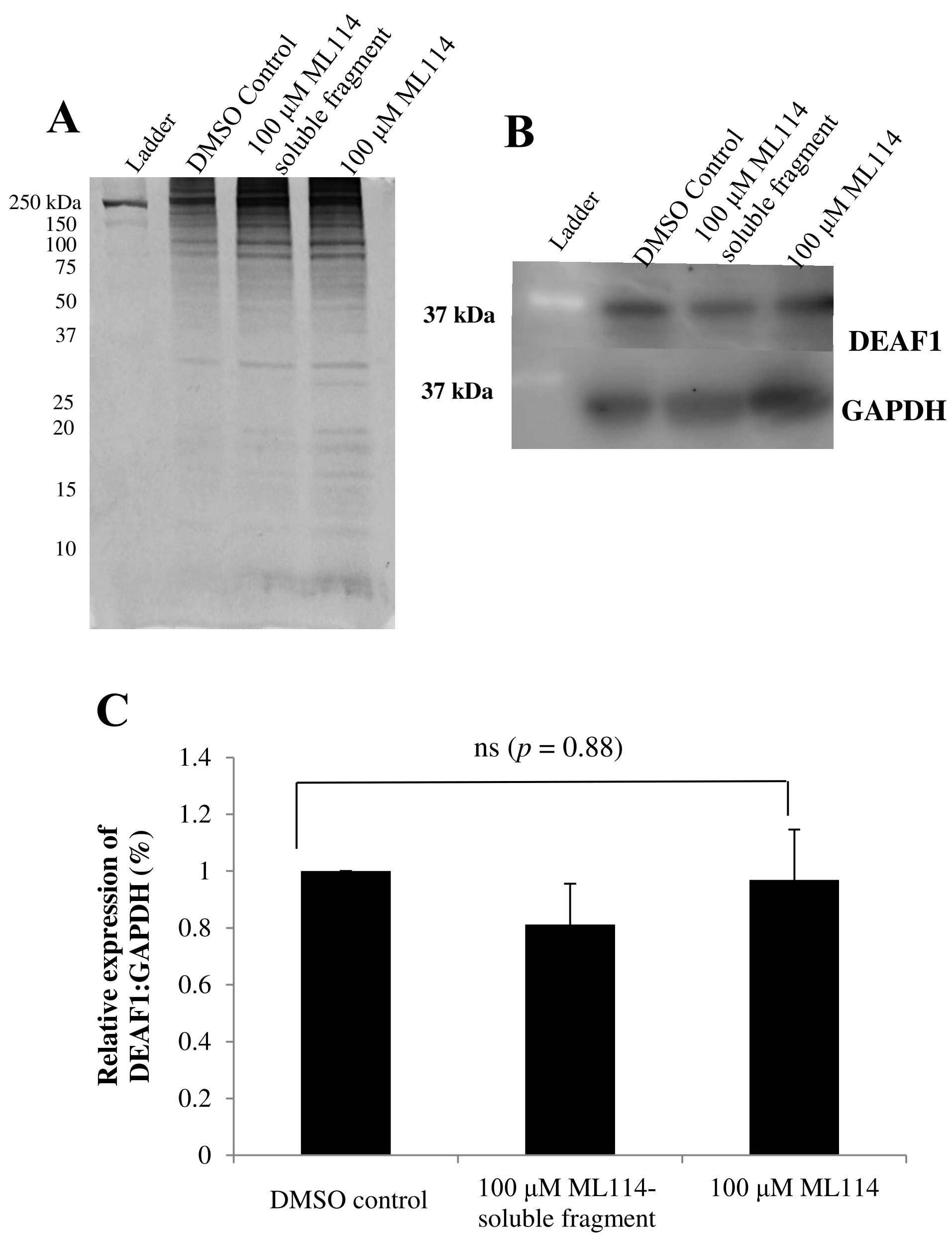

Figure 3.2 DEAF1 is not significantly increased in treated hPSCs A) Coomassie stained 1-DE gel of samples run in hPSCs treated with DMSO-control, ML114-soluble fragment treated, and ML114. B) Western blot detection of DEAF1 protein across all treatments. C) Analysis of western blots identified no significant changes in DEAF1 protein levels between DMSO-control, (n = 3), 100 μM ML114-soluble fragment (n = 2), and ML114-treated hPSCs (n = 3).

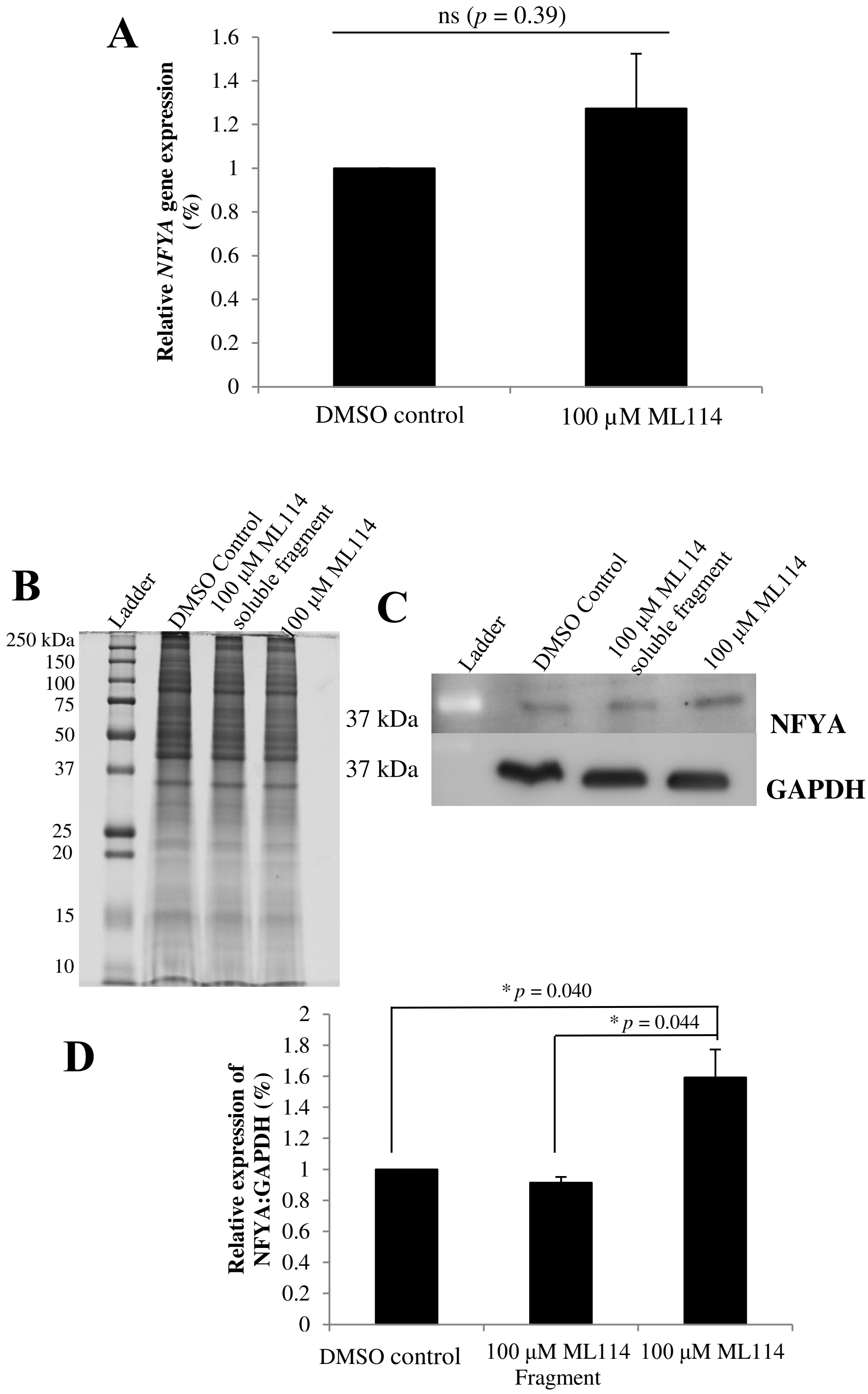

Figure 3.3 NFYA expression in hPSCs treated with ML114. A) qPCR revealed no significant increases in *NFYA* transcript levels in hPSCs treated with ML114. B) Coomassie stained 1DE gel of samples run with hPSCs treated with DMSO-control, ML114-soluble fragment treated, and ML114. C) Western blot detection of NFYA protein across all treatments. D). Analysis of western blots identified a significant increase in NFYA protein levels between DMSO-control, 100 µM ML114-soluble fragment, and ML114-treated hPSCs (n = 3).

3.4.1. DEAF1 & NFYA: pluripotency regulators as candidate RBBP9 SH effectors.

Affymetrix profiling revealed 2208 genes up-regulated as a result of ML114 treatment. The promoters of many of these differentially regulated genes contained a range of known and novel pluripotency-related transcription factors. DEAF1 and NFYA were selected for further investigation as they were high-confidence predicted regulators in both the distal and proximal promoter analyses of genes affected by both ML114 and RBBP9 siRNA treatments. DEAF1 and NFYA are reported to have roles in embryonic development and self-renewal in ESCs (Bolognese et al., 1999, Dolfini et al., 2012, Gu et al., 2010, Veraksa et al., 2002). For instance, a reduction of DEAF1 protein has been shown to induce embryonic arrest in the early stages of *Drosophila* development (Veraksa et al., 2002). Additionally, differentiation of mESCs and hESCs was found to decrease levels of DEAF1 similarly to OCT4 and NANOG. This decrease led the authors to conclude that DEAF1 has a role in self-renewal of both mESCs and hESCs (Gu et al., 2010). The lack of any decrease in OCT4, NANOG and DEAF1 transcript levels seen in this chapter provides further support for the idea that ML114 treatment did not induce hPSC differentiation.

NFYA has been shown to be a bifunctional transcription factor, where it has dual functions in transcriptional regulation by acting as either an activator or repressor (Ceribelli et al., 2008, Peng and Jahroudi, 2002, Deng et al., 2007, Peng and Jahroudi, 2003). For NFYA to act either as an activator or repressor of NFY targets there must be an active NFY trimer (NFYA, NFYB, or NFYC) present. These NFY subunits possess histone like properties, which enables specific binding to the CCAAT box, a common eukaryotic promoter element (Ceribelli et al., 2008). A study has shown subunits of NFY function in a cell-specific manner, where recruitment of histone deacetylases to the von Willebrand factor endothelial-specific promoter were found to repress promoter activity in non-endothelial cells and activate promoter activity in endothelial cells (Peng and Jahroudi, 2002).

Loss of *NFYA* in early embryogenesis was shown to result in early embryonic lethality, supporting the requirement of *NFYA* in early embryogenesis and ESCs (Bhattacharya et al., 2003). Chromatin immunoprecipitation data has shown NFY binds to the CCAAT-containing regions of *Cdc25c, Sall4,* and *Zic3*, which are highly expressed in pluripotent cells (Grskovic et al., 2007). The Affymetrix analyses showed here revealed up-regulation of *CDC25C* and *NANOG* with ML114 treatment. Compared with analysis of the published RBBP9 siRNA data showed increased *ZIC3* expression with RBBP9 siRNA treatment (O'Connor et al., 2011). During differentiation events in ESCs *NFYA* expression was shown to be significantly down-regulated, suggesting *NFYA* is required for assisting maintenance of pluripotency in ESCs (Grskovic et al., 2007). This suggests the up-regulation of NFYA might be a cellular consequence responsible for maintaining pluripotency in hESCs after selective inhibition of RBBP9 SH activity. In support of this idea, genes involved in differentiation were not significantly expressed with ML114 treatment; in contrast neurogenesis genes were upregulated with complete loss of RBBP9 protein.

The CCAAT binding motif bound by NFY has been shown to be part of the ESC transcription factor circuitry, promoting binding of master transcription factors such as OCT4, NANOG and SOX2 (Dolfini et al., 2012, Oldfield et al., 2014). Oldfield and colleagues showed silencing of *NFYA* resulted in significant loss of mESC Nanog protein, and gene expression analyses identifying depletion of NFY subunits resulted in down-regulation of pluripotency genes such as *Nanog* concomitantly with up-regulation of differentiation genes

(Oldfield et al., 2014). The Affymetrix data presented here also showed a small but significant increase in expression of *NANOG*, *SMAD1* and *TGF-β1*. High expression of *NANOG* is associated with pluripotency in hPSCs (Hart et al., 2004). Additionally, Nanog has been shown to bind to Smad1 and inhibit differentiation induced by bone morphogenic protein (BMP) signalling in mESCs (Suzuki et al., 2006). Thus ML114-treated hPSCs might retain pluripotency due to at least maintained, if not increased, levels of NANOG gene expression. Furthermore, NFYA expression has been shown to be regulated both at a transcriptional and translational level, with significant losses of NFYA identified in differentiated cells (Farina et al., 1999). Chromatin immunoprecipitation experiments performed in another study had also identified a high percentage of NFY motifs are present in the promoters of genes that are regulated by well-known regulators of pluripotency such as NANOG (47%), and SOX2 (43%), with addition of NFYA resulting in up-regulation of *Nanog* in mESCs (Dolfini et al., 2012). Curiously, this also increased proliferation of the mESCs, opposite to the effect seen with ML114 on hPSCs. As NFYA can act as a transcriptional activator or repressor, the different effect of increased NFYA protein on hESCs (used here) compared to the Dolfini mESC study could be due to the known and quite large differences in chromatin between these 2 different pluripotent states. In support of this idea, overexpression of the short isoform NFYA *via* protein transduction in the pluripotent NT2/D1 human embryonal carcinoma cells was shown to significantly reduce growth rates by 50-60% (Mojsin et al., 2015). Also, siRNA-mediated loss of RBBP9 protein in NT2/D1 cells resulted in reduced proliferation but also initiation of neural differentiation (O'Connor et al., 2011).

3.4.2. Potential mechanisms for effect of ML114 on hPSCs mediated by DEAF1.

Both DEAF1 and NFYA have reported roles in the regulation of proliferation in other, non-pluripotent cell types. Increased proliferation was shown with overexpression of DEAF1 in human breast epithelial cells *in vitro*, and mouse epithelial cells *in vivo* (Barker et al., 2008). In contrast, up-regulation of NFYA resulted in reduced proliferation in cell types including human embryonal carcinoma cells, and mouse erythroleukemia cells (Mojsin et al., 2015, Bolognese et al., 1999). However, depletion of various subunits of NFY trimers have also been shown to result in reduced proliferation of human carcinoma cells (Benatti et al., 2011). These differences may be due to the dual role of NFY trimers, more specifically NFYA to act as both a transcriptional activator and repressor in a cell-type specific manner (Peng and Jahroudi, 2002, Mojsin et al., 2015).

The lack of any increase in DEAF1 transcript or protein levels suggests that DEAF1 is unlikely to be a direct target of RBBP9 SH activity and thus may be an indirect proteolysis target (e.g., through RBBP9 SH-mediated proteolysis of kinases, phosphatases or other proteins that post-translationally regulate DEAF1). In contrast, the combination of no consistent increase in NFYA transcript between the Affymetrix and PCR analyses, together with the increased NFYA protein levels seen by Western blotting, suggests NFYA may be a direct target of RBBP9 SH proteolytic activity. In support of this conclusion, NFYA has previously been reported as a putative target of SH activity through mass spectrometry analyses in HIV-1 cells (Impens et al., 2012).

3.4.3. Potential mechanisms for NFYA-mediated effect of ML114 on hPSCs.

NFYA has been shown to have a role in cellular proliferation in many cell types. For example, loss of NFYA in hematopoietic stem cells resulted in cells accumulating in G_2/M and apoptosis (Bungartz et al., 2012). Additionally, it has been reported that in a mouse erythroleukemia cell line, the mRNA and protein levels of NFYB and NFYC do not vary during the cell cycle. In contrast, i) NFYA protein but not mRNA is maximal in mid-S phase and decreased in G2/M, and ii) CCAAT-binding activity follows NFYA protein levels. Based on this it has been suggested that NFYA is the limiting subunit within the NFY complex, and that post-transcriptional mechanisms regulate NFYA levels (Bolognese et al., 1999). These published findings therefore suggest that the increase in NFYA protein seen here after ML114 treatment is consistent with the conclusion that NFYA protein levels are regulated post-translationally by RBBP9 SH activity.

NFYA has been shown to regulate many cell cycle regulatory genes such as *SOX9, CCNB1, CCNB2, CDK1,* and *TOP2A* that are enriched with the CCAAT binding motif of NFY (Shi et al., 2015). Overexpression of the NFYA target gene SOX9 has been reported to decrease proliferation of prostate tumor cells (Drivdahl et al., 2004), and cyclin B is reported to be the only cell cycle-regulated cyclin in hPSCs (Stead et al., 2002). The Affymetrix analyses presented here revealed a small but significant increase in expression of particular NFYA target genes (as a result of both ML114 and RBBP9 siRNA) involved in cell cycle regulation including *CCNB2* and *SOX9*. Thus the Affymetrix data supports the idea that altered expression of NFYA target genes plays a role in the reduced hPSC proliferation and population growth rates that resulted from ML14 treatment.

The Affymetrix analysis of ML114-treated hPSCs also revealed a small but significant up-regulation of *CDC25C* and *CDK5* expression. This is interesting as *CDC25C* has previously been associated with *NFYA* and cell cycle regulation (Lucibello et al., 1995, Zwicker et al., 1995, Manni et al., 2001). Members of the CDC family, including *Cdc25c* have been identified as direct targets of *Cdk5* in mouse brain lysates (Chang et al., 2012). Both *CDC25C* and *CDK5* have been reported to work together to create a proliferative block in DU145 androgen-independent prostate cancer cells. Up-regulation of *CDK5* resulted in an accumulation of cells in G_1 phase, similar to the effects seen in hPSCs treated with ML114 (Lin et al., 2014). Thus in ML114-treated hPSCs, up-regulation of both *CDC25C* and *CDK5* expression as a result of increased NFYA protein levels could account for the temporary proliferative changes observed.

Overall, the data presented here suggests that the decreased proliferation seen in Chapter 2 is due to loss of RBBP9 SH activity resulting in increased levels of NFYA protein. This then leads to small but statistically-significant changes in gene expression for a range of genes known to regulate the cell cycle in pluripotent cells. The observed increase in NFYA protein levels as a result of ML114 treatment is consistent with published reports that NFYA is a known target of SH (Impens et al., 2012), and that NFYA activity is regulated by post-translational modification (Manni et al., 2008, Bolognese et al., 1999). As a note of caution, the small fold changes seen with the differentially-expressed genes suggest that further investigation into the molecular mechanisms of RBBP9 SH activity in hPSCs would benefit from proteomic approaches to look at protein levels and/or protein activity - both global proteomic analyses and specific analyses targeting NFYA and DEAF1. Given that RBBP9 and NFYA are both involved in hPSC maintenance and are both expressed during embryonic development, further investigation into the consequences of RBBP9 SH inhibition during development is also of interest. Other transcription factors affected by ML114 might also be worth investigating such as YY1 which has also been reported to be an essential regulator of stem cell maintenance and associated with cancer (Gangaraju and Lin, 2009, Kaufhold et al., 2016). The relationship of YY1 and RBBP9 SH activity loss could be investigated via gene expression and western blot analyses similarly to the assessment of NFYA and DEAF1.

CHAPTER 4: Investigating the role of Rbbp9 in embryonic zebrafish development

4.1. INTRODUCTION

Data presented in Chapter 2 showed ML114 treatment decoupled hPSC proliferation and differentiation capabilities, i.e., ML114 reduced hPSC proliferation but the treated cells retained pluripotency markers and the capacity to form tri-lineage teratomas after treatment was removed. Having an appropriate balance between stem cell maintenance, proliferation, and differentiation is essential for normal embryonic development. For example, published studies have shown that loss of key regulators of proliferation such as cyclins results in developmental abnormalities in mouse embryogenesis (Kozar et al., 2004). Serine proteases have previously been implicated in Drosophila gastrulation, with loss of serine protease function due to mutations seen to result in incomplete neural development during early embryogenesis (Han et al., 2000). In addition, the serine protease Furin: has been shown to be essential for the formation of key tissues derived from all three cell lineages. Disruption of this enzymatic activity has been shown to result in malformation of epiblast derivatives such as the primitive heart, gut, and extraembryonic mesoderm in mouse models (Roebroek et al., 1998).

To understand the role of Rbbp9 SH activity during embryonic development *in vivo*, zebrafish embryos were treated with ML114. Zebrafish are a useful model of vertebrate embryonic development as they are fertilised and develop outside the mother's body, have rapid development (i.e., a well-developed body and organ systems within three to four days), and are optically transparent so their development can be followed *via* simple microscopy (Streisinger et al., 1981, Kimmel et al., 1995). Zebrafish also display molecular similarities to human and hPSC development. This includes high levels of *oct4* in blastomeres of zebrafish embryos (Robles et al., 2011) – cells equivalent to the source of hESCs derived from the blastocyst of the inner cell mass. Other studies have successfully generated PSCs from zebrafish embryos at the mid-blastula stage (~2.25 hpf) and gastrula stage (~5.5 hpf) that have the potential to generate tissue specific cell lineages, similarly to hPSCs (Fan et al., 2004, Ghosh and Collodi, 1994).

Investigation *via* the Bgee gene expression browser shows *rbbp9* transcripts are expressed in at least 10 zebrafish organs at 40 different stages. This includes in the eye, heart, brain, and digestive tract, from fertilisation through to adult stages (Bastian et al., 2008). ML114-treated zebrafish were assessed for developmental changes *via* live animal imaging, PCR and histology. These studies confirmed *rbbp9* transcripts were expressed throughout the early stages of zebrafish development. ML114 treatment resulted in phenotypic changes to zebrafish eye, heart, brain and digestive tract morphology. To assess how these changes compared to the loss of entire Rbbp9 protein during zebrafish development, *rbbp9* morpholino (i.e., gene expression knockdown *via* blocking translation) experiments were performed. The changes seen were similar, though not identical, to those seen with ML114-treated zebrafish. The combined ML114 and *rbbp9* morpholino data presented here suggests Rbbp9 activities might be required for normal embryonic development in zebrafish, thus raising the possibility that RBBP9 SH activity plays a role in normal human tissue development.

4.2. METHODS

4.2.1. Zebrafish husbandry and housekeeping.

Tübingen/AB (TAB) strain zebrafish were maintained under standard housing conditions (Westerfield, 2000). Briefly, zebrafish were fed twice daily and kept at 28 °C, pH 7.4, and average conductance of 800 µS maintained by a ZebTEC automated zebrafish housing system (Techniplast, Buguggiate, Italy). An automated 14 hour light and 10 hour dark photoperiod cycle was used, with 1 hour of dim light used to mimic sunrise and 1 hour of dim light used to mimic sunset. All zebrafish protocols were approved by the Western Sydney University Animal Ethics Committee (approval number A9713).

4.2.1.1. Zebrafish embryo production.

Female and male zebrafish aged between 4-10 months were selected and placed in a breeding tank comprised of an outer tank (to hold water) and an inner tank (a smaller tank with small grooves for eggs to pass through) with a divider separating the two fish overnight (Techniplast). Spawning was carried out upon the start of the light cycle (Kimmel et al., 1995). The divider was removed from the breeding tank, and eggs released from the female were fertilised within the first 30 minutes upon removal of the divider. Fertilised embryos were then collected and maintained in 1 X E3 medium (5 mM NaCl, 0.17 mM KCl, 0.33 mM $CaCl_2$, 0.33 mM $MgSO_4$, pH 7.4) at 28 °C for the duration of the experiment (i.e. up to 7 days).

4.2.2. Treatment of zebrafish embryos with ML114 chemical inhibitor.

At the 1-cell stage post-fertilisation, 15-20 embryos were collected and maintained in 1 X E3 medium in 35 mm Petri dishes (Corning). Embryos were immediately treated with either: vehicle-only control consisting of 0.25% DMSO (Sigma Aldrich), a concentration known to not affect zebrafish development (Parng et al., 2002, Milan et al., 2003); or with up to 100 µM of ML114 or ML114 soluble fragment dissolved in 0.25% DMSO. Treatments were replenished daily for 7 days. Zebrafish embryos were counted 24 hours post treatment to determine the survival rate of treated embryos. Live embryos were imaged as described in 4.2.3, before being fixed with 4% PFA at 4 °C for 1 week for downstream applications.

4.2.3. Live imaging of zebrafish.

Phenotypic changes of zebrafish larvae were documented with live imaging at 24 hpf and 7 days post-fertilisation (dpf). Zebrafish larvae at 24 hpf were carefully manually dechorinated individually using Dumostar #5 fine point tweezers (Electron Microscopy Sciences, Pennsylvania, USA) to enable orientation for live imaging. Prior to imaging, zebrafish larvae were anesthetised with 0.4 mg/mL tricaine (Sigma Aldrich) and embedded in cooled, 1% low melting point agarose (Thermo Fisher Scientific) in a 35 mm glass bottom petri dish (14 mm micro-well, and #0 glass thickness) (MatTek Corporation, Massachusetts, USA). Images of anesthetised fish were captured using an Olympus MVX10 Stereomicroscope (Olympus), a Q-Imaging Retiga-4000 DC Fast 1394 camera (Q-Imaging, Brisbane, Australia), and Q Capture Pro 7 software. Images of morpholino-injected zebrafish were also imaged using a FITC-filter and visualised with the aid of an external light source provided by an X-cite® 120Q fluorescence illuminator (Excelitas Technologies, Waltham, MA, USA). Zebrafish measurements were obtained from images using ImageJ software (Schneider et al., 2012). Measurement parameters were input into ImageJ based on the objective lens magnification used to capture the image. Length measurements were taken for the body, yolk sac, gastrointestinal space, pericardial cavity as well as the area of the eye. Body length was measured from tip of the head to the end of the tail following the contours of the body. Eye area was calculated for each eye by placing a circle on the outer perimeter of the eye and using ImageJ to calculate the area within. Width of the gastrointestinal space was determined by measuring a line from the outer gastrointestinal wall to the swim bladder at the widest point between the two tissues. Pericardial cavity was determined by measuring a line from the junction of the ear and start of the yolk sac to the apex of the pericardial cavity. Statistical-significance was determined with a paired one-tail student's t-Test.

4.2.4. Extraction and purification of zebrafish DNA.

Healthy adult zebrafish (6-8 months) were euthanized with 8 mg/mL of tricaine (Sigma Aldrich). Zebrafish DNA was then extracted using the Purelink Genomic DNA Mini Kit (Thermo Fisher Scientific) following the manufacturer's instructions. Purified DNA samples were stored at -20 °C for downstream applications.

4.2.5. Zebrafish primer design for DNA sequencing.

Forward and reverse primers for specific genes were designed using Primer3Plus online software (Untergasser et al., 2007). Exon and intron sequences were obtained using the Ensembl online genome browser (http://asia.ensembl.org/index.html). Intronic gene sequences were selected for primer design if they displayed identical sequence across all four different mRNA isoforms of available *rbbp9* transcripts provided from different databases for zebrafish DNA sequence. DNA sequences derived from the 3' region of one exon and the 5' region of the next exon were input into Primer3Plus. Primer design was then initiated using parameters including 60 °C melting temperature, and 300-600 base amplicon pair (bp) length. To check whether the predicted primers bound anywhere else in the genome, the predicted primers were searched against the entire zebrafish genome and transcriptome using the BLAST nucleotide browser (https://blast.ncbi.nlm.nih.gov/Blast.cgi?PAGE_TYPE=BlastSearch&BLAST_SPEC=OGP__7955__9557). In the event primers were predicted to bind to other locations in the genome, the primer design process was repeated until unique primers were obtained. Primers were synthesised by GeneWorks (Sydney Australia).

Rbbp9 forward primer for DNA sequencing: aacttcagctcgtttgcag

Rbbp9 reverse primer for DNA sequencing: tgtgcgaataaaagcttcacc

Optimal working temperatures for each PCR primer set were obtained by performing a trial PCR reaction at temperatures ranging between 55-60 °C. Each PCR reaction consisted of 5 µL of 5 X Go-Taq Flexi PCR Buffer, 1.5 µL 25 mM $MgCl_2$, 1 µL 10 mM dNTPs, 2 µL 12.5 µM forward and reverse primers, 14 µL RNase/DNase free water, 0.5 µL Go-Taq Flexi, and 1 µL of cDNA. Samples were placed into an Eppendorf Mastercycler® (Eppendorf, North Ryde, Australia) using appropriate temperature profiles to determine the optimal temperature of each primer starting at 60 °C. The PCR reaction consisted of a 3 step process: denaturation (95 °C, 5 minutes and 30 seconds); followed by annealing of primers to target regions of DNA (55-60 °C, 20 seconds); and finally extension (72 °C, 2 minutes and 30 seconds). PCR products were loaded into a 2% agarose gel with 5 µL of 10, 000 X Gel Red Nucleic Acid (Bioline) as was a 100 bp DNA ladder (4 µL of 50 µg/µL) (FisherBiotec, Wembley, Australia). PCR products were separated using 100 V, 300 mA, and 50 W for 40 minutes. The gel was then imaged using a Gel Dock Transilumminator (Fisher Biotec) and E-box software.

4.2.5.1. DNA sequencing.

PCR products were excised from the agarose gel, extracted using the PureLink® Quick Gel Extraction Kit (Thermo Fisher Scientific), and 18 ng per sample was sequenced by the Australian Genome Research Facility using both the forward and reverse primers. The resulting sequences were compared against the entire zebrafish genome using the NCBI BLAST browser.

4.2.6. qPCR analysis of developing zebrafish larvae.

Zebrafish embryos pooled into respective treatment groups were homogenised on ice using a glass tissue homogeniser before being resuspended in RNA lysis buffer. RNA samples were then purified as described in section *3.2.2.1* and cDNA synthesis performed as described in section *3.2.2.2.* Primer design was performed using exonic zebrafish sequences obtained using the Ensembl genome browser, and following the steps outlined in section *3.2.2.3*. Primer sequences used are shown in Table 4.1. PCR amplification of zebrafish mRNA transcripts was performed as described in section *3.2.2.4* and quantification of zebrafish target transcripts were performed *via* qPCR as described in section *3.2.3*.

Table 4.1 Zebrafish primer sequences (5’ to 3’)		
Gene	**Forward primer sequence**	**Reverse primer sequence**
rbbp9	CCTGTAACGGCCAGAGAGAG	GTCCGATGATGAGCGTTTCT
tp53	GCGAGCAAATTACAGGGAAG	CAGTTGTCCATTCAGCACCA
actb1	CCCAGACATCAGGGAGTGAT	CACAATACCGTGCTCAATGG
eef1a1	GATGGCACGGTGACAACAT	ACCGCTAGCATTACCCTCCT

4.2.7. Western blot detection of Rbbp9 protein in zebrafish.

Untreated zebrafish embryos at 24 hpf were resuspended in calcium free Ringers solution (116 mM NaCl, 2.9 mM KCl, and 5 mM HEPES, pH 7.2) on ice to isolate the yolk sac from the embryo. Samples were centrifuged (500 × *g,* 5 minutes, 4 °C) and the supernatant (containing the yolk sac) was removed leaving the pellet containing the zebrafish larvae. The pellet was washed with 1 X PBS on ice, centrifuged (500 × *g,* 5 minutes, 4 °C), the supernatant removed and the remaining pellet resuspended in RIPA buffer containing 50 mM Tris-HCl, 150 mM NaCl, 1 mM EDTA, 1% Triton-X-100, 1% sodium deoxycholate, 0.1% SDS, and protease inhibitors (Promega). Lysed samples were then centrifuged at 18,000 × *g,* 20 minutes, 4 °C.

Protein estimations were performed as described in section *3.2.8.1*; 1-DE and Western blotting performed as described in section *3.2.8.2*. Transferred membranes were probed overnight with a 1/1,000 dilution of either an anti-RBBP9 rabbit polyclonal antibody (Proteintech, Chicago IL, USA), or an anti-alpha tubulin [EP1332Y] rabbit monoclonal antibody (Abcam, Massachusetts, USA). Membranes were then washed twice with 1 X PBST for 15 minutes and probed with a 1/2,500 dilution of anti-rabbit IgG peroxidase raised in goat HRP (Sigma Aldrich) secondary antibody for 1 hour at room temperature. Membranes were then washed twice with 1 X PBST for 15 minutes, followed by 1 X PBS wash for 15 minutes before exposure to the Luminata Cresendo Western HRP Substrate (Merck Millipore) and imaging as detailed in section *3.2.8.6.*

4.2.8. Histology.

4.2.8.1. Paraffin embedding.

Treated zebrafish larvae were fixed in 4% PFA for 1 week, then washed twice in 1 X PBS and embedded and secured in a 1% agarose block to prevent loss of zebrafish during automated processing. The 1% agarose block with zebrafish underwent dehydration and paraffin infiltration using a Ziess Microm STP120 Automated Tissue Processor (Ziess, North Ryde, Australia) and the following settings: 50% EtOH, 3 hours; 70% EtOH, 1 hour; 80% EtOH, 1 hour; 95% EtOH, 1 hour (twice); 100% EtOH, 1 hour (twice); Xylene, 1 hour; Xylene, 2 hours (twice); and paraffin at 60 °C, 2 hours (twice). The paraffin-infiltrated samples were then embedded into a paraffin block and solidified with a minimum time of 2 hours at -9 °C. Serial sections of 8 μM thickness were produced from the paraffin block using a microtome (Thermo Scientific). Paraffin ribbons were placed into a water bath held at 30 °C and captured using a glass slide (Sail, Wetherill Park, Australia). Slides were dried overnight at 30 °C in an oven prior to staining procedures.

4.2.8.2. Haemotoxylin and Eosin (H & E) staining and imaging.

Slides with sectioned material were rehydrated using the following procedure adapted from (Sabaliauskas et al., 2006): xylene, 15 minutes (twice); 100% EtOH, 2 minutes (twice); 95% EtOH, 3 minutes; and 70% EtOH, 2 minutes. Slides were then rinsed in dH_2O and stained with Haematoxylin for 3 minutes, rinsed with cool running tap water for 2 minutes, then dipped into acid alcohol (0.5% HCl in 70% EtOH) 4 times to de-stain the slides. Slides were further developed by brief exposure to Scott's bluing solution for 30 seconds, stained with Eosin for 40 seconds, and then dipped in dH_2O until all excess Eosin was removed. Slides were then dehydrated with 10 × dips in 70% EtOH, 10 × dips in 95% EtOH, equilibrated in 100% EtOH for 2 minutes, and finally briefly exposed to Xylene twice. Slides were then dried, and coverslips were applied to the slides using DPX as an adhering agent. Slides were imaged using a Ziess Apo Tome Microscope (Ziess), and virtual tissue images captured using Stereo Investigator version 11 software (MBF Biosciences, Williston, USA). Images were then compared at similar sections for morphological similarities and differences brought upon by ML114 treatment. Histological images of the acellular space surrounding the brain were determined by measuring 3 lines from the border of the brain (near the white matter, as indicated by pink staining) to the outer margin of the head at 3 separate landmarks and measuring 3 lines from landmarks near the white matter (parallel to lower body anatomy of zebrafish marked by chondrocraniumm and gastrointestinal tract) to cells of the chondrocranium (indicated by purple stain) then averaged. Statistical-significance was determined using a paired student's t-Test.

4.2.9. Morpholino targeted gene knockdown.

4.2.9.1. Morpholino oligonucleotide preparation.

Translation-blocking morpholino oligonucleotides were generated by Gene Tools (Oregon, USA) based on the specific rbbp9 sequence obtained as described above, and resuspended in dH_2O.

rbbp9 (5' TCACAACTCTCTTCA GAGGCATTAT 3')

tp53 (5' GCGCCATTTGCTTTGC AAGAATTG 3')

4.2.9.2. Preparation and calibration of microinjection pipettes.

Borosilicate glass pipette needles were freshly pulled prior to each microinjection. To do this, 10 cm long (1.0 mm OD, 0.78 mm ID), thin-wall borosilicate glass capillaries (Sutter Instrument Co., Novato, CA, USA) were placed into a Flaming/Brown micropipette puller, Model P-97 (Sutter Instrument Co.) and pulled under the following parameters: heat = 645; pull = 60; and velocity = 80 (Dean, 2006). Prior to use microinjection pipettes were broken at the tip with Dumostar #5 fine point tweezers (Electron Microscopy Sciences). Pipettes were then backfilled with 0.05% phenol red or 0.3 X Danieau Buffer and the volume delivered from them calibrated using an Olympus stereomicroscope SZ61 (Olympus), a MP-285 micromanipulator (Sutter Instrument Co.), and injection pressure controlled by a PLI-100 Picoinjector microinjection system (Harvard Apparatus, Massachusetts, USA). Injection pressure was adjusted to obtain a consistent injection volume of 4 nL calculated by measuring droplet size in mineral oil over a micrometer (Rosen et al., 2009). This volume was selected based on the total volume of zebrafish embryo at the 1-2 cell stage (Leung et al., 1998).

4.2.9.4. Morpholino injection and observations.

To determine optimal working concentration, morpholino's at a stock concentration of 1 mM were resuspended into working concentrations ranging from 8-16 ng. Prepared micropipettes were backfilled with 0.05% phenol red as a control, or morpholino in 0.3 X Danieau Buffer containing 17.4 mM NaCl, 0.21 mM KCl, 0.12 mM $MgSO_4 \cdot 7H_2O$, 0.18 mM $Ca(NO_3)_2$, 1.5 mM HEPES, pH 7.4 (Timme-Laragy et al., 2012). Fertilised zebrafish embryos at the 1-2 cell stage were injected with *rbbp9* and/or *tp53* morpholino. Injected embryos were maintained for 7 days as described in 4.2.1 with daily E3 medium changes. Zebrafish imaged at 24 hpf and 7 dpf as described in 4.2.3 before being fixed with 4% PFA for 1 week for downstream applications.

4.3. RESULTS

4.3.1. *rbbp9* is expressed by TAB zebrafish.

As a first step towards determining whether Rbbp9 SH is required during embryonic development of TAB strain zebrafish, embryos at various stages of early development were tested for *rbbp9* expression. Due to known differences in genomic sequences between different zebrafish strains (Coe et al., 2009), the precise genomic *rbbp9* sequence for the TAB strain used here was obtained through DNA sequencing (Figure 4.1). Based on this sequence, PCR analysis of *rbbp9* expression was performed across various stages of zebrafish embryonic development. These analyses confirmed expression of *rbbp9* transcripts during the early stages of zebrafish development from the 1-2 cell stage through to 7 dpf (Figure 4.2).

A

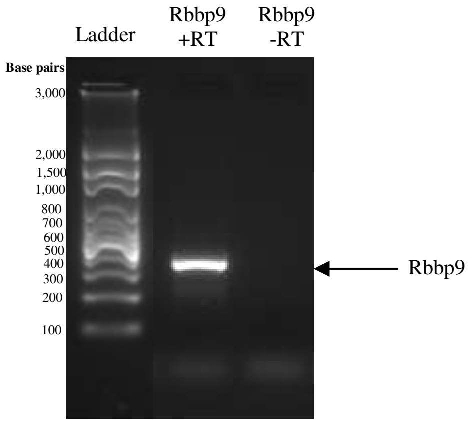

B

Danio rerio retinoblastoma binding protein 9 (rbbp9), mRNA
Sequence ID: **ref|NM_001042748.1|** Length: 1390 Number of Matches: 1
Range 1: 89 to 258

Score	Expect	Identities	Gaps	Strand	Frame
261 bits(141)	1e-65()	161/170(95%)	4/170(2%)	Plus/Plus	

Features:

```
Query  7    GTCGGAG-AGTT--AACTCAGAGC-AGATGGCGGACTGACCTCAAGGAGGCGCTGCGCTG  62
Sbjct  89   GTCGGAGAAGTTAAAACTCAGAGCAAGATGGCGGACTGACCTCCAGGAGGCGCTGCGCTG  148
Query  63   CGGAATATCGCTCCACATGCCGTCTGGGGTGTTTCCGTGTATGAGTTTTTGAGTAAGGAG  122
Sbjct  149  CGGAATATCGCTCCACATGCCGTCTGGGGTGTTTCCGTGTATGAGTTTTTGAGTAAGGAG  208
Query  123  CTGGATTTTTCTGTTAAAATGCCTCTGAAGAAAGTTGTGATTGTGTCTGG  172
Sbjct  209  CTGGATTTTGCTGTTATAATGCCTCTGAAGAGAGTTGTGATTGTGCCTGG  258
```

C

Danio rerio retinoblastoma binding protein 9 (rbbp9), mRNA
Sequence ID: **ref|NM_001042748.1|** Length: 1390 Number of Matches: 1
Range 1: 183 to 322

Score	Expect	Identities	Gaps	Strand	Frame
191 bits(103)	2e-44()	128/140(91%)	1/140(0%)	Plus/Minus	

Features:

```
Query  49   CTCATTTATTCGTTTGTTGGCCCATCCGTACAAGTTGCTACGCTCAACATCCCCTGCGCC  108
Sbjct  322  CTCATTTATTCGTTTGTTGGCCCATCCGTACCAGTTGCTACGCTCAACATCTCCTGCGCC  263
Query  109  GTTCCAAGGCACAATCACAACTCTCTTCACAGGCATTTTAACAGAAAAATCAAGCTCTTT  168
Sbjct  262  GTTCCCAGGCACAATCACAACTCTCTTCAGAGGCATTATAACAGCAAAATCCAGCTCCTT  203
Query  169  AATCAAAATCTTATAC-CGG  187
Sbjct  202  ACTCAAAAACTCATACACGG  183
```

Figure 4.1 Rbbp9 DNA sequence is conserved in TAB strain zebrafish. A) Rbbp9 transcripts detected in genomic DNA (gDNA) of adult zebrafish. **B)** DNA sequencing revealed a match for Rbbp9 sequences from online databases (National Centre for Biotechnology Information, NCBI) for **B)** forward (5'-3') and **C)** reverse primer (3'-5'). Where 'Query' = primer sequences input to verify detection of gene primer has been designed to detect by comparing with 'Sbjct' = annotated mRNA sequences.

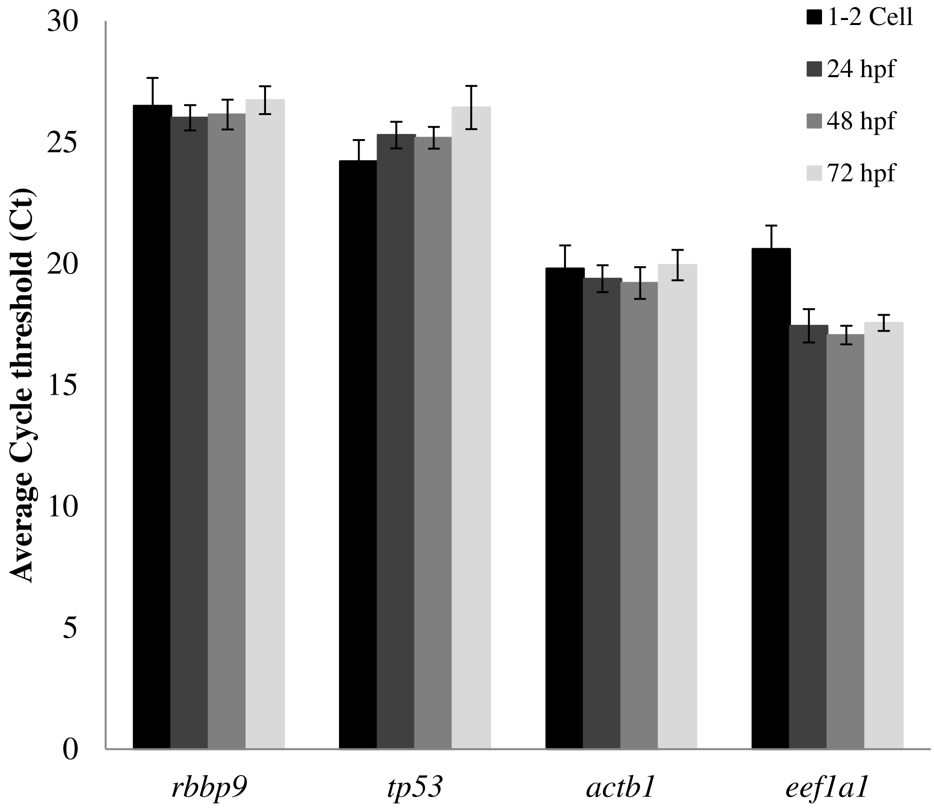

Figure 4.2 Early-stage zebrafish larvae express *rbbp9* and *tp53* transcripts. Zebrafish larvae express *rbbp9* and *tp53* genes as well as the housekeeping genes *actb1* and *eef1a1* from the 1-2 cell stage immediately post fertilisation through to 72 hpf. (n = 3).

To investigate expression of Rbbp9 protein in developing zebrafish, Western blot analysis was performed using an antibody previously shown by our group to detect human RBBP9 protein (O'Connor et al., 2011). Comparison of human and zebrafish Rbbp9 protein sequences identified 67% of residues fully conserved across the entire protein sequence between the two species. Within the N-terminal region detected by the Rbbp9 antibody 55% of the sequence contained conserved residues between human and zebrafish (Figure 4.3 A). Despite this similarity, Western blotting of 24 hpf zebrafish embryos using the validated anti-human RBBP9 antibody revealed a large amount of non-specific binding due to the primary but not secondary antibody, with no band corresponding to the predicted Rbbp9 molecular weight (Figure 4.3 B-C). This outcome necessitated detection of *rbbp9 via* mRNA levels for subsequent analyses.

4.3.2. ML114 treatment affects zebrafish development.

To test whether ML114 treatment affected zebrafish development, zebrafish embryos were treated with ML114, ML114 soluble fragment, or DMSO. Embryos were exposed to a range of ML114 and soluble fragment concentrations compared to DMSO using standard zebrafish embryo maintenance medium (E3). With no treatment at all (i.e., maintenance in E3 medium alone), approximately 65% of zebrafish embryos were alive at 24 hpf (Figure 4.4). Similarly, approximately 60-65% of zebrafish embryos treated with 0.25% DMSO, or DMSO plus 100 µM soluble ML114 fragment also survived after 24 hpf (Figure 4.4). A small but statistically-significant decrease in embryo viability was seen at 24 hpf, with control, 25 µM and 100 µM ML114.

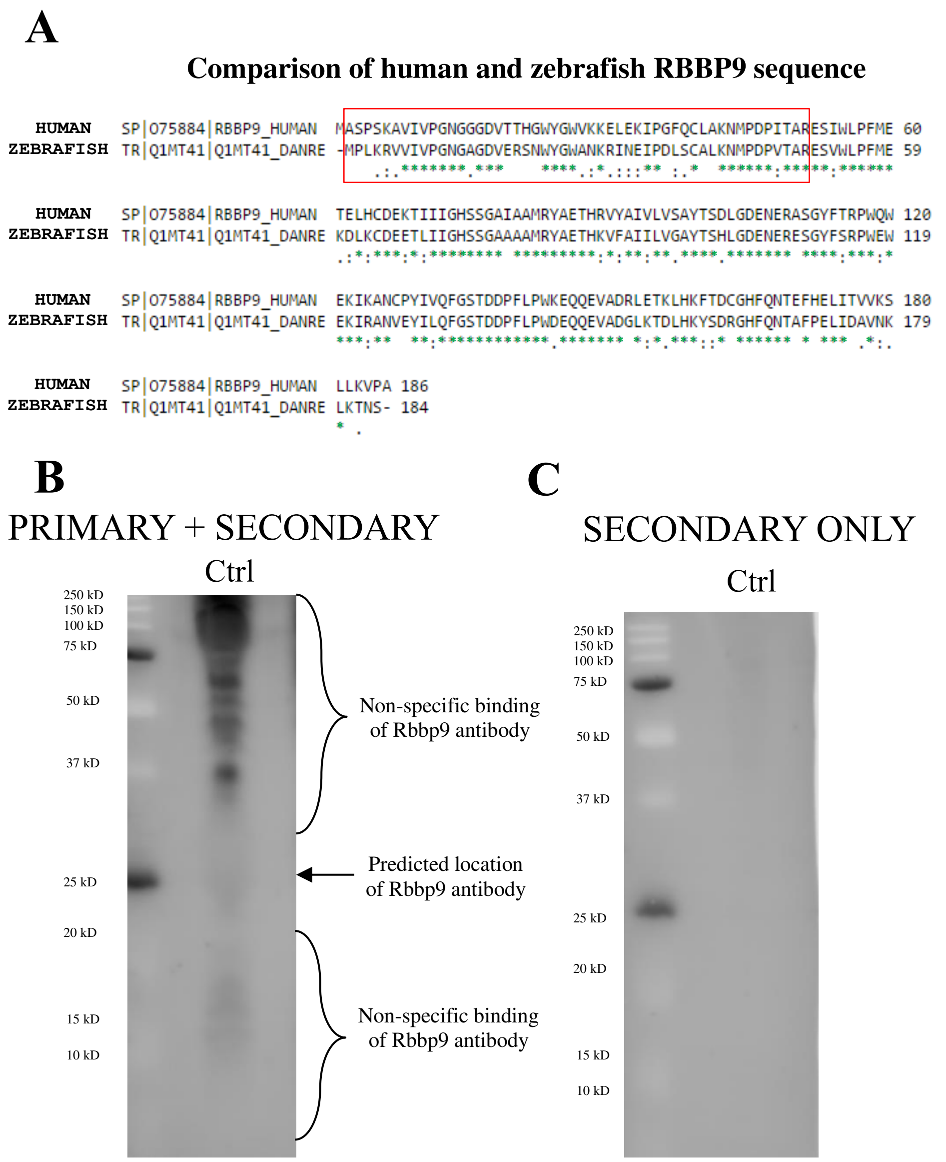

Figure 4.3 Protein expression of RBBP9 in zebrafish. A) RBBP9 protein sequence comparison between human and zebrafish (Universal Protein Resource, UniProt). Where '*****' indicates positions which have a single, fully conserved residue between human and zebrafish (67%), '**:**' indicates conservation between groups of strongly similar properties, '**.**' indicates conservation between groups of weakly similar properties (7.6%), and the '**blank space**' indicating non-conserved residues (12.6%). The red box corresponds to a region within the N-terminal amino acids 2-51 where the antibody was raised to detect. Within this region 55% of the sequence is conserved between human and zebrafish Rbbp9 sequences **B)** Western blot of 24 hpf untreated zebrafish lysate to detect RBBP9 protein using anti-RBBP9 antibody, and anti-rabbit secondary antibody, and **C)** Anti-rabbit secondary antibody only control.

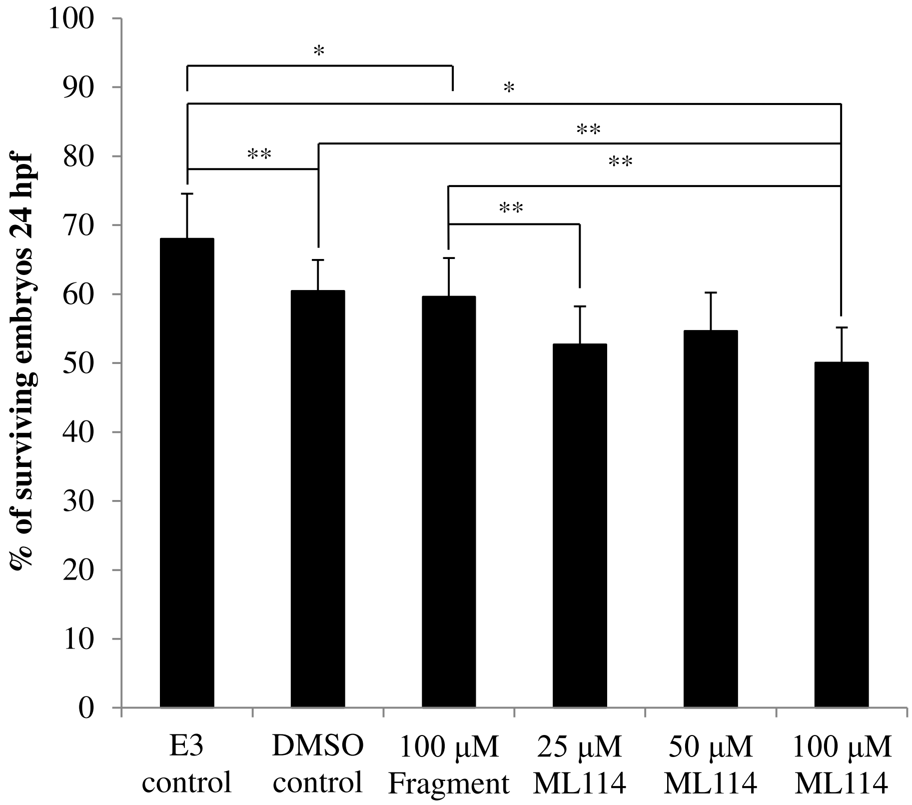

Figure 4.4 Survival of treated zebrafish 24 hpf. Zebrafish treated with higher concentrations of ML114 have a significantly reduced rate of survival 24 hpf compared to control treated zebrafish. E3 control (n=12), DMSO control (n=33), 100 µM Fragment (n=29), 25 µM- (n=24), 50 µM- (n=24) and 100 µM-ML114 (n=33); * p < 0.05, ** p < 0.01.

However, as over half of the embryos treated with higher concentrations of ML114 (~50-55%) were still viable at 24 hpf, the effects of ML114 treatment on zebrafish embryo development could be observed.

Phenotypic differences were visible at 24 hpf between zebrafish embryos treated with either DMSO or 100 μM ML114 soluble fragment, and those embryos treated with 100 μM ML114 (Figure 4.5). This included shorter overall body length, reduced area (and possibly pigmentation) of the eye, but no significant change in size of the pericardial cavity (Figure 4.6). As at 24 hpf, embryos treated for 7 days with DMSO and 100 μM soluble ML114 fragment developed normally (Figure 4.7 A-D). In contrast, zebrafish treated with ML114 for 7 days showed gross anatomical changes (Figure 4.7 E-H). Body length and eye area was still significantly smaller in the ML114-treated embryos, though pigmentation levels seemed similar. The size of the pericardial cavity was significantly increased compared to DMSO- and soluble fragment-treated embryos (Figure 4.8). However, all the treated embryos had functioning hearts as seen by movement of blood cells. By 7 dpf control-treated zebrafish larvae had lost their yolk sac and developed in place a well-defined gastrointestinal tract (Figure 4.7 A-B). In contrast, zebrafish treated with ML114 had an enlarged gastrointestinal cavity with poorly-developed gastrointestinal tissue (Figures 4.7 C-D and 4.8 D). Changes due to ML114-treatment were observed at all concentrations, but were pronounced with higher concentrations.

Histological analyses of DMSO- and ML114-treated zebrafish larvae 7 dpf was performed to identify anatomical and cellular changes responsible for the morphological differences observed *via* live imaging. Representative brightfield images and H & E stained sections showed changes in cellular morphology between control- and ML114-treated zebrafish that were consistent with the changes observed *via* whole animal imaging (Figure 4.9). For example, ML114 treatment reduced eye size and altered eye anatomy (Figure 4.9 and 4.10). All layers of the eye appeared to be present including; the outer plexiform layer, ganglion cell layer, inner plexiform layer, inner nuclear layer, outer nuclear layer, inner segment/outer segment of photoreceptor cells, and retinal epithelial cells. However, arrangement of cells within the layers of the eye appeared to be less organised and smaller in size after exposure to ML114-treatment compared with the even distribution of these layers seen in control-treated zebrafish (Figure 4.10 A-B).

ML114 treatment also resulted in muscle fibres which appeared to have a more disorganised arrangement compared to the expected parallel alignment of muscle fibres seen with control-treated zebrafish (Figure 4.10 C-D). In addition, differences in development of the gastrointestinal tract were also seen with ML114-treated zebrafish. The area previously occupied by the yolk sac in control-treated embryos had been replaced by the gastrointestinal tract (Figure 4.10 E). In contrast, ML114-treated embryos displayed enlarged gastrointestinal spaces and abnormal looking gastrointestinal tissue (Figure 4.10 F). Interestingly, zebrafish brain development also appeared to be affected by ML114 treatment. Similarities in morphological landmarks such as white- (represented by pink stain) and grey-matter (represented by purple stain) were present between the two treatments. However, the grey matter arrangement appeared to be more disorganised in ML114-treated zebrafish compared to the neat and tightly packed arrangement of the grey matter seen in DMSO control-treated zebrafish (Figure 11 A-D). A significant difference was also seen in acellular space surrounding the brain between DMSO control- and ML114-treated zebrafish at 7 dpf (Figure 4.11 E).

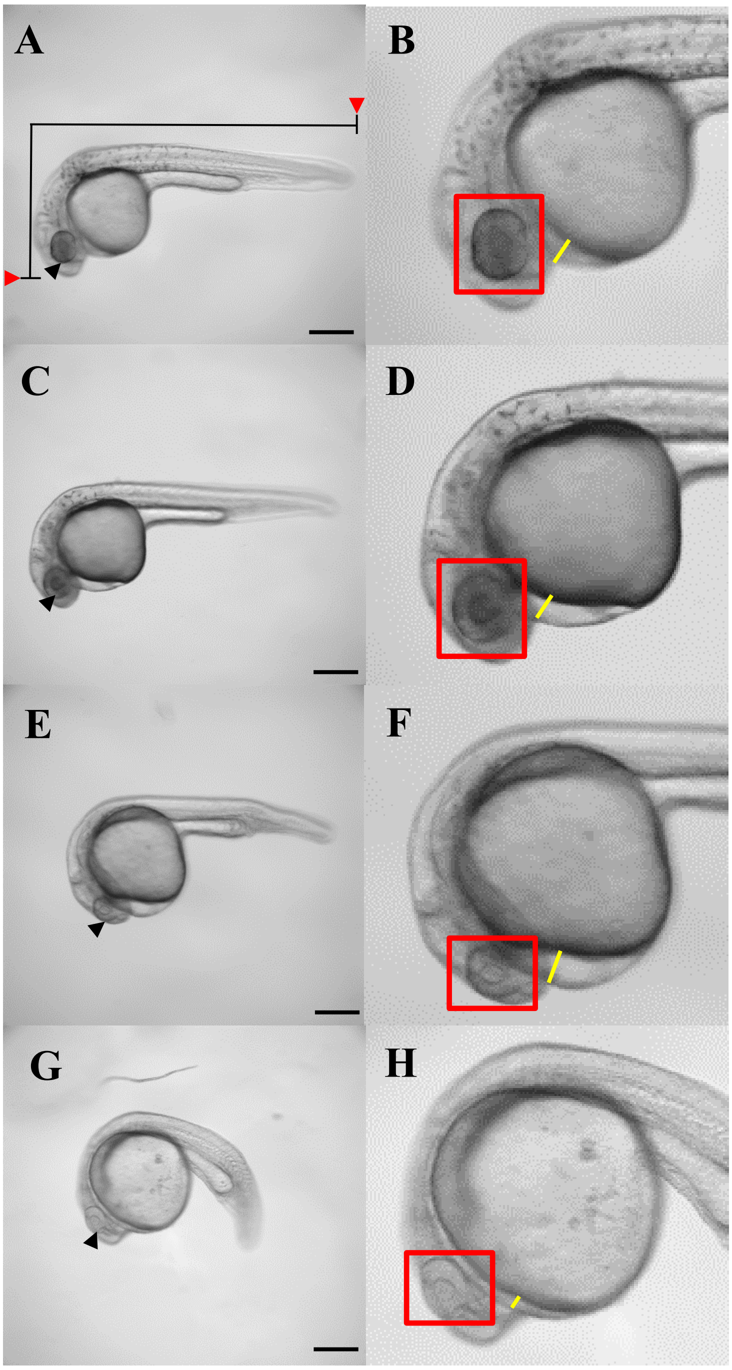

Figure 4.5 ML114 affects embryonic development 24 hpf. Representative images of treated zebrafish demonstrate phenotypic differences 24 hpf, where; **A-B)** DMSO control- and **C-D)** 100 µM ML114 soluble fragment-treated zebrafish display no developmental abnormalities whilst, **E-F)** 50 µM and **G-H)** 100 µM ML114-treated zebrafish show visible developmental differences in; body length and shape (red arrows) and stage of eye development (black arrows and red boxes), with no differences observed in pericardial cavity space (yellow lines). Scale bar = 200 µM.

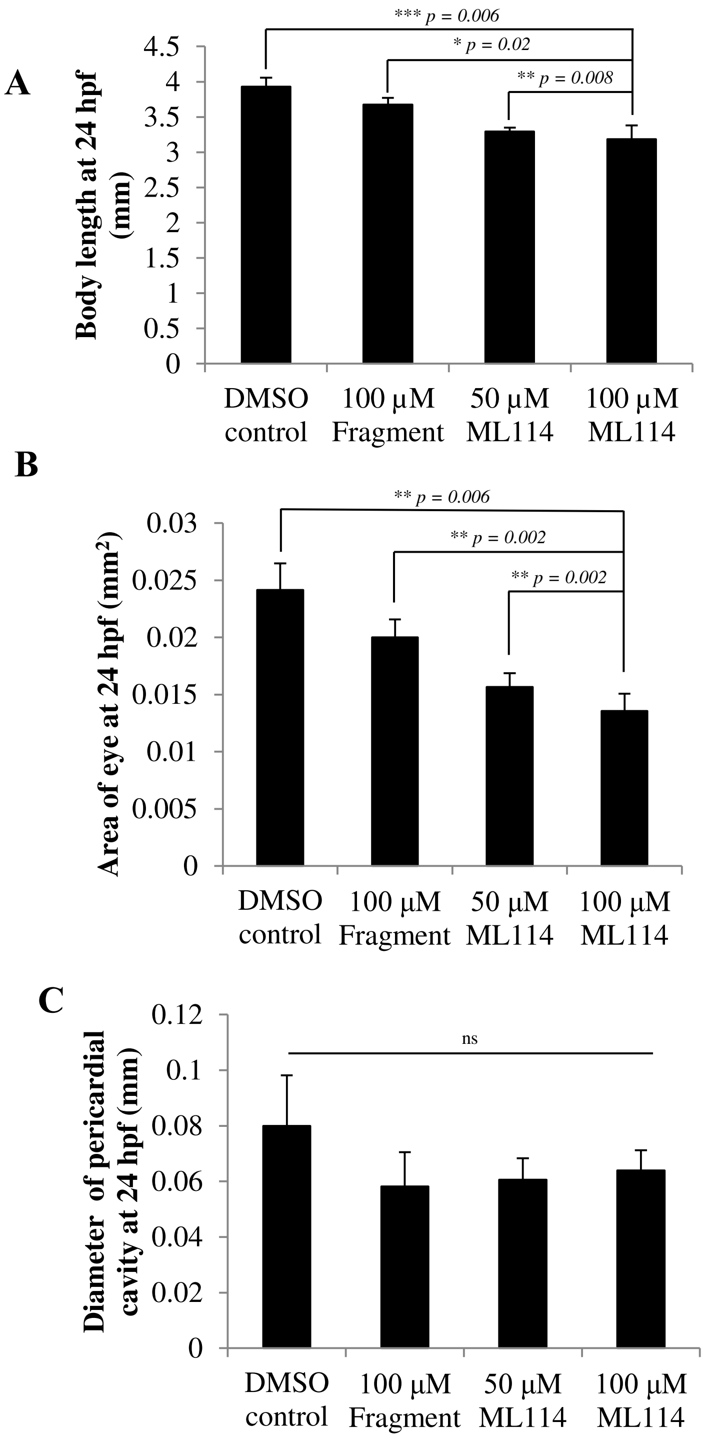

Figure 4.6 ML114 affects embryonic development of body and eye 24 hpf. Zebrafish treated with ML114 (50-100 µM) appeared to be behind in overall development at 24 hpf compared to control treated zebrafish (DMSO- and 100 µM ML114 soluble fragment. Differences were observed with treated zebrafish demonstrating; **A)** a shorter body length, and **B)** smaller eyes, **C)** with no differences in pericardial cavity. No differences were observed between DMSO-control and 100 µM ML114 soluble fragment treated zebrafish 24 hpf. DMSO-control (n=7), 100 µM ML114 soluble fragment (n=5), 50 µM ML114 (n=3), and 100 µM ML114 (n=7).

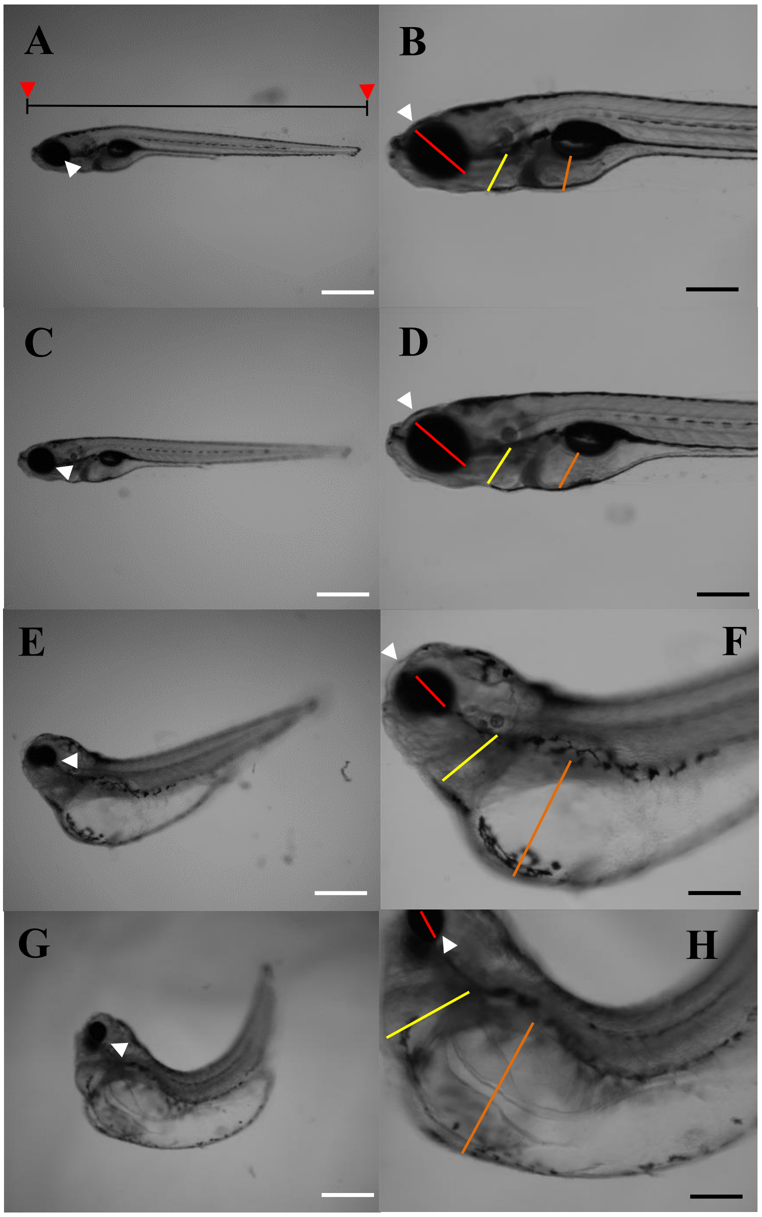

Figure 4.7 Anatomical changes resulting from ML114 treatment 7 dpf. Representative images of treated zebrafish demonstrate phenotypic differences 7 dpf, where; **A)** DMSO control- and **B)** 100 µM ML114 soluble fragment treated zebrafish display no developmental abnormalities whilst, **C)** 50 µM and **D)** 100 µM ML114-treated zebrafish exhibit developmental abnormalities with apparent differences in eye (red arrows), pericardial cavity space (yellow lines), yolk sac (orange lines) as well as body shape and size (white arrows and red lines). White scale bars = 600 µM and black scale bars = 300 µM.

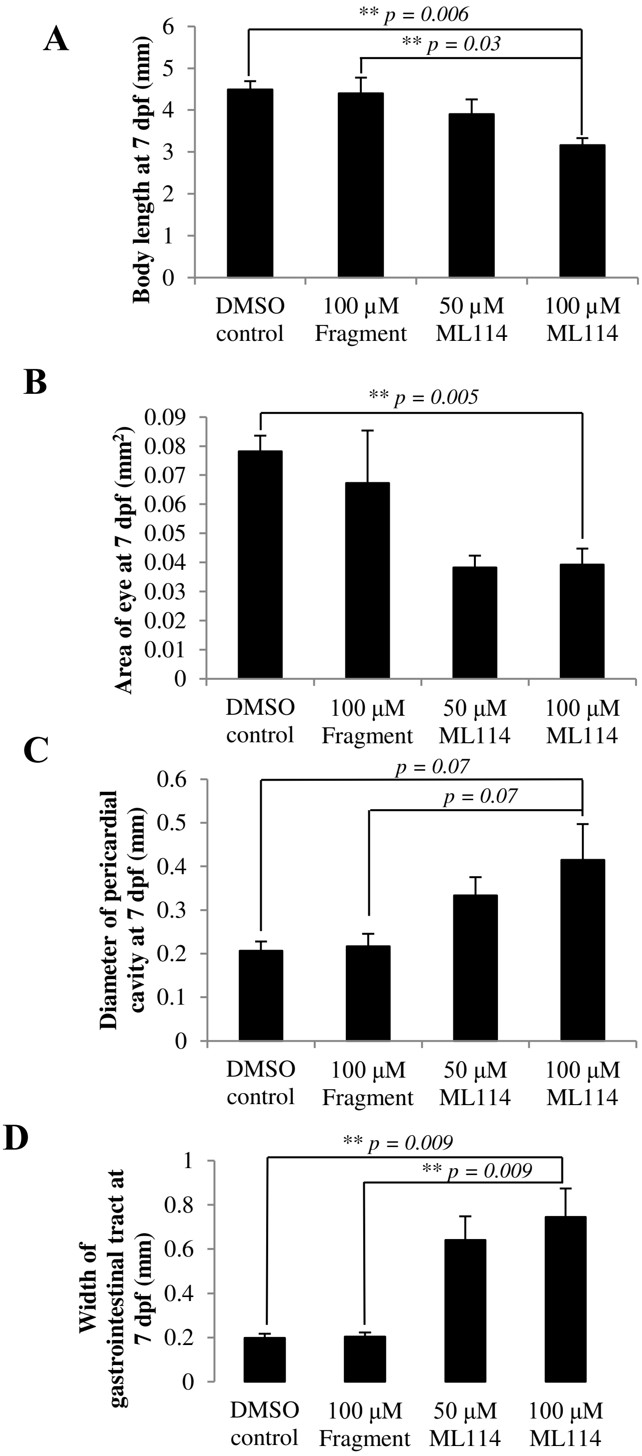

Figure 4.8 ML114 affects embryonic development 7 dpf. Treated zebrafish (50 µM and 100 µM ML114) were found to have severe developmental abnormalities. Treated zebrafish display; **A)** significantly shorter body length due to curvature, **B)** smaller eyes, **C)** increased pericardial cavity, and **D)** increased gastrointestinal space compared to DMSO-control and 100 µM ML114 soluble fragment-treated zebrafish 7 dpf which had no significant differences. DMSO-control (n=5), 100 µM ML114 soluble fragment (n=4), 50 µM ML114 (n=3), and 100 µM ML114 (n=5).

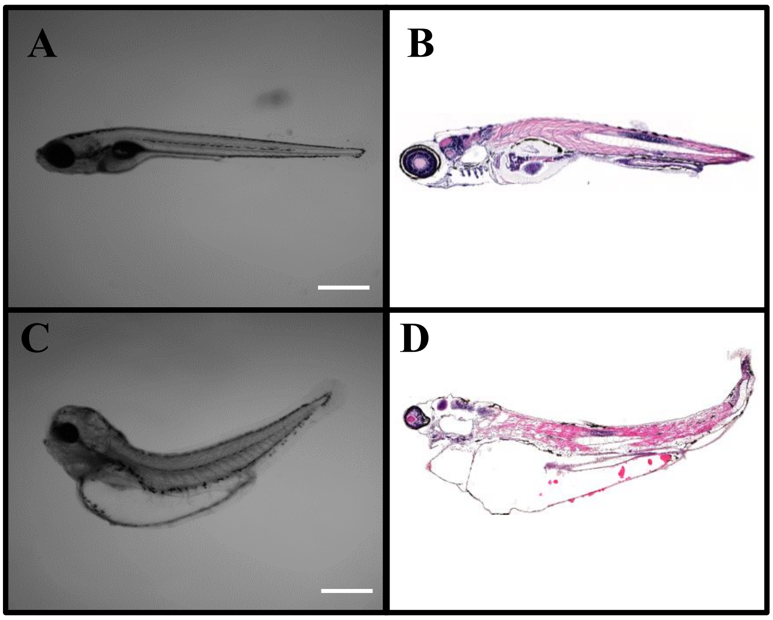

Figure 4.9 Histological representations of developmental changes in ML114-treated zebrafish 7 dpf. Histological analysis of treated zebrafish 7 dpf show morphological differences between **A-B)** DMSO control-, and **C-D)** 100 µM ML114-treatments. Representative images demonstrate changes in muscle fibre distribution, cellular distribution in zebrafish eye, and differences in size of pericardial space, and yolk sac. White scale bar = 600 µm.

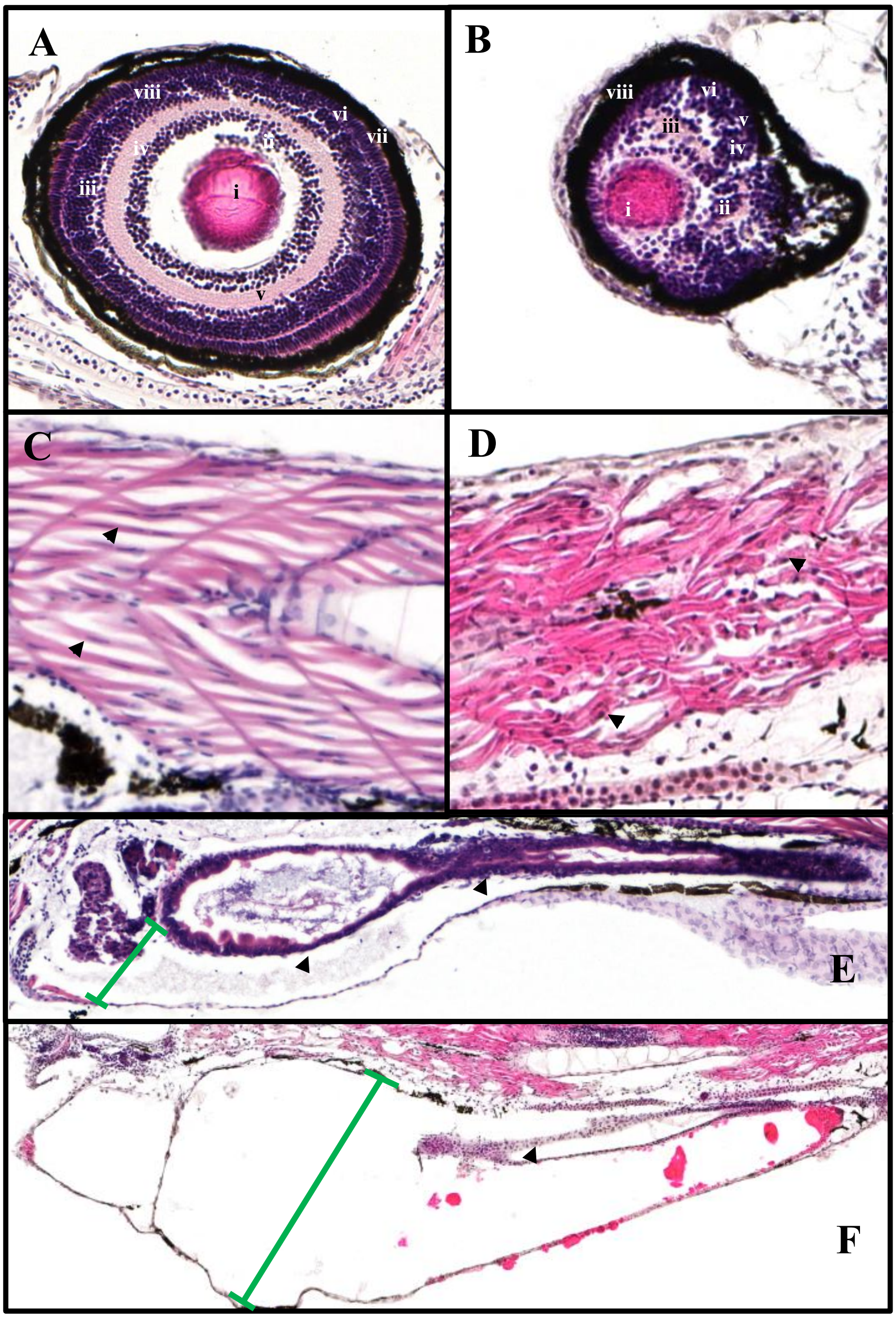

Figure 4.10 Morphological changes due to ML114 treatment at 7 dpf. Histological analysis of treated zebrafish 7 dpf show morphological differences between; **A, C, E)** DMSO control-, and **B, D, F)** 100 µM ML114-treatments. Representative images demonstrate changes in; **A-B)** cellular distribution in zebrafish eye, where all layers of the eye were present in both DMSO control- and ML114-treated zebrafish larvae: showing all layers including: i) lens, ii) ganglion cell layer, iii) inner plexiform layer, iv) inner nuclear layer, v) outer plexiform layer, vi) outer nuclear layer, vii) inner segment/outer segment of photoreceptor cells, and viii) retinal pigment epithelium. However, zebrafish treated with ML114 is missing the inner segment/outer segment of photoreceptor cells. Changes were also shown in: **C-D)** muscle fibre distribution where DMSO control- zebrafish show parallel alignment of normal muscle fibres, whereas ML114-treated zebrafish muscle arrangement do not follow this pattern (black arrows), and **E-F)** differences in size of pericardial space, yolk sac size (green lines) and gastrointestinal tract (black arrows).

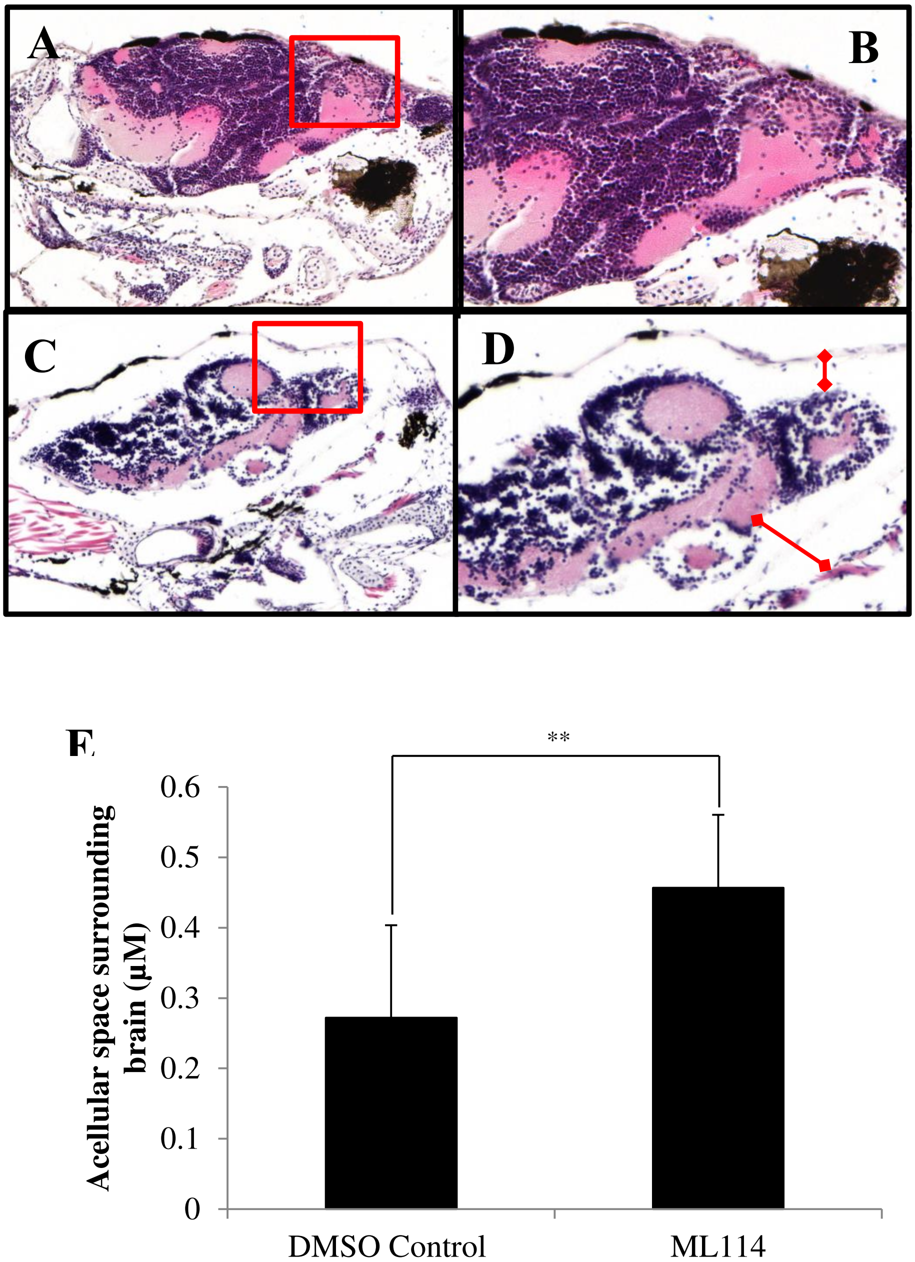

Figure 4.11 Increases in acellular space surrounding brain due to ML114 treatment at 7 dpf. Histological analysis of treated zebrafish 7 dpf show lack of acellular space (red lines) surrounding the brains white- (pink stain) and grey-matter (purple stain) (red boxes) in **A-B)** DMSO control-, when compared to **C-D)** 100 µM ML114-treatments. **E)** Significant differences were seen in the acellular space surrounding the brain between DMSO control- and ML114 treatments. (n=3; ** p = 0.01).

4.3.3. Effect of *rbbp9* and *p53* morpholino's in developing zebrafish.

To investigate whether the observed anatomical and histological changes resulting from ML114 treatment might be due to p53-related stress responses, *p53* transcript levels were assessed in control- and ML114-treated zebrafish embryos at 24 hpf and 7 dpf. These analyses showed no significant increase in *p53* expression in zebrafish across all treatments (Figure 4.12). To identify the effects of Rbbp9 protein loss in zebrafish development, a translation-blocking morpholino (Summerton, 1999) was obtained based on the DNA sequence of the TAB strain zebrafish identified in this study (Figure 4.1). Morpholinos with a FITC tag were used to allow for visualisation of morpholino location in the developing zebrafish embryo after microinjection. Zebrafish embryos injected with phenol red but no morpholino showed no fluorescence at 24 hpf or 7 dpf, and did not present any phenotypic abnormalities (Figure 4.13 A-B and 4.14 A-B). In contrast, embryos injected with *rbbp9* morpholino's showed fluorescence indicating the presence of morpholino's within the developing embryos. Additionally, these embryos showed phenotypic abnormalities proportional to the amount of morpholino used (Figure 4.13 and 4.14). For instance embryos injected with 16 ng of *rbbp9* morpholino showed changes most similar to those seen with ML114 treatment at 24 hpf, such as lack of eye pigmentation (Figure 4.13 E-F). At 7 dpf (Figure 4.14), zebrafish treated with both 8 ng and 16 ng of *rbbp9* morpholino showed changes consistent with ML114 treatment. This included decreased body size, decreased eye size, and abnormal gastrointestinal tract anatomy (Figure 4.15 A-B). Some variation in the degree of these changes was observed, such that statistically-significant changes were only seen with 16 ng of *rbbp9* morpholino. A slight but statistically insignificant difference was noted in the pericardial and gastrointestinal cavity (Figure 4.15 C-D) and a functioning heart was observed moving blood cells in the morpholino-treated zebrafish.

Histological analyses of zebrafish embryos at 7 dpf revealed that embryos injected with the *rbbp9* morpholino had some anatomical changes similar to those seen with ML114 treatment (Figure 4.16)**.** Unlike ML114-treatment, histological analyses showed normal organisation of the eye layers in both control- and *rbbp9* morpholino treated zebrafish (Figure 4.17 A,C,E). However, shortened body length due to *rbbp9* morpholino treatment was accompanied by loosely assembled and disorganised muscle fibres similar to that seen with ML114 treatment (Figure 4.17 B, D, F). Differences in development of the gastrointestinal tract were also seen that were comparable to the changes seen with ML114-treated zebrafish. With the microinjection control, the gastrointestinal cavity was the expected size and contained properly-formed gastrointestinal tissue (Figure 4.18 A). However, *rbbp9* morpholino-treated zebrafish had an enlarged gastrointestinal cavity with large amounts of acellular space (Figure 4.18 C-B). Additionally, the cellular tissues within the gastrointestinal space of the *rbbp9* morpholino-treated zebrafish looked abnormal in morphology compared to the control-treated zebrafish. Interestingly, comparison of brain development in the controls (DMSO and phenol red) showed brain development was affected by loss of Rbbp9 activity *via* 100 μM ML114, 8 ng- and 16 ng *rbbp9*-morpholino. The positioning of morphological landmarks of the brain appear to be similar such as white matter (represented by pink stain), however there appears to be more acellular space surrounding the grey matter (represented by purple stain) in zebrafish with loss of Rbbp9 (Figure 4.19 A-F). Investigation of the head showed acellular space surrounding the brain in *rbbp9* morpholino treated zebrafish, an effect not seen in control–treated zebrafish. This difference in acellular space surrounding the brain was significant in both 8 ng- and 16 ng *rbbp9* morpholino-treated zebrafish (Figure 4.19 G).

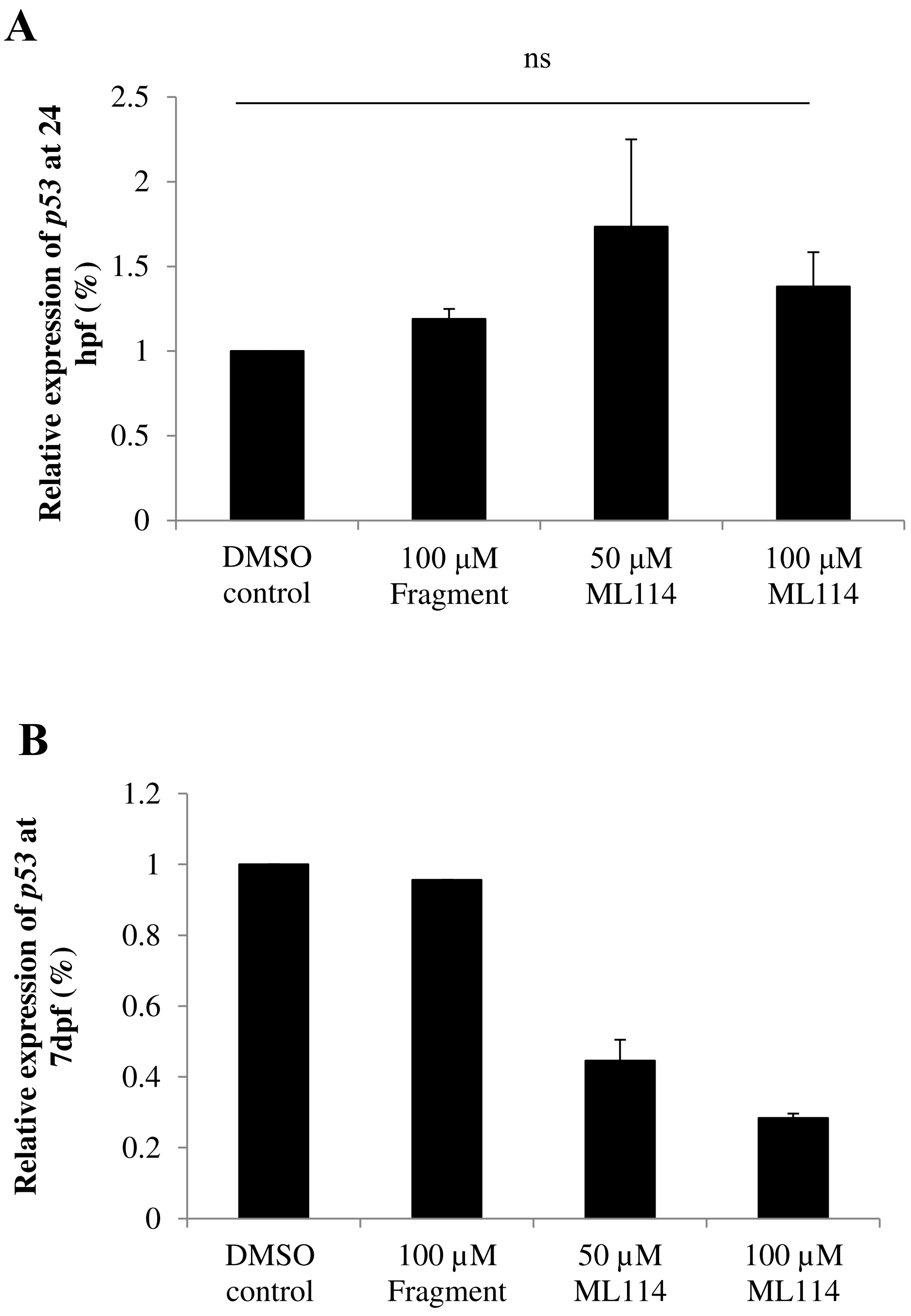

Figure 4.12 ML114-treatment does not up-regulate *p53* mRNA expression. A) ML114-treatment does not significantly up-regulate expression of *p53* 24 hpf across all treatments using *actb1* as a housekeeping control. (n=3), **B)** ML114-treatment does not result in increased *p53* mRNA expression using *actb1* as a housekeeping control. (n=2).

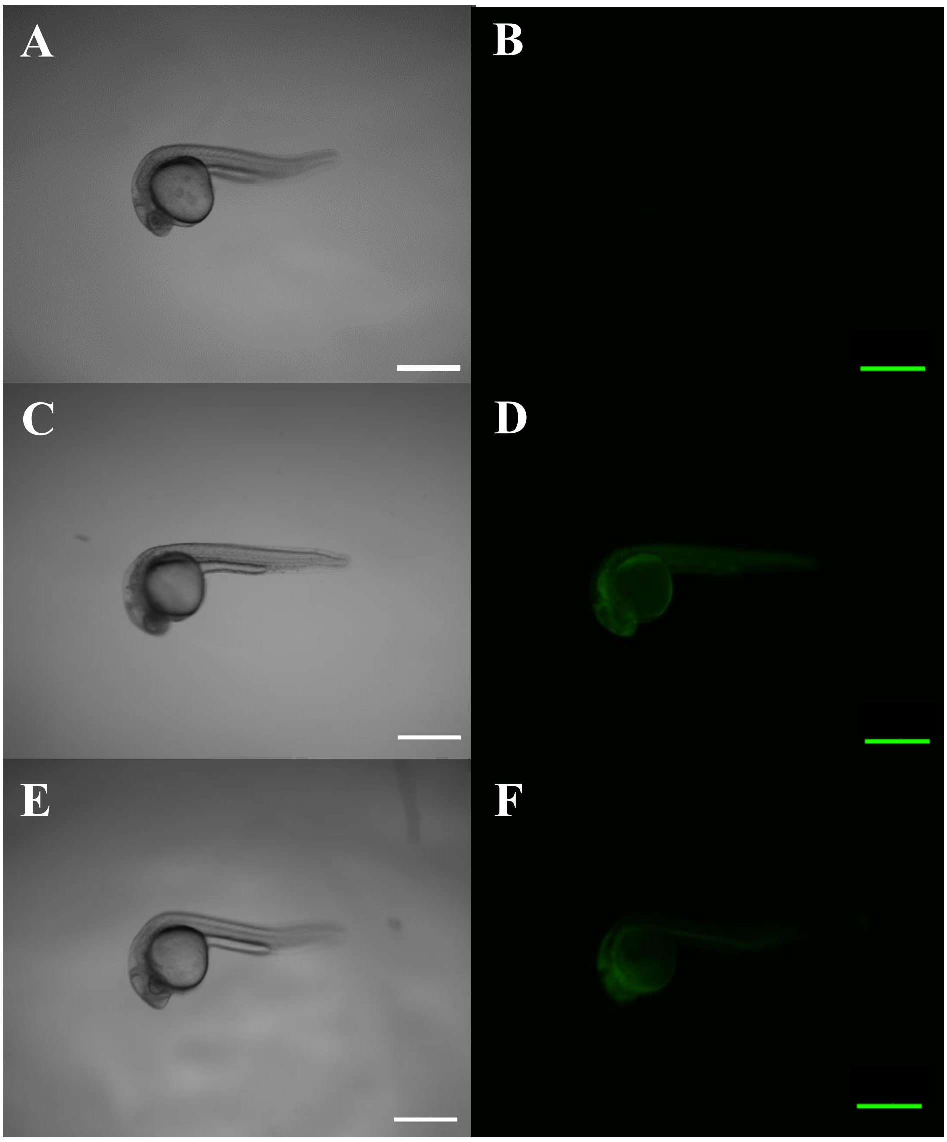

Figure 4.13 *rbbp9* morpholino affects embryonic development 24 hpf. Representative images of zebrafish 24 hpf which have been injected with; **A-B)** phenol red control, **C-D)** 8 ng of *rbbp9* morpholino, and **E-F)** 16 ng of *rbbp9* morpholino. Differences in body shape were identified at higher concentrations of *rbbp9* morpholino. Incorporation of morpholino was confirmed by positive FITC fluorescence (indicated by green dye). Scale bars = 600 µm.

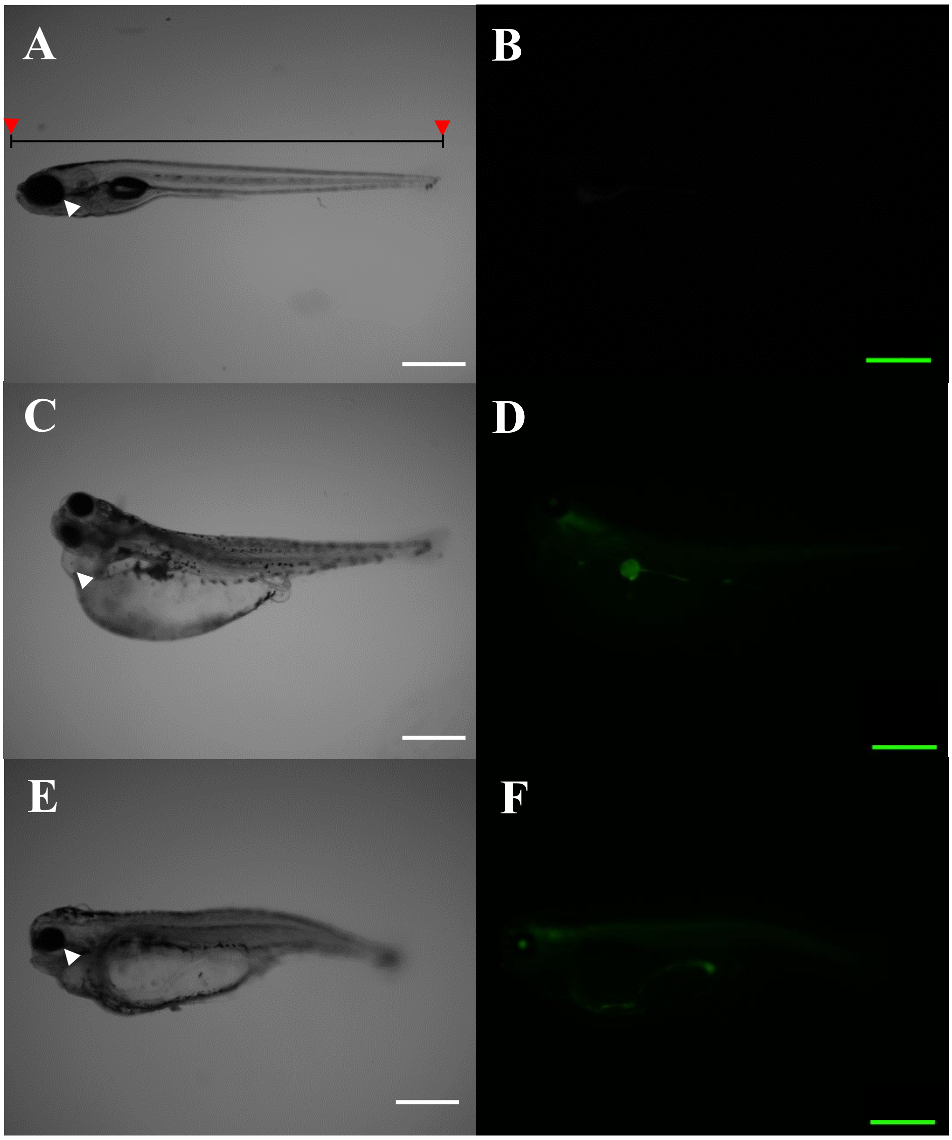

Figure 4.14 *rbbp9* morpholino affects embryonic development 7 dpf. Representative images of zebrafish larvae 7 dpf, which have been injected with; **A-B)** a phenol red control, **C-D)** 8 ng of *rbbp9* morpholino, and **E-F)** 16 ng of *rbbp9* morpholino. Higher concentrations of rbbp9 morpholino result in phenotypic changes in body size (black arrow), and eye development (red arrow). Incorporation of morpholino was confirmed by FITC fluorescence (indicated by green dye). Scale bars = 600 µm.

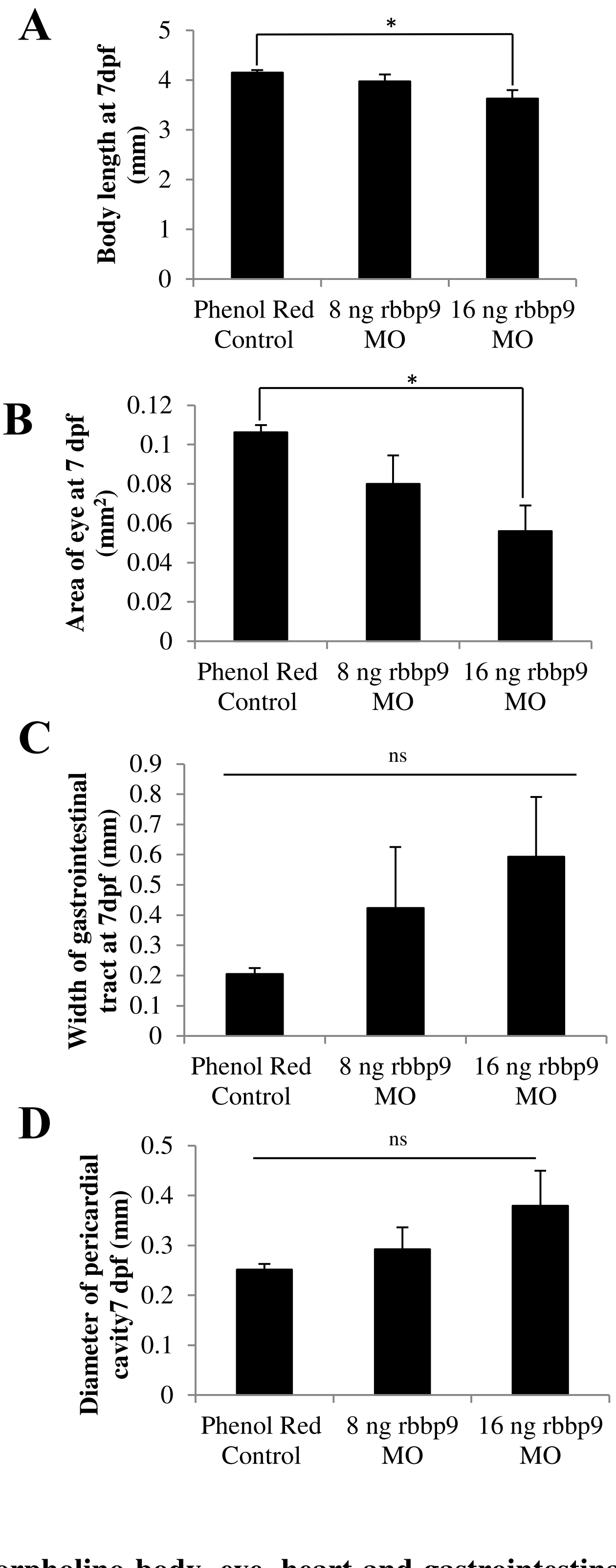

Figure 4.15 *rbbp9* morpholino body, eye, heart and gastrointestinal development 7 dpf. *rbbp9* morpholino (MO) resulted in; **A)** reduced body length, and **B)** smaller eyes, **C)** with no significant changes to the yolk sac and **D)** pericardial cavity. (n=3; $p < 0.05$).

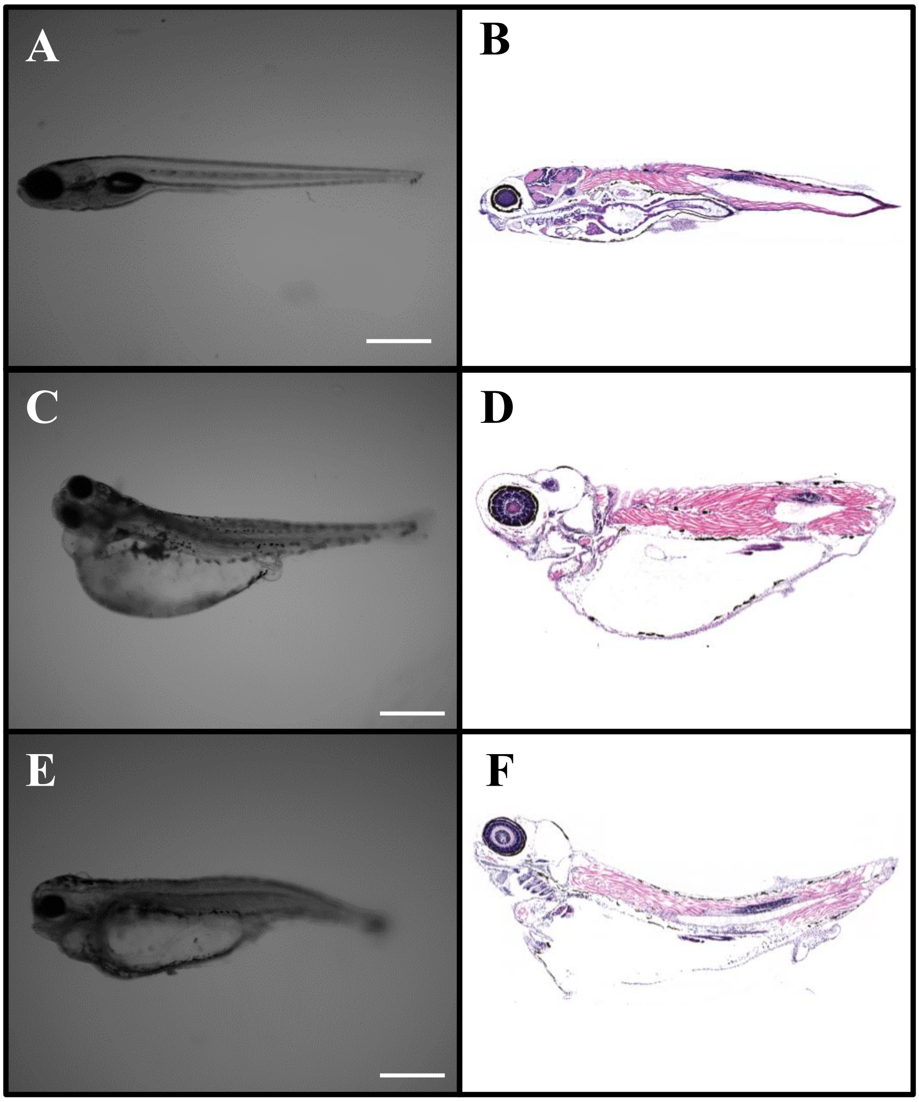

Figure 4.16 Histological representation of developmental changes in zebrafish treated with *rbbp9* morpholino 7dpf. Representative histological images of zebrafish larvae 7 dpf, which have been injected with: **A-B)** a phenol red control, **C-D)** 8 ng of *rbbp9* morpholino, and **E-F)** 16 ng of *rbbp9* morpholino. Higher concentrations of rbbp9 morpholino result in phenotypic changes in body size, eye development, gastrointestinal cavity and tract. White scale bar = 600 µm.

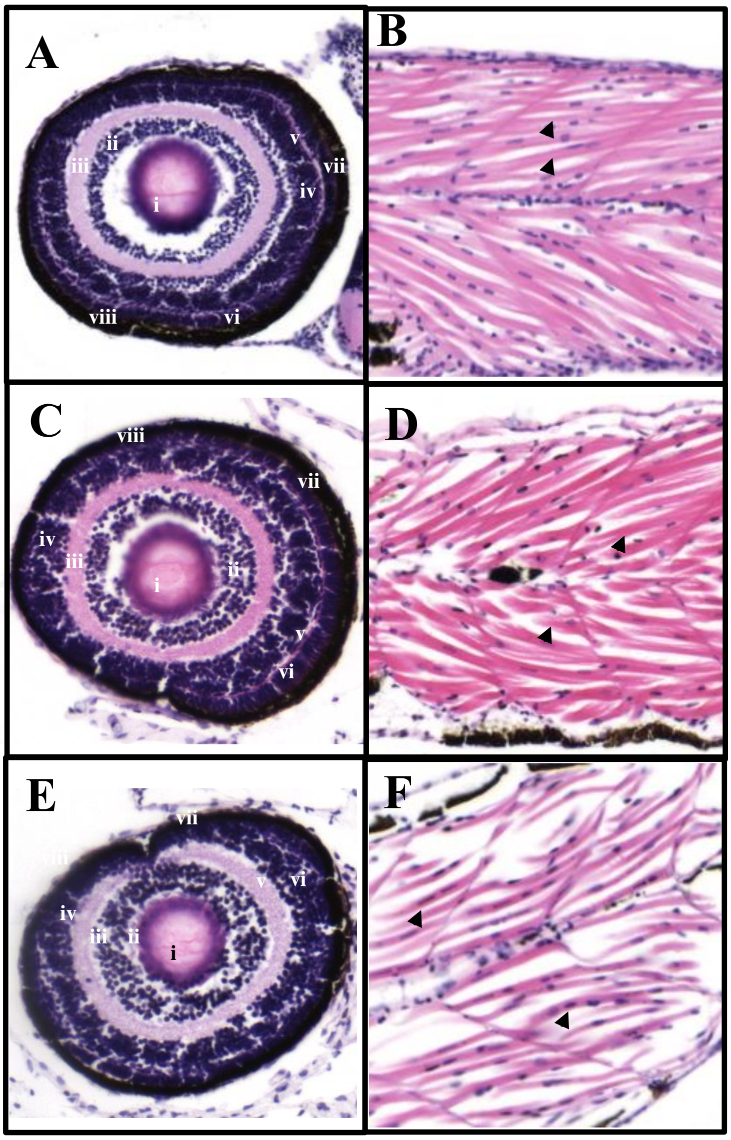

Figure 4.17 Morphological differences of developmental changes to the eye and muscle in zebrafish treated with *rbbp9* morpholino 7 dpf. Representative histological images of zebrafish larvae 7 dpf, which have been injected with; **A-B)** a phenol red control, **C-D)** 8 ng of *rbbp9* morpholino, and **E-F)** 16 ng of *rbbp9* morpholino. Higher concentrations of rbbp9 morpholino result in; **A, C, E)** normal eye morphology showing all layers including: i) lens, ii) ganglion cell layer, iii) inner plexiform layer, iv) inner nuclear layer, v) outer plexiform layer, vi) outer nuclear layer, vii) inner segment/outer segment of photoreceptor cells, and viii) retinal pigment epithelium. Changes in morphology between treatments were seen in: **B, D, F)** muscle fibre distribution in zebrafish treated with *rbbp9* morpholino's (black arrows).

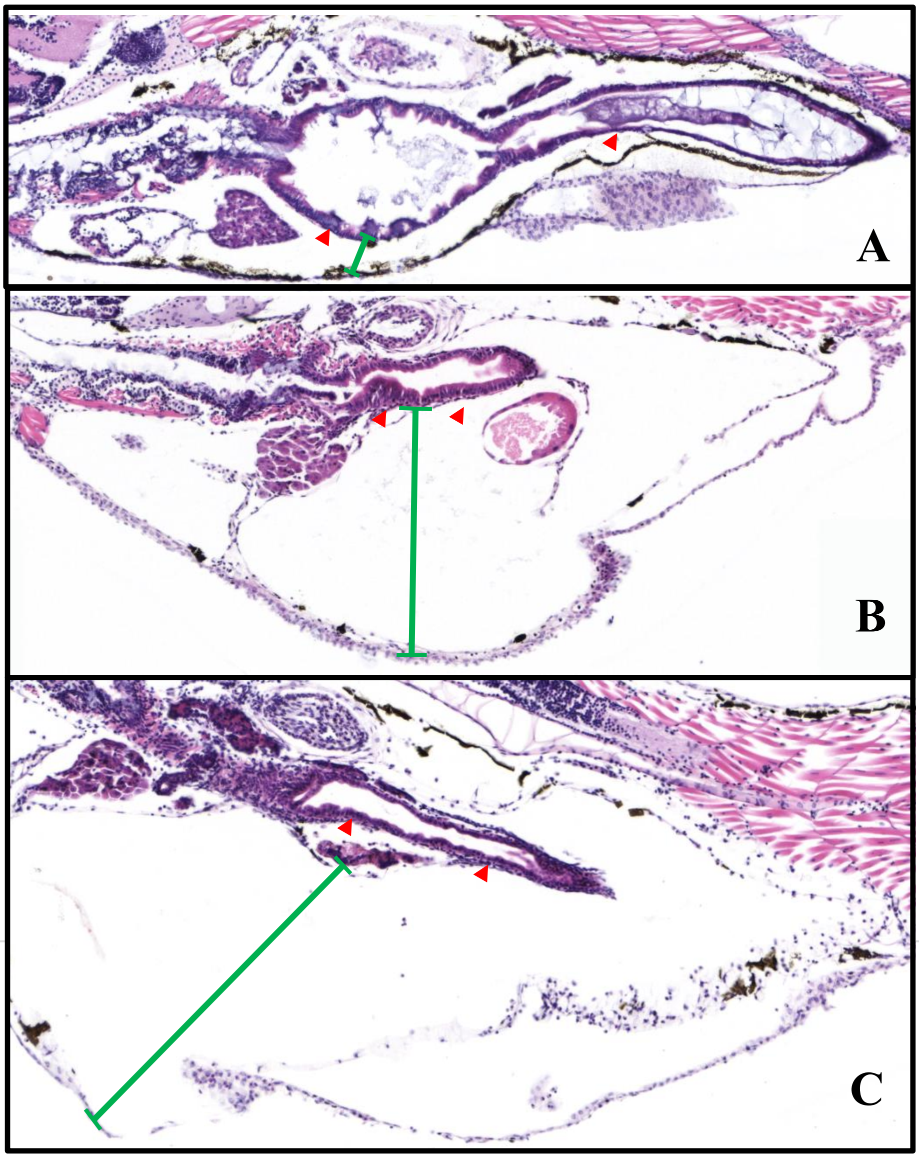

Figure 4.18 Morphological differences of developmental changes of the gastrointestinal tract in zebrafish treated with *rbbp9* morpholino 7 dpf. Representative histological images of zebrafish larvae 7 dpf, show changes at the gastrointestinal tract (red arrows) and yolk sac (green lines) between **A)** Phenol red control, **B)** 8 ng of *rbbp9* morpholino, and **C)** 16 ng of *rbbp9* morpholino.

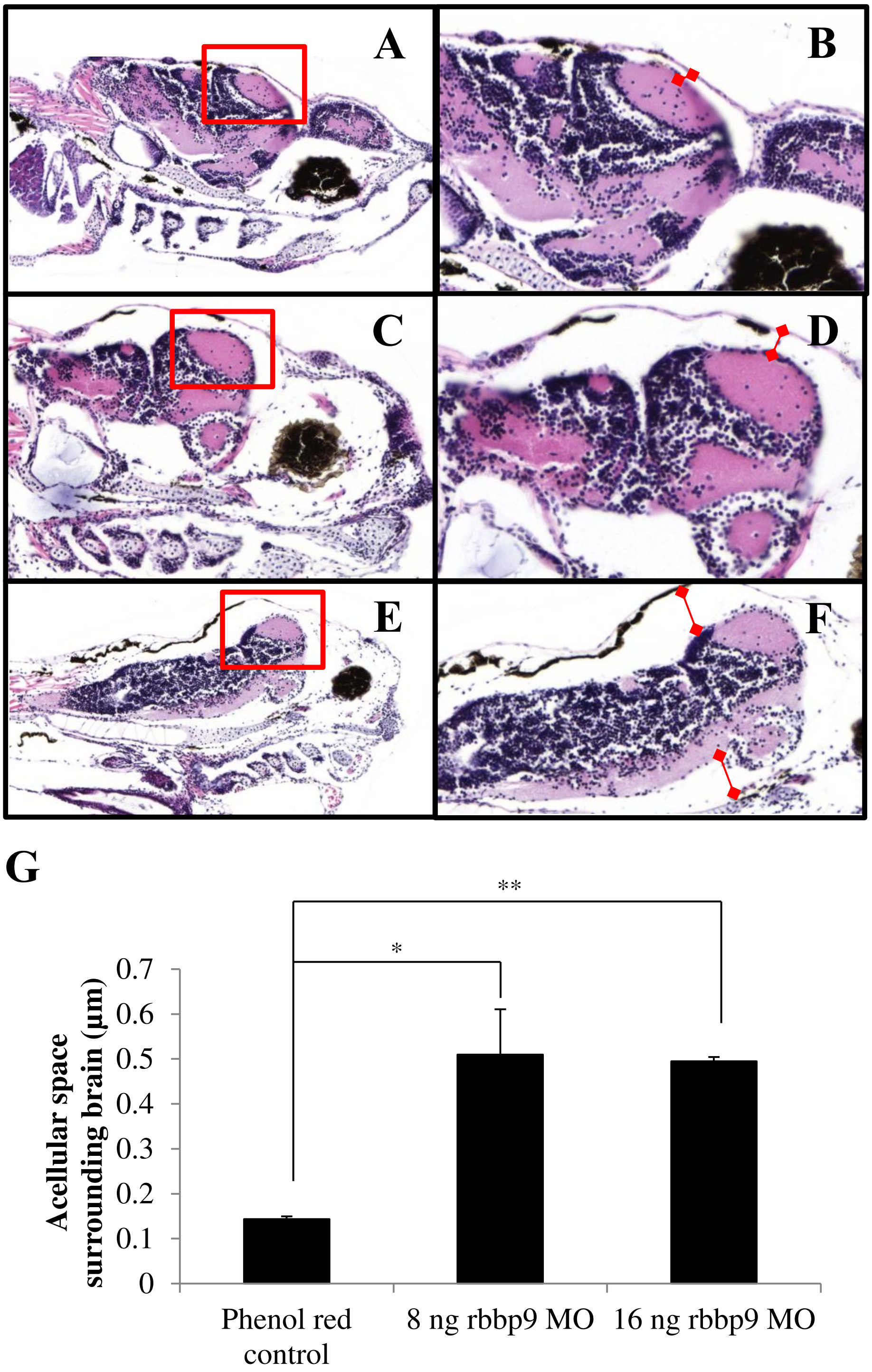

Figure 4.19 Increased acellular space surrounding the brain due to treatment with *rbbp9* morpholino at 7 dpf. Histological analysis of treated zebrafish 7 dpf show lack of acellular space (red lines) surrounding the brains white- (pink stain) and grey-matter (purple stain) (red boxes) in **A-B)** Phenol control-, when compared to **C-D)** 8 ng *rbbp9* morpholino (MO) and **E-F)** 16 ng *rbbp9* morpholino. **G)** Significant changes were seen in the acellular space surrounding the brain between the Phenol red control- and 8 ng *rbbp9*- and 16 ng *rbbp9*-morpholino treated zebrafish. (n=3; * p = 0.0358; ** p = 0.0007).

A *tp53* morpholino was used to assess whether changes seen with *rbbp9* morpholino treatment might be due to activation of the tp53 pathway, a classical indicator of non-specificity with morpholino treatments (Robu et al., 2007, Langheinrich et al., 2002). Fluorescence microscopy showed the *tp53* morpholino was present throughout the zebrafish embryos up to 7 dpf. Consistent with published reports, use of this *tp53* morpholino at concentrations up to 16 ng did not result in any phenotypic changes at either 24 hpf (Figure 4.20) or 7 dpf (Figure 4.21). Notably, co-injection of 8 ng *rbbp9* and 8 ng of *tp53* morpholino's into zebrafish embryos resulted in the same range of phenotypic changes seen with both *rbbp9* morpholino treatment and also ML114 treatment at 24 hpf and 7 dpf (Figure 4.22 and 4.23). These data suggest that p53 activation may not be responsible for the phenotype that resulted from *rbbp9* morpholino treatment.

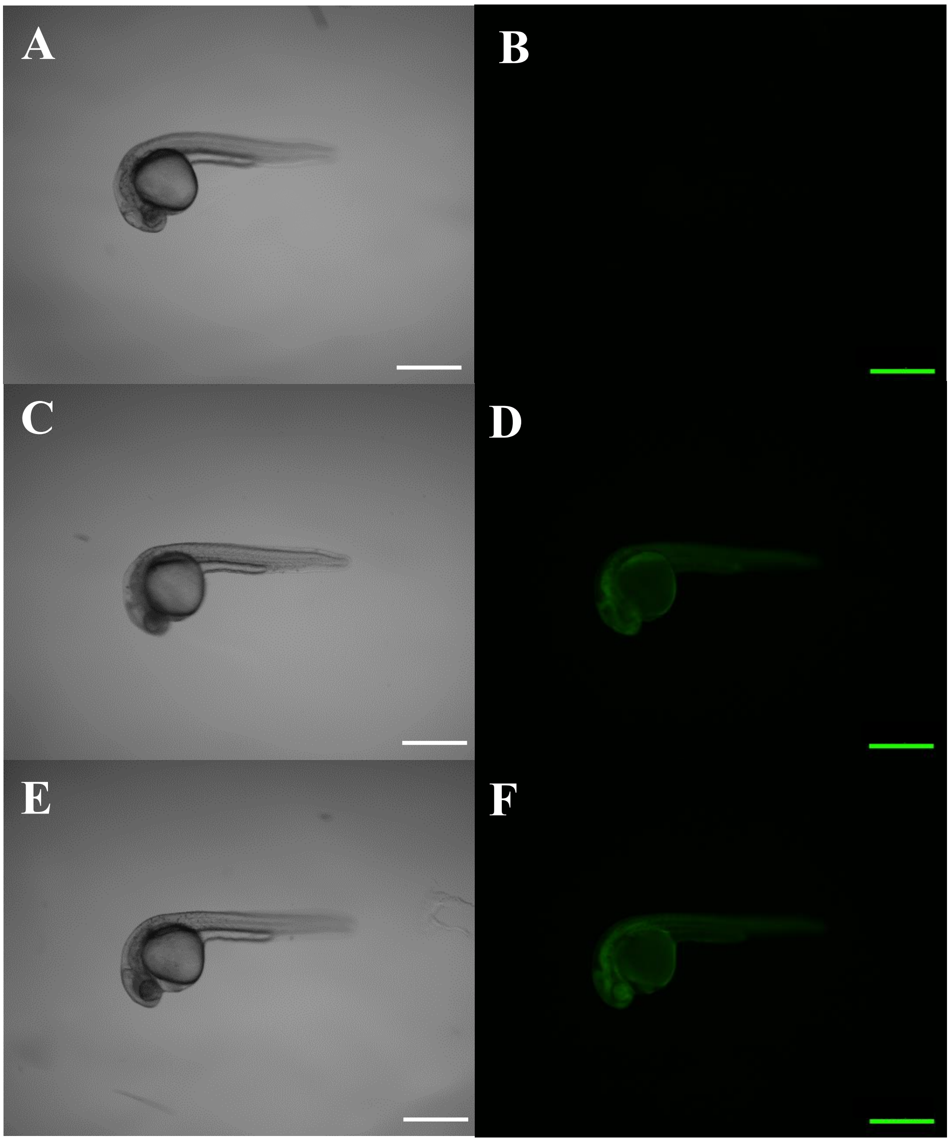

Figure 4.20 *tp53* morpholino does not affect embryonic development 24 hpf. Representative images of 24 hpf zebrafish which have been injected with; **A-B)** phenol red control, **C-D)** 8 ng of *tp53* morpholino, and **E-F)** 16 ng *tp53* morpholino. No changes in phenotype were seen in zebrafish injected with *tp53* morpholino. Incorporation of morpholino was confirmed by FITC fluorescence (indicated by green dye). Scale bars = 600 µm.

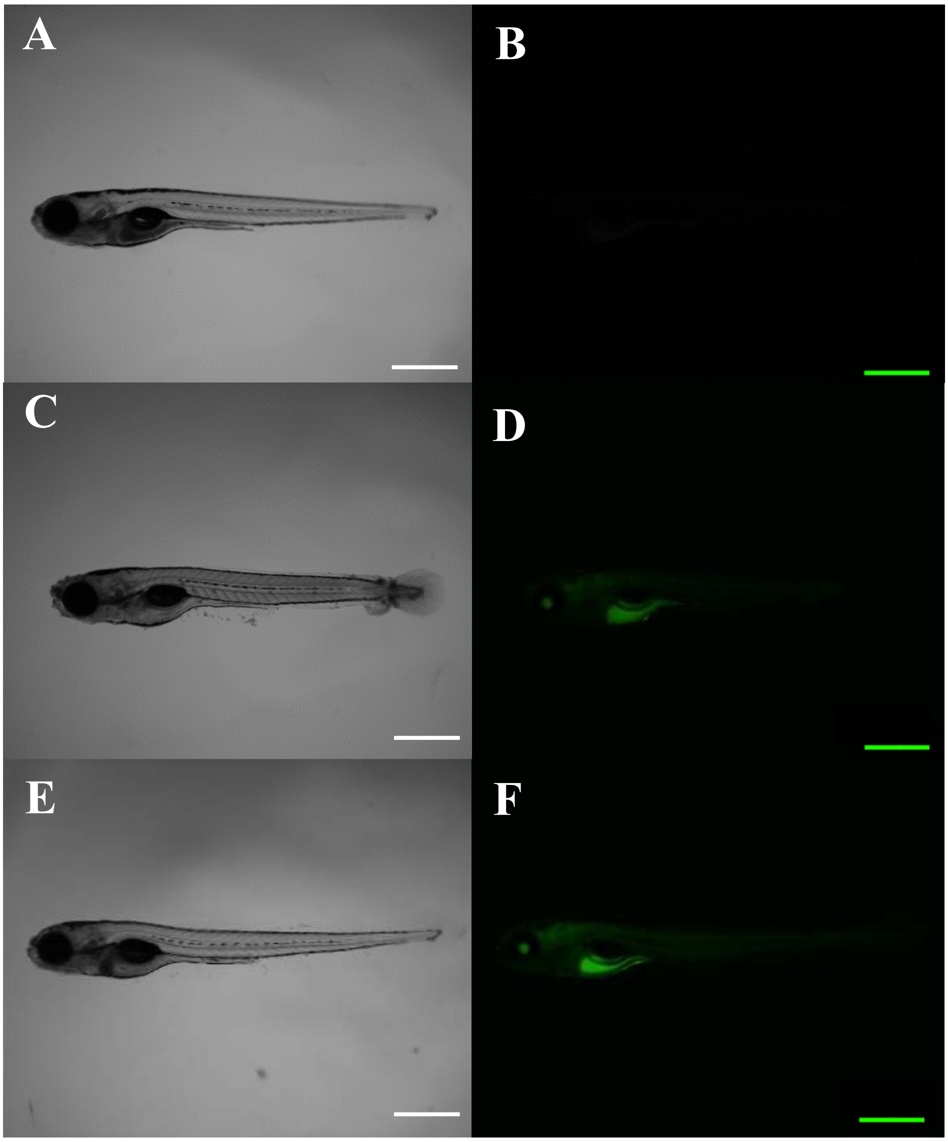

Figure 4.21 *tp53* morpholino does not affect embryonic development 7 dpf. Representative images of 7 dpf zebrafish which have been injected with; **A-B)** phenol red control, **C-D)** 8 ng of *tp53* morpholino, and **E-F)** 16 ng *tp53* morpholino. No changes in phenotype were seen in zebrafish injected with *tp53* morpholino. Incorporation of morpholino was confirmed by positive FITC fluorescence (indicated by green dye). Scale bars = 600 µm.

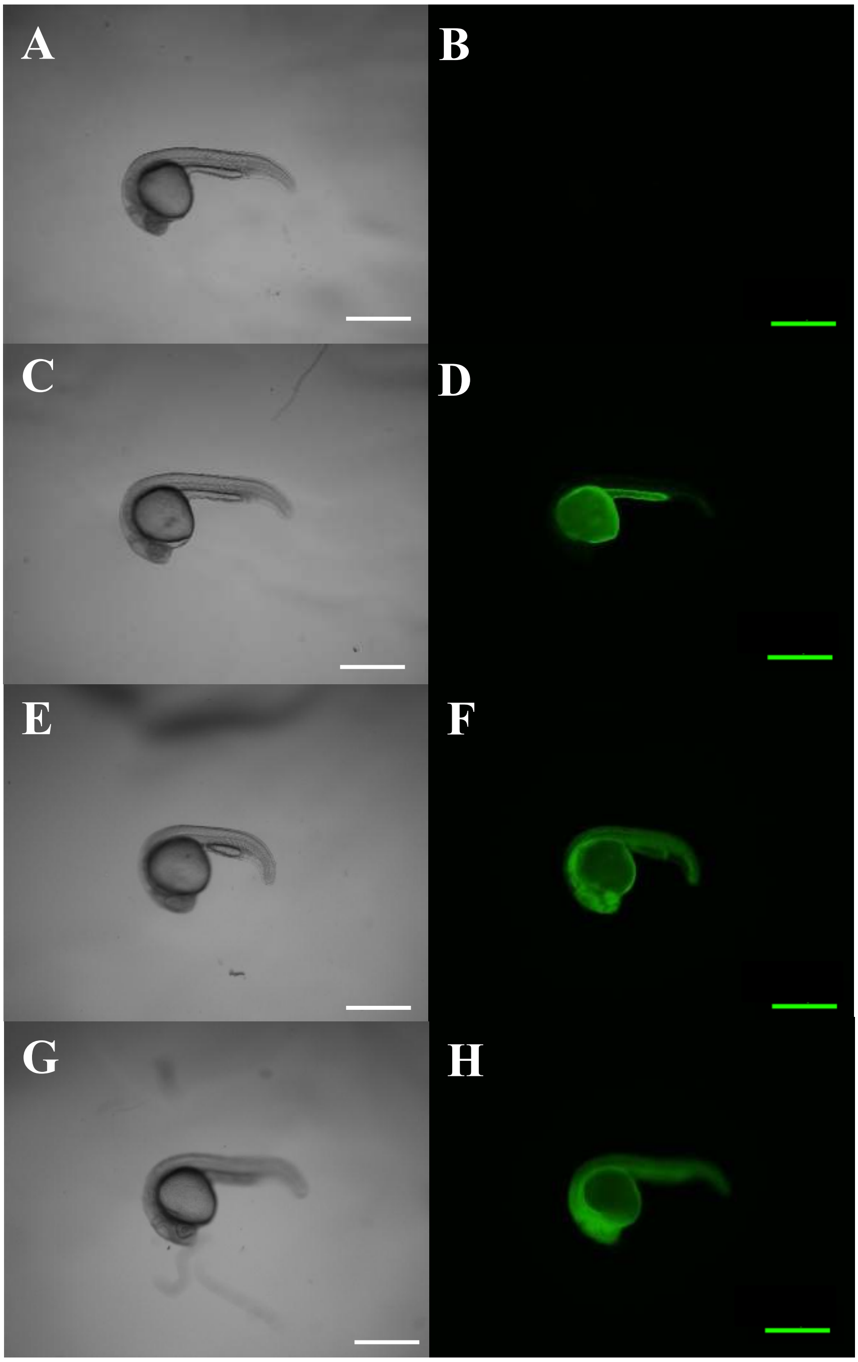

Figure 4.22 Incorporation of *rbbp9* and *tp53* morpholino's 24 hpf. Representative images of zebrafish at 24 hpf which have been injected with; **A-B)** a phenol red control, **C-D)** 16 ng of *tp53* morpholino, **E-F)** 8 ng *rbbp9* morpholino, and **G-H)** a co-injection of 8 ng *rbbp9* and 8 ng *tp53* morpholino. Incorporation of morpholino was confirmed by FITC fluorescence (indicated by green dye). Scale bars = 600 µm.

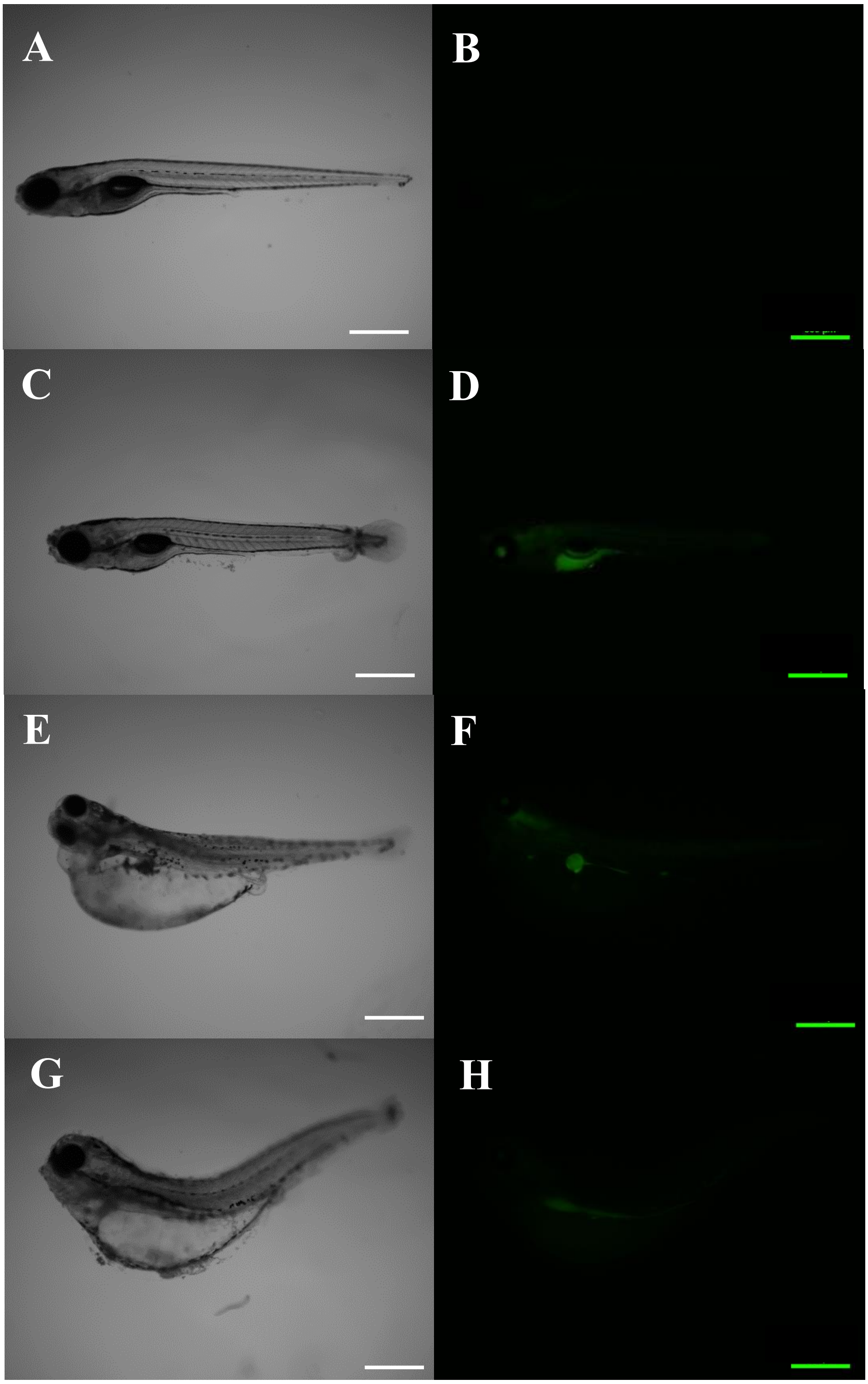

Figure 4.23 Co-injection of *rbbp9* and *tp53* morpholino's result in developmental changes 7 dpf. Representative images of zebrafish at 7 dpf which have been injected with; **A-B)** a phenol red control, **C-D)** 16 ng of *tp53* morpholino, **E-F)** 8 ng *rbbp9* morpholino, and **G-H)** a co-injection of 8 ng *rbbp9* and 16 ng *tp53* morpholino. Developmental changes seen with *rbbp9* morpholino are phenocopied with the addition of *tp53* morpholino. Incorporation of morpholino was confirmed by FITC fluorescence (indicated by green dye). Scale bars = 600 µm.

4.4. DISCUSSION

Rbbp9 is expressed in a variety of tissues throughout development (Bastian et al., 2008). However, whether it is critical for the development of any particular tissue is unknown. As a first step towards defining the role of Rbbp9 during embryonic development, this chapter investigated the effects of both ML114 and *rbbp9* morpholino on zebrafish embryos. Specific anatomical and histological defects were consistently observed with both ML114 and *rbbp9* morpholino treatments including anatomical defects relating to body size/shape, eye size, pericardial cavity, muscle, brain and the gastrointestinal system. Interestingly, ML114 but not *rbbp9* morpholino also affected organisation of the eye tissues.

4.4.1. Comparison of consequences due to loss of Rbbp9 activities.

Publically available online Affymetrix gene expression datasets show *rbbp9* transcripts are expressed in many tissues during zebrafish development, particularly in the eye, heart, brain, liver, and digestive tract (Bastian et al., 2008). Interestingly the eye, heart, brain and gastrointestinal tract were greatly affected by ML114 treatment. This suggests the abnormalities observed with ML114 treatment could be due to loss of Rbbp9 SH activity in these tissues. This conclusion is supported by the finding that use of the *rbbp9* morpholino resulted in a very similar set of anatomical and histological abnormalities that were not abolished by co-injection of the *tp53* morpholino at high concentrations.

4.4.2. Effects of ML114 and *rbbp9* morpholino treatments appear specific.

The validated anti-human RBBP9 antibody (O'Connor et al., 2011, Shields et al., 2010, Nachmany et al., 2012) could not reliably detect changes in Rbbp9 protein expression, and currently no zebrafish-specific Rbbp9 antibody exists. Thus to determine whether the effects resulting from ML114 and *rbbp9* morpholino treatment were specific, it is useful to compare against other zebrafish-based studies.

Specific anatomical and cellular changes were observed here due to both ML114 and *rbbp9* morpholino treatments. This included shortened body length, bent bodies (though not in all treated zebrafish), disorganised muscle fibres, differences in brain anatomy and malformation of the gastrointestinal tract are all tissues which has been shown to express Rbbp9 (Bastian et al., 2008). Published reports show that both morpholino- and chemical-based investigations in zebrafish have, in some instances, been capable of initiating p53-mediated toxicity responses (Robu et al., 2007, Langheinrich et al., 2002, Jeon and Lee, 2013, Ekker and Larson, 2001). Classic markers of p53-mediated toxicity include: spinal curvature (or U-shaped body), body shortening, smaller eyes and head, pericardial edema and enlarged yolk sac (Robu et al., 2007, Bilotta et al., 2004, Zhang et al., 2010, Shi et al., 2011, Jeon and Lee, 2013, Melo et al., 2015, Peng et al., 2015, Henry et al., 1997). Co-incident with these changes is the up-regulation of *p53* mRNA transcripts, enabling *p53* mRNA expression to be used as an indicator of toxic effects in zebrafish. In contrast, embryos with suppressed *p53* activity have been found to be morphologically indistinguishable from control embryos (Langheinrich et al., 2002). p53-mediated zebrafish toxicity due to the commonly used agricultural pesticide, cypermethrin, resulted in a clear upregulation of *p53* transcripts in a concentration-dependent manner (fold increases from 1.62-3.47) (Shi et al., 2011). Toxicity assays using silver, gold and platinum nanoparticles in zebrafish embryos also resulted in developmental defects (Asharani et al., 2011). High mortality rates were a result of toxicity due to nanoparticle treatments. Control-treated zebrafish had a mortality rate of less than 3%, whereas the mortality rate of zebrafish treated with nanoparticles showed a concentration-dependent effect ranging from 10-43% (Asharani et al., 2011). Interestingly, there was a small difference in survival rate between no-treatment control zebrafish (68%) and DMSO control-treated zebrafish (60%), soluble fragment (60%) as well as 50% of 100 μM ML114-treated zebrafish surviving 24 hours post treatment. These data indicate that the differences in survival rates due to ML114 toxicity were much smaller (at ~10%) than published chemical/nanopartical toxicity effects. Phenotypic changes observed as a result of exposure to nanoparticles also included: pericardial effusion, abnormal cardiac morphology, micropthalmia and malpigmented eyes (Asharani et al., 2011, Kim et al., 2013). Importantly, these morphological changes associated with toxicity were also accompanied with high expression of *p53* (with increases between 2-6 fold) suggesting these changes were due to activation of the p53 pathway (Kim et al., 2013, Shi et al., 2008). In comparison, no increase in *p53* expression was seen in the studies shown here.

Interestingly, ML114-treated zebrafish all had functioning hearts, as observed by circulating blood cells. Similar effects have been seen in published zebrafish toxicity studies, for example in a study that investigated the effects of acetylcholine esterase (AChE) inhibitors used to treat glaucoma and Alzheimer's disease (Behra et al., 2004). In that study, the chemical AChE inhibitor GAL phenocopied the effects of *ache* gene mutation, namely reduced motility and myopathy/abnormal muscle distribution. However, two other AChE inhibitors did not induce the same myopathy; instead they induced non-specific/off-target effects on neural development that were unrelated to AChE activity, although it is unknown whether this effect was mediated by activation of the p53 pathway. However, this toxicity was considered unlikely to be a generalized toxicity as all the embryos treated with AChE inhibitors had functioning hearts. This data suggests the phenotypes seen with ML114 treatment could be specifically due to ML114-selective inhibition of Rbbp9 SH activity as phenotypic changes were accompanied with functional hearts and most phenotypes were phenocopied with loss of Rbbp9 *via* morpholino treatment.

From the data shown here, zebrafish embryos treated with ML114 showed phenotypic changes similar to published effects attributed to p53-mediated toxicity. In addition to the fact that *p53* mRNA levels weren't increased by ML114 or *rbbp9* morpholino treatment, *p53* morpholino was unable to rescue the effects of *rbbp9* morpholino. However, it may still be possible the effects of ML114 and rbbp9 morpholino could have been non-specific, as the affected tissues are known to be affected by non-specific toxicity. For example, the observed phenotypes could be due to as yet undefined, *p53*-independent toxicity pathways. A curious difference between ML114 and *rbbp9* morpholino was that ML114 affected eye anatomy in addition to eye size. If all the ML114 and *rbbp9* morpholino effects were non-specific, it might be expected that the ML114 effect on eye anatomy would occur with both treatments. Alternately, if the effects are specific, it could be that eye development can accommodate loss of Rbbp9 protein by altering expression of other genes in the Rbbp9 pathway in a way that selective inhibition of Rbbp9 SH activity by ML114 cannot.

4.4.3. Off-target effects and Rbbp9 activities.

Overexpression of the serine/threonine mitotic kinase Aurora-A has been implicated in many cancers such as breast, colon, and pancreatic cancers (Bischoff et al., 1998, Zhou et al., 1998). Interestingly, these are the same cancers in which RBBP9 has been found to be overexpressed in (Lee et al., 1988, Shields et al., 2010). Loss of Aurora-A in zebrafish embryogenesis has been shown to result in specific (i.e., not non-specific) phenotypic changes such as short bent bodies and growth retardation (Jeon and Lee, 2013), similar to the phenotypes observed here with ML114 and *rbbp9* morpholino treatment. Co-injection of *tp53* morpholino was found to partially rescue the phenotypic changes due to loss of Aurora-A (Jeon and Lee, 2013), whereas co-injection of *tp53* morpholino did not rescue the changes brought upon by knockdown of Rbbp9.Although not explored in this study (due to time constraints), Western blot identification of p53 protein levels might provide further support for verifying p53 knockdown in zebrafish. Another informative control for future studies to address whether the rbbp9 morpholino affects are off-target effects would be to introduce *rbbp9* cDNA or mRNA which is not targeted by the current *rbbp9* morpholino (Ekker and Larson, 2001).

Overall, the combined ML114 and *rbbp9* morpholino data presented here suggest inhibition of Rbbp9 SH and Rb-binding activities could lead to abnormal development of tissues in which *rbbp9* is expressed. This interpretation is consistent with the known requirement for other serine proteases during development (e.g., Furin). Further support for the specificity of these effects is still required, such as assessment of p53 protein levels *via* Western blotting or cDNA/mRNA rescue assays together with *rbbp9* morpholino. Further understanding of the role of Rbbp9 activities *in vivo* will be beneficial for understanding its role in normal and cancer development.

CHAPTER 5: General Discussion

5.1. RBBP9 and the embryonic state.

RBBP9 is reported to be expressed in hPSCs, many cell types during early embryogenesis (including the eye, muscle, heart, brain and digestive tract), and in cancer cells (Shields et al., 2010, Woitach et al., 1998, Bastian et al., 2008, O'Connor et al., 2011). Currently, RBBP9 has two proposed mechanisms of action; i) RB-binding activity, and ii) SH activity (Shields et al., 2010, Woitach et al., 1998). RBBP9 is thought to have a role in cell cycle regulation due to its ability to bind to RB protein, which itself regulates the activity of E2F transcription factors required for cell cycle progression (Woitach et al., 1998). RBBP9 has also been shown to have SH activity (Shields et al., 2010), and loss of RBBP9 SH activity resulted in decreased proliferation of human pancreatic carcinoma cells and consequently reduced tumorigenesis in an *in vivo* assay. More recently, RBBP9 was identified as a candidate regulator of PSC maintenance. siRNA-mediated loss of RBBP9 protein resulted in down-regulation of pluripotency-associated markers, decreased expression of some cell cycle genes, and up-regulation of genes associated with neural differentiation (O'Connor et al., 2011). However, of the two proposed RBBP9 activities it was unclear what contribution each made to the regulation of pluripotency in hPSCs.

The discovery of ML114 as a highly potent and selective inhibitor of RBBP9 SH activity (Bachovchin et al., 2010b) enabled the studies presented here to begin defining the relative contribution of RBBP9 SH activity to hPSC maintenance and also embryonic development. Data presented within this thesis show the requirement for RBBP9 SH activity in hPSC maintenance, and possibly also embryogenesis. Chapter 2 shows RBBP9 SH activity appears to be required to promote hPSC transition from G_0/G_1 to S-phase, but has no noticeable effect on hPSC differentiation within the 7-day timeframe studied. This finding is consistent with recent literature that shows decreased PSC proliferation does not necessarily induce differentiation. Chapter 3 suggests RBBP9 SH activity may regulate hPSC proliferation by acting directly on NFYA and indirectly on DEAF1. This finding is consistent with the emerging role for NFYA and DEAF1 in PSC maintenance. Chapter 4 begins to investigate the role of RBBP9 SH activity in early embryogenesis, with the data not discounting the possibility that it is required for normal eye, gut, brain and muscle development, at least in zebrafish embryos. This would be consistent with the known role for other SH proteins during embryonic development.. However, even though Rbbp9 is expressed in all these zebrafish tissues, the degree of overlap between ML114- and *rbbp9* morpholino-treated zebrafish with zebrafish toxicity phenotypes makes it difficult to conclusively interpret this data.

Data presented here supporting the conclusion that the effects of ML114 were selective include the consistent dose-dependent effects caused by ML114 treatment in both hPSCs and zebrafish, and the lack of any effect resulting from treatment with the soluble ML114 cleavage product. From the ML114 identification study, incubation of cell-free RBBP9 protein with ML114 was found to increase the mass of the RBBP9 peptide fragment containing Ser75 by 110.09 Da (Bachovchin et al., 2010b). Therefore, more formal demonstration that the effects of ML114 on hPSCs are due to inhibition of RBBP9 SH activity could be performed in future by assessment of RBBP9 peptides from ML114-treated hPSCs; however, this was not possible for this thesis.

5.2. RBBP9 SH activity and its role in hPSC maintenance.

5.2.1. ML114 selectively affects cell proliferation in hPSCs.

Proper integration of a range of molecular networks is required to work together to govern the maintenance of key characteristics unique to hPSCs, i.e.: the ability to self-renew indefinitely and the potential to form any cell type of the body (Martin, 1981, Thomson et al., 1998). To elucidate the role of RBBP9 SH activity in hPSCs, the highly selective chemical inhibitor ML114 was used (Bachovchin et al., 2010b, O'Connor et al., 2011, Shields et al., 2010, Vorobiev et al., 2012, Woitach et al., 1998) and resulted in decreased hPSC proliferation without noticeably inducing differentiation during a 7 day assay period (see 2.4.1). Investigating the effect of ML114 at later time points could also be informative. Depletion of PRMT5 in hPSCs has similarly been shown to result in decreased proliferation of hPSCs whilst retaining markers of pluripotency (Gkountela et al., 2014). Additionally, loss of RBBP9 SH activity has been shown to reduce proliferation of human pancreatic carcinoma cells, similarly to the observed effects in hPSCs after ML114 treatment (Shields et al., 2010). Taken together, these data suggest that decreased proliferation observed with ML114 treatment is also due to loss of SH activity. Comparison of the data presented here with published effects of siRNA-mediated loss of RBBP9 in hPSCs suggests RB-binding activity appears to be: i) required for inhibiting neural differentiation of hPSCs; ii) may also be involved in regulating hPSC proliferation (given the known role for RB/E2F interaction); and iii) may not be required for normal embryonic development if the effects seen in Chapter 4 are specific (as ML114 treatment essentially phenocopied the effects of *rbbp9* morpholino in zebrafish development).

5.2.2. Future opportunities for studying RBBP9 and its effectors in hPSCs.

Gene expression profiling of ML114-treated hPSCs suggested that NFYA and DEAF1 may be direct and indirect (respectively) effectors of RBBP9 SH activity. Both NFYA and DEAF1 are reported to have roles in embryonic development and self-renewal in various PSCs including hPSCs (Bolognese et al., 1999, Dolfini et al., 2012, Gu et al., 2010, Veraksa et al., 2002, Bhattacharya et al., 2003, Farina et al., 1999, Grskovic et al., 2007, Mojsin et al., 2015, Oldfield et al., 2014). NFY binding motifs are located in the promoters of known hPSC regulatory genes such as *OCT4, NANOG* and *SOX2* (Dolfini et al., 2012), and NFYA can act as both a transcriptional activator and repressor (Ceribelli et al., 2008, Peng and Jahroudi, 2002, Deng et al., 2007, Peng and Jahroudi, 2003). Gene expression profiling of ML114-treated hPSCs revealed a small but significant increase in *NANOG* transcripts, which has been shown to interact with NFYA in ESCs (Bhattacharya et al., 2003, Farina et al., 1999, Grskovic et al., 2007, Oldfield et al., 2014). Loss of NFYA has been shown in a few studies to also reduce expression of NANOG, as well as embryo death occurring with decreased levels of NFYA similar to the effects seen with depletion of Nanog in mESCs (Bhattacharya et al., 2003, Farina et al., 1999, Oldfield et al., 2014, Mitsui et al., 2003).

As previously mentioned, the gene expression fold changes associated with ML114 treatment of hPSCs were quite small, although still statistically significant based both on raw *p*-values and *p*-values taking into account a false discovery rate cut off <0.05 (Kuehn et al., 2008). Interestingly, a study in which NFYA was overexpressed in pluripotent human embryonal carcinoma cells showed high levels of NFYA decreased cell proliferation and expression of pluripotency markers (Mojsin et al., 2015, Grskovic et al., 2007). However, a separate study showed that shRNA-mediated loss of NFYA decreases mESC proliferation, and NFYA expression has also been shown to decrease during hPSC differentiation (Grskovic et al., 2007). When viewed together with the data presented in Chapters 2 and 3, it is possible that NFYA protein levels need to be kept within strict limits (similar to OCT4, NANOG and SOX2) in order to maintain a pluripotent state. Alternately, there may be species-specific differences in the role of NFYA, and/or differences in its role in epiblast-like pluripotent cells (e.g., hPSCs) vs mESC-like pluripotent cells.

Although currently not completely understood, tight regulation of transcription factors is required to both maintain a state of pluripotency within an ESC, but also reprogram a somatic cell back into a pluripotent state (Hanna et al., 2002, Alon, 2007, Boyer et al., 2005, Gurdon, 1962, Takahashi and Yamanaka, 2006). From the data presented in this thesis, it appears that both proposed mechanisms of action of RBBP9 are beneficial to maintaining pluripotency. It would therefore be interesting to see whether inclusion of RBBP9 in the reprogramming cocktail would increase the efficiency of hiPSC production. Additionally, understanding mechanisms of RBBP9 in both naïve and primed stem cells would be useful. Both primed and naïve hPSCs retain the characteristics unique to stem cells with some key differences. Naïve hPSCs have better survival as single cells, shorter doubling time and can form germline chimeras *in vivo* while primed hPSCs do not have these characteristics (Tesar et al., 2007, Ware et al., 2014). Primed hPSCs were used in this study (Brons et al., 2007, Nichols and Smith, 2009, Tesar et al., 2007, Thomson et al., 1998). Further investigation of RBBP9 SH activity loss in naïve stem cells and its effect on the naïve hPSC cell cycle would be of interest. As naïve stem cells have a shorter doubling time than primed hPSCs, the effect of RBBP9 SH activity loss on naïve cell cycle could be compared to effects seen in primed hPSCs (Ware et al., 2014). Additional testing could also include more ESC lines such as the NTeraD2 and iPSC65 (O'Connor et al., 2011). This would allow for a more comprehensive comparison with loss of RBBP9 activities in other ESCs enabling this work to be applicable to a broader audience in the hPSC field.

Currently there are no reports of DEAF1 or NFYA in reprogramming, however stable expression of DEAF1 has been shown to be required to maintain a pluripotent state in both mESCs and hESCs (Gu et al., 2010). However, based on data presented in Chapters 2 and 3, overexpression of NFYA outside a useful range might decrease the efficiency of hiPSC production by decreasing cell proliferation.

5.3. RBBP9 SH and its effectors in cancer progression.

Self-renewal is a defining feature of both stem cells and cancer, where cancer is thought to be a disease of unregulated proliferation, including self-renewal of cancer stem cells (Bisson and Prowse, 2009, Reya et al., 2001, Reya et al., 2003, Bonnet and Dick, 1997, Wong et al., 2008). RBBP9 expression has also been reported in human cancer cells, with one of the studies identifying its role as a SH in promoting proliferation of human pancreatic carcinoma cells (Shields et al., 2010, Woitach et al., 1998, O'Connor et al., 2011). Interestingly NFYA and DEAF1 have known roles in regulating cancer cells (Dai et al., 2015, Barker et al., 2008, Cubeddu et al., 2012, Benatti et al., 2016, Charafe-Jauffret et al., 2009). Loss of NFYA subunits has been found to result in differentiation of hESCs as well as reducing expression of *CDCA8*, a gene required in some human cancers such as lung cancer. Further investigations into RBBP9 SH and its effect on NFYA and DEAF1 could prove useful in understanding cancer cell proliferation and differentiation pathways, and potentially also for identification of new anti-cancer targets.

5.4. Rbbp9 SH and embryonic development.

Chapter 4 showed that both ML114 and *rbbp9* morpholino resulted in abnormal muscle, eye, heart, brain and gastrointestinal development. The RBBP9 expression pattern and results shown in Chapter 2 support a role for RBBP9 in embryonic development; however, specific technical issues limit the conclusions that can be drawn from the data in zebrafish. Recently, morpholino technology has been shown to have more off-target effects than previously reported (Kok et al., 2015). For example, poor correlation was identified between morpholino-induced and mutant phenotypes in zebrafish with the *megamind* morpholino. At present there is no available mutant Rbbp9 zebrafish to compare phenotypic changes arising from either *rbbp9* morpholino or ML114 inhibition of Rbbp9 SH activity. The ML114 soluble fragment and *p53* morpholino controls used here suggest the ML114 and *rbbp9* morpholino treatment phenotypes could be specifically due to loss of RBBP9 activities (Langheinrich et al., 2002, Robu et al., 2007). This is supported by the lack of any increase in *p53* transcript levels with the treatments, and the known role for SHs in embryonic development. However, as previously described, future studies could address the specificity/non-specific toxicity issue by assessing p53 protein levels, by cDNA/mRNA rescue experiments for the *rbbp9* morpholino work, or perhaps more effectively by using other gene knockdown technologies not available at the time of this thesis such as Clustered Regularly Interspaced Short Palindromic Repeats (CRISPR) technology (Gaj et al., 2013, Ablain et al., 2015, Hruscha et al., 2013, Hwang et al., 2013). Should the effects prove to be specific, then it would be interesting for future studies to explore whether NFYA or DEAF1 are involved in these developmental changes seen.

5.5. Summary.

This thesis strongly suggests that RBBP9 SH activity is required for proliferation (but not differentiation) of hPSCs, and that it may also have a role in regulating normal development during early embryogenesis. The data presented also suggest that NFYA, and possibly also DEAF1, may be targets of RBBP9 SH activity. Overall, the results suggest that further investigation of RBBP9 activities could lead to a better understanding of the mechanisms behind normal and abnormal development and perhaps also improved methods of somatic cell reprogramming and cancer therapy.

References

ABLAIN, J., DURAND, E. M., YANG, S., ZHOU, Y. & ZON, L. I. 2015. A CRISPR/Cas9 vector system for tissue-specific gene disruption in zebrafish. *Dev Cell,* 32**,** 756-64.

ADEWUMI, O., AFLATOONIAN, B., AHRLUND-RICHTER, L., AMIT, M., ANDREWS, P. W., BEIGHTON, G., BELLO, P. A., BENVENISTY, N., BERRY, L. S., BEVAN, S., BLUM, B., BROOKING, J., CHEN, K. G., CHOO, A. B., CHURCHILL, G. A., CORBEL, M., DAMJANOV, I., DRAPER, J. S., DVORAK, P., EMANUELSSON, K., FLECK, R. A., FORD, A., GERTOW, K., GERTSENSTEIN, M., GOKHALE, P. J., HAMILTON, R. S., HAMPL, A., HEALY, L. E., HOVATTA, O., HYLLNER, J., IMREH, M. P., ITSKOVITZ-ELDOR, J., JACKSON, J., JOHNSON, J. L., JONES, M., KEE, K., KING, B. L., KNOWLES, B. B., LAKO, M., LEBRIN, F., MALLON, B. S., MANNING, D., MAYSHAR, Y., MCKAY, R. D., MICHALSKA, A. E., MIKKOLA, M., MILEIKOVSKY, M., MINGER, S. L., MOORE, H. D., MUMMERY, C. L., NAGY, A., NAKATSUJI, N., O'BRIEN, C. M., OH, S. K., OLSSON, C., OTONKOSKI, T., PARK, K. Y., PASSIER, R., PATEL, H., PATEL, M., PEDERSEN, R., PERA, M. F., PIEKARCZYK, M. S., PERA, R. A., REUBINOFF, B. E., ROBINS, A. J., ROSSANT, J., RUGG-GUNN, P., SCHULZ, T. C., SEMB, H., SHERRER, E. S., SIEMEN, H., STACEY, G. N., STOJKOVIC, M., SUEMORI, H., SZATKIEWICZ, J., TURETSKY, T., TUURI, T., VAN DEN BRINK, S., VINTERSTEN, K., VUORISTO, S., WARD, D., WEAVER, T. A., YOUNG, L. A. & ZHANG, W. 2007. Characterization of human embryonic stem cell lines by the International Stem Cell Initiative. *Nat Biotechnol,* 25**,** 803-16.

ADJAYE, J., HUNTRISS, J., HERWIG, R., BENKAHLA, A., BRINK, T. C., WIERLING, C., HULTSCHIG, C., GROTH, D., YASPO, M. L., PICTON, H. M., GOSDEN, R. G. & LEHRACH, H. 2005. Primary differentiation in the human blastocyst: comparative molecular portraits of inner cell mass and trophectoderm cells. *Stem Cells,* 23**,** 1514-25.

ALON, U. 2007. Network motifs: theory and experimental approaches. *Nat Rev Genet,* 8**,** 450-61.

AMIT, M., CARPENTER, M. K., INOKUMA, M. S., CHIU, C. P., HARRIS, C. P., WAKNITZ, M. A., ITSKOVITZ-ELDOR, J. & THOMSON, J. A. 2000. Clonally derived human embryonic stem cell lines maintain pluripotency and proliferative potential for prolonged periods of culture. *Dev Biol,* 227**,** 271-8.

AMSTERDAM, A., BURGESS, S., GOLLING, G., CHEN, W., SUN, Z., TOWNSEND, K., FARRINGTON, S., HALDI, M. & HOPKINS, N. 1999. A large-scale insertional mutagenesis screen in zebrafish. *Genes Dev,* 13**,** 2713-24.

AOYAMA, A. & CHEN, W. T. 1990. A 170-kDa membrane-bound protease is associated with the expression of invasiveness by human malignant melanoma cells. *Proc Natl Acad Sci U S A,* 87**,** 8296-300.

ASHARANI, P. V., LIANWU, Y., GONG, Z. & VALIYAVEETTIL, S. 2011. Comparison of the toxicity of silver, gold and platinum nanoparticles in developing zebrafish embryos. *Nanotoxicology,* 5**,** 43-54.

AVILION, A. A., NICOLIS, S. K., PEVNY, L. H., PEREZ, L., VIVIAN, N. & LOVELL-BADGE, R. 2003. Multipotent cell lineages in early mouse development depend on SOX2 function. *Genes Dev,* 17**,** 126-40.

BACHOVCHIN, D. A., SPEERS, A. E., BROWN, S. J., CRAVATT, B. F., SPICER, T., MERCER, B. A., FERGUSON, J., HODDER, P. & ROSEN, H. R. 2010a. Probe Report for RBBP9 Inhibitors - Probe 2. *Probe Reports from the NIH Molecular Libraries Program.* Bethesda (MD).

BACHOVCHIN, D. A., WOLFE, M. R., MASUDA, K., BROWN, S. J., SPICER, T. P., FERNANDEZ-VEGA, V., CHASE, P., HODDER, P. S., ROSEN, H. & CRAVATT, B. F. 2010b. Oxime esters as selective, covalent inhibitors of the serine hydrolase retinoblastoma-binding protein 9 (RBBP9). *Bioorg Med Chem Lett,* 20**,** 2254-8.

BAIN, G., RAY, W. J., YAO, M. & GOTTLIEB, D. I. 1996. Retinoic acid promotes neural and represses mesodermal gene expression in mouse embryonic stem cells in culture. *Biochem Biophys Res Commun,* 223**,** 691-4.

BARKER, H. E., SMYTH, G. K., WETTENHALL, J., WARD, T. A., BATH, M. L., LINDEMAN, G. J. & VISVADER, J. E. 2008. Deaf-1 regulates epithelial cell proliferation and side-branching in the mammary gland. *BMC Dev Biol,* 8**,** 94.

BASTIAN, F., PARMENTIER, G., ROUX, J., MORETTI, S., LAUDET, V. & ROBINSON-RECHAVI, M. 2008. Bgee: Integrating and comparing heterogeneous transcriptome data among species. *Data Integration in the Life Sciences, Proceedings,* 5109**,** 124-131.

BECKER, K. A., GHULE, P. N., THERRIEN, J. A., LIAN, J. B., STEIN, J. L., VAN WIJNEN, A. J. & STEIN, G. S. 2006. Self-renewal of human embryonic stem cells is supported by a shortened G1 cell cycle phase. *J Cell Physiol,* 209**,** 883-93.

BEHRA, M., ETARD, C., COUSIN, X. & STRAHLE, U. 2004. The use of zebrafish mutants to identify secondary target effects of acetylcholine esterase inhibitors. *Toxicol Sci,* 77**,** 325-33.

BENATTI, P., CHIARAMONTE, M. L., LORENZO, M., HARTLEY, J. A., HOCHHAUSER, D., GNESUTTA, N., MANTOVANI, R., IMBRIANO, C. & DOLFINI, D. 2016. NF-Y activates genes of metabolic pathways altered in cancer cells. *Oncotarget,* 7**,** 1633-50.

BENATTI, P., DOLFINI, D., VIGANO, A., RAVO, M., WEISZ, A. & IMBRIANO, C. 2011. Specific inhibition of NF-Y subunits triggers different cell proliferation defects. *Nucleic Acids Res,* 39**,** 5356-68.

BERG, R. W. & MCBURNEY, M. W. 1990. Cell density and cell cycle effects on retinoic acid-induced embryonal carcinoma cell differentiation. *Dev Biol,* 138**,** 123-35.

BHATTACHARYA, A., DENG, J. M., ZHANG, Z. P., BEHRINGER, R., DE CROMBRUGGHE, B. & MAITY, S. N. 2003. The B subunit of the CCAAT box binding transcription factor complex (CBF/NF-Y) is essential for early mouse development and cell proliferation. *Cancer Research,* 63**,** 8167-8172.

BILOTTA, J., BARNETT, J. A., HANCOCK, L. & SASZIK, S. 2004. Ethanol exposure alters zebrafish development: a novel model of fetal alcohol syndrome. *Neurotoxicol Teratol,* 26**,** 737-43.

BISCHOFF, J. R., ANDERSON, L., ZHU, Y., MOSSIE, K., NG, L., SOUZA, B., SCHRYVER, B., FLANAGAN, P., CLAIRVOYANT, F., GINTHER, C., CHAN, C. S., NOVOTNY, M., SLAMON, D. J. & PLOWMAN, G. D. 1998. A homologue of Drosophila aurora kinase is oncogenic and amplified in human colorectal cancers. *EMBO J,* 17**,** 3052-65.

BISSON, I. & PROWSE, D. M. 2009. WNT signaling regulates self-renewal and differentiation of prostate cancer cells with stem cell characteristics. *Cell Res,* 19**,** 683-97.

BOLOGNESE, F., WASNER, M., DOHNA, C. L., GURTNER, A., RONCHI, A., MULLER, H., MANNI, I., MOSSNER, J., PIAGGIO, G., MANTOVANI, R. & ENGELAND, K. 1999. The cyclin B2 promoter depends on NF-Y, a trimer whose CCAAT-binding activity is cell-cycle regulated. *Oncogene,* 18**,** 1845-53.

BONNET, D. & DICK, J. E. 1997. Human acute myeloid leukemia is organized as a hierarchy that originates from a primitive hematopoietic cell. *Nat Med,* 3**,** 730-7.

BOYER, L. A., LEE, T. I., COLE, M. F., JOHNSTONE, S. E., LEVINE, S. S., ZUCKER, J. P., GUENTHER, M. G., KUMAR, R. M., MURRAY, H. L., JENNER, R. G., GIFFORD, D. K., MELTON, D. A., JAENISCH, R. & YOUNG, R. A. 2005. Core transcriptional regulatory circuitry in human embryonic stem cells. *Cell,* 122**,** 947-56.

BOYER, S. N., WAZER, D. E. & BAND, V. 1996. E7 protein of human papilloma virus-16 induces degradation of retinoblastoma protein through the ubiquitin-proteasome pathway. *Cancer Res,* 56**,** 4620-4.

BRONS, I. G., SMITHERS, L. E., TROTTER, M. W., RUGG-GUNN, P., SUN, B., CHUVA DE SOUSA LOPES, S. M., HOWLETT, S. K., CLARKSON, A., AHRLUND-RICHTER, L., PEDERSEN, R. A. & VALLIER, L. 2007. Derivation of pluripotent epiblast stem cells from mammalian embryos. *Nature,* 448**,** 191-5.

BUNGARTZ, G., LAND, H., SCADDEN, D. T. & EMERSON, S. G. 2012. NF-Y is necessary for hematopoietic stem cell proliferation and survival. *Blood,* 119**,** 1380-9.

CALDER, A., ROTH-ALBIN, I., BHATIA, S., PILQUIL, C., LEE, J. H., BHATIA, M., LEVADOUX-MARTIN, M., MCNICOL, J., RUSSELL, J., COLLINS, T. & DRAPER, J. S. 2013. Lengthened G1 phase indicates differentiation status in human embryonic stem cells. *Stem Cells Dev,* 22**,** 279-95.

CALLAGHAN, D. A., DONG, L., CALLAGHAN, S. M., HOU, Y. X., DAGNINO, L. & SLACK, R. S. 1999. Neural precursor cells differentiating in the absence of Rb exhibit delayed terminal mitosis and deregulated E2F 1 and 3 activity. *Dev Biol,* 207**,** 257-70.

CARTWRIGHT, P., MCLEAN, C., SHEPPARD, A., RIVETT, D., JONES, K. & DALTON, S. 2005. LIF/STAT3 controls ES cell self-renewal and pluripotency by a Myc-dependent mechanism. *Development,* 132**,** 885-96.

CAZENAVE, C., STEIN, C. A., LOREAU, N., THUONG, N. T., NECKERS, L. M., SUBASINGHE, C., HELENE, C., COHEN, J. S. & TOULME, J. J. 1989. Comparative inhibition of rabbit globin mRNA translation by modified antisense oligodeoxynucleotides. *Nucleic Acids Res,* 17**,** 4255-73.

CERIBELLI, M., DOLFINI, D., MERICO, D., GATTA, R., VIGANO, A. M., PAVESI, G. & MANTOVANI, R. 2008. The histone-like NF-Y is a bifunctional transcription factor. *Mol Cell Biol,* 28**,** 2047-58.

CHAMBERS, I., COLBY, D., ROBERTSON, M., NICHOLS, J., LEE, S., TWEEDIE, S. & SMITH, A. 2003. Functional expression cloning of Nanog, a pluripotency sustaining factor in embryonic stem cells. *Cell,* 113**,** 643-55.

CHAMBERS, I., SILVA, J., COLBY, D., NICHOLS, J., NIJMEIJER, B., ROBERTSON, M., VRANA, J., JONES, K., GROTEWOLD, L. & SMITH, A. 2007. Nanog safeguards pluripotency and mediates germline development. *Nature,* 450**,** 1230-4.

CHANG, K. H., VINCENT, F. & SHAH, K. 2012. Deregulated Cdk5 triggers aberrant activation of cell cycle kinases and phosphatases inducing neuronal death. *J Cell Sci,* 125**,** 5124-37.

CHARAFE-JAUFFRET, E., GINESTIER, C., IOVINO, F., WICINSKI, J., CERVERA, N., FINETTI, P., HUR, M. H., DIEBEL, M. E., MONVILLE, F., DUTCHER, J., BROWN, M., VIENS, P., XERRI, L., BERTUCCI, F., STASSI, G., DONTU, G., BIRNBAUM, D. & WICHA, M. S. 2009. Breast cancer cell lines contain functional cancer stem cells with metastatic capacity and a distinct molecular signature. *Cancer Res,* 69**,** 1302-13.

CHELLAPPAN, S. P., HIEBERT, S., MUDRYJ, M., HOROWITZ, J. M. & NEVINS, J. R. 1991. The E2F transcription factor is a cellular target for the RB protein. *Cell,* 65**,** 1053-61.

CHEN, C. C., ZHU, X. G. & ZHONG, S. 2008. Selection of thermodynamic models for combinatorial control of multiple transcription factors in early differentiation of embryonic stem cells. *BMC Genomics,* 9 Suppl 1**,** S18.

CHEN, M., CHEN, S., DU, M., TANG, S., CHEN, M., WANG, W., YANG, H., CHEN, Q. & CHEN, J. 2015a. Toxic effect of palladium on embryonic development of zebrafish. *Aquat Toxicol,* 159**,** 208-16.

CHEN, X., XU, B., HAN, X., MAO, Z., CHEN, M., DU, G., TALBOT, P., WANG, X. & XIA, Y. 2015b. The effects of triclosan on pluripotency factors and development of mouse embryonic stem cells and zebrafish. *Arch Toxicol,* 89**,** 635-46.

CHIANG, K. P., NIESSEN, S., SAGHATELIAN, A. & CRAVATT, B. F. 2006. An enzyme that regulates ether lipid signaling pathways in cancer annotated by multidimensional profiling. *Chem Biol,* 13**,** 1041-50.

CHIN, M. H., MASON, M. J., XIE, W., VOLINIA, S., SINGER, M., PETERSON, C., AMBARTSUMYAN, G., AIMIUWU, O., RICHTER, L., ZHANG, J., KHVOROSTOV, I., OTT, V., GRUNSTEIN, M., LAVON, N., BENVENISTY, N., CROCE, C. M., CLARK, A. T., BAXTER, T., PYLE, A. D., TEITELL, M. A., PELEGRINI, M., PLATH, K. & LOWRY, W. E. 2009. Induced pluripotent stem cells and embryonic stem cells are distinguished by gene expression signatures. *Cell Stem Cell,* 5**,** 111-23.

CHUANG, J. Y., WU, C. H., LAI, M. D., CHANG, W. C. & HUNG, J. J. 2009. Overexpression of Sp1 leads to p53-dependent apoptosis in cancer cells. *Int J Cancer,* 125**,** 2066-76.

COE, T. S., HAMILTON, P. B., GRIFFITHS, A. M., HODGSON, D. J., WAHAB, M. A. & TYLER, C. R. 2009. Genetic variation in strains of zebrafish (Danio rerio) and the implications for ecotoxicology studies. *Ecotoxicology,* 18**,** 144-50.

COLE, M. F., JOHNSTONE, S. E., NEWMAN, J. J., KAGEY, M. H. & YOUNG, R. A. 2008. Tcf3 is an integral component of the core regulatory circuitry of embryonic stem cells. *Genes Dev,* 22**,** 746-55.

CONKLIN, J. F., BAKER, J. & SAGE, J. 2012. The RB family is required for the self-renewal and survival of human embryonic stem cells. *Nat Commun,* 3**,** 1244.

CONSTAM, D. B. & ROBERTSON, E. J. 2000. Tissue-specific requirements for the proprotein convertase furin/SPC1 during embryonic turning and heart looping. *Development,* 127**,** 245-54.

COREY, D. R. & ABRAMS, J. M. 2001. Morpholino antisense oligonucleotides: tools for investigating vertebrate development. *Genome Biol,* 2**,** REVIEWS1015.

COWAN, C. A., KLIMANSKAYA, I., MCMAHON, J., ATIENZA, J., WITMYER, J., ZUCKER, J. P., WANG, S., MORTON, C. C., MCMAHON, A. P., POWERS, D. & MELTON, D. A. 2004. Derivation of embryonic stem-cell lines from human blastocysts. *N Engl J Med,* 350**,** 1353-6.

CUBEDDU, L., JOSEPH, S., RICHARD, D. J. & MATTHEWS, J. M. 2012. Contribution of DEAF1 structural domains to the interaction with the breast cancer oncogene LMO4. *PLoS One,* 7**,** e39218.

DAHERON, L., OPITZ, S. L., ZAEHRES, H., LENSCH, M. W., ANDREWS, P. W., ITSKOVITZ-ELDOR, J. & DALEY, G. Q. 2004. LIF/STAT3 signaling fails to maintain self-renewal of human embryonic stem cells. *Stem Cells,* 22**,** 770-8.

DAI, C., MIAO, C. X., XU, X. M., LIU, L. J., GU, Y. F., ZHOU, D., CHEN, L. S., LIN, G. & LU, G. X. 2015. Transcriptional activation of human CDCA8 gene regulated by transcription factor NF-Y in embryonic stem cells and cancer cells. *J Biol Chem,* 290**,** 22423-34.

DAVIE, J. R., HE, S., LI, L., SEKHAVAT, A., ESPINO, P., DROBIC, B., DUNN, K. L., SUN, J. M., CHEN, H. Y., YU, J., PRITCHARD, S. & WANG, X. 2008. Nuclear organization and chromatin dynamics--Sp1, Sp3 and histone deacetylases. *Adv Enzyme Regul,* 48**,** 189-208.

DEAN, D. A. 2006. Preparation (pulling) of needles for gene delivery by microinjection. *CSH Protoc,* 2006.

DENG, H., SUN, Y., ZHANG, Y., LUO, X., HOU, W., YAN, L., CHEN, Y., TIAN, E., HAN, J. & ZHANG, H. 2007. Transcription factor NFY globally represses the expression of the C. elegans Hox gene Abdominal-B homolog egl-5. *Dev Biol,* 308**,** 583-92.

DOLFINI, D., MINUZZO, M., PAVESI, G. & MANTOVANI, R. 2012. The short isoform of NF-YA belongs to the embryonic stem cell transcription factor circuitry. *Stem Cells,* 30**,** 2450-9.

DRAPER, B. W., MORCOS, P. A. & KIMMEL, C. B. 2001. Inhibition of zebrafish fgf8 pre-mRNA splicing with morpholino oligos: a quantifiable method for gene knockdown. *Genesis,* 30**,** 154-6.

DRAPER, J. S., PIGOTT, C., THOMSON, J. A. & ANDREWS, P. W. 2002. Surface antigens of human embryonic stem cells: changes upon differentiation in culture. *J Anat,* 200**,** 249-58.

DRIEVER, W., SOLNICA-KREZEL, L., SCHIER, A. F., NEUHAUSS, S. C., MALICKI, J., STEMPLE, D. L., STAINIER, D. Y., ZWARTKRUIS, F., ABDELILAH, S., RANGINI, Z., BELAK, J. & BOGGS, C. 1996. A genetic screen for mutations affecting embryogenesis in zebrafish. *Development,* 123**,** 37-46.

DRIVDAHL, R., HAUGK, K. H., SPRENGER, C. C., NELSON, P. S., TENNANT, M. K. & PLYMATE, S. R. 2004. Suppression of growth and tumorigenicity in the prostate tumor cell line M12 by overexpression of the transcription factor SOX9. *Oncogene,* 23**,** 4584-93.

EISEN, J. S. & SMITH, J. C. 2008. Controlling morpholino experiments: don't stop making antisense. *Development,* 135**,** 1735-43.

EKKER, S. C. & LARSON, J. D. 2001. Morphant technology in model developmental systems. *Genesis,* 30**,** 89-93.

FAN, L., CRODIAN, J., LIU, X., ALESTROM, A., ALESTROM, P. & COLLODI, P. 2004. Zebrafish embryo cells remain pluripotent and germ-line competent for multiple passages in culture. *Zebrafish,* 1**,** 21-6.

FARINA, A., MANNI, I., FONTEMAGGI, G., TIAINEN, M., CENCIARELLI, C., BELLORINI, M., MANTOVANI, R., SACCHI, A. & PIAGGIO, G. 1999. Down-regulation of cyclin B1 gene transcription in terminally differentiated skeletal muscle cells is associated with loss of functional CCAAT-binding NF-Y complex. *Oncogene,* 18**,** 2818-27.

FILIPCZYK, A. A., LASLETT, A. L., MUMMERY, C. & PERA, M. F. 2007. Differentiation is coupled to changes in the cell cycle regulatory apparatus of human embryonic stem cells. *Stem Cell Res,* 1**,** 45-60.

FLEMING, T. P. 1987. A quantitative analysis of cell allocation to trophectoderm and inner cell mass in the mouse blastocyst. *Dev Biol,* 119**,** 520-31.

FLUCKIGER, A. C., MARCY, G., MARCHAND, M., NEGRE, D., COSSET, F. L., MITALIPOV, S., WOLF, D., SAVATIER, P. & DEHAY, C. 2006. Cell cycle features of primate embryonic stem cells. *Stem Cells,* 24**,** 547-56.

FONG, H., HOHENSTEIN, K. A. & DONOVAN, P. J. 2008. Regulation of self-renewal and pluripotency by Sox2 in human embryonic stem cells. *Stem Cells,* 26**,** 1931-8.

GAJ, T., GERSBACH, C. A. & BARBAS, C. F., 3RD 2013. ZFN, TALEN, and CRISPR/Cas-based methods for genome engineering. *Trends Biotechnol,* 31**,** 397-405.

GANGARAJU, V. K. & LIN, H. 2009. MicroRNAs: key regulators of stem cells. *Nat Rev Mol Cell Biol,* 10**,** 116-25.

GARDNER, R. L. & ROSSANT, J. 1979. Investigation of the fate of 4-5 day post-coitum mouse inner cell mass cells by blastocyst injection. *J Embryol Exp Morphol,* 52**,** 141-52.

GERLOFF, A., DITTMER, A., OERLECKE, I., HOLZHAUSEN, H. J. & DITTMER, J. 2011. Protein expression of the Ets transcription factor Elf-1 in breast cancer cells is negatively correlated with histological grading, but not with clinical outcome. *Oncol Rep,* 26**,** 1121-5.

GHANEM, N., ANDRUSIAK, M. G., SVOBODA, D., AL LAFI, S. M., JULIAN, L. M., MCCLELLAN, K. A., DE REPENTIGNY, Y., KOTHARY, R., EKKER, M., BLAIS, A., PARK, D. S. & SLACK, R. S. 2012. The Rb/E2F pathway modulates neurogenesis through direct regulation of the Dlx1/Dlx2 bigene cluster. *J Neurosci,* 32**,** 8219-30.

GHOSH, C. & COLLODI, P. 1994. Culture of cells from zebrafish (Brachydanio rerio) blastula-stage embryos. *Cytotechnology,* 14**,** 21-6.

GKOUNTELA, S., LI, Z., CHIN, C. J., LEE, S. A. & CLARK, A. T. 2014. PRMT5 is required for human embryonic stem cell proliferation but not pluripotency. *Stem Cell Rev,* 10**,** 230-9.

GOLDSTEIN, L. A., GHERSI, G., PINEIRO-SANCHEZ, M. L., SALAMONE, M., YEH, Y., FLESSATE, D. & CHEN, W. T. 1997. Molecular cloning of seprase: a serine integral membrane protease from human melanoma. *Biochim Biophys Acta,* 1361**,** 11-9.

GREBER, B., LEHRACH, H. & ADJAYE, J. 2007. Fibroblast growth factor 2 modulates transforming growth factor beta signaling in mouse embryonic fibroblasts and human ESCs (hESCs) to support hESC self-renewal. *Stem Cells,* 25**,** 455-64.

GRSKOVIC, M., CHAIVORAPOL, C., GASPAR-MAIA, A., LI, H. & RAMALHO-SANTOS, M. 2007. Systematic identification of cis-regulatory sequences active in mouse and human embryonic stem cells. *PLoS Genet,* 3**,** e145.

GU, B., ZHANG, J., CHEN, Q., TAO, B., WANG, W., ZHOU, Y., CHEN, L., LIU, Y. & ZHANG, M. 2010. Aire regulates the expression of differentiation-associated genes and self-renewal of embryonic stem cells. *Biochem Biophys Res Commun,* 394**,** 418-23.

GUO, Y., COSTA, R., RAMSEY, H., STARNES, T., VANCE, G., ROBERTSON, K., KELLEY, M., REINBOLD, R., SCHOLER, H. & HROMAS, R. 2002. The embryonic stem cell transcription factors Oct-4 and FoxD3 interact to regulate endodermal-specific promoter expression. *Proc Natl Acad Sci U S A,* 99**,** 3663-7.

GURDON, J. B. 1962. The transplantation of nuclei between two species of Xenopus. *Dev Biol,* 5**,** 68-83.

HAFFTER, P., GRANATO, M., BRAND, M., MULLINS, M. C., HAMMERSCHMIDT, M., KANE, D. A., ODENTHAL, J., VAN EEDEN, F. J., JIANG, Y. J., HEISENBERG, C. P., KELSH, R. N., FURUTANI-SEIKI, M., VOGELSANG, E., BEUCHLE, D., SCHACH, U., FABIAN, C. & NUSSLEIN-VOLHARD, C. 1996. The identification of genes with unique and essential functions in the development of the zebrafish, Danio rerio. *Development,* 123**,** 1-36.

HAN, J. H., LEE, S. H., TAN, Y. Q., LEMOSY, E. K. & HASHIMOTO, C. 2000. Gastrulation defective is a serine protease involved in activating the receptor toll to polarize the Drosophila embryo. *Proc Natl Acad Sci U S A,* 97**,** 9093-7.

HANNA, J., CHENG, A. W., SAHA, K., KIM, J., LENGNER, C. J., SOLDNER, F., CASSADY, J. P., MUFFAT, J., CAREY, B. W. & JAENISCH, R. 2010. Human embryonic stem cells with biological and epigenetic characteristics similar to those of mouse ESCs. *Proc Natl Acad Sci U S A,* 107**,** 9222-7.

HANNA, L. A., FOREMAN, R. K., TARASENKO, I. A., KESSLER, D. S. & LABOSKY, P. A. 2002. Requirement for Foxd3 in maintaining pluripotent cells of the early mouse embryo. *Genes Dev,* 16**,** 2650-61.

HART, A. H., HARTLEY, L., IBRAHIM, M. & ROBB, L. 2004. Identification, cloning and expression analysis of the pluripotency promoting Nanog genes in mouse and human. *Dev Dyn,* 230**,** 187-98.

HATANO, S. Y., TADA, M., KIMURA, H., YAMAGUCHI, S., KONO, T., NAKANO, T., SUEMORI, H., NAKATSUJI, N. & TADA, T. 2005. Pluripotential competence of cells associated with Nanog activity. *Mech Dev,* 122**,** 67-79.

HAY, D. C., SUTHERLAND, L., CLARK, J. & BURDON, T. 2004. Oct-4 knockdown induces similar patterns of endoderm and trophoblast differentiation markers in human and mouse embryonic stem cells. *Stem Cells,* 22**,** 225-35.

HEASMAN, J., KOFRON, M. & WYLIE, C. 2000. Beta-catenin signaling activity dissected in the early Xenopus embryo: a novel antisense approach. *Dev Biol,* 222**,** 124-34.

HEINS, N., ENGLUND, M. C., SJOBLOM, C., DAHL, U., TONNING, A., BERGH, C., LINDAHL, A., HANSON, C. & SEMB, H. 2004. Derivation, characterization, and differentiation of human embryonic stem cells. *Stem Cells,* 22**,** 367-76.

HENRY, T. R., SPITSBERGEN, J. M., HORNUNG, M. W., ABNET, C. C. & PETERSON, R. E. 1997. Early life stage toxicity of 2,3,7,8-tetrachlorodibenzo-p-dioxin in zebrafish (Danio rerio). *Toxicol Appl Pharmacol,* 142**,** 56-68.

HIRST, M., DELANEY, A., ROGERS, S. A., SCHNERCH, A., PERSAUD, D. R., O'CONNOR, M. D., ZENG, T., MOKSA, M., FICHTER, K., MAH, D., GO, A., MORIN, R. D., BAROSS, A., ZHAO, Y., KHATTRA, J., PRABHU, A. L., PANDOH, P., MCDONALD, H., ASANO, J., DHALLA, N., MA, K., LEE, S., ALLY, A., CHAHAL, N., MENZIES, S., SIDDIQUI, A., HOLT, R., JONES, S., GERHARD, D. S., THOMSON, J. A., EAVES, C. J. & MARRA, M. A. 2007. LongSAGE profiling of nine human embryonic stem cell lines. *Genome Biol,* 8**,** R113.

HOUGH, S. R., CLEMENTS, I., WELCH, P. J. & WIEDERHOLT, K. A. 2006. Differentiation of mouse embryonic stem cells after RNA interference-mediated silencing of OCT4 and Nanog. *Stem Cells,* 24**,** 1467-75.

HOWE, K., CLARK, M. D., TORROJA, C. F., TORRANCE, J., BERTHELOT, C., MUFFATO, M., COLLINS, J. E., HUMPHRAY, S., MCLAREN, K., MATTHEWS, L., MCLAREN, S., SEALY, I., CACCAMO, M., CHURCHER, C., SCOTT, C., BARRETT, J. C., KOCH, R., RAUCH, G. J., WHITE, S., CHOW, W., KILIAN, B., QUINTAIS, L. T., GUERRA-ASSUNCAO, J. A., ZHOU, Y., GU, Y., YEN, J., VOGEL, J. H., EYRE, T., REDMOND, S., BANERJEE, R., CHI, J., FU, B., LANGLEY, E., MAGUIRE, S. F., LAIRD, G. K., LLOYD, D., KENYON, E., DONALDSON, S., SEHRA, H., ALMEIDA-KING, J., LOVELAND, J., TREVANION, S., JONES, M., QUAIL, M., WILLEY, D., HUNT, A., BURTON, J., SIMS, S., MCLAY, K., PLUMB, B., DAVIS, J., CLEE, C., OLIVER, K., CLARK, R., RIDDLE, C., ELLIOT, D., THREADGOLD, G., HARDEN, G., WARE, D., BEGUM, S., MORTIMORE, B., KERRY, G., HEATH, P., PHILLIMORE, B., TRACEY, A., CORBY, N., DUNN, M., JOHNSON, C., WOOD, J., CLARK, S., PELAN, S., GRIFFITHS, G., SMITH, M., GLITHERO, R., HOWDEN, P., BARKER, N., LLOYD, C., STEVENS, C., HARLEY, J., HOLT, K., PANAGIOTIDIS, G., LOVELL, J., BEASLEY, H., HENDERSON, C., GORDON, D., AUGER, K., WRIGHT, D., COLLINS, J., RAISEN, C., DYER, L., LEUNG, K., ROBERTSON, L., AMBRIDGE, K., LEONGAMORNLERT, D., MCGUIRE, S., GILDERTHORP, R., GRIFFITHS, C., MANTHRAVADI, D., NICHOL, S., BARKER, G., et al. 2013. The zebrafish reference genome sequence and its relationship to the human genome. *Nature,* 496**,** 498-503.

HRUSCHA, A., KRAWITZ, P., RECHENBERG, A., HEINRICH, V., HECHT, J., HAASS, C. & SCHMID, B. 2013. Efficient CRISPR/Cas9 genome editing with low off-target effects in zebrafish. *Development,* 140**,** 4982-7.

HUANG, D. W., SHERMAN, B. T., TAN, Q., COLLINS, J. R., ALVORD, W. G., ROAYAEI, J., STEPHENS, R., BASELER, M. W., LANE, H. C. & LEMPICKI, R. A. 2007. The DAVID Gene Functional Classification Tool: a novel biological module-centric algorithm to functionally analyze large gene lists. *Genome Biol,* 8**,** R183.

HUANGFU, D., OSAFUNE, K., MAEHR, R., GUO, W., EIJKELENBOOM, A., CHEN, S., MUHLESTEIN, W. & MELTON, D. A. 2008. Induction of pluripotent stem cells from primary human fibroblasts with only Oct4 and Sox2. *Nat Biotechnol,* 26**,** 1269-75.

HUMPHREY, R. K., BEATTIE, G. M., LOPEZ, A. D., BUCAY, N., KING, C. C., FIRPO, M. T., ROSE-JOHN, S. & HAYEK, A. 2004. Maintenance of pluripotency in human embryonic stem cells is STAT3 independent. *Stem Cells,* 22**,** 522-30.

HWANG, W. Y., FU, Y., REYON, D., MAEDER, M. L., TSAI, S. Q., SANDER, J. D., PETERSON, R. T., YEH, J. R. & JOUNG, J. K. 2013. Efficient genome editing in zebrafish using a CRISPR-Cas system. *Nat Biotechnol,* 31**,** 227-9.

HYSLOP, L., STOJKOVIC, M., ARMSTRONG, L., WALTER, T., STOJKOVIC, P., PRZYBORSKI, S., HERBERT, M., MURDOCH, A., STRACHAN, T. & LAKO, M. 2005. Downregulation of NANOG induces differentiation of human embryonic stem cells to extraembryonic lineages. *Stem Cells,* 23**,** 1035-43.

IMPENS, F., TIMMERMAN, E., STAES, A., MOENS, K., ARIEN, K. K., VERHASSELT, B., VANDEKERCKHOVE, J. & GEVAERT, K. 2012. A catalogue of putative HIV-1 protease host cell substrates. *Biol Chem,* 393**,** 915-31.

IRION, S., NOSTRO, M. C., KATTMAN, S. J. & KELLER, G. M. 2008. Directed differentiation of pluripotent stem cells: from developmental biology to therapeutic applications. *Cold Spring Harb Symp Quant Biol,* 73**,** 101-10.

ITSKOVITZ-ELDOR, J., SCHULDINER, M., KARSENTI, D., EDEN, A., YANUKA, O., AMIT, M., SOREQ, H. & BENVENISTY, N. 2000. Differentiation of human embryonic stem cells into embryoid bodies compromising the three embryonic germ layers. *Mol Med,* 6**,** 88-95.

IVANOVA, N., DOBRIN, R., LU, R., KOTENKO, I., LEVORSE, J., DECOSTE, C., SCHAFER, X., LUN, Y. & LEMISCHKA, I. R. 2006. Dissecting self-renewal in stem cells with RNA interference. *Nature,* 442**,** 533-8.

JAMES, D., LEVINE, A. J., BESSER, D. & HEMMATI-BRIVANLOU, A. 2005. TGFbeta/activin/nodal signaling is necessary for the maintenance of pluripotency in human embryonic stem cells. *Development,* 132**,** 1273-82.

JEON, H. Y. & LEE, H. 2013. Depletion of Aurora-A in zebrafish causes growth retardation due to mitotic delay and p53-dependent cell death. *FEBS J,* 280**,** 1518-30.

JESSANI, N., LIU, Y., HUMPHREY, M. & CRAVATT, B. F. 2002. Enzyme activity profiles of the secreted and membrane proteome that depict cancer cell invasiveness. *Proc Natl Acad Sci U S A,* 99**,** 10335-40.

JIA, F., WILSON, K. D., SUN, N., GUPTA, D. M., HUANG, M., LI, Z., PANETTA, N. J., CHEN, Z. Y., ROBBINS, R. C., KAY, M. A., LONGAKER, M. T. & WU, J. C. 2010. A nonviral minicircle vector for deriving human iPS cells. *Nat Methods,* 7**,** 197-9.

KAUFHOLD, S., GARBAN, H. & BONAVIDA, B. 2016. Yin Yang 1 is associated with cancer stem cell transcription factors (SOX2, OCT4, BMI1) and clinical implication. *J Exp Clin Cancer Res,* 35**,** 84.

KIM, J., CHU, J., SHEN, X., WANG, J. & ORKIN, S. H. 2008. An extended transcriptional network for pluripotency of embryonic stem cells. *Cell,* 132**,** 1049-61.

KIM, K. T., ZAIKOVA, T., HUTCHISON, J. E. & TANGUAY, R. L. 2013. Gold nanoparticles disrupt zebrafish eye development and pigmentation. *Toxicol Sci,* 133**,** 275-88.

KIMMEL, C. B., BALLARD, W. W., KIMMEL, S. R., ULLMANN, B. & SCHILLING, T. F. 1995. Stages of embryonic development of the zebrafish. *Dev Dyn,* 203**,** 253-310.

KIMMEL, C. B. & WARGA, R. M. 1986. Tissue-specific cell lineages originate in the gastrula of the zebrafish. *Science,* 231**,** 365-8.

KOK, F. O., SHIN, M., NI, C. W., GUPTA, A., GROSSE, A. S., VAN IMPEL, A., KIRCHMAIER, B. C., PETERSON-MADURO, J., KOURKOULIS, G., MALE, I., DESANTIS, D. F., SHEPPARD-TINDELL, S., EBARASI, L., BETSHOLTZ, C., SCHULTE-MERKER, S., WOLFE, S. A. & LAWSON, N. D. 2015. Reverse genetic screening reveals poor correlation between morpholino-induced and mutant phenotypes in zebrafish. *Dev Cell,* 32**,** 97-108.

KOPP, J. L., ORMSBEE, B. D., DESLER, M. & RIZZINO, A. 2008. Small increases in the level of Sox2 trigger the differentiation of mouse embryonic stem cells. *Stem Cells,* 26**,** 903-11.

KOTKAMP, K., KUR, E., WENDIK, B., POLOK, B. K., BEN-DOR, S., ONICHTCHOUK, D. & DRIEVER, W. 2014. Pou5f1/Oct4 promotes cell survival via direct activation of mych expression during zebrafish gastrulation. *PLoS One,* 9**,** e92356.

KOZAR, K., CIEMERYCH, M. A., REBEL, V. I., SHIGEMATSU, H., ZAGOZDZON, A., SICINSKA, E., GENG, Y., YU, Q., BHATTACHARYA, S., BRONSON, R. T., AKASHI, K. & SICINSKI, P. 2004. Mouse development and cell proliferation in the absence of D-cyclins. *Cell,* 118**,** 477-91.

KRISHNAKUMAR, R., CHEN, A. F., PANTOVICH, M. G., DANIAL, M., PARCHEM, R. J., LABOSKY, P. A. & BLELLOCH, R. 2016. FOXD3 Regulates Pluripotent Stem Cell Potential by Simultaneously Initiating and Repressing Enhancer Activity. *Cell Stem Cell,* 18**,** 104-17.

KUEHN, H., LIBERZON, A., REICH, M. & MESIROV, J. P. 2008. Using GenePattern for gene expression analysis. *Curr Protoc Bioinformatics,* Chapter 7**,** Unit 7 12.

KURODA, T., TADA, M., KUBOTA, H., KIMURA, H., HATANO, S. Y., SUEMORI, H., NAKATSUJI, N. & TADA, T. 2005. Octamer and Sox elements are required for transcriptional cis regulation of Nanog gene expression. *Mol Cell Biol,* 25**,** 2475-85.

LANGHEINRICH, U., HENNEN, E., STOTT, G. & VACUN, G. 2002. Zebrafish as a model organism for the identification and characterization of drugs and genes affecting p53 signaling. *Curr Biol,* 12**,** 2023-8.

LEE, E. Y., TO, H., SHEW, J. Y., BOOKSTEIN, R., SCULLY, P. & LEE, W. H. 1988. Inactivation of the retinoblastoma susceptibility gene in human breast cancers. *Science,* 241**,** 218-21.

LENSCH, M. W., SCHLAEGER, T. M., ZON, L. I. & DALEY, G. Q. 2007. Teratoma formation assays with human embryonic stem cells: a rationale for one type of human-animal chimera. *Cell Stem Cell,* 1**,** 253-8.

LEUNG, C. F., WEBB, S. E. & MILLER, A. L. 1998. Calcium transients accompany ooplasmic segregation in zebrafish embryos. *Dev Growth Differ,* 40**,** 313-26.

LI, Y., MCCLINTICK, J., ZHONG, L., EDENBERG, H. J., YODER, M. C. & CHAN, R. J. 2005. Murine embryonic stem cell differentiation is promoted by SOCS-3 and inhibited by the zinc finger transcription factor Klf4. *Blood,* 105**,** 635-7.

LIN, E., CHEN, M. C., HUANG, C. Y., HSU, S. L., HUANG, W. J., LIN, M. S., WU, J. C. & LIN, H. 2014. All-trans retinoic acid induces DU145 cell cycle arrest through Cdk5 activation. *Cell Physiol Biochem,* 33**,** 1620-30.

LIN, T., CHAO, C., SAITO, S., MAZUR, S. J., MURPHY, M. E., APPELLA, E. & XU, Y. 2005. p53 induces differentiation of mouse embryonic stem cells by suppressing Nanog expression. *Nat Cell Biol,* 7**,** 165-71.

LIU, Y. & LABOSKY, P. A. 2008. Regulation of embryonic stem cell self-renewal and pluripotency by Foxd3. *Stem Cells,* 26**,** 2475-84.

LOH, Y. H., WU, Q., CHEW, J. L., VEGA, V. B., ZHANG, W., CHEN, X., BOURQUE, G., GEORGE, J., LEONG, B., LIU, J., WONG, K. Y., SUNG, K. W., LEE, C. W., ZHAO, X. D., CHIU, K. P., LIPOVICH, L., KUZNETSOV, V. A., ROBSON, P., STANTON, L. W., WEI, C. L., RUAN, Y., LIM, B. & NG, H. H. 2006. The Oct4 and Nanog transcription network regulates pluripotency in mouse embryonic stem cells. *Nat Genet,* 38**,** 431-40.

LUCIBELLO, F. C., TRUSS, M., ZWICKER, J., EHLERT, F., BEATO, M. & MULLER, R. 1995. Periodic cdc25C transcription is mediated by a novel cell cycle-regulated repressor element (CDE). *EMBO J,* 14**,** 132-42.

LUDWIG, T. E., LEVENSTEIN, M. E., JONES, J. M., BERGGREN, W. T., MITCHEN, E. R., FRANE, J. L., CRANDALL, L. J., DAIGH, C. A., CONARD, K. R., PIEKARCZYK, M. S., LLANAS, R. A. & THOMSON, J. A. 2006. Derivation of human embryonic stem cells in defined conditions. *Nat Biotechnol,* 24**,** 185-7.

MANNI, I., CARETTI, G., ARTUSO, S., GURTNER, A., EMILIOZZI, V., SACCHI, A., MANTOVANI, R. & PIAGGIO, G. 2008. Posttranslational regulation of NF-YA modulates NF-Y transcriptional activity. *Mol Biol Cell,* 19**,** 5203-13.

MANNI, I., MAZZARO, G., GURTNER, A., MANTOVANI, R., HAUGWITZ, U., KRAUSE, K., ENGELAND, K., SACCHI, A., SODDU, S. & PIAGGIO, G. 2001. NF-Y mediates the transcriptional inhibition of the cyclin B1, cyclin B2, and cdc25C promoters upon induced G2 arrest. *J Biol Chem,* 276**,** 5570-6.

MARTIN, G. R. 1981. Isolation of a pluripotent cell line from early mouse embryos cultured in medium conditioned by teratocarcinoma stem cells. *Proc Natl Acad Sci U S A,* 78**,** 7634-8.

MASUI, S., NAKATAKE, Y., TOYOOKA, Y., SHIMOSATO, D., YAGI, R., TAKAHASHI, K., OKOCHI, H., OKUDA, A., MATOBA, R., SHAROV, A. A., KO, M. S. & NIWA, H. 2007. Pluripotency governed by Sox2 via regulation of Oct3/4 expression in mouse embryonic stem cells. *Nat Cell Biol,* 9**,** 625-35.

MATSUDA, T., NAKAMURA, T., NAKAO, K., ARAI, T., KATSUKI, M., HEIKE, T. & YOKOTA, T. 1999. STAT3 activation is sufficient to maintain an undifferentiated state of mouse embryonic stem cells. *EMBO J,* 18**,** 4261-9.

MELO, K. M., OLIVEIRA, R., GRISOLIA, C. K., DOMINGUES, I., PIECZARKA, J. C., DE SOUZA FILHO, J. & NAGAMACHI, C. Y. 2015. Short-term exposure to low doses of rotenone induces developmental, biochemical, behavioral, and histological changes in fish. *Environ Sci Pollut Res Int,* 22**,** 13926-38.

MILAN, D. J., PETERSON, T. A., RUSKIN, J. N., PETERSON, R. T. & MACRAE, C. A. 2003. Drugs that induce repolarization abnormalities cause bradycardia in zebrafish. *Circulation,* 107**,** 1355-8.

MITALIPOVA, M., CALHOUN, J., SHIN, S., WININGER, D., SCHULZ, T., NOGGLE, S., VENABLE, A., LYONS, I., ROBINS, A. & STICE, S. 2003. Human embryonic stem cell lines derived from discarded embryos. *Stem Cells,* 21**,** 521-6.

MITSUI, K., TOKUZAWA, Y., ITOH, H., SEGAWA, K., MURAKAMI, M., TAKAHASHI, K., MARUYAMA, M., MAEDA, M. & YAMANAKA, S. 2003. The homeoprotein Nanog is required for maintenance of pluripotency in mouse epiblast and ES cells. *Cell,* 113**,** 631-42.

MOJSIN, M., TOPALOVIC, V., MARJANOVIC VICENTIC, J. & STEVANOVIC, M. 2015. Transcription factor NF-Y inhibits cell growth and decreases SOX2 expression in human embryonal carcinoma cell line NT2/D1. *Biochemistry (Mosc),* 80**,** 202-7.

MULLER, H. & HELIN, K. 2000. The E2F transcription factors: key regulators of cell proliferation. *Biochim Biophys Acta,* 1470**,** M1-12.

MUMMERY, C. L., VAN DEN BRINK, C. E. & DE LAAT, S. W. 1987. Commitment to differentiation induced by retinoic acid in P19 embryonal carcinoma cells is cell cycle dependent. *Dev Biol,* 121**,** 10-9.

NACHMANY, H., WALD, S., ABEKASIS, M., BULVIK, S. & WEIL, M. 2012. Two potential biomarkers identified in mesenchymal stem cells and leukocytes of patients with sporadic amyotrophic lateral sclerosis. *Dis Markers,* 32**,** 211-20.

NARSINH, K. H., JIA, F., ROBBINS, R. C., KAY, M. A., LONGAKER, M. T. & WU, J. C. 2011. Generation of adult human induced pluripotent stem cells using nonviral minicircle DNA vectors. *Nat Protoc,* 6**,** 78-88.

NASEVICIUS, A. & EKKER, S. C. 2000. Effective targeted gene 'knockdown' in zebrafish. *Nat Genet,* 26**,** 216-20.

NICHOLS, J. & SMITH, A. 2009. Naive and primed pluripotent states. *Cell Stem Cell,* 4**,** 487-92.

NICHOLS, J., ZEVNIK, B., ANASTASSIADIS, K., NIWA, H., KLEWE-NEBENIUS, D., CHAMBERS, I., SCHOLER, H. & SMITH, A. 1998. Formation of pluripotent stem cells in the mammalian embryo depends on the POU transcription factor Oct4. *Cell,* 95**,** 379-91.

NIWA, H., BURDON, T., CHAMBERS, I. & SMITH, A. 1998. Self-renewal of pluripotent embryonic stem cells is mediated via activation of STAT3. *Genes Dev,* 12**,** 2048-60.

NIWA, H., MIYAZAKI, J. & SMITH, A. G. 2000. Quantitative expression of Oct-3/4 defines differentiation, dedifferentiation or self-renewal of ES cells. *Nat Genet,* 24**,** 372-6.

O'CONNOR, M. D., KARDEL, M. D., IOSFINA, I., YOUSSEF, D., LU, M., LI, M. M., VERCAUTEREN, S., NAGY, A. & EAVES, C. J. 2008. Alkaline phosphatase-positive colony formation is a sensitive, specific, and quantitative indicator of undifferentiated human embryonic stem cells. *Stem Cells,* 26**,** 1109-16.

O'CONNOR, M. D., WEDERELL, E., ROBERTSON, G., DELANEY, A., MOROZOVA, O., POON, S. S., YAP, D., FEE, J., ZHAO, Y., MCDONALD, H., ZENG, T., HIRST, M., MARRA, M. A., APARICIO, S. A. & EAVES, C. J. 2011. Retinoblastoma-binding proteins 4 and 9 are important for human pluripotent stem cell maintenance. *Exp Hematol,* 39**,** 866-79 e1.

OGAWA, K., SAITO, A., MATSUI, H., SUZUKI, H., OHTSUKA, S., SHIMOSATO, D., MORISHITA, Y., WATABE, T., NIWA, H. & MIYAZONO, K. 2007. Activin-Nodal signaling is involved in propagation of mouse embryonic stem cells. *J Cell Sci,* 120**,** 55-65.

OKITA, K., NAKAGAWA, M., HYENJONG, H., ICHISAKA, T. & YAMANAKA, S. 2008. Generation of mouse induced pluripotent stem cells without viral vectors. *Science,* 322**,** 949-53.

OLDFIELD, A. J., YANG, P., CONWAY, A. E., CINGHU, S., FREUDENBERG, J. M., YELLABOINA, S. & JOTHI, R. 2014. Histone-fold domain protein NF-Y promotes chromatin accessibility for cell type-specific master transcription factors. *Mol Cell,* 55**,** 708-22.

OLLIS, D. L., CHEAH, E., CYGLER, M., DIJKSTRA, B., FROLOW, F., FRANKEN, S. M., HAREL, M., REMINGTON, S. J., SILMAN, I., SCHRAG, J. & ET AL. 1992. The alpha/beta hydrolase fold. *Protein Eng,* 5**,** 197-211.

PAN, G., LI, J., ZHOU, Y., ZHENG, H. & PEI, D. 2006. A negative feedback loop of transcription factors that controls stem cell pluripotency and self-renewal. *FASEB J,* 20**,** 1730-2.

PAN, G. & PEI, D. 2005. The stem cell pluripotency factor NANOG activates transcription with two unusually potent subdomains at its C terminus. *J Biol Chem,* 280**,** 1401-7.

PARK, I. H., ZHAO, R., WEST, J. A., YABUUCHI, A., HUO, H., INCE, T. A., LEROU, P. H., LENSCH, M. W. & DALEY, G. Q. 2008. Reprogramming of human somatic cells to pluripotency with defined factors. *Nature,* 451**,** 141-6.

PARNG, C. 2005. In vivo zebrafish assays for toxicity testing. *Curr Opin Drug Discov Devel,* 8**,** 100-6.

PARNG, C., ANDERSON, N., TON, C. & MCGRATH, P. 2004. Zebrafish apoptosis assays for drug discovery. *Methods Cell Biol,* 76**,** 75-85.

PARNG, C., SENG, W. L., SEMINO, C. & MCGRATH, P. 2002. Zebrafish: a preclinical model for drug screening. *Assay Drug Dev Technol,* 1**,** 41-8.

PAUKLIN, S. & VALLIER, L. 2013. The cell-cycle state of stem cells determines cell fate propensity. *Cell,* 155**,** 135-47.

PENG, W. H., LEE, Y. C., CHAU, Y. P., LU, K. S. & KUNG, H. N. 2015. Short-term exposure of zebrafish embryos to arecoline leads to retarded growth, motor impairment, and somite muscle fiber changes. *Zebrafish,* 12**,** 58-70.

PENG, Y. & JAHROUDI, N. 2002. The NFY transcription factor functions as a repressor and activator of the von Willebrand factor promoter. *Blood,* 99**,** 2408-17.

PENG, Y. & JAHROUDI, N. 2003. The NFY transcription factor inhibits von Willebrand factor promoter activation in non-endothelial cells through recruitment of histone deacetylases. *J Biol Chem,* 278**,** 8385-94.

QIU, C., MA, Y., WANG, J., PENG, S. & HUANG, Y. 2010. Lin28-mediated post-transcriptional regulation of Oct4 expression in human embryonic stem cells. *Nucleic Acids Res,* 38**,** 1240-8.

REICH, M., LIEFELD, T., GOULD, J., LERNER, J., TAMAYO, P. & MESIROV, J. P. 2006. GenePattern 2.0. *Nat Genet,* 38**,** 500-1.

REUBINOFF, B. E., PERA, M. F., FONG, C. Y., TROUNSON, A. & BONGSO, A. 2000. Embryonic stem cell lines from human blastocysts: somatic differentiation in vitro. *Nat Biotechnol,* 18**,** 399-404.

REYA, T., DUNCAN, A. W., AILLES, L., DOMEN, J., SCHERER, D. C., WILLERT, K., HINTZ, L., NUSSE, R. & WEISSMAN, I. L. 2003. A role for Wnt signalling in self-renewal of haematopoietic stem cells. *Nature,* 423**,** 409-14.

REYA, T., MORRISON, S. J., CLARKE, M. F. & WEISSMAN, I. L. 2001. Stem cells, cancer, and cancer stem cells. *Nature,* 414**,** 105-11.

RICHARDS, M., TAN, S. P., TAN, J. H., CHAN, W. K. & BONGSO, A. 2004. The transcriptome profile of human embryonic stem cells as defined by SAGE. *Stem Cells,* 22**,** 51-64.

ROBLES, V., MARTI, M. & IZPISUA BELMONTE, J. C. 2011. Study of pluripotency markers in zebrafish embryos and transient embryonic stem cell cultures. *Zebrafish,* 8**,** 57-63.

ROBU, M. E., LARSON, J. D., NASEVICIUS, A., BEIRAGHI, S., BRENNER, C., FARBER, S. A. & EKKER, S. C. 2007. p53 activation by knockdown technologies. *PLoS Genet,* 3**,** e78.

RODDA, D. J., CHEW, J. L., LIM, L. H., LOH, Y. H., WANG, B., NG, H. H. & ROBSON, P. 2005. Transcriptional regulation of nanog by OCT4 and SOX2. *J Biol Chem,* 280**,** 24731-7.

RODOLFA, K. T. & EGGAN, K. 2006. A transcriptional logic for nuclear reprogramming. *Cell,* 126**,** 652-5.

RODRIGUEZ, R. T., VELKEY, J. M., LUTZKO, C., SEERKE, R., KOHN, D. B., O'SHEA, K. S. & FIRPO, M. T. 2007. Manipulation of OCT4 levels in human embryonic stem cells results in induction of differential cell types. *Exp Biol Med (Maywood),* 232**,** 1368-80.

ROEBROEK, A. J., UMANS, L., PAULI, I. G., ROBERTSON, E. J., VAN LEUVEN, F., VAN DE VEN, W. J. & CONSTAM, D. B. 1998. Failure of ventral closure and axial rotation in embryos lacking the proprotein convertase Furin. *Development,* 125**,** 4863-76.

ROIDER, H. G., MANKE, T., O'KEEFFE, S., VINGRON, M. & HAAS, S. A. 2009. PASTAA: identifying transcription factors associated with sets of co-regulated genes. *Bioinformatics,* 25**,** 435-42.

ROSEN, J. N., SWEENEY, M. F. & MABLY, J. D. 2009. Microinjection of zebrafish embryos to analyze gene function. *J Vis Exp*.

SABALIAUSKAS, N. A., FOUTZ, C. A., MEST, J. R., BUDGEON, L. R., SIDOR, A. T., GERSHENSON, J. A., JOSHI, S. B. & CHENG, K. C. 2006. High-throughput zebrafish histology. *Methods,* 39**,** 246-54.

SAVATIER, P., HUANG, S., SZEKELY, L., WIMAN, K. G. & SAMARUT, J. 1994. Contrasting patterns of retinoblastoma protein expression in mouse embryonic stem cells and embryonic fibroblasts. *Oncogene,* 9**,** 809-18.

SAVATIER, P., LAPILLONNE, H., VAN GRUNSVEN, L. A., RUDKIN, B. B. & SAMARUT, J. 1996. Withdrawal of differentiation inhibitory activity/leukemia inhibitory factor up-regulates D-type cyclins and cyclin-dependent kinase inhibitors in mouse embryonic stem cells. *Oncogene,* 12**,** 309-22.

SCHNEIDER, C. A., RASBAND, W. S. & ELICEIRI, K. W. 2012. NIH Image to ImageJ: 25 years of image analysis. *Nat Methods,* 9**,** 671-5.

SCHULDINER, M., YANUKA, O., ITSKOVITZ-ELDOR, J., MELTON, D. A. & BENVENISTY, N. 2000. Effects of eight growth factors on the differentiation of cells derived from human embryonic stem cells. *Proc Natl Acad Sci U S A,* 97**,** 11307-12.

SCUDELLARI, M. 2016. How iPS cells changed the world. *Nature,* 534**,** 310-2.

SHAMBLOTT, M. J., AXELMAN, J., WANG, S., BUGG, E. M., LITTLEFIELD, J. W., DONOVAN, P. J., BLUMENTHAL, P. D., HUGGINS, G. R. & GEARHART, J. D.

1998. Derivation of pluripotent stem cells from cultured human primordial germ cells. *Proc Natl Acad Sci U S A,* 95**,** 13726-31.

SHI, X., DU, Y., LAM, P. K., WU, R. S. & ZHOU, B. 2008. Developmental toxicity and alteration of gene expression in zebrafish embryos exposed to PFOS. *Toxicol Appl Pharmacol,* 230**,** 23-32.

SHI, X., GU, A., JI, G., LI, Y., DI, J., JIN, J., HU, F., LONG, Y., XIA, Y., LU, C., SONG, L., WANG, S. & WANG, X. 2011. Developmental toxicity of cypermethrin in embryo-larval stages of zebrafish. *Chemosphere,* 85**,** 1010-6.

SHI, Z., CHIANG, C. I., LABHART, P., ZHAO, Y., YANG, J., MISTRETTA, T. A., HENNING, S. J., MAITY, S. N. & MORI-AKIYAMA, Y. 2015. Context-specific role of SOX9 in NF-Y mediated gene regulation in colorectal cancer cells. *Nucleic Acids Res,* 43**,** 6257-69.

SHIELDS, D. J., NIESSEN, S., MURPHY, E. A., MIELGO, A., DESGROSELLIER, J. S., LAU, S. K., BARNES, L. A., LESPERANCE, J., BOUVET, M., TARIN, D., CRAVATT, B. F. & CHERESH, D. A. 2010. RBBP9: a tumor-associated serine hydrolase activity required for pancreatic neoplasia. *Proc Natl Acad Sci U S A,* 107**,** 2189-94.

SINGH, A. M., CHAPPELL, J., TROST, R., LIN, L., WANG, T., TANG, J., MATLOCK, B. K., WELLER, K. P., WU, H., ZHAO, S., JIN, P. & DALTON, S. 2013. Cell-cycle control of developmentally regulated transcription factors accounts for heterogeneity in human pluripotent cells. *Stem Cell Reports,* 1**,** 532-44.

SPERGER, J. M., CHEN, X., DRAPER, J. S., ANTOSIEWICZ, J. E., CHON, C. H., JONES, S. B., BROOKS, J. D., ANDREWS, P. W., BROWN, P. O. & THOMSON, J. A.

2003. Gene expression patterns in human embryonic stem cells and human pluripotent germ cell tumors. *Proc Natl Acad Sci U S A,* 100**,** 13350-5.

STADTFELD, M., NAGAYA, M., UTIKAL, J., WEIR, G. & HOCHEDLINGER, K. 2008. Induced pluripotent stem cells generated without viral integration. *Science,* 322**,** 945-9.

STAINIER, D. Y., KONTARAKIS, Z. & ROSSI, A. 2015. Making sense of anti-sense data. *Dev Cell,* 32**,** 7-8.

STEAD, E., WHITE, J., FAAST, R., CONN, S., GOLDSTONE, S., RATHJEN, J., DHINGRA, U., RATHJEN, P., WALKER, D. & DALTON, S. 2002. Pluripotent cell division cycles are driven by ectopic Cdk2, cyclin A/E and E2F activities. *Oncogene,* 21**,** 8320-33.

STEINER, A. B., ENGLEKA, M. J., LU, Q., PIWARZYK, E. C., YAKLICHKIN, S., LEFEBVRE, J. L., WALTERS, J. W., PINEDA-SALGADO, L., LABOSKY, P. A. & KESSLER, D. S. 2006. FoxD3 regulation of Nodal in the Spemann organizer is essential for Xenopus dorsal mesoderm development. *Development,* 133**,** 4827-38.

STREISINGER, G., WALKER, C., DOWER, N., KNAUBER, D. & SINGER, F. 1981. Production of clones of homozygous diploid zebra fish (Brachydanio rerio). *Nature,* 291**,** 293-6.

SUMMERTON, J. 1999. Morpholino antisense oligomers: the case for an RNase H-independent structural type. *Biochim Biophys Acta,* 1489**,** 141-58.

SUMMERTON, J. & BARTLETT, P. A. 1978. Sequence-specific crosslinking agents for nucleic acids. Use of 6-bromo-5,5-dimethoxyhexanohydrazide for crosslinking cytidine to guanosine and crosslinking RNA to complementary sequences of DNA. *J Mol Biol,* 122**,** 145-62.

SUMMERTON, J. & WELLER, D. 1997. Morpholino antisense oligomers: design, preparation, and properties. *Antisense Nucleic Acid Drug Dev,* 7**,** 187-95.

SUZUKI, A., RAYA, A., KAWAKAMI, Y., MORITA, M., MATSUI, T., NAKASHIMA, K., GAGE, F. H., RODRIGUEZ-ESTEBAN, C. & IZPISUA BELMONTE, J. C. 2006. Nanog binds to Smad1 and blocks bone morphogenetic protein-induced differentiation of embryonic stem cells. *Proc Natl Acad Sci U S A,* 103**,** 10294-9.

SUZUKI, D. E., NAKAHATA, A. M. & OKAMOTO, O. K. 2014. Knockdown of E2F2 inhibits tumorigenicity, but preserves stemness of human embryonic stem cells. *Stem Cells Dev,* 23**,** 1266-74.

TAKAHASHI, K., OKITA, K., NAKAGAWA, M. & YAMANAKA, S. 2007a. Induction of pluripotent stem cells from fibroblast cultures. *Nat Protoc,* 2**,** 3081-9.

TAKAHASHI, K., TANABE, K., OHNUKI, M., NARITA, M., ICHISAKA, T., TOMODA, K. & YAMANAKA, S. 2007b. Induction of pluripotent stem cells from adult human fibroblasts by defined factors. *Cell,* 131**,** 861-72.

TAKAHASHI, K., TANABE, K., OHNUKI, M., NARITA, M., SASAKI, A., YAMAMOTO, M., NAKAMURA, M., SUTOU, K., OSAFUNE, K. & YAMANAKA, S. 2014. Induction of pluripotency in human somatic cells via a transient state resembling primitive streak-like mesendoderm. *Nat Commun,* 5**,** 3678.

TAKAHASHI, K. & YAMANAKA, S. 2006. Induction of pluripotent stem cells from mouse embryonic and adult fibroblast cultures by defined factors. *Cell,* 126**,** 663-76.

TESAR, P. J., CHENOWETH, J. G., BROOK, F. A., DAVIES, T. J., EVANS, E. P., MACK, D. L., GARDNER, R. L. & MCKAY, R. D. 2007. New cell lines from mouse epiblast share defining features with human embryonic stem cells. *Nature,* 448**,** 196-9.

THOMSON, J. A., ITSKOVITZ-ELDOR, J., SHAPIRO, S. S., WAKNITZ, M. A., SWIERGIEL, J. J., MARSHALL, V. S. & JONES, J. M. 1998. Embryonic stem cell lines derived from human blastocysts. *Science,* 282**,** 1145-7.

THOMSON, J. A., KALISHMAN, J., GOLOS, T. G., DURNING, M., HARRIS, C. P., BECKER, R. A. & HEARN, J. P. 1995. Isolation of a primate embryonic stem cell line. *Proc Natl Acad Sci U S A,* 92**,** 7844-8.

TIMME-LARAGY, A. R., KARCHNER, S. I. & HAHN, M. E. 2012. Gene knockdown by morpholino-modified oligonucleotides in the zebrafish (Danio rerio) model: applications for developmental toxicology. *Methods Mol Biol,* 889**,** 51-71.

UNTERGASSER, A., NIJVEEN, H., RAO, X., BISSELING, T., GEURTS, R. & LEUNISSEN, J. A. 2007. Primer3Plus, an enhanced web interface to Primer3. *Nucleic Acids Res,* 35**,** W71-4.

VALLIER, L., MENDJAN, S., BROWN, S., CHNG, Z., TEO, A., SMITHERS, L. E., TROTTER, M. W., CHO, C. H., MARTINEZ, A., RUGG-GUNN, P., BRONS, G. & PEDERSEN, R. A. 2009. Activin/Nodal signalling maintains pluripotency by controlling Nanog expression. *Development,* 136**,** 1339-49.

VANDEL, L., NICOLAS, E., VAUTE, O., FERREIRA, R., AIT-SI-ALI, S. & TROUCHE, D. 2001. Transcriptional repression by the retinoblastoma protein through the recruitment of a histone methyltransferase. *Mol Cell Biol,* 21**,** 6484-94.

VERAKSA, A., KENNISON, J. & MCGINNIS, W. 2002. DEAF-1 function is essential for the early embryonic development of Drosophila. *Genesis,* 33**,** 67-76.

VOROBIEV, S. M., HUANG, Y. J., SEETHARAMAN, J., XIAO, R., ACTON, T. B., MONTELIONE, G. T. & TONG, L. 2012. Human retinoblastoma binding protein 9, a serine hydrolase implicated in pancreatic cancers. *Protein Pept Lett,* 19**,** 194-7.

VOROBIEV, S. M., SU, M., SEETHARAMAN, J., HUANG, Y. J., CHEN, C. X., MAGLAQUI, M., JANJUA, H., PROUDFOOT, M., YAKUNIN, A., XIAO, R., ACTON, T. B., MONTELIONE, G. T. & TONG, L. 2009. Crystal structure of human retinoblastoma binding protein 9. *Proteins,* 74**,** 526-9.

WANG, J., RAO, S., CHU, J., SHEN, X., LEVASSEUR, D. N., THEUNISSEN, T. W. & ORKIN, S. H. 2006. A protein interaction network for pluripotency of embryonic stem cells. *Nature,* 444**,** 364-8.

WANG, Z., ORON, E., NELSON, B., RAZIS, S. & IVANOVA, N. 2012. Distinct lineage specification roles for NANOG, OCT4, and SOX2 in human embryonic stem cells. *Cell Stem Cell,* 10**,** 440-54.

WARE, C. B., NELSON, A. M., MECHAM, B., HESSON, J., ZHOU, W., JONLIN, E. C., JIMENEZ-CALIANI, A. J., DENG, X., CAVANAUGH, C., COOK, S., TESAR, P. J., OKADA, J., MARGARETHA, L., SPERBER, H., CHOI, M., BLAU, C. A., TREUTING, P. M., HAWKINS, R. D., CIRULLI, V. & RUOHOLA-BAKER, H. 2014. Derivation of naive human embryonic stem cells. *Proc Natl Acad Sci U S A,* 111**,** 4484-9.

WATANABE, K., UENO, M., KAMIYA, D., NISHIYAMA, A., MATSUMURA, M., WATAYA, T., TAKAHASHI, J. B., NISHIKAWA, S., NISHIKAWA, S., MUGURUMA, K. & SASAI, Y. 2007. A ROCK inhibitor permits survival of dissociated human embryonic stem cells. *Nat Biotechnol,* 25**,** 681-6.

WEI, C. L., MIURA, T., ROBSON, P., LIM, S. K., XU, X. Q., LEE, M. Y., GUPTA, S., STANTON, L., LUO, Y., SCHMITT, J., THIES, S., WANG, W., KHREBTUKOVA, I., ZHOU, D., LIU, E. T., RUAN, Y. J., RAO, M. & LIM, B. 2005. Transcriptome profiling of human and murine ESCs identifies divergent paths required to maintain the stem cell state. *Stem Cells,* 23**,** 166-85.

WESTERFIELD, M. 2000. *The Zebrafish Book. A Guide for the Laboratory Use of Zebrafish (Danio rerio).* University of Oregon Press, Eugene.

WOITACH, J. T., ZHANG, M., NIU, C. H. & THORGEIRSSON, S. S. 1998. A retinoblastoma-binding protein that affects cell-cycle control and confers transforming ability. *Nat Genet,* 19**,** 371-4.

WOLTJEN, K., MICHAEL, I. P., MOHSENI, P., DESAI, R., MILEIKOVSKY, M., HAMALAINEN, R., COWLING, R., WANG, W., LIU, P., GERTSENSTEIN, M., KAJI, K., SUNG, H. K. & NAGY, A. 2009. piggyBac transposition reprograms fibroblasts to induced pluripotent stem cells. *Nature,* 458**,** 766-70.

WONG, D. J., LIU, H., RIDKY, T. W., CASSARINO, D., SEGAL, E. & CHANG, H. Y. 2008. Module map of stem cell genes guides creation of epithelial cancer stem cells. *Cell Stem Cell,* 2**,** 333-44.

WOOLF, T. M., JENNINGS, C. G., REBAGLIATI, M. & MELTON, D. A. 1990. The stability, toxicity and effectiveness of unmodified and phosphorothioate antisense oligodeoxynucleotides in Xenopus oocytes and embryos. *Nucleic Acids Res,* 18**,** 1763-9.

WU, D. Y. & YAO, Z. 2006. Functional analysis of two Sp1/Sp3 binding sites in murine Nanog gene promoter. *Cell Res,* 16**,** 319-22.

WU, Q., CHEN, X., ZHANG, J., LOH, Y. H., LOW, T. Y., ZHANG, W., ZHANG, W., SZE, S. K., LIM, B. & NG, H. H. 2006. Sall4 interacts with Nanog and co-occupies Nanog genomic sites in embryonic stem cells. *J Biol Chem,* 281**,** 24090-4.

XU, R. H., SAMPSELL-BARRON, T. L., GU, F., ROOT, S., PECK, R. M., PAN, G., YU, J., ANTOSIEWICZ-BOURGET, J., TIAN, S., STEWART, R. & THOMSON, J. A. 2008. NANOG is a direct target of TGFbeta/activin-mediated SMAD signaling in human ESCs. *Cell Stem Cell,* 3**,** 196-206.

YU, J., VODYANIK, M. A., SMUGA-OTTO, K., ANTOSIEWICZ-BOURGET, J., FRANE, J. L., TIAN, S., NIE, J., JONSDOTTIR, G. A., RUOTTI, V., STEWART, R., SLUKVIN, II & THOMSON, J. A. 2007. Induced pluripotent stem cell lines derived from human somatic cells. *Science,* 318**,** 1917-20.

ZAMECNIK, P. C. & STEPHENSON, M. L. 1978. Inhibition of Rous sarcoma virus replication and cell transformation by a specific oligodeoxynucleotide. *Proc Natl Acad Sci U S A,* 75**,** 280-4.

ZHANG, J., TAM, W. L., TONG, G. Q., WU, Q., CHAN, H. Y., SOH, B. S., LOU, Y., YANG, J., MA, Y., CHAI, L., NG, H. H., LUFKIN, T., ROBSON, P. & LIM, B. 2006. Sall4 modulates embryonic stem cell pluripotency and early embryonic development by the transcriptional regulation of Pou5f1. *Nat Cell Biol,* 8**,** 1114-23.

ZHANG, Y., SHAO, M., WANG, L., LIU, Z., GAO, M., LIU, C. & ZHANG, H. 2010. Ethanol exposure affects cell movement during gastrulation and induces split axes in zebrafish embryos. *Int J Dev Neurosci,* 28**,** 283-8.

ZHOU, H., KUANG, J., ZHONG, L., KUO, W. L., GRAY, J. W., SAHIN, A., BRINKLEY, B. R. & SEN, S. 1998. Tumour amplified kinase STK15/BTAK induces centrosome amplification, aneuploidy and transformation. *Nat Genet,* 20**,** 189-93.

ZHU, L., ZHANG, S. & JIN, Y. 2014. Foxd3 suppresses NFAT-mediated differentiation to maintain self-renewal of embryonic stem cells. *EMBO Rep,* 15**,** 1286-96.

ZOU, P., WU, S. Y., KOTEICHE, H. A., MISHRA, S., LEVIC, D. S., KNAPIK, E., CHEN, W. & MCHAOURAB, H. S. 2015. A conserved role of alphaA-crystallin in the development of the zebrafish embryonic lens. *Exp Eye Res,* 138**,** 104-13.

ZWICKER, J., LUCIBELLO, F. C., WOLFRAIM, L. A., GROSS, C., TRUSS, M., ENGELAND, K. & MULLER, R. 1995. Cell cycle regulation of the cyclin A, cdc25C and cdc2 genes is based on a common mechanism of transcriptional repression. *EMBO J,* 14**,** 4514-22.

Appendix

Appendix 1: Transcripts up-regulated by ML114 treatment.

Gene Symbol	Score	Feature P	FDR (BH)	Fold Change	Gene Symbol	Score	Feature P	FDR (BH)	Fold Change
REPS2	-1.2799934	0.001996	0.0213908	1.0049805	RNU6ATAC3P	-1.724531	0.001996	0.0213908	1.0260427
HHIPL2	-1.2835035	0.001996	0.0213908	1.0060279	RIIAD1	-1.7384378	0.001996	0.0213908	1.0107409
SNX14	-1.3174063	0.001996	0.0213908	1.0045622	GGCX	-1.7411335	0.001996	0.0213908	1.0051136
FGF14	-1.3203425	0.001996	0.0213908	1.012611	LARP7	-1.7413593	0.001996	0.0213908	1.0136518
C9orf152	-1.3608531	0.001996	0.0213908	1.0116378	C2orf73	-1.7455232	0.001996	0.0213908	1.0154788
THEMIS	-1.3704425	0.001996	0.0213908	1.008913	ST8SIA6	-1.7517903	0.001996	0.0213908	1.0231708
GSK3B	-1.3962801	0.001996	0.0213908	1.0016071	ZNF563	-1.7541013	0.001996	0.0213908	1.0183376
LGALS17A	-1.3976835	0.001996	0.0213908	1.0140159	PFKFB2	-1.7558437	0.001996	0.0213908	1.0071522
ALKBH6	-1.4011802	0.001996	0.0213908	1.00215	NPR1	-1.7572846	0.001996	0.0213908	1.010633
OR13A1	-1.4018358	0.001996	0.0213908	1.0082079	CBR1	-1.7624861	0.001996	0.0213908	1.0064749
MAP4K4	-1.4349339	0.001996	0.0213908	1.0024057	ZRANB2	-1.7635249	0.001996	0.0213908	1.0027059
TSC22D4	-1.4411056	0.001996	0.0213908	1.0037394	DLX5	-1.7707034	0.001996	0.0213908	1.0126272
RNASEH2B	-1.477176	0.001996	0.0213908	1.0037863	PITRM1	-1.7724285	0.001996	0.0213908	1.0014494
NWD1	-1.4854658	0.001996	0.0213908	1.0127319	F13A1	-1.7728683	0.001996	0.0213908	1.0137054
NAPRT1	-1.4995182	0.001996	0.0213908	1.0035046	ARHGAP28	-1.7749045	0.001996	0.0213908	1.0082186
APP	-1.5000075	0.001996	0.0213908	1.0014371	SCML2	-1.7749857	0.001996	0.0213908	1.0029493
PRAMEF6	-1.5007834	0.001996	0.0213908	1.0070778	HECTD2	-1.7789108	0.001996	0.0213908	1.0076337
GPR19	-1.5145234	0.001996	0.0213908	1.0036769	KIAA0825	-1.7795945	0.001996	0.0213908	1.0247834
SLC35F3	-1.5160319	0.001996	0.0213908	1.0021253	C8orf49	-1.7828204	0.001996	0.0213908	1.010407
GRAMD1C	-1.5166785	0.001996	0.0213908	1.0097952	CTPS2	-1.7848877	0.001996	0.0213908	1.0032021
UCA1	-1.5240129	0.001996	0.0213908	1.0104064	KIAA1009	-1.7858151	0.001996	0.0213908	1.0244315
ZNF304	-1.5457414	0.001996	0.0213908	1.0042737	NEMF	-1.7915964	0.001996	0.0213908	1.0063361
HMGB3P30	-1.5479308	0.001996	0.0213908	1.0122679	ETV4	-1.7946588	0.001996	0.0213908	1.0114889
HNRNPM	-1.5552876	0.001996	0.0213908	1.0024612	MIR451B	-1.7984893	0.001996	0.0213908	1.0196429
SNRPD2P2	-1.556235	0.001996	0.0213908	1.0111087	PEX1	-1.8019079	0.001996	0.0213908	1.0051587
ABT1	-1.563308	0.001996	0.0213908	1.0036556	PMS2	-1.8048815	0.001996	0.0213908	1.0068138
RNY5P3	-1.6008215	0.001996	0.0213908	1.0122257	ACN9	-1.8073221	0.001996	0.0213908	1.0084744
RNF215	-1.6042401	0.001996	0.0213908	1.0050034	AKR7A2	-1.8108251	0.001996	0.0213908	1.0030517
GRIK2	-1.6193135	0.001996	0.0213908	1.0159427	ZNF844	-1.8143813	0.001996	0.0213908	1.0118251
SEC23B	-1.6211225	0.001996	0.0213908	1.0024199	MPV17	-1.8204109	0.001996	0.0213908	1.0019042
ESRRB	-1.6212719	0.001996	0.0213908	1.0124959	TSTA3	-1.820872	0.001996	0.0213908	1.0055397
APH1B	-1.6243191	0.001996	0.0213908	1.0078585	VPS8	-1.8248973	0.001996	0.0213908	1.0018282
FIGNL1	-1.6309397	0.001996	0.0213908	1.0112131	RALGAPB	-1.8287274	0.001996	0.0213908	1.0027687
ABCG2	-1.6342263	0.001996	0.0213908	1.0139283	PTK7	-1.833024	0.001996	0.0213908	1.0057195
ERCC6	-1.6396575	0.001996	0.0213908	1.0054655	PRKCQ	-1.8359992	0.001996	0.0213908	1.0054168
CCDC104	-1.6493947	0.001996	0.0213908	1.0077587	ERO1LB	-1.8417381	0.001996	0.0213908	1.0061446
C17orf78	-1.6621901	0.001996	0.0213908	1.0152651	HGF	-1.8449903	0.001996	0.0213908	1.0109299
NAT8L	-1.6657251	0.001996	0.0213908	1.0035682	PILRB	-1.8556796	0.001996	0.0213908	1.0058306
RN5S466	-1.6660628	0.001996	0.0213908	1.0267446	LDHC	-1.8558353	0.001996	0.0213908	1.0127872
DNAJC18	-1.666802	0.001996	0.0213908	1.0038215	BGN	-1.8637839	0.001996	0.0213908	1.0163933
RAB13	-1.6697817	0.001996	0.0213908	1.005622	POGZ	-1.8656599	0.001996	0.0213908	1.0021406
FERMT1	-1.6709535	0.001996	0.0213908	1.0124099	MED30	-1.8692246	0.001996	0.0213908	1.0042039
RAD9B	-1.683909	0.001996	0.0213908	1.0075428	HSD3B7	-1.8694492	0.001996	0.0213908	1.0028069
RIMBP3	-1.6915288	0.001996	0.0213908	1.0116905	SLC35G1	-1.8742526	0.001996	0.0213908	1.0118028
FGF16	-1.696589	0.001996	0.0213908	1.0233463	RN5S458	-1.875796	0.001996	0.0213908	1.0179922
ARHGAP30	-1.7022305	0.001996	0.0213908	1.0058592	FYTTD1	-1.8812502	0.001996	0.0213908	1.0103096
CAPS2	-1.7034143	0.001996	0.0213908	1.0179727	AK091192	-1.882605	0.001996	0.0213908	1.0170274
MIR129-2	-1.7042131	0.001996	0.0213908	1.0163127	EIF4EBP2	-1.8835027	0.001996	0.0213908	1.0019466
MDK	-1.7147409	0.001996	0.0213908	1.00278[illegible]	ZNF548	-1.8842995	0.001996	0.0213908	1.0045969
PHLDA1	-1.7169625	0.001996	0.0213908	1.004435	DKKL1	-1.8847324	0.001996	0.0213908	1.0164519

Gene Symbol	Score	Feature P	FDR (BH)	Fold Change	Gene Symbol	Score	Feature P	FDR (BH)	Fold Change
TBX3	-1.8927929	0.001996	0.0213908	1.0188518	TTC13	-1.9837686	0.001996	0.0213908	1.0030217
PATL2	-1.894749	0.001996	0.0213908	1.0113072	CCDC93	-1.9840628	0.001996	0.0213908	1.0063568
WASH3P	-1.9037443	0.001996	0.0213908	1.0044533	STEAP4	-1.9846812	0.001996	0.0213908	1.0244252
PHLDB2	-1.9051029	0.001996	0.0213908	1.0218127	DACT1	-1.9854626	0.001996	0.0213908	1.0172366
ACPL2	-1.9052909	0.001996	0.0213908	1.0051831	ALX1	-1.9877526	0.001996	0.0213908	1.0133995
HECW2	-1.9131447	0.001996	0.0213908	1.0061169	PFKFB4	-1.9882408	0.001996	0.0213908	1.0090425
GLT25D1	-1.9178778	0.001996	0.0213908	1.0024711	CNTRL	-1.9907414	0.001996	0.0213908	1.0149388
C2orf80	-1.9194862	0.001996	0.0213908	1.0160613	KGFLP1	-1.9907962	0.001996	0.0213908	1.0060402
KLF6	-1.9289713	0.001996	0.0213908	1.005873	CST4	-1.9917296	0.001996	0.0213908	1.0065932
LAPTM4A	-1.9292309	0.001996	0.0213908	1.0019748	TLE1	-1.9922362	0.001996	0.0213908	1.0061362
CYP2B6	-1.9292499	0.001996	0.0213908	1.0283802	RPS15A	-1.9936416	0.001996	0.0213908	1.0010796
KLK13	-1.9331532	0.001996	0.0213908	1.0099579	RING1	-1.994076	0.001996	0.0213908	1.0022953
CYTH1	-1.9337715	0.001996	0.0213908	1.0056183	ACOX1	-1.9953366	0.001996	0.0213908	1.0048574
KDM4D	-1.9352649	0.001996	0.0213908	1.0169751	C9orf9	-1.9970024	0.001996	0.0213908	1.0043258
CXXC4	-1.9361418	0.001996	0.0213908	1.006845	C1orf101	-1.9972491	0.001996	0.0213908	1.0151335
KRT86	-1.936355	0.001996	0.0213908	1.004514	RN5S401	-1.9980244	0.001996	0.0213908	1.0203739
DAAM2	-1.9378208	0.001996	0.0213908	1.0076092	NFU1	-1.9988124	0.001996	0.0213908	1.0071422
ZNF187	-1.9382203	0.001996	0.0213908	1.0094795	STK17B	-1.9997521	0.001996	0.0213908	1.0044921
GALNT1	-1.9410724	0.001996	0.0213908	1.0049106	LGI4	-2.0002979	0.001996	0.0213908	1.0042544
LINC00575	-1.9420804	0.001996	0.0213908	1.0172468	CCDC141	-2.0030082	0.001996	0.0213908	1.0192075
LYPLA2	-1.9430473	0.001996	0.0213908	1.0021635	GPR25	-2.0032111	0.001996	0.0213908	1.0061546
SKIV2L	-1.9441851	0.001996	0.0213908	1.0043741	SLC46A3	-2.0057046	0.001996	0.0213908	1.0185128
TMEM210	-1.9449658	0.001996	0.0213908	1.0064999	PLDN	-2.0057221	0.001996	0.0213908	1.0070059
IKBKE	-1.9475891	0.001996	0.0213908	1.0080946	WDR41	-2.0065056	0.001996	0.0213908	1.0027827
ITIH4	-1.9500919	0.001996	0.0213908	1.0121804	CRYBB1	-2.0129294	0.001996	0.0213908	1.0046499
KAT5	-1.9507203	0.001996	0.0213908	1.0044563	FNIP1	-2.0139917	0.001996	0.0213908	1.0071651
ADAM21	-1.9507797	0.001996	0.0213908	1.025773	ELP3	-2.016264	0.001996	0.0213908	1.0049722
TRPC7	-1.9538273	0.001996	0.0213908	1.0165523	SKIDA1	-2.0181877	0.001996	0.0213908	1.003
IL2RB	-1.9544275	0.001996	0.0213908	1.0076873	C10orf76	-2.0216457	0.001996	0.0213908	1.0041522
THAP9	-1.9545734	0.001996	0.0213908	1.0066431	CST5	-2.0225996	0.001996	0.0213908	1.0132322
ZIC4	-1.954857	0.001996	0.0213908	1.0125145	IL1RAP	-2.0232337	0.001996	0.0213908	1.0127351
C6orf170	-1.9577676	0.001996	0.0213908	1.0085179	ZNF37BP	-2.0244333	0.001996	0.0213908	1.0030395
DGKD	-1.9580713	0.001996	0.0213908	1.0025134	HERC6	-2.0255001	0.001996	0.0213908	1.011871
C17orf49	-1.9611016	0.001996	0.0213908	1.0022326	OLR1	-2.0261353	0.001996	0.0213908	1.0099345
ST3GAL2	-1.9631641	0.001996	0.0213908	1.0040502	CDCA2	-2.0291809	0.001996	0.0213908	1.0033184
CEP290	-1.9635031	0.001996	0.0213908	1.016618	LRRIQ4	-2.0295222	0.001996	0.0213908	1.0106741
HEXB	-1.9636455	0.001996	0.0213908	1.0036351	LGI1	-2.0296884	0.001996	0.0213908	1.0810722
CACNB2	-1.9642332	0.001996	0.0213908	1.0079583	BCL2L14	-2.0303368	0.001996	0.0213908	1.0030714
R3HCC1L	-1.9643728	0.001996	0.0213908	1.0085145	C2orf77	-2.0329033	0.001996	0.0213908	1.0092366
KAZN	-1.9664383	0.001996	0.0213908	1.0139674	MPLKIP	-2.0345015	0.001996	0.0213908	1.0038451
RN5S252	-1.9676021	0.001996	0.0213908	1.0137326	RPS29	-2.0349801	0.001996	0.0213908	1.0028445
NPAS2	-1.968039	0.001996	0.0213908	1.006897	RN5S147	-2.0427551	0.001996	0.0213908	1.0263534
CLDN16	-1.9698736	0.001996	0.0213908	1.0136818	C14orf1	-2.0501118	0.001996	0.0213908	1.0012593
PRLR	-1.9701979	0.001996	0.0213908	1.0072737	DYNC2LI1	-2.0554236	0.001996	0.0213908	1.019091
ARFGEF1	-1.9711575	0.001996	0.0213908	1.004876	ACAD9	-2.0583484	0.001996	0.0213908	1.0046863
FAHD2A	-1.973668	0.001996	0.0213908	1.0061959	POTEE	-2.0600194	0.001996	0.0213908	1.0067738
ZNF124	-1.9747501	0.001996	0.0213908	1.0100759	MALL	-2.0625612	0.001996	0.0213908	1.0031395
SNX7	-1.9748245	0.001996	0.0213908	1.0126125	VWDE	-2.0641244	0.001996	0.0213908	1.0040763
RBP5	-1.9768652	0.001996	0.0213908	1.0100435	KCNA3	-2.0646698	0.001996	0.0213908	1.0058022
ACSM3	-1.9830687	0.001996	0.0213908	1.0117302	DALRD3	-2.0650276	0.001996	0.0213908	1.0019815

Gene Symbol	Score	Feature P	FDR (BH)	Fold Change	Gene Symbol	Score	Feature P	FDR (BH)	Fold Change
JAG2	-2.0699287	0.001996	0.0213908	1.0046483	ALOX12P2	-2.1540121	0.001996	0.0213908	1.0076398
TACSTD2	-2.0736111	0.001996	0.0213908	1.0097622	PJA1	-2.1558155	0.001996	0.0213908	1.0071788
PRELID2	-2.074852	0.001996	0.0213908	1.0059201	MDH1B	-2.1560985	0.001996	0.0213908	1.0199387
GBP4	-2.0768307	0.001996	0.0213908	1.0143858	TDRD9	-2.1577314	0.001996	0.0213908	1.0086261
RPS7P10	-2.0793556	0.001996	0.0213908	1.0138692	POLR2J4	-2.1640253	0.001996	0.0213908	1.0033752
TRIM4	-2.0824415	0.001996	0.0213908	1.0037465	TBC1D20	-2.1677669	0.001996	0.0213908	1.0019575
TP53INP2	-2.0829377	0.001996	0.0213908	1.0101357	DDX11L2	-2.1681626	0.001996	0.0213908	1.0070005
DIP2A	-2.0847955	0.001996	0.0213908	1.0038225	RPL32P3	-2.169936	0.001996	0.0213908	1.0043728
IDH1	-2.0880066	0.001996	0.0213908	1.0025683	BRWD3	-2.1719996	0.001996	0.0213908	1.0047059
SPG20OS	-2.0883352	0.001996	0.0213908	1.0332299	RALGDS	-2.1741414	0.001996	0.0213908	1.0054976
PCNP	-2.0888	0.001996	0.0213908	1.0042352	RN5S169	-2.1763193	0.001996	0.0213908	1.0192246
TNMD	-2.0889825	0.001996	0.0213908	1.0067554	FAM21A	-2.1777316	0.001996	0.0213908	1.0033646
KIAA1257	-2.0930533	0.001996	0.0213908	1.01126	NTN1	-2.1801825	0.001996	0.0213908	1.0049303
OR2A4	-2.0931675	0.001996	0.0213908	1.0211309	PDHA1	-2.181244	0.001996	0.0213908	1.0030058
DARS2	-2.0959582	0.001996	0.0213908	1.0062112	SRGAP2	-2.1854109	0.001996	0.0213908	1.0032583
FGF13	-2.0991968	0.001996	0.0213908	1.007385	KIAA1109	-2.1875205	0.001996	0.0213908	1.0043452
CD44	-2.0995949	0.001996	0.0213908	1.0071113	ZNF300	-2.1901555	0.001996	0.0213908	1.0104705
PPP2R5A	-2.102642	0.001996	0.0213908	1.0060636	RASSF4	-2.191064	0.001996	0.0213908	1.0042317
INVS	-2.1036416	0.001996	0.0213908	1.0096472	ZAR1L	-2.1913549	0.001996	0.0213908	1.0094806
TACC2	-2.104876	0.001996	0.0213908	1.0073431	NTN4	-2.1932044	0.001996	0.0213908	1.012505
HINT3	-2.1054207	0.001996	0.0213908	1.0157575	MTMR11	-2.1933873	0.001996	0.0213908	1.0079339
OR52L1	-2.1071619	0.001996	0.0213908	1.0157486	MTERF	-2.1938963	0.001996	0.0213908	1.0060936
FNDC7	-2.1072835	0.001996	0.0213908	1.0249714	ZSWIM1	-2.1944651	0.001996	0.0213908	1.0043079
PIGN	-2.1074875	0.001996	0.0213908	1.0087646	FUT10	-2.1952191	0.001996	0.0213908	1.0021169
DNAJA4	-2.1111346	0.001996	0.0213908	1.0091457	MRPS11	-2.1957038	0.001996	0.0213908	1.0027853
MEIS3P2	-2.1132045	0.001996	0.0213908	1.0106444	FOXB1	-2.1971836	0.001996	0.0213908	1.0169448
HAGH	-2.1132232	0.001996	0.0213908	1.0050674	ECI2	-2.1987346	0.001996	0.0213908	1.0066732
KIAA0913	-2.1134607	0.001996	0.0213908	1.0080219	PLXND1	-2.1993385	0.001996	0.0213908	1.0075863
OR6Y1	-2.1191086	0.001996	0.0213908	1.0149698	RENBP	-2.2017271	0.001996	0.0213908	1.0084113
MEAF6	-2.1199019	0.001996	0.0213908	1.0059864	LRRIQ1	-2.2019911	0.001996	0.0213908	1.0243809
DIRC1	-2.1212216	0.001996	0.0213908	1.0150113	BCKDHB	-2.2023005	0.001996	0.0213908	1.0032739
FAM108B1	-2.1215154	0.001996	0.0213908	1.0099885	SETD9	-2.2057233	0.001996	0.0213908	1.0076584
XRCC5	-2.1225097	0.001996	0.0213908	1.0016368	SYPL2	-2.2061465	0.001996	0.0213908	1.0084411
SPAG1	-2.1251891	0.001996	0.0213908	1.0132762	SFXN1	-2.2076774	0.001996	0.0213908	1.0045718
CWC25	-2.1265825	0.001996	0.0213908	1.0047966	ABCB4	-2.2077353	0.001996	0.0213908	1.0164739
KDM8	-2.1304069	0.001996	0.0213908	1.0055506	LRCH3	-2.2091355	0.001996	0.0213908	1.0029145
CDK9	**-2.1310958**	**0.001996**	**0.0213908**	**1.0029795**	CLEC4D	-2.2093228	0.001996	0.0213908	1.0222178
SULT1A2	-2.1326131	0.001996	0.0213908	1.0045052	SOGA1	-2.2095608	0.001996	0.0213908	1.003413
ENDOD1	-2.1327645	0.001996	0.0213908	1.0037097	TEKT3	-2.2102722	0.001996	0.0213908	1.0136562
ZNF133	-2.1328718	0.001996	0.0213908	1.0046269	PROS1	-2.2106755	0.001996	0.0213908	1.0238451
ZNF230	-2.1346284	0.001996	0.0213908	1.0149737	GLT25D2	-2.2112843	0.001996	0.0213908	1.0274081
SPINK2	-2.1346884	0.001996	0.0213908	1.0241619	CABYR	-2.2113578	0.001996	0.0213908	1.0030743
KDELC1	-2.1423582	0.001996	0.0213908	1.0047919	DLK1	-2.2133829	0.001996	0.0213908	1.0303672
GBA	-2.1432765	0.001996	0.0213908	1.0091013	C6orf10	-2.2147427	0.001996	0.0213908	1.0219906
FAM107B	-2.1435695	0.001996	0.0213908	1.0057873	GAA	-2.2154108	0.001996	0.0213908	1.0080524
BHLHE22	-2.1465201	0.001996	0.0213908	1.007612	FAM211B	-2.217049	0.001996	0.0213908	1.0053218
DLG5	-2.1477206	0.001996	0.0213908	1.0023397	ANKK1	-2.2185168	0.001996	0.0213908	1.0048648
ATF7IP2	-2.147842	0.001996	0.0213908	1.0141226	RWDD2A	-2.2186788	0.001996	0.0213908	1.0109222
TCEAL8	-2.1509434	0.001996	0.0213908	1.012523	PYGO1	-2.21981	0.001996	0.0213908	1.0161079
MRPS14	-2.1517015	0.001996	0.0213908	1.002564	HNRNPA2B1	-2.2210485	0.001996	0.0213908	1.0028571

Gene Symbol	Score	Feature P	FDR (BH)	Fold Change	Gene Symbol	Score	Feature P	FDR (BH)	Fold Change
C9orf40	-2.2210552	0.001996	0.0213908	1.0039761	GSC	-2.2799763	0.001996	0.02139076	1.0265194
AP3B2	-2.2243813	0.001996	0.0213908	1.0164718	TMEM187	-2.2808468	0.001996	0.02139076	1.0150119
PAK1	-2.2244025	0.001996	0.0213908	1.0042106	OXER1	-2.2812943	0.001996	0.02139076	1.007213
CXorf58	-2.2244146	0.001996	0.0213908	1.0112538	WBSCR17	-2.2819431	0.001996	0.02139076	1.0076466
CDC42SE1	-2.224568	0.001996	0.0213908	1.0040474	RABL2A	-2.2844062	0.001996	0.02139076	1.0055271
ETFA	-2.2250061	0.001996	0.0213908	1.0040042	ITPRIPL2	-2.2854381	0.001996	0.02139076	1.0055761
RORA	-2.2256215	0.001996	0.0213908	1.0089713	DEFB109P1B	-2.2882232	0.001996	0.02139076	1.0175794
KLHL4	-2.2289661	0.001996	0.0213908	1.0223595	MCL1	-2.2896337	0.001996	0.02139076	1.0028051
C5orf60	-2.2302147	0.001996	0.0213908	1.0110504	BSDC1	-2.2899424	0.001996	0.02139076	1.0028184
AAAS	-2.2302438	0.001996	0.0213908	1.0020823	IRAK3	-2.2905969	0.001996	0.02139076	1.0161446
CD79B	-2.2320422	0.001996	0.0213908	1.0079027	AK123300	-2.2924893	0.001996	0.02139076	1.0210274
HPS6	-2.232197	0.001996	0.0213908	1.0040556	RAB7A	-2.2935063	0.001996	0.02139076	1.0023525
UNC45A	-2.2342121	0.001996	0.0213908	1.001968	HDAC3	-2.29403	0.001996	0.02139076	1.0020831
WNK1	-2.2363948	0.001996	0.0213908	1.0095624	CRIPAK	-2.2959411	0.001996	0.02139076	1.0078865
SF3B1	-2.2392839	0.001996	0.0213908	1.0019713	LOC349196	-2.2960041	0.001996	0.02139076	1.0210847
ADH1A	-2.2398547	0.001996	0.0213908	1.0074848	PXDC1	-2.29635	0.001996	0.02139076	1.0232355
PHOX2A	-2.2429524	0.001996	0.0213908	1.0058183	NKD1	-2.2965053	0.001996	0.02139076	1.0101542
PTH1R	-2.2453753	0.001996	0.0213908	1.0122004	ACVR1C	-2.2974534	0.001996	0.02139076	1.0078979
FAM222B	-2.245568	0.001996	0.0213908	1.0035874	NIT2	-2.2999532	0.001996	0.02139076	1.003787
TRIM66	-2.2489402	0.001996	0.0213908	1.0156932	MRP63	-2.3000595	0.001996	0.02139076	1.0012488
TRAPPC6B	-2.2501614	0.001996	0.0213908	1.0074496	NM_033490.1	-2.3009322	0.001996	0.02139076	1.004476
CCNT2	-2.25027	0.001996	0.0213908	1.0036533	PHC2	-2.3016874	0.001996	0.02139076	1.0109197
DDX50	-2.2506276	0.001996	0.0213908	1.00344	IPP	-2.3024306	0.001996	0.02139076	1.0161808
IARS2	-2.250767	0.001996	0.0213908	1.0036751	STX5	-2.3030033	0.001996	0.02139076	1.004657
TSPEAR	-2.2507692	0.001996	0.0213908	1.0150528	NPIP	-2.3042784	0.001996	0.02139076	1.0011828
INPP5K	-2.2518873	0.001996	0.0213908	1.006631	ADRA2C	-2.3049498	0.001996	0.02139076	1.0048342
ARHGAP5-AS1	-2.2519491	0.001996	0.0213908	1.012561	SEC16A	-2.3058304	0.001996	0.02139076	1.001863
ZBTB38	-2.2530067	0.001996	0.0213908	1.0109068	GTF2B	-2.3065654	0.001996	0.02139076	1.0038333
GRM6	-2.2547148	0.001996	0.0213908	1.0043836	IMPDH2	-2.3065812	0.001996	0.02139076	1.0013444
KIAA1324L	-2.2555783	0.001996	0.0213908	1.0050584	FBXL5	-2.3066514	0.001996	0.02139076	1.0041682
TMEM135	-2.2557232	0.001996	0.0213908	1.003258	CTSK	-2.3072115	0.001996	0.02139076	1.0120857
LPHN1	-2.257415	0.001996	0.0213908	1.0015623	AS3MT	-2.3104214	0.001996	0.02139076	1.0065473
NECAB2	-2.2578534	0.001996	0.0213908	1.0076653	AKAP6	-2.3106135	0.001996	0.02139076	1.0196738
AGR2	-2.2579141	0.001996	0.0213908	1.0165457	NUCB1	-2.3106754	0.001996	0.02139076	1.0038482
PRUNE	-2.2596546	0.001996	0.0213908	1.0037655	ATP5S	-2.3118794	0.001996	0.02139076	1.0051228
BCMO1	-2.2610851	0.001996	0.0213908	1.008286	ANP32A	-2.3130231	0.001996	0.02139076	1.0026923
TTLL7	-2.2612976	0.001996	0.0213908	1.0093028	FAM86B2	-2.315678	0.001996	0.02139076	1.0047083
FAM86B1	-2.2629094	0.001996	0.0213908	1.0063884	PEX7	-2.3175685	0.001996	0.02139076	1.0058856
MAP2	-2.2629546	0.001996	0.0213908	1.0301178	MC3R	-2.3212314	0.001996	0.02139076	1.0078109
GFM2	-2.2642055	0.001996	0.0213908	1.0049669	ELK3	-2.3216879	0.001996	0.02139076	1.012423
NKAIN2	-2.2667648	0.001996	0.0213908	1.0279418	SLC35E3	-2.3232867	0.001996	0.02139076	1.0143825
NANOG	**-2.2722202**	**0.001996**	**0.0213908**	**1.0074623**	PBXIP1	-2.3240384	0.001996	0.02139076	1.0076985
ZFAND3	-2.2731239	0.001996	0.0213908	1.0036872	CBR3	-2.3242885	0.001996	0.02139076	1.0062393
NXF2B	-2.2731584	0.001996	0.0213908	1.0125143	RASA4CP	-2.325357	0.001996	0.02139076	1.0117645
NAA30	-2.2738485	0.001996	0.0213908	1.0045424	ATP8A1	-2.3262725	0.001996	0.02139076	1.0038645
KCTD15	-2.2740946	0.001996	0.0213908	1.005924	FASTK	-2.3267687	0.001996	0.02139076	1.0026126
FDXACB1	-2.2755055	0.001996	0.0213908	1.010671	PHF7	-2.3300934	0.001996	0.02139076	1.010596
RRAGB	-2.2767712	0.001996	0.0213908	1.0110133	BAP1	-2.3306709	0.001996	0.02139076	1.0026515
TMBIM4	-2.2775936	0.001996	0.0213908	1.0080686	GDPD1	-2.3320256	0.001996	0.02139076	1.0136154
NMI	-2.2789717	0.001996	0.0213908	1.02123	FYCO1	-2.3327109	0.001996	0.02139076	1.0057486

Gene Symbol	Score	Feature P	FDR (BH)	Fold Change	Gene Symbol	Score	Feature P	FDR (BH)	Fold Change
GRK4	-2.3327715	0.001996	0.0213908	1.0130738	C21orf90	-2.3847203	0.001996	0.0213908	1.0198372
RN5S496	-2.3335358	0.001996	0.0213908	1.0300294	HJURP	-2.3851503	0.001996	0.0213908	1.0043893
ANKRD36P1	-2.3338601	0.001996	0.0213908	1.0170667	SPG20	-2.3866169	0.001996	0.0213908	1.0091405
PRDM5	-2.3339789	0.001996	0.0213908	1.0056678	HSD17B14	-2.3892067	0.001996	0.0213908	1.0108347
WDR55	-2.3404909	0.001996	0.0213908	1.0051425	DNHD1	-2.3892378	0.001996	0.0213908	1.0172192
SFXN2	-2.3409586	0.001996	0.0213908	1.0082796	RHBDF1	-2.389297	0.001996	0.0213908	1.0111794
C18orf32	-2.3419861	0.001996	0.0213908	1.0077326	TCEA2	-2.3899112	0.001996	0.0213908	1.0102906
CYLC1	-2.3423593	0.001996	0.0213908	1.0202801	RPS19	-2.3913066	0.001996	0.0213908	1.0016791
ZNF706	-2.3443576	0.001996	0.0213908	1.0066051	KIF24	-2.3915567	0.001996	0.0213908	1.0092832
TGFB2	-2.3468009	0.001996	0.0213908	1.025841	LYSMD1	-2.392519	0.001996	0.0213908	1.0049364
C7orf55	-2.3468227	0.001996	0.0213908	1.0028876	ERMP1	-2.3925448	0.001996	0.0213908	1.0039636
VMA21	-2.3481078	0.001996	0.0213908	1.0023859	TRPV1	-2.3928469	0.001996	0.0213908	1.0047232
RNF139	-2.3487549	0.001996	0.0213908	1.003806	ACACB	-2.3961854	0.001996	0.0213908	1.0036717
PPIC	-2.3496056	0.001996	0.0213908	1.0063746	GMPPA	-2.3979221	0.001996	0.0213908	1.0063678
LAMP1	-2.3519578	0.001996	0.0213908	1.0025274	HIBADH	-2.3980151	0.001996	0.0213908	1.0073
DYNC1I1	-2.3539169	0.001996	0.0213908	1.0070699	NIN	-2.399713	0.001996	0.0213908	1.0090056
USP30	-2.3539604	0.001996	0.0213908	1.0086677	RBM43	-2.3998581	0.001996	0.0213908	1.0121187
OPN5	-2.3548689	0.001996	0.0213908	1.020126	ARAP1	-2.4005239	0.001996	0.0213908	1.0041229
TRA2A	-2.3549497	0.001996	0.0213908	1.0082881	NEU1	-2.4025721	0.001996	0.0213908	1.0041659
SPRY1	-2.3570037	0.001996	0.0213908	1.0042264	TTC33	-2.4035983	0.001996	0.0213908	1.0097887
UEVLD	-2.3585836	0.001996	0.0213908	1.0115425	TIMELESS	-2.4056442	0.001996	0.0213908	1.0055838
HCG4	-2.3602228	0.001996	0.0213908	1.012532	TP53INP1	-2.4062547	0.001996	0.0213908	1.0110482
SLC35D2	-2.3618173	0.001996	0.0213908	1.0135391	SPATA12	-2.406866	0.001996	0.0213908	1.0167304
PBLD	-2.3620587	0.001996	0.0213908	1.0168008	SMAD5	-2.4073775	0.001996	0.0213908	1.0022683
SSTR1	-2.3649206	0.001996	0.0213908	1.0114066	CXXC5	-2.4078018	0.001996	0.0213908	1.0036897
OR6C6	-2.36503	0.001996	0.0213908	1.018775	TAS2R20	-2.4104515	0.001996	0.0213908	1.02365
FLJ35776	-2.3661543	0.001996	0.0213908	1.0168766	TUBE1	-2.4110589	0.001996	0.0213908	1.0093267
GTF2A1	-2.366582	0.001996	0.0213908	1.003515	LRRC9	-2.4113358	0.001996	0.0213908	1.0396942
ZBTB48	-2.3666492	0.001996	0.0213908	1.0025895	ANKRD20A3	-2.4118545	0.001996	0.0213908	1.010526
RILPL2	-2.3671837	0.001996	0.0213908	1.0079884	ENTPD1	-2.413175	0.001996	0.0213908	1.0162499
MANBA	-2.3696204	0.001996	0.0213908	1.0053559	ILDR2	-2.414227	0.001996	0.0213908	1.0189193
ZEB2	-2.370172	0.001996	0.0213908	1.0402385	LTB4R	-2.4143386	0.001996	0.0213908	1.008113
IFT140	-2.3707002	0.001996	0.0213908	1.002783	PCMTD1	-2.4152095	0.001996	0.0213908	1.0039651
WDR96	-2.3726477	0.001996	0.0213908	1.0319513	LRP4	-2.4158842	0.001996	0.0213908	1.0080327
C3orf67	-2.3734712	0.001996	0.0213908	1.0081389	LOC100129534	-2.4159697	0.001996	0.0213908	1.0126652
ABCD1	-2.3739416	0.001996	0.0213908	1.0082842	PPFIBP1	-2.4172405	0.001996	0.0213908	1.0096642
KAT7	-2.3760821	0.001996	0.0213908	1.0040655	NFATC4	-2.4177063	0.001996	0.0213908	1.0113541
BEX5	-2.3764752	0.001996	0.0213908	1.0084192	C20orf132	-2.4177322	0.001996	0.0213908	1.0130384
KLF7	-2.3772576	0.001996	0.0213908	1.0033724	HEBP2	-2.4184816	0.001996	0.0213908	1.0078271
KRT8P11	-2.3773588	0.001996	0.0213908	1.0011793	FRYL	-2.4206998	0.001996	0.0213908	1.0043793
USP3	-2.3777031	0.001996	0.0213908	1.0143411	MST1	-2.4226339	0.001996	0.0213908	1.0116151
CBFA2T2	-2.3779619	0.001996	0.0213908	1.0060233	DOCK4	-2.4243904	0.001996	0.0213908	1.0120587
TMTC2	-2.3783865	0.001996	0.0213908	1.0263994	OR4D1	-2.4250242	0.001996	0.0213908	1.0168026
PRRG2	-2.3784915	0.001996	0.0213908	1.0109105	SOX11	-2.4264617	0.001996	0.0213908	1.0048257
TSPAN3	-2.3800234	0.001996	0.0213908	1.0029844	C11orf63	-2.4296445	0.001996	0.0213908	1.018876
MAGEH1	-2.3809688	0.001996	0.0213908	1.0078878	FAM172A	-2.4297378	0.001996	0.0213908	1.0085444
SRP9	-2.3821653	0.001996	0.0213908	1.0009578	TMEM204	-2.4298258	0.001996	0.0213908	1.0042499
TMEM63A	-2.3823342	0.001996	0.0213908	1.0182832	FAM125B	-2.4307193	0.001996	0.0213908	1.0031486
C10orf107	-2.3842859	0.001996	0.0213908	1.024969	OR5H1	-2.4307227	0.001996	0.0213908	1.0857778
F8	-2.3847142	0.001996	0.0213908	1.0123029	PPP3CC	-2.4307249	0.001996	0.0213908	1.0075042

Gene Symbol	Score	Feature P	FDR (BH)	Fold Change	Gene Symbol	Score	Feature P	FDR (BH)	Fold Change
TM9SF1	-2.432294	0.001996	0.0213908	1.00700008	CNOT6L	-2.4880493	0.001996	0.0213908	1.00388975
SCAND3	-2.4326407	0.001996	0.0213908	1.008165029	CRYBG3	-2.4902677	0.001996	0.0213908	1.00991161
RIT1	-2.4326521	0.001996	0.0213908	1.010143473	ESYT1	-2.49037	0.001996	0.0213908	1.00590625
AMOTL1	-2.4329134	0.001996	0.0213908	1.010929875	ZNF793	-2.4905476	0.001996	0.0213908	1.00380815
VKORC1	-2.4336966	0.001996	0.0213908	1.001817081	PON2	-2.4917048	0.001996	0.0213908	1.0016526
C15orf44	-2.4349872	0.001996	0.0213908	1.004840995	ARL6IP5	-2.4923503	0.001996	0.0213908	1.00454273
GPR50	-2.4366815	0.001996	0.0213908	1.013241732	DBP	-2.4952871	0.001996	0.0213908	1.00585979
KIAA1586	-2.4380922	0.001996	0.0213908	1.001726349	LOC93463	-2.4988241	0.001996	0.0213908	1.0095541
KIAA0895L	-2.4383058	0.001996	0.0213908	1.009817162	RSPH3	-2.5014912	0.001996	0.0213908	1.01064198
MAPK10	-2.4391153	0.001996	0.0213908	1.021687287	ZC3H11A	-2.5034792	0.001996	0.0213908	1.00494645
BSCL2	-2.4427872	0.001996	0.0213908	1.003350015	C15orf29	-2.5054595	0.001996	0.0213908	1.00309491
KRTAP27-1	-2.450433	0.001996	0.0213908	1.017529081	AP2B1	-2.5055991	0.001996	0.0213908	1.00130068
RIPK4	-2.4531427	0.001996	0.0213908	1.009185237	PDE8A	-2.506371	0.001996	0.0213908	1.01216466
KLHL36	-2.454288	0.001996	0.0213908	1.001278032	HIP1R	-2.5079905	0.001996	0.0213908	1.00844312
FAM20C	-2.4548965	0.001996	0.0213908	1.008011149	SENP8	-2.508438	0.001996	0.0213908	1.00529727
OLIG3	-2.4549056	0.001996	0.0213908	1.021899222	SUGT1P3	-2.5101267	0.001996	0.0213908	1.01324046
RHBDD1	-2.4553436	0.001996	0.0213908	1.009215075	TSHZ1	-2.5109085	0.001996	0.0213908	1.01232422
PDXDC2P	-2.4560243	0.001996	0.0213908	1.007036087	TRIM36	-2.5116104	0.001996	0.0213908	1.01731037
RASA1	-2.4561751	0.001996	0.0213908	1.006946036	HDAC5	-2.51295	0.001996	0.0213908	1.00617208
CAPZA3	-2.4565347	0.001996	0.0213908	1.046710823	GPR137C	-2.5142599	0.001996	0.0213908	1.00562081
RIMKLBP1	-2.4577065	0.001996	0.0213908	1.004029657	MLLT4-AS1	-2.517251	0.001996	0.0213908	1.00843189
SRPX2	-2.4589453	0.001996	0.0213908	1.015328365	CD177	-2.5197366	0.001996	0.0213908	1.01109401
RPS28	-2.4602337	0.001996	0.0213908	1.00172198	USP20	-2.5201991	0.001996	0.0213908	1.00437166
AK021889	-2.4606101	0.001996	0.0213908	1.027998992	SLC12A7	-2.5207188	0.001996	0.0213908	1.00374131
IL10RB	-2.4617718	0.001996	0.0213908	1.009860047	FBXL4	-2.5223723	0.001996	0.0213908	1.00746524
PFKL	-2.4628987	0.001996	0.0213908	1.004677399	TFF3	-2.5276949	0.001996	0.0213908	1.01135453
SDHAF2	-2.4632655	0.001996	0.0213908	1.002712592	WNT11	-2.5282852	0.001996	0.0213908	1.00695652
ARF6	-2.4639365	0.001996	0.0213908	1.003302893	CCL2	-2.5289608	0.001996	0.0213908	1.00448384
NONO	-2.4639562	0.001996	0.0213908	1.00242173	C6orf165	-2.5293177	0.001996	0.0213908	1.0118106
OGT	-2.4647152	0.001996	0.0213908	1.004036113	NADKD1	-2.5312118	0.001996	0.0213908	1.00992297
LYRM1	-2.4649736	0.001996	0.0213908	1.003899503	ZNF160	-2.5315384	0.001996	0.0213908	1.00693807
TRIP11	-2.4677641	0.001996	0.0213908	1.011120299	FAM160B1	-2.5353564	0.001996	0.0213908	1.00612919
MSX2	-2.4678131	0.001996	0.0213908	1.03840718	MAPRE3	-2.5367042	0.001996	0.0213908	1.00797748
NDUFA2	-2.4680542	0.001996	0.0213908	1.003355805	DCAF5	-2.5397185	0.001996	0.0213908	1.00596003
TMEM186	-2.4680743	0.001996	0.0213908	1.007826571	CENPA	-2.5400845	0.001996	0.0213908	1.00464927
CMPK2	-2.4694419	0.001996	0.0213908	1.005087749	NSMCE1	-2.5410872	0.001996	0.0213908	1.00844785
TMEM59	-2.470586	0.001996	0.0213908	1.0018463	TACR1	-2.5411062	0.001996	0.0213908	1.03061224
METTL4	-2.4712039	0.001996	0.0213908	1.006636435	UBA1	-2.5416162	0.001996	0.0213908	1.00263295
TBL1XR1	-2.4730486	0.001996	0.0213908	1.004583921	WNT8A	-2.5417745	0.001996	0.0213908	1.02667588
PCDHB8	-2.4734645	0.001996	0.0213908	1.041739034	BLVRA	-2.5423064	0.001996	0.0213908	1.004817
CCHCR1	-2.4742135	0.001996	0.0213908	1.003423489	GNG2	-2.5427996	0.001996	0.0213908	1.01270972
OR10T1P	-2.4788582	0.001996	0.0213908	1.017198472	ZNF600	-2.5471296	0.001996	0.0213908	1.01330857
ANKRD36C	-2.4804077	0.001996	0.0213908	1.006858435	NODAL	-2.5475595	0.001996	0.0213908	1.04161647
GPSM3	-2.4804699	0.001996	0.0213908	1.011917527	ANKRD20A8P	-2.5485548	0.001996	0.0213908	1.01499081
LIPH	-2.4819038	0.001996	0.0213908	1.034492071	NAA40	-2.5485956	0.001996	0.0213908	1.00467922
NM_023011.2	-2.4833234	0.001996	0.0213908	1.002494608	C19orf70	-2.5492099	0.001996	0.0213908	1.0037304
PKDCC	-2.4844849	0.001996	0.0213908	1.029561846	PLSCR1	-2.5494657	0.001996	0.0213908	1.01783948
FN3KRP	-2.4846304	0.001996	0.0213908	1.00556311	DDHD1	-2.5502626	0.001996	0.0213908	1.004928
NGEF	-2.4852998	0.001996	0.0213908	1.006564882	ELMOD3	-2.552865	0.001996	0.0213908	1.00993112
MIF4GD	-2.4859416	0.001996	0.0213908	1.010201511	SNX30	-2.5548191	0.001996	0.0213908	1.00686611

Gene Symbol	Score	Feature P	FDR (BH)	Fold Change	Gene Symbol	Score	Feature P	FDR (BH)	Fold Change
RNF24	-2.5549472	0.001996	0.0213908	1.0047028	CSMD3	-2.6028321	0.001996	0.0213908	1.0072171
ARID5A	-2.5551175	0.001996	0.0213908	1.0133329	SEMA3D	-2.6031283	0.001996	0.0213908	1.0151722
STAG3L3	-2.5562453	0.001996	0.0213908	1.0069181	DNAH12	-2.603146	0.001996	0.0213908	1.0209615
KLF5	-2.5562678	0.001996	0.0213908	1.0106869	HNF1B	-2.6047558	0.001996	0.0213908	1.0232646
GDPGP1	-2.5581433	0.001996	0.0213908	1.0077368	JAKMIP3	-2.6058272	0.001996	0.0213908	1.0080203
CTBP1-AS1	-2.5582541	0.001996	0.0213908	1.0056498	TBC1D28	-2.6062318	0.001996	0.0213908	1.0119632
MLH3	-2.5591133	0.001996	0.0213908	1.0110073	HNRNPA1	-2.6072685	0.001996	0.0213908	1.0013975
VGLL4	-2.5602132	0.001996	0.0213908	1.0030359	AY358241	-2.6074937	0.001996	0.0213908	1.0369273
TMEM198B	-2.5607995	0.001996	0.0213908	1.0093052	SCARNA9L	-2.6081294	0.001996	0.0213908	1.0176228
MYEF2	-2.5608657	0.001996	0.0213908	1.0030971	AK098314	-2.609661	0.001996	0.0213908	1.0071255
PRKAR1A	-2.5608757	0.001996	0.0213908	1.0036244	SP5	-2.6099224	0.001996	0.0213908	1.0328157
LINC00173	-2.5609812	0.001996	0.0213908	1.0114476	SLC40A1	-2.6103525	0.001996	0.0213908	1.0430797
PIGB	-2.5622685	0.001996	0.0213908	1.009066	LZIC	-2.6108068	0.001996	0.0213908	1.0073221
LINC00467	-2.5632256	0.001996	0.0213908	1.0283903	UGT3A1	-2.610956	0.001996	0.0213908	1.0157043
EZH1	-2.5648081	0.001996	0.0213908	1.0091792	FAM83F	-2.6140043	0.001996	0.0213908	1.0052526
TIRAP	-2.565106	0.001996	0.0213908	1.0147642	COPG1	-2.6141548	0.001996	0.0213908	1.0024959
SPTBN1	-2.5659816	0.001996	0.0213908	1.0029979	PDE9A	-2.6141837	0.001996	0.0213908	1.0031622
ICAM3	-2.5660412	0.001996	0.0213908	1.0096561	TMEM194B	-2.6149215	0.001996	0.0213908	1.0072006
CAPN7	-2.5687421	0.001996	0.0213908	1.0058037	EHD3	-2.6187588	0.001996	0.0213908	1.0047239
RYR2	-2.5689597	0.001996	0.0213908	1.0139063	UBL3	-2.6192716	0.001996	0.0213908	1.0033744
FAM167A	-2.5690995	0.001996	0.0213908	1.048299	EBAG9	-2.6200021	0.001996	0.0213908	1.0062548
PHKA1	-2.5702083	0.001996	0.0213908	1.0084419	GFRA3	-2.6205884	0.001996	0.0213908	1.0080065
LYPLAL1	-2.571339	0.001996	0.0213908	1.0198868	USP41	-2.6213366	0.001996	0.0213908	1.016804
SPA17	-2.5729475	0.001996	0.0213908	1.0128341	PLXNA3	-2.6215163	0.001996	0.0213908	1.0082091
DZIP3	-2.574858	0.001996	0.0213908	1.0077124	DCLK2	-2.6219428	0.001996	0.0213908	1.0270821
CCDC92	-2.5755603	0.001996	0.0213908	1.0497748	LOC440173	-2.6219998	0.001996	0.0213908	1.0210912
TMEM144	-2.5777999	0.001996	0.0213908	1.0228469	KBTBD2	-2.6223786	0.001996	0.0213908	1.0064897
ST6GAL1	-2.5778454	0.001996	0.0213908	1.0026718	CD40	-2.6239402	0.001996	0.0213908	1.0133534
RHPN1-AS1	-2.5794775	0.001996	0.0213908	1.0037498	ABL1	-2.6248008	0.001996	0.0213908	1.0019138
FAM213A	-2.5808093	0.001996	0.0213908	1.0070278	MYO3B	-2.6282256	0.001996	0.0213908	1.0441029
RNF5	-2.5808421	0.001996	0.0213908	1.003066	FAM125A	-2.6283685	0.001996	0.0213908	1.0093727
METTL20	-2.5815363	0.001996	0.0213908	1.019442	NIPAL3	-2.629674	0.001996	0.0213908	1.0069267
IL1RAPL1	-2.5830552	0.001996	0.0213908	1.0429608	ARSD	-2.6297321	0.001996	0.0213908	1.005765
CCDC82	-2.5845311	0.001996	0.0213908	1.0051897	TNFAIP8L1	-2.6304088	0.001996	0.0213908	1.0105815
VPS13C	-2.584809	0.001996	0.0213908	1.011586	ARMCX4	-2.6308385	0.001996	0.0213908	1.0095408
DCP1B	-2.58512	0.001996	0.0213908	1.0051781	ARHGEF11	-2.6315128	0.001996	0.0213908	1.0026988
OMA1	-2.5867204	0.001996	0.0213908	1.0153549	FMO4	-2.6316586	0.001996	0.0213908	1.0080619
TIA1	-2.5874357	0.001996	0.0213908	1.005081	TMEM120A	-2.6322788	0.001996	0.0213908	1.0043739
ASB5	-2.5877983	0.001996	0.0213908	1.0607262	DENND1B	-2.6331821	0.001996	0.0213908	1.0132699
TMEM87B	-2.5896898	0.001996	0.0213908	1.0122226	IER3	-2.6340002	0.001996	0.0213908	1.0101389
CTSA	-2.5910132	0.001996	0.0213908	1.0025431	RNU1-17P	-2.6341368	0.001996	0.0213908	1.0050547
MTMR10	-2.591687	0.001996	0.0213908	1.0112477	TAF6L	-2.6342661	0.001996	0.0213908	1.006748
CEP44	-2.5934557	0.001996	0.0213908	1.0086845	RIOK3	-2.6344542	0.001996	0.0213908	1.003893
IL12RB2	-2.5936504	0.001996	0.0213908	1.0143816	SNORD115-35	-2.6356645	0.001996	0.0213908	1.0158439
TPD52	-2.5938389	0.001996	0.0213908	1.0024854	LAS1L	-2.638295	0.001996	0.0213908	1.0031024
DUX4L7	-2.5942263	0.001996	0.0213908	1.0160225	RNF103	-2.6385226	0.001996	0.0213908	1.0123151
NLRP12	-2.5964835	0.001996	0.0213908	1.0102364	EFHA2	-2.6426884	0.001996	0.0213908	1.0041393
KIF27	-2.5965973	0.001996	0.0213908	1.0111717	PYROXD2	-2.6442531	0.001996	0.0213908	1.0156009
SLC25A20	-2.5998713	0.001996	0.0213908	1.0119392	LCK	-2.6442923	0.001996	0.0213908	1.0023846
MARVELD2	-2.600306	0.001996	0.0213908	1.0093074	LANCL3	-2.6446746	0.001996	0.0213908	1.0351982

Gene Symbol	Score	Feature P	FDR (BH)	Fold Change	Gene Symbol	Score	Feature P	FDR (BH)	Fold Change
INPPL1	-2.6448093	0.001996	0.0213908	1.0058163	YAP1	-2.6930984	0.001996	0.0213908	1.0040751
PPM1H	-2.6451518	0.001996	0.0213908	1.0052473	RNF122	-2.6940034	0.001996	0.0213908	1.013324
CLCN5	-2.645847	0.001996	0.0213908	1.008109	TMEM123	-2.695709	0.001996	0.0213908	1.0055757
CARKD	-2.6469192	0.001996	0.0213908	1.0052465	ZHX2	-2.6967569	0.001996	0.0213908	1.0050857
GLI3	-2.6470121	0.001996	0.0213908	1.0085213	SP110	-2.6975587	0.001996	0.0213908	1.0152551
DDB1	-2.6477036	0.001996	0.0213908	1.0020567	C1orf210	-2.6977332	0.001996	0.0213908	1.0031685
POLR2J3	-2.648229	0.001996	0.0213908	1.0054889	LRRC3	-2.6978334	0.001996	0.0213908	1.0263937
PTTG2	-2.6490159	0.001996	0.0213908	1.0244172	ZNF627	-2.699059	0.001996	0.0213908	1.0057793
RBM4B	-2.6493874	0.001996	0.0213908	1.00633	ZNF688	-2.7004914	0.001996	0.0213908	1.0103215
DCBLD1	-2.6505891	0.001996	0.0213908	1.0117881	SFT2D2	-2.7007001	0.001996	0.0213908	1.0045406
SPCS3	-2.6509556	0.001996	0.0213908	1.0043749	TIMM8B	-2.7015659	0.001996	0.0213908	1.0042838
UBXN4	-2.6521108	0.001996	0.0213908	1.0053404	C19orf54	-2.7020023	0.001996	0.0213908	1.0070612
SUSD2	-2.6537375	0.001996	0.0213908	1.0103668	POLR2J2	-2.7036314	0.001996	0.0213908	1.0040749
AADAT	-2.6548402	0.001996	0.0213908	1.0115668	TARBP1	-2.7050889	0.001996	0.0213908	1.0133729
PLA2G5	-2.6566135	0.001996	0.0213908	1.0202548	ZKSCAN1	-2.7071145	0.001996	0.0213908	1.0115951
FBXO11	-2.6574804	0.001996	0.0213908	1.0035718	FAM159B	-2.7071939	0.001996	0.0213908	1.035621
ANKRD32	-2.657658	0.001996	0.0213908	1.0190915	PPP1R3B	-2.7072477	0.001996	0.0213908	1.0175357
REEP4	-2.6580669	0.001996	0.0213908	1.0061704	DNAJC4	-2.7086577	0.001996	0.0213908	1.0098773
C6orf57	-2.6584747	0.001996	0.0213908	1.013086	HFM1	-2.7086708	0.001996	0.0213908	1.033095
RAC2	-2.6598794	0.001996	0.0213908	1.0078102	ZNF285	-2.7090795	0.001996	0.0213908	1.0289051
TEN1-CDK3	-2.66049	0.001996	0.0213908	1.0071613	POLK	-2.7112375	0.001996	0.0213908	1.0084708
CHKB-CPT1B	-2.6617041	0.001996	0.0213908	1.011305	TRIM68	-2.7115853	0.001996	0.0213908	1.0155321
LHX5	-2.6617545	0.001996	0.0213908	1.0535917	CLMN	-2.7119131	0.001996	0.0213908	1.0118516
STK38	-2.6658469	0.001996	0.0213908	1.0026591	EPHB2	-2.712277	0.001996	0.0213908	1.0049093
MGC21881	-2.6688291	0.001996	0.0213908	1.0088579	SULT4A1	-2.7132519	0.001996	0.0213908	1.0092513
SIPA1L2	-2.6732476	0.001996	0.0213908	1.0195142	PEX26	-2.7136021	0.001996	0.0213908	1.0059576
GGT2	-2.6746738	0.001996	0.0213908	1.0077617	PCDHB7	-2.7137021	0.001996	0.0213908	1.0202507
TBX6	-2.6755041	0.001996	0.0213908	1.0109733	TPST1	-2.7141699	0.001996	0.0213908	1.0035748
UNK	-2.6768322	0.001996	0.0213908	1.0077793	TYK2	-2.7147781	0.001996	0.0213908	1.006555
TOB2	-2.6783767	0.001996	0.0213908	1.0100388	ENTPD4	-2.7150507	0.001996	0.0213908	1.0041463
WASH4P	-2.6785763	0.001996	0.0213908	1.0069506	GALE	-2.7152076	0.001996	0.0213908	1.0111807
ZNF135	-2.6799304	0.001996	0.0213908	1.0087484	FAM70A	-2.7166352	0.001996	0.0213908	1.0210204
CDAN1	-2.6799915	0.001996	0.0213908	1.0068565	SLC16A5	-2.7176281	0.001996	0.0213908	1.0093457
DHRS13	-2.6803325	0.001996	0.0213908	1.0056276	MGARP	-2.7182168	0.001996	0.0213908	1.0121596
C11orf52	-2.6806229	0.001996	0.0213908	1.0100454	ZDHHC17	-2.718603	0.001996	0.0213908	1.0057697
RP2	-2.6819539	0.001996	0.0213908	1.0105222	CNKSR3	-2.7199487	0.001996	0.0213908	1.0082597
CFLAR	-2.6822966	0.001996	0.0213908	1.0247582	GNGT1	-2.7202059	0.001996	0.0213908	1.0261263
DOC2A	-2.6826635	0.001996	0.0213908	1.007887	FAM184A	-2.7206483	0.001996	0.0213908	1.0206624
SEPP1	-2.68354	0.001996	0.0213908	1.0174517	COPA	-2.7222051	0.001996	0.0213908	1.0026822
HEY2	-2.6855718	0.001996	0.0213908	1.0209729	SNX33	-2.7250302	0.001996	0.0213908	1.0013401
C9orf64	-2.686357	0.001996	0.0213908	1.0139226	ACBD4	-2.7251293	0.001996	0.0213908	1.0087409
NUDT6	-2.6869908	0.001996	0.0213908	1.0079725	LOC440434	-2.7257073	0.001996	0.0213908	1.0037979
CREBRF	-2.6887124	0.001996	0.0213908	1.019673	DAK	-2.7261771	0.001996	0.0213908	1.007363
ATG7	-2.6896295	0.001996	0.0213908	1.0059085	HOXB9	-2.7268804	0.001996	0.0213908	1.0103033
ATAT1	-2.6908549	0.001996	0.0213908	1.0093893	RN5S290	-2.728045	0.001996	0.0213908	1.0113838
MTMR14	-2.6911253	0.001996	0.0213908	1.0039977	ZNF433	-2.7309792	0.001996	0.0213908	1.0133523
ROGDI	-2.691295	0.001996	0.0213908	1.0044563	KIF1B	-2.7320095	0.001996	0.0213908	1.0042549
HEATR7A	-2.6918523	0.001996	0.0213908	1.0040286	GATA4	-2.732201	0.001996	0.0213908	1.0240351
DCK	-2.6925737	0.001996	0.0213908	1.0020613	PLGRKT	-2.7339234	0.001996	0.0213908	1.0200531
C6orf203	-2.6927586	0.001996	0.0213908	1.0140014	PIP4K2B	-2.735092	0.001996	0.0213908	1.0030366

Gene Symbol	Score	Feature P	FDR (BH)	Fold Change	Gene Symbol	Score	Feature P	FDR (BH)	Fold Change
WDR91	-2.7364379	0.001996	0.0213908	1.0036236	APOF	-2.7805427	0.001996	0.0213908	1.0146593
RTTN	-2.7376664	0.001996	0.0213908	1.0067717	FMO5	-2.7817463	0.001996	0.0213908	1.0200564
ST3GAL6	-2.7383972	0.001996	0.0213908	1.0136095	CCDC53	-2.7824047	0.001996	0.0213908	1.0181206
ZBTB41	-2.7385102	0.001996	0.0213908	1.0087422	CALCR	-2.7832145	0.001996	0.0213908	1.0561191
GPX7	-2.7389362	0.001996	0.0213908	1.0096626	ANO1	-2.7834848	0.001996	0.0213908	1.0157689
C1orf201	-2.739234	0.001996	0.0213908	1.0141375	UBE2H	-2.7847267	0.001996	0.0213908	1.0034443
NR1H3	-2.7402555	0.001996	0.0213908	1.0083355	ZNF658	-2.7852789	0.001996	0.0213908	1.0166759
C1orf115	-2.7404561	0.001996	0.0213908	1.0075938	LIPT2	-2.7878058	0.001996	0.0213908	1.0063445
VPS39	-2.7414879	0.001996	0.0213908	1.0046705	CD99L2	-2.7883938	0.001996	0.0213908	1.0123109
ITLN2	-2.7459558	0.001996	0.0213908	1.0125294	CECR1	-2.7886562	0.001996	0.0213908	1.0057536
GSTM1	-2.7463566	0.001996	0.0213908	1.0070916	FZD1	-2.7903684	0.001996	0.0213908	1.0099043
SUMF2	-2.7465956	0.001996	0.0213908	1.008403	L3MBTL1	-2.7914209	0.001996	0.0213908	1.0141398
C1orf74	-2.7469741	0.001996	0.0213908	1.0059368	WDR78	-2.7915238	0.001996	0.0213908	1.016088
ZSCAN23	-2.7486771	0.001996	0.0213908	1.0175226	RAB5B	-2.7926185	0.001996	0.0213908	1.0043175
BVES	-2.7542943	0.001996	0.0213908	1.011552	FBXO7	-2.7944442	0.001996	0.0213908	1.0039703
BMP1	-2.7558519	0.001996	0.0213908	1.0080778	FTSJD2	-2.7950888	0.001996	0.0213908	1.0037807
LHX1	-2.7559317	0.001996	0.0213908	1.0452115	MMS19	-2.7955176	0.001996	0.0213908	1.0036295
MEIS2	-2.7566875	0.001996	0.0213908	1.038354	CYP39A1	-2.796556	0.001996	0.0213908	1.0153949
NR2C1	-2.7572606	0.001996	0.0213908	1.0053668	LRRC3DN	-2.7970082	0.001996	0.0213908	1.0295634
CTAGE4	-2.7575353	0.001996	0.0213908	1.031192	SMAD3	-2.7973678	0.001996	0.0213908	1.0035796
SPO11	-2.7601983	0.001996	0.0213908	1.0145872	DMTF1	-2.7976912	0.001996	0.0213908	1.0016645
AKAP14	-2.7610928	0.001996	0.0213908	1.0125935	STAG3L1	-2.7989814	0.001996	0.0213908	1.007244
COPZ1	-2.7617793	0.001996	0.0213908	1.0035035	KLF12	-2.8004885	0.001996	0.0213908	1.0098426
PLA2G7	-2.7620385	0.001996	0.0213908	1.0184331	CDK5	-2.8013669	0.001996	0.0213908	1.0072982
SLC38A3	-2.7628577	0.001996	0.0213908	1.008805	PMS2P1	-2.8016617	0.001996	0.0213908	1.0059359
BRE	-2.7633672	0.001996	0.0213908	1.0044053	PYDC1	-2.8027237	0.001996	0.0213908	1.0069039
ZNF233	-2.7634397	0.001996	0.0213908	1.0091701	ZMAT2	-2.8033931	0.001996	0.0213908	1.0055151
TBX19	-2.7635828	0.001996	0.0213908	1.0111541	FAM122A	-2.804524	0.001996	0.0213908	1.0080114
STIM1	-2.7638572	0.001996	0.0213908	1.0129129	KRT18	-2.8047655	0.001996	0.0213908	1.0072592
HNRNPUL2	-2.7642578	0.001996	0.0213908	1.0055326	GUCY1A2	-2.8060361	0.001996	0.0213908	1.0106536
PTPDC1	-2.7642983	0.001996	0.0213908	1.0081087	DDX60	-2.8087759	0.001996	0.0213908	1.0286048
TOP2A	-2.7649929	0.001996	0.0213908	1.0044281	TENC1	-2.8091848	0.001996	0.0213908	1.0182109
FRMPD4	-2.7655968	0.001996	0.0213908	1.0270721	TSC2	-2.8092112	0.001996	0.0213908	1.0029877
APLF	-2.7661331	0.001996	0.0213908	1.0081897	MDP1	-2.8103337	0.001996	0.0213908	1.0081349
RASGRP1	-2.7661401	0.001996	0.0213908	1.0148993	EPHX2	-2.8105353	0.001996	0.0213908	1.0145533
GLS	-2.767505	0.001996	0.0213908	1.0142614	RAB14	-2.8106708	0.001996	0.0213908	1.002921
WDR81	-2.7678502	0.001996	0.0213908	1.0082758	WNT8B	-2.8124654	0.001996	0.0213908	1.0258083
SYPL1	-2.768931	0.001996	0.0213908	1.0035349	KRCC1	-2.8163698	0.001996	0.0213908	1.0166484
SETD4	-2.7689743	0.001996	0.0213908	1.0141859	AHNAK	-2.8181197	0.001996	0.0213908	1.0243512
MCF2L2	-2.7694008	0.001996	0.0213908	1.0037509	OR5H14	-2.8186226	0.001996	0.0213908	1.1685847
RNF31	-2.7695117	0.001996	0.0213908	1.0021348	FRRS1	-2.8188875	0.001996	0.0213908	1.0133706
FAT4	-2.7707077	0.001996	0.0213908	1.0322178	PYGL	-2.8189096	0.001996	0.0213908	1.0038651
RNF152	-2.7733793	0.001996	0.0213908	1.0220043	GDPD3	-2.8200675	0.001996	0.0213908	1.0106394
ARHGAP24	-2.7741889	0.001996	0.0213908	1.0369961	DTWD2	-2.8211728	0.001996	0.0213908	1.0326057
SNX16	-2.7753298	0.001996	0.0213908	1.0125857	RHOBTB3	-2.8212489	0.001996	0.0213908	1.0168825
RNY4P30	-2.777371	0.001996	0.0213908	1.0176737	EDIL3	-2.8213442	0.001996	0.0213908	1.0069528
INMT	-2.7782702	0.001996	0.0213908	1.0106154	SLC30A4	-2.8230965	0.001996	0.0213908	1.0298606
CD48	-2.7784757	0.001996	0.0213908	1.0212601	NAT9	-2.8264013	0.001996	0.0213908	1.0128533
ABHD13	-2.7787201	0.001996	0.0213908	1.0055982	BBS2	-2.8272836	0.001996	0.0213908	1.0142159
CRYGA	-2.7803199	0.001996	0.0213908	1.0217278	CKMT2	-2.8280552	0.001996	0.0213908	1.0173699

Gene Symbol	Score	Feature P	FDR (BH)	Fold Change	Gene Symbol	Score	Feature P	FDR (BH)	Fold Change
CPT2	-2.8287072	0.001996	0.0213908	1.0061314	ATM	-2.8944487	0.001996	0.0213908	1.004428
CSRNP3	-2.828827	0.001996	0.0213908	1.0095512	TPTE2P6	-2.8945999	0.001996	0.0213908	1.0277127
CHST9	-2.8293535	0.001996	0.0213908	1.0111598	SNX1	-2.8955948	0.001996	0.0213908	1.005052
CACNB3	-2.8299959	0.001996	0.0213908	1.0118004	OR52A5	-2.897135	0.001996	0.0213908	1.054863
FZD4	-2.8313063	0.001996	0.0213908	1.0089175	ZYG11A	-2.8976858	0.001996	0.0213908	1.0153166
CDC25C	**-2.8325804**	**0.001996**	**0.0213908**	**1.0086812**	UHRF2	-2.8996646	0.001996	0.0213908	1.0054175
GNB4	-2.8344565	0.001996	0.0213908	1.0103999	TUBB2A	-2.9011045	0.001996	0.0213908	1.0091155
RNF32	-2.8362624	0.001996	0.0213908	1.0049363	RAB38	-2.9011066	0.001996	0.0213908	1.0078001
TRPV4	-2.8377799	0.001996	0.0213908	1.0126901	DCAF7	-2.904022	0.001996	0.0213908	1.0049878
LIX1	-2.838939	0.001996	0.0213908	1.0679879	SEC24C	-2.9046041	0.001996	0.0213908	1.0035148
CHURC1-FNTB	-2.8406086	0.001996	0.0213908	1.0022673	RBM11	-2.9069914	0.001996	0.0213908	1.0095239
KCNG1	-2.841635	0.001996	0.0213908	1.0112267	CXorf23	-2.9071726	0.001996	0.0213908	1.01093
ODF2L	-2.8417196	0.001996	0.0213908	1.0065522	SVOPL	-2.9090971	0.001996	0.0213908	1.008431
RPS20	-2.8420663	0.001996	0.0213908	1.0024903	C1orf145	-2.9093295	0.001996	0.0213908	1.0046377
FLJ43879	-2.8425812	0.001996	0.0213908	1.0111566	TXNIP	-2.9094082	0.001996	0.0213908	1.0213546
ZNF512	-2.8426206	0.001996	0.0213908	1.0031921	BMPR1A	-2.9101174	0.001996	0.0213908	1.0059206
PURG	-2.8428312	0.001996	0.0213908	1.005746	GLTP	-2.9108919	0.001996	0.0213908	1.0082679
C17orf65	-2.8443053	0.001996	0.0213908	1.0066045	ZNF578	-2.9120673	0.001996	0.0213908	1.0271875
C4orf46	-2.8448648	0.001996	0.0213908	1.0041824	RPS2	-2.9125639	0.001996	0.0213908	1.0005038
STK33	-2.8470006	0.001996	0.0213908	1.0094431	IL17RA	-2.9127516	0.001996	0.0213908	1.0055695
CLK2P	-2.8471041	0.001996	0.0213908	1.0051862	MITD1	-2.9132125	0.001996	0.0213908	1.0125545
NUDT16P1	-2.8475408	0.001996	0.0213908	1.0055412	NGLY1	-2.9166067	0.001996	0.0213908	1.0093824
TGIF2	-2.8487108	0.001996	0.0213908	1.0051353	GLB1L	-2.9182019	0.001996	0.0213908	1.01281
NFASC	-2.849162	0.001996	0.0213908	1.0153685	MPDU1	-2.9185707	0.001996	0.0213908	1.002452
BCAR3	-2.8525564	0.001996	0.0213908	1.0142452	MR1	-2.9195786	0.001996	0.0213908	1.0231215
ZNF396	-2.8532088	0.001996	0.0213908	1.0217288	ZNF385C	-2.9223455	0.001996	0.0213908	1.0052891
LANCL1	-2.8535146	0.001996	0.0213908	1.0062251	TPST2	-2.9237057	0.001996	0.0213908	1.0043109
KRT78	-2.8538472	0.001996	0.0213908	1.004586	BAZ2A	-2.9247398	0.001996	0.0213908	1.0023571
ALG10	-2.8553	0.001996	0.0213908	1.006987	C10orf131	-2.9256899	0.001996	0.0213908	1.039316
FAM193B	-2.8600027	0.001996	0.0213908	1.0051477	ACTR2	-2.9258841	0.001996	0.0213908	1.0023076
CDH9	-2.8626926	0.001996	0.0213908	1.0482886	MFAP3L	-2.9267721	0.001996	0.0213908	1.0319356
GSTO1	-2.8628633	0.001996	0.0213908	1.0164517	CABIN1	-2.9272306	0.001996	0.0213908	1.0026438
SIPA1L1	-2.8637594	0.001996	0.0213908	1.0046187	MOCS1	-2.9311546	0.001996	0.0213908	1.0062888
FLOT2	-2.8679866	0.001996	0.0213908	1.0045047	ING4	-2.9319054	0.001996	0.0213908	1.0068795
ECM1	-2.8687358	0.001996	0.0213908	1.0155275	ITPR3	-2.9323614	0.001996	0.0213908	1.0044521
TSPYL4	-2.8695636	0.001996	0.0213908	1.0035741	USP11	-2.9336864	0.001996	0.0213908	1.0037499
THBS3	-2.8737768	0.001996	0.0213908	1.027034	LRRN2	-2.9339241	0.001996	0.0213908	1.0269785
MYO6	-2.8756931	0.001996	0.0213908	1.0115793	CHST4	-2.9345399	0.001996	0.0213908	1.009198
PPP1CA	-2.8791323	0.001996	0.0213908	1.004462	ATG10	-2.9353012	0.001996	0.0213908	1.0143411
PLCB2	-2.8796207	0.001996	0.0213908	1.0090012	MED23	-2.9355717	0.001996	0.0213908	1.0076282
PGLS	-2.8796535	0.001996	0.0213908	1.0104799	MDFIC	-2.9365053	0.001996	0.0213908	1.0026
CCNB2	**-2.8801734**	**0.001996**	**0.0213908**	**1.0028086**	LRRCC1	-2.9368965	0.001996	0.0213908	1.0077966
TCTA	-2.8818887	0.001996	0.0213908	1.0061805	TUBG2	-2.9378549	0.001996	0.0213908	1.0100611
CCPG1	-2.8847779	0.001996	0.0213908	1.0209846	FLJ30403	-2.9406968	0.001996	0.0213908	1.0228534
NMNAT1	-2.8854033	0.001996	0.0213908	1.0129707	ZC3HAV1L	-2.9429644	0.001996	0.0213908	1.0083574
LRIG3	-2.8875046	0.001996	0.0213908	1.0195268	ERLIN2	-2.9480365	0.001996	0.0213908	1.0058345
POMT1	-2.8915738	0.001996	0.0213908	1.0065066	MYD88	-2.9490222	0.001996	0.0213908	1.0041355
FST	-2.8923689	0.001996	0.0213908	1.033116	C12orf57	-2.9492276	0.001996	0.0213908	1.0018601
GOLGA2	-2.8934672	0.001996	0.0213908	1.0031289	MAN1A1	-2.9494963	0.001996	0.0213908	1.0152507
GSTO2	-2.8942318	0.001996	0.0213908	1.0103263	ZNF839	-2.9501752	0.001996	0.0213908	1.0136366

Gene Symbol	Score	Feature P	FDR (BH)	Fold Change	Gene Symbol	Score	Feature P	FDR (BH)	Fold Change
ZNF765	-2.9521591	0.001996	0.0213908	1.0027661	PABPC1L	-3.0044798	0.001996	0.0213908	1.0091152
SGPP1	-2.9530702	0.001996	0.0213908	1.0038663	COG1	-3.0061015	0.001996	0.0213908	1.0048289
TSPYL1	-2.9536475	0.001996	0.0213908	1.0019171	DDX25	-3.0066884	0.001996	0.0213908	1.0073857
NRIP1	-2.9542162	0.001996	0.0213908	1.0118123	LRRC20	-3.006736	0.001996	0.0213908	1.0073977
CSTB	-2.9549433	0.001996	0.0213908	1.0017827	THAP6	-3.0099412	0.001996	0.0213908	1.0090609
TMEM185B	-2.9552388	0.001996	0.0213908	1.0058906	TRNAL41P	-3.0102755	0.001996	0.0213908	1.0133628
C4orf37	-2.9552823	0.001996	0.0213908	1.0143474	DDX11	-3.0104736	0.001996	0.0213908	1.0044576
MAN1B1	-2.9560727	0.001996	0.0213908	1.001368	SCN5A	-3.0123762	0.001996	0.0213908	1.0020891
CAPN11	-2.9562417	0.001996	0.0213908	1.0202911	RNF141	-3.0129233	0.001996	0.0213908	1.0047569
RFXANK	-2.9564308	0.001996	0.0213908	1.0039486	IL13RA1	-3.0150038	0.001996	0.0213908	1.0101275
SNX10	-2.9604664	0.001996	0.0213908	1.0080638	USP51	-3.0150775	0.001996	0.0213908	1.0059521
ZMYM6	-2.9623321	0.001996	0.0213908	1.0083322	SEPSECS	-3.0161184	0.001996	0.0213908	1.020082
ITGA2B	-2.9639059	0.001996	0.0213908	1.0052855	CHMP4C	-3.0181644	0.001996	0.0213908	1.027344
CDC7	-2.9647221	0.001996	0.0213908	1.0059498	SLC26A8	-3.0184641	0.001996	0.0213908	1.0149676
KRT18P28	-2.9666076	0.001996	0.0213908	1.008598	GSN	-3.0192308	0.001996	0.0213908	1.0032227
NICN1	-2.9672722	0.001996	0.0213908	1.0080517	GPR126	-3.0195075	0.001996	0.0213908	1.018272
LOC284788	-2.9675944	0.001996	0.0213908	1.0209701	MBTPS2	-3.0197275	0.001996	0.0213908	1.0055311
CHFR	-2.9682855	0.001996	0.0213908	1.0089779	RAD23A	-3.0220992	0.001996	0.0213908	1.002498
C19orf40	-2.9686228	0.001996	0.0213908	1.0056043	ATP2A1	-3.0221835	0.001996	0.0213908	1.0104831
P2RX4	-2.9707286	0.001996	0.0213908	1.0153621	FBLN2	-3.0231294	0.001996	0.0213908	1.0108298
PTBP3	-2.972676	0.001996	0.0213908	1.0034729	MCTP2	-3.0233415	0.001996	0.0213908	1.0134147
WDR60	-2.9727863	0.001996	0.0213908	1.009275	ENGASE	-3.0233727	0.001996	0.0213908	1.0080385
STRADB	-2.9743028	0.001996	0.0213908	1.0040575	ZNF137P	-3.0241415	0.001996	0.0213908	1.0156706
MTERFD3	-2.9781661	0.001996	0.0213908	1.0055351	STIL	-3.0241722	0.001996	0.0213908	1.0062831
OLFM3	-2.9782262	0.001996	0.0213908	1.0330947	SIX3	-3.0245612	0.001996	0.0213908	1.0120452
SETD8	-2.9802718	0.001996	0.0213908	1.0041193	NPY1R	-3.0246521	0.001996	0.0213908	1.0133587
C7orf25	-2.9806818	0.001996	0.0213908	1.0220618	LRRIQ3	-3.0259285	0.001996	0.0213908	1.0339327
CHRNB4	-2.9806929	0.001996	0.0213908	1.0159376	MAP2K3	-3.0282126	0.001996	0.0213908	1.0076589
ATP5H	-2.9817383	0.001996	0.0213908	1.0055624	RWDD2B	-3.0294556	0.001996	0.0213908	1.0234685
ITGA2	-2.986624	0.001996	0.0213908	1.0012569	TXLNG2P	-3.0305861	0.001996	0.0213908	1.0059031
PTGES3L-AARSD1	-2.9896642	0.001996	0.0213908	1.0044692	CCDC125	-3.0312353	0.001996	0.0213908	1.017356
FAM21C	-2.9897245	0.001996	0.0213908	1.0045813	MSI1	-3.0336236	0.001996	0.0213908	1.0121332
MINK1	-2.9898477	0.001996	0.0213908	1.0025639	WSB1	-3.0365371	0.001996	0.0213908	1.0072885
CHRD	-2.9909454	0.001996	0.0213908	1.0197771	MTA2	-3.0366387	0.001996	0.0213908	1.0035113
PEX12	-2.9914286	0.001996	0.0213908	1.0135272	MSN	-3.037024	0.001996	0.0213908	1.0028033
SMARCAL1	-2.9916604	0.001996	0.0213908	1.0046313	ZFP2	-3.0377222	0.001996	0.0213908	1.0142558
ATP5A1	-2.9931034	0.001996	0.0213908	1.001407	APOL2	-3.0387823	0.001996	0.0213908	1.0074528
LRP10	-2.9940664	0.001996	0.0213908	1.0120088	AKAP7	-3.0389184	0.001996	0.0213908	1.0196578
GABPB2	-2.9942596	0.001996	0.0213908	1.0149817	KLRC4-KLRK1	-3.0391849	0.001996	0.0213908	1.0140192
DSCAM	-2.9950003	0.001996	0.0213908	1.0074479	RNF181	-3.0401698	0.001996	0.0213908	1.0019089
RCBTB1	-2.9958011	0.001996	0.0213908	1.0044403	WDR31	-3.0403489	0.001996	0.0213908	1.0167761
PLA2G6	-2.9969234	0.001996	0.0213908	1.0248277	USF2	-3.0446261	0.001996	0.0213908	1.0034742
RNFT1	-2.9971025	0.001996	0.0213908	1.0184363	ZNF436	-3.0452978	0.001996	0.0213908	1.010903
EGFLAM	-2.9974842	0.001996	0.0213908	1.0326713	RNY4P22	-3.0458643	0.001996	0.0213908	1.0117841
CYP11A1	-2.9975845	0.001996	0.0213908	1.019591	FES	-3.046452	0.001996	0.0213908	1.0121581
CDH20	-2.9984768	0.001996	0.0213908	1.0121747	APLNR	-3.047093	0.001996	0.0213908	1.066052
TTC8	-2.9988312	0.001996	0.0213908	1.0084055	USP4	-3.0506356	0.001996	0.0213908	1.0035548
SP1	-3.0012182	0.001996	0.0213908	1.0031993	NKX2-1	-3.0527072	0.001996	0.0213908	1.0116203
UBE2Q2P2	-3.003238	0.001996	0.0213908	1.0074425	RN5S109	-3.0549076	0.001996	0.0213908	1.0288522
PBX2	-3.0041125	0.001996	0.0213908	1.00383	PDK1	-3.0552711	0.001996	0.0213908	1.0168755

Gene Symbol	Score	Feature P	FDR (BH)	Fold Change	Gene Symbol	Score	Feature P	FDR (BH)	Fold Change
SHISA6	-3.0555033	0.001996	0.0213908	1.0095357	AK024925	-3.1176179	0.001996	0.0213908	1.0351756
PIK3R3	-3.0565898	0.001996	0.0213908	1.0072183	UBR1	-3.119722	0.001996	0.0213908	1.0070521
CEP112	-3.05905	0.001996	0.0213908	1.015582	PCBD1	-3.120011	0.001996	0.0213908	1.0050841
TCL1B	-3.0601417	0.001996	0.0213908	1.0143597	HERPUD2	-3.1209167	0.001996	0.0213908	1.0040449
PITPNM2	-3.0609809	0.001996	0.0213908	1.011088	ZNF546	-3.1217648	0.001996	0.0213908	1.0232335
ADAMTS16	-3.0620462	0.001996	0.0213908	1.0127794	MTRF1	-3.1220417	0.001996	0.0213908	1.004802
KDM4C	-3.0635391	0.001996	0.0213908	1.0097736	AP2A2	-3.1257053	0.001996	0.0213908	1.0015304
DIAPH2	-3.0661688	0.001996	0.0213908	1.0105172	SST	-3.1278234	0.001996	0.0213908	1.0090555
PLCG1	-3.0696989	0.001996	0.0213908	1.0045909	ABLIM1	-3.1282816	0.001996	0.0213908	1.0051687
TGFA	-3.0718985	0.001996	0.0213908	1.0123743	ZSWIM4	-3.1283172	0.001996	0.0213908	1.005373
IGSF9B	-3.0725733	0.001996	0.0213908	1.017475	BOC	-3.1284243	0.001996	0.0213908	1.016266
CD1D	-3.073723	0.001996	0.0213908	1.013935	SYNJ2	-3.1322744	0.001996	0.0213908	1.0065214
IQCH	-3.0762358	0.001996	0.0213908	1.0141442	GIT2	-3.1326648	0.001996	0.0213908	1.0057697
TMPRSS11E	-3.0769319	0.001996	0.0213908	1.0259925	NCOA4	-3.1328261	0.001996	0.0213908	1.0055042
TMLHE	-3.0771365	0.001996	0.0213908	1.0036979	ROR2	-3.1334369	0.001996	0.0213908	1.0353599
FAM18B2	-3.0785837	0.001996	0.0213908	1.0103436	TMEM185A	-3.1346568	0.001996	0.0213908	1.004569
RNF180	-3.0792785	0.001996	0.0213908	1.0091393	TSHB	-3.1356361	0.001996	0.0213908	1.0118427
ALDH9A1	-3.0806933	0.001996	0.0213908	1.0032696	NCKAP1L	-3.1356413	0.001996	0.0213908	1.0146991
HTRA2	-3.0812652	0.001996	0.0213908	1.0049404	C4orf36	-3.1361726	0.001996	0.0213908	1.0331368
FBXL20	-3.0819544	0.001996	0.0213908	1.0101215	GUSBP1	-3.1372872	0.001996	0.0213908	1.0052025
SLC4A4	-3.0826862	0.001996	0.0213908	1.0117506	PNMA1	-3.1376218	0.001996	0.0213908	1.0062606
ZIC2	-3.0828928	0.001996	0.0213908	1.0081305	FAM72D	-3.1379234	0.001996	0.0213908	1.0051616
C6orf223	-3.0839455	0.001996	0.0213908	1.0114365	PDK3	-3.1381425	0.001996	0.0213908	1.0053912
ZNF503	-3.0853795	0.001996	0.0213908	1.0105508	VRK3	-3.1387945	0.001996	0.0213908	1.0057904
PLEKHM1	-3.0870562	0.001996	0.0213908	1.0052701	VANGL1	-3.1403714	0.001996	0.0213908	1.0265676
TRAPPC11	-3.0871295	0.001996	0.0213908	1.0089235	KIAA1456	-3.1413877	0.001996	0.0213908	1.0277534
SLC25A16	-3.0878678	0.001996	0.0213908	1.0076057	FLJ46010	-3.1424961	0.001996	0.0213908	1.0241925
PION	-3.0896472	0.001996	0.0213908	1.0346055	ZNF671	-3.1432261	0.001996	0.0213908	1.008367
HOMER3	-3.0909259	0.001996	0.0213908	1.0024579	MOSPD1	-3.143373	0.001996	0.0213908	1.0180044
DMD	-3.0920136	0.001996	0.0213908	1.0136019	HEATR4	-3.1434861	0.001996	0.0213908	1.021422
ARHGAP11B	-3.0947413	0.001996	0.0213908	1.0073051	RCAN2	-3.1465961	0.001996	0.0213908	1.0094633
TMEM106B	-3.0949487	0.001996	0.0213908	1.0073649	SIRT5	-3.1487103	0.001996	0.0213908	1.0073739
SPRED2	-3.095924	0.001996	0.0213908	1.0066967	FAM219B	-3.1488656	0.001996	0.0213908	1.0055733
LCA5L	-3.0959858	0.001996	0.0213908	1.008856	ERVH-6	-3.1489588	0.001996	0.0213908	1.023276
ELMO1	-3.0960466	0.001996	0.0213908	1.0112031	TCTN1	-3.1496987	0.001996	0.0213908	1.0104451
B4GALT1	-3.09879	0.001996	0.0213908	1.0067053	C18orf56	-3.1497502	0.001996	0.0213908	1.0068118
STAT5B	-3.0996771	0.001996	0.0213908	1.0037145	PAH	-3.1506536	0.001996	0.0213908	1.0119685
LRIG1	-3.1002411	0.001996	0.0213908	1.0061958	EPC1	-3.1522932	0.001996	0.0213908	1.004228
CSTF2T	-3.1007064	0.001996	0.0213908	1.0048882	NIPA1	-3.1533923	0.001996	0.0213908	1.0206771
LPXN	-3.1023567	0.001996	0.0213908	1.0272264	PLIN2	-3.1550249	0.001996	0.0213908	1.0076055
NPM3	-3.1026734	0.001996	0.0213908	1.0123678	REST	-3.1566872	0.001996	0.0213908	1.0061295
SMA5	-3.1033453	0.001996	0.0213908	1.0054074	CEP41	-3.1569384	0.001996	0.0213908	1.0053255
SLC5A9	-3.1055295	0.001996	0.0213908	1.0351958	GXYLT2	-3.1588468	0.001996	0.0213908	1.0122503
CETN3	-3.1073088	0.001996	0.0213908	1.0165832	C8orf44	-3.15896	0.001996	0.0213908	1.0222096
EPB42	-3.1081889	0.001996	0.0213908	1.0174556	SERPINE2	-3.1590743	0.001996	0.0213908	1.026012
BAI1	-3.1084275	0.001996	0.0213908	1.005135	RAB43	-3.160237	0.001996	0.0213908	1.0065512
APTX	-3.1111776	0.001996	0.0213908	1.0012798	KLF11	-3.1617389	0.001996	0.0213908	1.0184969
ANKRA2	-3.1125184	0.001996	0.0213908	1.0207129	ARL6IP1	-3.1637039	0.001996	0.0213908	1.0037589
BIN2P1	-3.1153264	0.001996	0.0213908	1.019097	KIF20A	-3.1664216	0.001996	0.0213908	1.0039574
HIC2	-3.1168952	0.001996	0.0213908	1.0064114	CUL9	-3.1664819	0.001996	0.0213908	1.0093638

Gene Symbol	Score	Feature P	FDR (BH)	Fold Change	Gene Symbol	Score	Feature P	FDR (BH)	Fold Change
SPATA7	-3.1667102	0.001996	0.0213908	1.0129955	ARMC9	-3.2216305	0.001996	0.0213908	1.0065887
PRDM1	-3.1702813	0.001996	0.0213908	1.0527297	RN5S504	-3.2291	0.001996	0.0213908	1.0344208
XYLB	-3.1704737	0.001996	0.0213908	1.0073867	CENPC1	-3.2298121	0.001996	0.0213908	1.0063006
PRKCH	-3.1711361	0.001996	0.0213908	1.0081907	ZNF75D	-3.235701	0.001996	0.0213908	1.005434
NUDT15	-3.1717951	0.001996	0.0213908	1.0149169	EGLN1	-3.2358968	0.001996	0.0213908	1.0078781
RAB18	-3.1736116	0.001996	0.0213908	1.0115526	C1orf126	-3.2360597	0.001996	0.0213908	1.0334151
OR8G3P	-3.1749306	0.001996	0.0213908	1.0222257	ADHFE1	-3.236599	0.001996	0.0213908	1.0437104
MAP3K1	-3.1764119	0.001996	0.0213908	1.0141771	EPB41L3	-3.2367952	0.001996	0.0213908	1.0183884
NEK7	-3.1776408	0.001996	0.0213908	1.0092114	MS4A13	-3.2372413	0.001996	0.0213908	1.0153929
SULT1C4	-3.1776409	0.001996	0.0213908	1.0210033	HECTD3	-3.2385693	0.001996	0.0213908	1.0069338
ZNF692	-3.1815822	0.001996	0.0213908	1.0065517	HSD17B4	-3.2438064	0.001996	0.0213908	1.0075297
ZFYVE27	-3.1829507	0.001996	0.0213908	1.0034773	CYB5R1	-3.2457291	0.001996	0.0213908	1.0051611
FBXO4	-3.1831965	0.001996	0.0213908	1.0276872	C1orf192	-3.2494098	0.001996	0.0213908	1.0215175
FITM2	-3.1836336	0.001996	0.0213908	1.0060158	SLA	-3.2505097	0.001996	0.0213908	1.0084758
LPCAT4	-3.1849435	0.001996	0.0213908	1.0064157	BMS1P5	-3.250716	0.001996	0.0213908	1.0076194
S100A11	-3.18607	0.001996	0.0213908	1.0116296	VARS2	-3.2533419	0.001996	0.0213908	1.0051501
XK	-3.1861212	0.001996	0.0213908	1.0168246	UNC93A	-3.2556246	0.001996	0.0213908	1.0200482
YPEL1	-3.1863151	0.001996	0.0213908	1.0207503	SCP2	-3.2557124	0.001996	0.0213908	1.0138908
TRAF3IP2	-3.1876395	0.001996	0.0213908	1.0093658	FOXK1	-3.2589555	0.001996	0.0213908	1.0078199
GSTM4	-3.188083	0.001996	0.0213908	1.0109176	LRFN5	-3.2593678	0.001996	0.0213908	1.0231462
MTHFR	-3.1904683	0.001996	0.0213908	1.0127084	RWDD3	-3.2596603	0.001996	0.0213908	1.0142571
ANKRD31	-3.1918657	0.001996	0.0213908	1.0233083	ELAC1	-3.2600889	0.001996	0.0213908	1.0193061
LMNB1	-3.1920022	0.001996	0.0213908	1.007957	C8orf40	-3.2603623	0.001996	0.0213908	1.0098898
PSKH2	-3.1928977	0.001996	0.0213908	1.0280119	HDHD2	-3.262779	0.001996	0.0213908	1.0060423
APOBEC3C	-3.1932738	0.001996	0.0213908	1.0088964	GUCA1A	-3.2633312	0.001996	0.0213908	1.0025728
EAPP	-3.1946781	0.001996	0.0213908	1.0074694	C2orf68	-3.2643099	0.001996	0.0213908	1.0038507
FAM173B	-3.1954489	0.001996	0.0213908	1.0180108	PDCD4	-3.2673532	0.001996	0.0213908	1.0233876
EIF2C4	-3.1970375	0.001996	0.0213908	1.0092374	GTF2H5	-3.2678754	0.001996	0.0213908	1.0070042
COX6A1	-3.1971708	0.001996	0.0213908	1.0024321	NNT	-3.2681803	0.001996	0.0213908	1.0069121
CSMD1	-3.1984772	0.001996	0.0213908	1.0450455	FNDC3A	-3.2688441	0.001996	0.0213908	1.0060032
HTR1D	-3.1985647	0.001996	0.0213908	1.0174246	AKAP13	-3.2699034	0.001996	0.0213908	1.0051399
ZNF652	-3.2001143	0.001996	0.0213908	1.0029238	AF118077	-3.2718519	0.001996	0.0213908	1.0219611
INTU	-3.2003915	0.001996	0.0213908	1.0090294	AKAP10	-3.2756084	0.001996	0.0213908	1.0062669
PCDHB13	-3.2038317	0.001996	0.0213908	1.0161432	FAM120B	-3.2790042	0.001996	0.0213908	1.0080894
LNX1	-3.2047995	0.001996	0.0213908	1.0100235	RN7SKP10	-3.2794121	0.001996	0.0213908	1.0094417
MYO15B	-3.2048028	0.001996	0.0213908	1.0142839	CD82	-3.2823474	0.001996	0.0213908	1.0106813
RAB30	-3.2051267	0.001996	0.0213908	1.0105208	OAS2	-3.2823715	0.001996	0.0213908	1.0094045
OR14A16	-3.2057081	0.001996	0.0213908	1.0446337	DDX59	-3.2842066	0.001996	0.0213908	1.0105633
UBP1	-3.2058957	0.001996	0.0213908	1.003226	C4orf34	-3.2849274	0.001996	0.0213908	1.0141296
FOXB2	-3.206654	0.001996	0.0213908	1.0090307	LLGL1	-3.2852503	0.001996	0.0213908	1.0039272
TNFRSF1A	-3.207058	0.001996	0.0213908	1.0052654	ARNT	-3.2853249	0.001996	0.0213908	1.006728
SLC16A3	-3.2079655	0.001996	0.0213908	1.0113457	RLIM	-3.2857143	0.001996	0.0213908	1.0016339
PER2	-3.2081743	0.001996	0.0213908	1.0056302	VEZT	-3.2873657	0.001996	0.0213908	1.0067698
SUPT4H1	-3.2086259	0.001996	0.0213908	1.002733	NUMA1	-3.2880635	0.001996	0.0213908	1.0046565
KCTD2	-3.2097152	0.001996	0.0213908	1.0026745	SLC22A23	-3.289769	0.001996	0.0213908	1.0099793
MANEAL	-3.2100657	0.001996	0.0213908	1.0057915	DHRS7	-3.2905647	0.001996	0.0213908	1.0109341
FAM19A2	-3.2164819	0.001996	0.0213908	1.028548	PHF8	-3.2931429	0.001996	0.0213908	1.0074616
TRMT112	-3.2168174	0.001996	0.0213908	1.001705	TACC1	-3.2961746	0.001996	0.0213908	1.0059356
SLC35E2	-3.2171002	0.001996	0.0213908	1.0030484	PXMP4	-3.2974328	0.001996	0.0213908	1.0128421
SCUBE3	-3.2173332	0.001996	0.0213908	1.0220849	CNGA2	-3.2979179	0.001996	0.0213908	1.0142121

Gene Symbol	Score	Feature P	FDR (BH)	Fold Change	Gene Symbol	Score	Feature P	FDR (BH)	Fold Change
TMC6	-3.2983663	0.001996	0.0213908	1.006839	THTPA	-3.3643112	0.001996	0.0213908	1.0087257
RRNAD1	-3.2996708	0.001996	0.0213908	1.0091424	TSPAN12	-3.3643668	0.001996	0.0213908	1.016302
SLC26A2	-3.3000509	0.001996	0.0213908	1.0123248	UBN2	-3.3674256	0.001996	0.0213908	1.0070703
PRKAR2A	-3.300548	0.001996	0.0213908	1.00192	ESPL1	-3.3675127	0.001996	0.0213908	1.0056956
LMO7	-3.3009529	0.001996	0.0213908	1.0254785	SLC47A1	-3.3693059	0.001996	0.0213908	1.0443924
STOX1	-3.3024618	0.001996	0.0213908	1.0168073	ERVH-4	-3.3699544	0.001996	0.0213908	1.0318449
MMRN1	-3.3034627	0.001996	0.0213908	1.0309247	TMED10	-3.3706594	0.001996	0.0213908	1.0009602
TMEM51	-3.303464	0.001996	0.0213908	1.0100269	KBTBD3	-3.3710139	0.001996	0.0213908	1.0292835
ZFP64	-3.303978	0.001996	0.0213908	1.0059439	PPIL6	-3.3720528	0.001996	0.0213908	1.0307025
ZNF679	-3.3047543	0.001996	0.0213908	1.0080174	MCOLN3	-3.3735346	0.001996	0.0213908	1.0322241
S100Z	-3.3051137	0.001996	0.0213908	1.0259826	ITGA5	-3.3738381	0.001996	0.0213908	1.0135648
JAKMIP1	-3.306888	0.001996	0.0213908	1.0145722	PRSS1	-3.3739321	0.001996	0.0213908	1.0383418
EFEMP1	-3.3083396	0.001996	0.0213908	1.0121802	C17orf57	-3.3770673	0.001996	0.0213908	1.0215438
WNT3	-3.309911	0.001996	0.0213908	1.0437062	TTC12	-3.3812794	0.001996	0.0213908	1.0088533
PRPF39	-3.3105434	0.001996	0.0213908	1.0087142	PTK2B	-3.3815692	0.001996	0.0213908	1.0081248
ZNF821	-3.3119951	0.001996	0.0213908	1.0130253	C2orf57	-3.384213	0.001996	0.0213908	1.0065825
GNA14	-3.3137822	0.001996	0.0213908	1.0284905	GSTZ1	-3.384389	0.001996	0.0213908	1.0111799
SAT1	-3.3138798	0.001996	0.0213908	1.0161245	RDM1	-3.3867416	0.001996	0.0213908	1.0145312
FAM218A	-3.3142603	0.001996	0.0213908	1.0060515	TRAPPC9	-3.3871999	0.001996	0.0213908	1.009603
BDKRB1	-3.3176182	0.001996	0.0213908	1.0616044	NRM	-3.3874448	0.001996	0.0213908	1.0056491
ATP5J2P3	-3.3181664	0.001996	0.0213908	1.0229613	STARD13	-3.3883627	0.001996	0.0213908	1.0078829
EWSR1	-3.319155	0.001996	0.0213908	1.00314	FAM126B	-3.3887112	0.001996	0.0213908	1.0060978
SLC12A6	-3.3197995	0.001996	0.0213908	1.009528	SZT2	-3.3906164	0.001996	0.0213908	1.0056282
HGSNAT	-3.3209753	0.001996	0.0213908	1.0214506	GPR37	-3.391974	0.001996	0.0213908	1.02855
C12orf55	-3.3215725	0.001996	0.0213908	1.0223279	CYP26A1	-3.3929346	0.001996	0.0213908	1.099315
RASGEF1B	-3.3218969	0.001996	0.0213908	1.029881	NBPF15	-3.3933352	0.001996	0.0213908	1.0012679
GIN1	-3.323031	0.001996	0.0213908	1.0155689	ADAMTS9	-3.3965119	0.001996	0.0213908	1.0309561
GRAMD1A	-3.3233068	0.001996	0.0213908	1.0044104	CTBS	-3.3975853	0.001996	0.0213908	1.0285733
SLCO2A1	-3.3236716	0.001996	0.0213908	1.0416111	C6orf89	-3.3975854	0.001996	0.0213908	1.0124358
CHD9	-3.3240472	0.001996	0.0213908	1.0037784	SOAT1	-3.3977016	0.001996	0.0213908	1.0346861
FAM54B	-3.3277188	0.001996	0.0213908	1.004275	DRAM2	-3.3979569	0.001996	0.0213908	1.0081485
C5orf24	-3.3313526	0.001996	0.0213908	1.0061665	HMGB2	-3.3989891	0.001996	0.0213908	1.006829
LOC554206	-3.3314159	0.001996	0.0213908	1.0051331	MAN2B1	-3.4000077	0.001996	0.0213908	1.0074866
DNAJB4	-3.3322387	0.001996	0.0213908	1.00694	RET	-3.4000832	0.001996	0.0213908	1.0229474
SP140L	-3.3331086	0.001996	0.0213908	1.0078571	PRPF8	-3.4031105	0.001996	0.0213908	1.0019789
EPSTI1	-3.3348298	0.001996	0.0213908	1.0354306	ANTXR2	-3.4081011	0.001996	0.0213908	1.0205912
PJA2	-3.3351654	0.001996	0.0213908	1.0049693	CD9	-3.408212	0.001996	0.0213908	1.0067344
C1orf168	-3.336721	0.001996	0.0213908	1.0392931	PCDHB9	-3.4109151	0.001996	0.0213908	1.0182276
IVNS1ABP	-3.3385626	0.001996	0.0213908	1.0099416	CCDC159	-3.4144684	0.001996	0.0213908	1.0229798
CHEK2	-3.3400049	0.001996	0.0213908	1.0130756	EFNB1	-3.4165648	0.001996	0.0213908	1.0161486
ARHGAP40	-3.3403562	0.001996	0.0213908	1.051158	MYF6	-3.4170618	0.001996	0.0213908	1.0192603
LEF1	-3.3416048	0.001996	0.0213908	1.0527489	SLC30A1	-3.419178	0.001996	0.0213908	1.0080125
GPX2	-3.3514018	0.001996	0.0213908	1.0278508	FAM208A	-3.4204346	0.001996	0.0213908	1.0151934
MAPK7	-3.3530387	0.001996	0.0213908	1.0050153	LIG4	-3.421977	0.001996	0.0213908	1.0060106
SLC39A8	-3.3556927	0.001996	0.0213908	1.0180867	PTPRB	-3.4223849	0.001996	0.0213908	1.0120689
IGHMBP2	-3.3569291	0.001996	0.0213908	1.0051353	NCKAP1	-3.4247813	0.001996	0.0213908	1.0047325
TOM1L2	-3.3580663	0.001996	0.0213908	1.0088514	EPHB3	-3.4259746	0.001996	0.0213908	1.0282459
MYO7A	-3.3583471	0.001996	0.0213908	1.0101284	ST14	-3.4272798	0.001996	0.0213908	1.0047619
CUL7	-3.3593805	0.001996	0.0213908	1.0079362	CYP2R1	-3.427912	0.001996	0.0213908	1.0103852
PRTG	-3.3608143	0.001996	0.0213908	1.053438	NIPAL2	-3.42854	0.001996	0.0213908	1.0098553

Gene Symbol	Score	Feature P	FDR (BH)	Fold Change	Gene Symbol	Score	Feature P	FDR (BH)	Fold Change
STX17	-3.4320238	0.001996	0.0213908	1.0116728	DAB1	-3.5046938	0.001996	0.0213908	1.0122632
FUT8	-3.4332393	0.001996	0.0213908	1.0189531	TTC39B	-3.5080469	0.001996	0.0213908	1.0346441
JHDM1D	-3.433332	0.001996	0.0213908	1.0184459	RBM47	-3.5084746	0.001996	0.0213908	1.0059998
LOC81691	-3.436161	0.001996	0.0213908	1.009877	WLS	-3.5093585	0.001996	0.0213908	1.0439572
SAYSD1	-3.4364252	0.001996	0.0213908	1.0061139	C6orf72	-3.5105504	0.001996	0.0213908	1.0027272
TINF2	-3.4382591	0.001996	0.0213908	1.0101684	DSEL	-3.5106913	0.001996	0.0213908	1.0254749
VAMP5	-3.4388686	0.001996	0.0213908	1.0056878	ZBTB10	-3.5117	0.001996	0.0213908	1.0087346
FAM47E-STBD1	-3.4405535	0.001996	0.0213908	1.0276524	CYHR1	-3.5125762	0.001996	0.0213908	1.0062466
INF2	-3.4413192	0.001996	0.0213908	1.0052006	CCKBR	-3.5128711	0.001996	0.0213908	1.0228656
HSD11B1L	-3.4436989	0.001996	0.0213908	1.0073807	CDC14B	-3.51384	0.001996	0.0213908	1.0094194
NME5	-3.4452345	0.001996	0.0213908	1.0331207	H2AFY	-3.5142356	0.001996	0.0213908	1.0080209
MLL5	-3.4482785	0.001996	0.0213908	1.0065884	SNX17	-3.5149794	0.001996	0.0213908	1.0059082
TMEM80	-3.4497376	0.001996	0.0213908	1.0086381	SPATA20	-3.5150637	0.001996	0.0213908	1.0131558
RPS9	-3.4498131	0.001996	0.0213908	1.0035826	CLIP2	-3.516365	0.001996	0.0213908	1.0042276
DENND4A	-3.4502052	0.001996	0.0213908	1.0132327	GOLGA8A	-3.5168567	0.001996	0.0213908	1.0126643
RNF187	-3.4508186	0.001996	0.0213908	1.0062522	CAPN2	-3.5175619	0.001996	0.0213908	1.0124461
HSBP1	-3.451573	0.001996	0.0213908	1.0060587	KIAA0146	-3.5192788	0.001996	0.0213908	1.0021841
PPP4R1L	-3.4521662	0.001996	0.0213908	1.0131382	CCNDBP1	-3.5242069	0.001996	0.0213908	1.0145965
NDRG3	-3.4530424	0.001996	0.0213908	1.0078724	ARL6IP6	-3.5249227	0.001996	0.0213908	1.0013867
ODZ4	-3.4537373	0.001996	0.0213908	1.0341937	FGF17	-3.5266407	0.001996	0.0213908	1.0334074
MON2	-3.454692	0.001996	0.0213908	1.0041666	TPT1-AS1	-3.5297642	0.001996	0.0213908	1.0057221
LAMB1	-3.4553389	0.001996	0.0213908	1.0101904	GSS	-3.531607	0.001996	0.0213908	1.0073241
EML3	-3.4567052	0.001996	0.0213908	1.0074938	AP4B1	-3.5326122	0.001996	0.0213908	1.004934
CUX1	-3.459115	0.001996	0.0213908	1.007378	WNT5B	-3.536455	0.001996	0.0213908	1.0069757
SERPINA1	-3.4600795	0.001996	0.0213908	1.0166951	C1GALT1C1	-3.5371982	0.001996	0.0213908	1.0145394
VPS29	-3.4618326	0.001996	0.0213908	1.0050493	LETMD1	-3.5400477	0.001996	0.0213908	1.006717
PAN2	-3.4618712	0.001996	0.0213908	1.017042	FUZ	-3.5405137	0.001996	0.0213908	1.0051694
KIAA1549	-3.464444	0.001996	0.0213908	1.0054821	PCED1B	-3.5405164	0.001996	0.0213908	1.0197074
FAM169B	-3.4645234	0.001996	0.0213908	1.0111499	C9orf135	-3.5425708	0.001996	0.0213908	1.0142174
ZNF701	-3.4648227	0.001996	0.0213908	1.0195576	SCYL3	-3.5429902	0.001996	0.0213908	1.0157234
WDR5B	-3.4698535	0.001996	0.0213908	1.0186145	HMG20A	-3.5430581	0.001996	0.0213908	1.0055641
C5orf4	-3.470266	0.001996	0.0213908	1.0282686	ADH1C	-3.543306	0.001996	0.0213908	1.0150683
CBR4	-3.4721796	0.001996	0.0213908	1.0151569	WDR19	-3.54368	0.001996	0.0213908	1.0094517
ADAMTS19	-3.4748244	0.001996	0.0213908	1.0066361	TMEM14A	-3.5446665	0.001996	0.0213908	1.0049307
GAPDHP22	-3.4776355	0.001996	0.0213908	1.0165414	PLXNA2	-3.5460586	0.001996	0.0213908	1.0415034
PPIL3	-3.4779393	0.001996	0.0213908	1.0032736	CACNA1F	-3.5463312	0.001996	0.0213908	1.0074191
FAM227A	-3.4789296	0.001996	0.0213908	1.00947	HMGCL	-3.5480544	0.001996	0.0213908	1.015728
TCEANC	-3.4855335	0.001996	0.0213908	1.0183503	EPM2AIP1	-3.5489216	0.001996	0.0213908	1.0066097
PRMT8	-3.4881539	0.001996	0.0213908	1.008405	MSI2	-3.5502307	0.001996	0.0213908	1.0078125
WDR25	-3.488313	0.001996	0.0213908	1.0026035	TMCO6	-3.5502724	0.001996	0.0213908	1.0076147
FAM63A	-3.4892859	0.001996	0.0213908	1.0105742	CARD8	-3.5515616	0.001996	0.0213908	1.0048367
CD164	-3.4894912	0.001996	0.0213908	1.0040351	CASP8	-3.5515931	0.001996	0.0213908	1.0170939
HMGN4	-3.4915436	0.001996	0.0213908	1.0041574	GLT1D1	-3.5522131	0.001996	0.0213908	1.0130655
PIGV	-3.4939493	0.001996	0.0213908	1.0155769	COX20	-3.5525189	0.001996	0.0213908	1.0059219
CLUAP1	-3.4958293	0.001996	0.0213908	1.0193328	BMF	-3.5541386	0.001996	0.0213908	1.0054398
ZNF526	-3.4960085	0.001996	0.0213908	1.00343	OBFC1	-3.556273	0.001996	0.0213908	1.0089021
SMYD2	-3.4968435	0.001996	0.0213908	1.0196931	BTBD3	-3.5564703	0.001996	0.0213908	1.0039299
CER1	-3.4977608	0.001996	0.0213908	1.0671656	EFNB2	-3.5579419	0.001996	0.0213908	1.0257286
GREB1L	-3.4980406	0.001996	0.0213908	1.0830315	FLJ31958	-3.5600073	0.001996	0.0213908	1.0172117
NAPB	-3.5000963	0.001996	0.0213908	1.0068422	PBX3	-3.561133	0.001996	0.0213908	1.0041117

Gene Symbol	Score	Feature P	FDR (BH)	Fold Change	Gene Symbol	Score	Feature P	FDR (BH)	Fold Change
FAM174B	-3.5630108	0.001996	0.0213908	1.0077694	ZNF266	-3.6514642	0.001996	0.0213908	1.0081925
BBS5	-3.5665669	0.001996	0.0213908	1.028075	GNS	-3.6516967	0.001996	0.0213908	1.0054545
CORO2A	-3.5685825	0.001996	0.0213908	1.0126804	ZNF83	-3.6534669	0.001996	0.0213908	1.0134731
FAM40B	-3.5725459	0.001996	0.0213908	1.010779	RXFP2	-3.6536238	0.001996	0.0213908	1.0131402
H2AFY2	-3.5763688	0.001996	0.0213908	1.0161316	NTPCR	-3.6564916	0.001996	0.0213908	1.0046338
TMEM27	-3.5808719	0.001996	0.0213908	1.0389853	AP2M1	-3.6573847	0.001996	0.0213908	1.0030771
FSHR	-3.5831269	0.001996	0.0213908	1.0312597	KCNH8	-3.6580781	0.001996	0.0213908	1.0168729
TOR3A	-3.5834402	0.001996	0.0213908	1.0091833	MPP2	-3.6590372	0.001996	0.0213908	1.0109143
RNF170	-3.5860529	0.001996	0.0213908	1.016164	SULF1	-3.6613678	0.001996	0.0213908	1.0204168
DDAH2	-3.5889463	0.001996	0.0213908	1.0053749	JRKL	-3.6628382	0.001996	0.0213908	1.0234779
KIF13B	-3.5929555	0.001996	0.0213908	1.0099804	MCF2L	-3.6637114	0.001996	0.0213908	1.0045812
FLJ20464	-3.5932889	0.001996	0.0213908	1.0177033	GPR108	-3.6640178	0.001996	0.0213908	1.0069846
CMC1	-3.5953044	0.001996	0.0213908	1.014432	CPA2	-3.6644885	0.001996	0.0213908	1.0127785
TAS2R4	-3.5992193	0.001996	0.0213908	1.0053828	IRAK4	-3.6702107	0.001996	0.0213908	1.0107287
RPS6KA4	-3.6019081	0.001996	0.0213908	1.0033826	NUF2	-3.6711908	0.001996	0.0213908	1.0149679
EPB49	-3.6021114	0.001996	0.0213908	1.0121031	FAM149B1	-3.6722917	0.001996	0.0213908	1.0083628
TXNRD3	-3.6034669	0.001996	0.0213908	1.013879	CCDC97	-3.6813205	0.001996	0.0213908	1.0048807
CD3D	-3.6043862	0.001996	0.0213908	1.011259	SMAD1	-3.6817633	0.001996	0.0213908	1.0033864
ARRDC4	-3.6051417	0.001996	0.0213908	1.0325387	ZNF781	-3.682609	0.001996	0.0213908	1.0491767
COQ6	-3.6074984	0.001996	0.0213908	1.0058211	TBC1D8	-3.6841902	0.001996	0.0213908	1.0082548
ZNF302	-3.6085054	0.001996	0.0213908	1.0114556	KLHL14	-3.6848773	0.001996	0.0213908	1.0223273
PARP11	-3.6092454	0.001996	0.0213908	1.0131456	TSPAN18	-3.6865137	0.001996	0.0213908	1.0069857
GLYATL1	-3.6093386	0.001996	0.0213908	1.0200416	ACOT11	-3.6912764	0.001996	0.0213908	1.0058386
COG7	-3.6123279	0.001996	0.0213908	1.0035146	NPRL2	-3.6931924	0.001996	0.0213908	1.0039038
DKK1	-3.6144198	0.001996	0.0213908	1.117376	TBX22	-3.6954663	0.001996	0.0213908	1.0603389
CDK5RAP3	-3.6191008	0.001996	0.0213908	1.0131049	GEMIN8	-3.6967136	0.001996	0.0213908	1.0182168
C9orf100	-3.6198041	0.001996	0.0213908	1.009707	RNF146	-3.6981389	0.001996	0.0213908	1.0081627
MARCH8	-3.6202414	0.001996	0.0213908	1.0098048	CHMP1B	-3.6984895	0.001996	0.0213908	1.0066936
LAMTOR2	-3.6216267	0.001996	0.0213908	1.0084197	AKR1E2	-3.7005817	0.001996	0.0213908	1.0186384
TMEM154	-3.6223914	0.001996	0.0213908	1.0295177	AASDH	-3.701064	0.001996	0.0213908	1.0123603
TAF15	-3.6241078	0.001996	0.0213908	1.0027766	TDP1	-3.7013037	0.001996	0.0213908	1.0040399
PPM1K	-3.62448	0.001996	0.0213908	1.0108786	BABAM1	-3.7087144	0.001996	0.0213908	1.0025385
CDH26	-3.626739	0.001996	0.0213908	1.0142837	C12orf76	-3.7155201	0.001996	0.0213908	1.007975
RN5S198	-3.6271448	0.001996	0.0213908	1.0753471	CTSO	-3.7163529	0.001996	0.0213908	1.0396996
PLEKHH2	-3.6330678	0.001996	0.0213908	1.0154253	SNAP91	-3.7203997	0.001996	0.0213908	1.0166659
YAF2	-3.6343532	0.001996	0.0213908	1.0293302	ZNF362	-3.7216426	0.001996	0.0213908	1.0050662
GPR128	-3.6353931	0.001996	0.0213908	1.0315477	IFITM1	-3.7221018	0.001996	0.0213908	1.0083864
ST8SIA4	-3.6362368	0.001996	0.0213908	1.0807968	GABARAP	-3.7222254	0.001996	0.0213908	1.0030474
SLC31A1	-3.6391267	0.001996	0.0213908	1.0013187	ZNF397	-3.722303	0.001996	0.0213908	1.0108809
P2RY1	-3.6396251	0.001996	0.0213908	1.0287583	TGFB1	-3.7246451	0.001996	0.0213908	1.0325713
EIF2D	-3.641228	0.001996	0.0213908	1.0063056	C6orf70	-3.7274885	0.001996	0.0213908	1.0300914
DKK4	-3.6424639	0.001996	0.0213908	1.1402494	MFAP4	-3.727642	0.001996	0.0213908	1.0675755
LAPTM4B	-3.6436728	0.001996	0.0213908	1.0030074	GYS1	-3.7283372	0.001996	0.0213908	1.0066134
SLC35G3	-3.6450082	0.001996	0.0213908	1.0250785	POLD4	-3.7288354	0.001996	0.0213908	1.0092837
C6orf130	-3.6453225	0.001996	0.0213908	1.0099752	PDE5A	-3.7296228	0.001996	0.0213908	1.017088
OSGEPL1	-3.6453519	0.001996	0.0213908	1.0140529	ZBTB25	-3.7383274	0.001996	0.0213908	1.0080071
PPFIBP2	-3.6471754	0.001996	0.0213908	1.0197017	AMELY	-3.7393839	0.001996	0.0213908	1.0162733
IFT122	-3.647177	0.001996	0.0213908	1.0051325	IPCEF1	-3.7396787	0.001996	0.0213908	1.0209014
KIFAP3	-3.6503234	0.001996	0.0213908	1.0178647	SYNRG	-3.7413363	0.001996	0.0213908	1.0042159
SH3BP1	-3.6505449	0.001996	0.0213908	1.003076	KIAA1244	-3.744904	0.001996	0.0213908	1.0052774

Gene Symbol	Score	Feature P	FDR (BH)	Fold Change	Gene Symbol	Score	Feature P	FDR (BH)	Fold Change
TCHP	-3.7467614	0.001996	0.0213908	1.012025	VANGL2	-3.828137	0.001996	0.0213908	1.0026303
PLCL1	-3.7469805	0.001996	0.0213908	1.0110224	TCEAL4	-3.8354354	0.001996	0.0213908	1.013034
DUSP18	-3.7483447	0.001996	0.0213908	1.0149989	ADCK4	-3.8419324	0.001996	0.0213908	1.0058342
DMXL2	-3.7504189	0.001996	0.0213908	1.0158793	RNF213	-3.8477847	0.001996	0.0213908	1.006892
CD200	-3.7539584	0.001996	0.0213908	1.0060795	FIBP	-3.8478829	0.001996	0.0213908	1.0033703
LRTM2	-3.7554167	0.001996	0.0213908	1.0040184	SAMD3	-3.8482021	0.001996	0.0213908	1.0848147
ANKRD6	-3.7568204	0.001996	0.0213908	1.0118838	RGL3	-3.8490334	0.001996	0.0213908	1.0114881
HDDC3	-3.7572219	0.001996	0.0213908	1.0081655	DHRS1	-3.8492023	0.001996	0.0213908	1.0108351
SHISA2	-3.7602361	0.001996	0.0213908	1.0382879	RGP1	-3.8510349	0.001996	0.0213908	1.00421
NFYA	**-3.7607691**	**0.001996**	**0.0213908**	**1.0052176**	AMPD3	-3.852034	0.001996	0.0213908	1.0064018
MAN2A2	-3.7620979	0.001996	0.0213908	1.0170061	CHIC2	-3.8543769	0.001996	0.0213908	1.0081031
UACA	-3.7649786	0.001996	0.0213908	1.0126765	VWF	-3.8583429	0.001996	0.0213908	1.0380063
GATA6	-3.7655198	0.001996	0.0213908	1.0357236	SLC35F1	-3.8591883	0.001996	0.0213908	1.0105496
ZIC1	-3.7675192	0.001996	0.0213908	1.0359554	PLEKHG3	-3.8609771	0.001996	0.0213908	1.0061981
RAPGEF3	-3.7684929	0.001996	0.0213908	1.0173433	ZNF280D	-3.8630386	0.001996	0.0213908	1.0116424
RYR1	-3.7689069	0.001996	0.0213908	1.006022	BIVM	-3.8658953	0.001996	0.0213908	1.0153586
SOX17	-3.7730084	0.001996	0.0213908	1.0248636	GTSE1	-3.8678315	0.001996	0.0213908	1.0069342
PSD4	-3.7751967	0.001996	0.0213908	1.0241871	ARAP3	-3.8704644	0.001996	0.0213908	1.0039851
NCAM1	-3.7764613	0.001996	0.0213908	1.0131579	CDH12	-3.8739153	0.001996	0.0213908	1.0381318
HEATR5B	-3.7778315	0.001996	0.0213908	1.0071029	ZFYVE1	-3.8761386	0.001996	0.0213908	1.0059303
BBS12	-3.7795579	0.001996	0.0213908	1.0116658	PTP4A3	-3.8766743	0.001996	0.0213908	1.0108482
TTC30B	-3.7819172	0.001996	0.0213908	1.0347673	FLOT1	-3.8830945	0.001996	0.0213908	1.0076006
DSP	-3.7845502	0.001996	0.0213908	1.0132054	CAMK2D	-3.8844203	0.001996	0.0213908	1.0157038
GOLGA1	-3.7848833	0.001996	0.0213908	1.0104361	ABHD12B	-3.8886528	0.001996	0.0213908	1.0579268
OAT	-3.7862969	0.001996	0.0213908	1.0052739	RPP25	-3.8904769	0.001996	0.0213908	1.0048909
FLRT3	-3.7878811	0.001996	0.0213908	1.0638391	LIN28B	-3.8926448	0.001996	0.0213908	1.0029361
STAT6	-3.7910116	0.001996	0.0213908	1.0126162	FOXRED1	-3.899359	0.001996	0.0213908	1.003062
FANCF	-3.7983556	0.001996	0.0213908	1.0127243	ALDH3A2	-3.8999487	0.001996	0.0213908	1.0130852
C3orf75	-3.7991276	0.001996	0.0213908	1.0112326	GSTT2	-3.9001452	0.001996	0.0213908	1.0210277
GRK5	-3.7995309	0.001996	0.0213908	1.0144377	BTN2A3P	-3.9004349	0.001996	0.0213908	1.0108685
FER1L5	-3.8008021	0.001996	0.0213908	1.0080788	AF090940	-3.9011068	0.001996	0.0213908	1.0173539
MYL6B	-3.8008924	0.001996	0.0213908	1.0032176	DDTL	-3.901626	0.001996	0.0213908	1.0045583
CRAT	-3.8030638	0.001996	0.0213908	1.0107487	CHRNA3	-3.9032305	0.001996	0.0213908	1.0092981
TCF12	-3.8058689	0.001996	0.0213908	1.0018644	THNSL2	-3.9045931	0.001996	0.0213908	1.0209475
NMRK1	-3.805998	0.001996	0.0213908	1.0335893	ZNF518B	-3.9048326	0.001996	0.0213908	1.0137359
VENTX	-3.8061339	0.001996	0.0213908	1.0124803	HAO2	-3.9084893	0.001996	0.0213908	1.0167264
SLC27A3	-3.8067929	0.001996	0.0213908	1.0110517	OR5T1	-3.9088454	0.001996	0.0213908	1.0167345
RBM5	-3.80733	0.001996	0.0213908	1.0135066	RHOH	-3.9105472	0.001996	0.0213908	1.0417874
SCNN1A	-3.8075711	0.001996	0.0213908	1.0046135	FSCB	-3.9116076	0.001996	0.0213908	1.020745
FAM214A	-3.8081791	0.001996	0.0213908	1.0223398	PBX1	-3.9139873	0.001996	0.0213908	1.0049962
FAM160B2	-3.8089611	0.001996	0.0213908	1.0161519	SEPT7L	-3.9140327	0.001996	0.0213908	1.0044566
MAPK3	-3.8095882	0.001996	0.0213908	1.0029953	ACBD5	-3.9173562	0.001996	0.0213908	1.0099406
TRAF5	-3.8105225	0.001996	0.0213908	1.0091211	ACTR3BP2	-3.9260773	0.001996	0.0213908	1.0135808
SERINC3	-3.8147077	0.001996	0.0213908	1.0048102	PIK3CA	-3.9300319	0.001996	0.0213908	1.007026
ELF2	-3.8173073	0.001996	0.0213908	1.0092537	HPS1	-3.9338611	0.001996	0.0213908	1.0064045
RPUSD3	-3.8173445	0.001996	0.0213908	1.0070738	LOH12CR1	-3.9341358	0.001996	0.0213908	1.010129
MMP2	-3.81809	0.001996	0.0213908	1.0042262	H6PD	-3.9355379	0.001996	0.0213908	1.0147523
MTHFSD	-3.8229865	0.001996	0.0213908	1.0138261	ARRB1	-3.9388304	0.001996	0.0213908	1.0351579
GSTK1	-3.8245487	0.001996	0.0213908	1.0109533	TPCN1	-3.9392111	0.001996	0.0213908	1.0098157
RN5S229	-3.8253458	0.001996	0.0213908	1.0379438	GLT8D1	-3.9413442	0.001996	0.0213908	1.0020783

Gene Symbol	Score	Feature P	FDR (BH)	Fold Change	Gene Symbol	Score	Feature P	FDR (BH)	Fold Change
ZNF76	-4.1275106	0.001996	0.0213908	1.0097682	RAD50	-4.2580521	0.001996	0.0213908	1.0096929
PLA2G2A	-4.1301084	0.001996	0.0213908	1.0319497	CSAD	-4.2598227	0.001996	0.0213908	1.0143814
NECAP1	-4.1345941	0.001996	0.0213908	1.0041567	HSD17B11	-4.2650749	0.001996	0.0213908	1.0057955
RNF19A	-4.1365048	0.001996	0.0213908	1.0261206	F2RL1	-4.2661322	0.001996	0.0213908	1.0116072
PLEKHA1	-4.1386905	0.001996	0.0213908	1.0067486	PEX11B	-4.2667174	0.001996	0.0213908	1.0099989
YIPF1	-4.1414098	0.001996	0.0213908	1.0058386	PIK3C2B	-4.2689912	0.001996	0.0213908	1.0109747
ARHGEF25	-4.1422086	0.001996	0.0213908	1.0057391	RNASEL	-4.2717031	0.001996	0.0213908	1.0258341
LRFN3	-4.1422661	0.001996	0.0213908	1.0078822	CCDC167	-4.2744557	0.001996	0.0213908	1.0176511
IL17RD	-4.1481659	0.001996	0.0213908	1.0227204	EHHADH	-4.2755141	0.001996	0.0213908	1.0271793
EXOC1	-4.1578603	0.001996	0.0213908	1.0074659	PARP6	-4.2765435	0.001996	0.0213908	1.0112319
MAST4	-4.1592251	0.001996	0.0213908	1.0054622	MLLT6	-4.2861125	0.001996	0.0213908	1.0171972
ANKRD36	-4.1614859	0.001996	0.0213908	1.0090916	C4orf3	-4.2903158	0.001996	0.0213908	1.0097699
FOXA2	-4.1622128	0.001996	0.0213908	1.0648303	CHN2	-4.2922966	0.001996	0.0213908	1.005724
ADRBK1	-4.1657873	0.001996	0.0213908	1.0082816	PIK3R1	-4.2925496	0.001996	0.0213908	1.0272621
CTNND1	-4.1696106	0.001996	0.0213908	1.004739	ZCCHC11	-4.2930727	0.001996	0.0213908	1.0066067
POLR3GL	-4.1720143	0.001996	0.0213908	1.0156923	MAGEF1	-4.2964968	0.001996	0.0213908	1.0066206
TLE3	-4.1720804	0.001996	0.0213908	1.0118599	DERA	-4.2995154	0.001996	0.0213908	1.0177412
GLIPR1L2	-4.1730271	0.001996	0.0213908	1.029033	FBXL14	-4.3039021	0.001996	0.0213908	1.0081089
ZBTB34	-4.1750669	0.001996	0.0213908	1.0024087	MYO3A	-4.3076049	0.001996	0.0213908	1.0139544
CPEB2	-4.1751991	0.001996	0.0213908	1.0093165	FGF8	-4.3078954	0.001996	0.0213908	1.040251
C12orf66	-4.1802243	0.001996	0.0213908	1.0172114	RIN2	-4.3142768	0.001996	0.0213908	1.0140724
KIAA1407	-4.1940433	0.001996	0.0213908	1.0292592	RIMKLB	-4.314412	0.001996	0.0213908	1.0063584
SLC24A6	-4.199591	0.001996	0.0213908	1.0081056	DOPEY1	-4.3148712	0.001996	0.0213908	1.0122388
DET1	-4.2020361	0.001996	0.0213908	1.016903	ZMIZ1	-4.3159165	0.001996	0.0213908	1.0034606
DHFRL1	-4.2052614	0.001996	0.0213908	1.010564	MFF	-4.319461	0.001996	0.0213908	1.005103
SLC35A5	-4.2055955	0.001996	0.0213908	1.0095388	ACOT4	-4.3202738	0.001996	0.0213908	1.0150331
SEPT14	-4.2085983	0.001996	0.0213908	1.0057511	HDAC11	-4.3221026	0.001996	0.0213908	1.0159161
MKRN1	-4.2110374	0.001996	0.0213908	1.0021029	CYP27A1	-4.3239144	0.001996	0.0213908	1.0197955
PRPF40B	-4.2146668	0.001996	0.0213908	1.0113982	PGK1	-4.3355583	0.001996	0.0213908	1.0011262
RBKS	-4.215676	0.001996	0.0213908	1.0073784	TMEM241	-4.3401554	0.001996	0.0213908	1.0052816
MMAA	-4.2164076	0.001996	0.0213908	1.0277209	NRSN2	-4.3466754	0.001996	0.0213908	1.0076329
PGPEP1	-4.2190337	0.001996	0.0213908	1.0082453	PAG1	-4.3472298	0.001996	0.0213908	1.027159
CHD2	-4.2216386	0.001996	0.0213908	1.0029037	XPC	-4.3480475	0.001996	0.0213908	1.01028
ANKRD26	-4.2258761	0.001996	0.0213908	1.0132955	PIGQ	-4.3483092	0.001996	0.0213908	1.0098073
PEX5	-4.2263666	0.001996	0.0213908	1.0044504	NBPF11	-4.3543062	0.001996	0.0213908	1.0033114
PCDH10	-4.2274743	0.001996	0.0213908	1.0813966	DDX60L	-4.3610767	0.001996	0.0213908	1.0312765
PLEKHG6	-4.2288606	0.001996	0.0213908	1.0077318	MGEA5	-4.3734688	0.001996	0.0213908	1.0042523
AGAP9	-4.2329822	0.001996	0.0213908	1.0073348	KEL	-4.3740865	0.001996	0.0213908	1.0229765
UFC1	-4.2344182	0.001996	0.0213908	1.0055724	ENPP2	-4.3753976	0.001996	0.0213908	1.0073459
STK19	-4.236345	0.001996	0.0213908	1.0051712	CYFIP1	-4.3805123	0.001996	0.0213908	1.0042517
FANCC	-4.2419509	0.001996	0.0213908	1.0144036	RNF43	-4.3819038	0.001996	0.0213908	1.0341472
HP1BP3	-4.242069	0.001996	0.0213908	1.0063379	TTC9	-4.383179	0.001996	0.0213908	1.0029936
AK3	-4.2425463	0.001996	0.0213908	1.002064	EPHA4	-4.3839431	0.001996	0.0213908	1.0412992
WASH1	-4.2436681	0.001996	0.0213908	1.0054604	ACOX3	-4.3858699	0.001996	0.0213908	1.010467
CSTL1	-4.243723	0.001996	0.0213908	1.0417671	SLC43A2	-4.3970521	0.001996	0.0213908	1.0168033
SVIL	-4.2454042	0.001996	0.0213908	1.0174664	COQ2	-4.3977681	0.001996	0.0213908	1.0024483
TMTC1	-4.2457102	0.001996	0.0213908	1.0133636	ZFPL1	-4.3980012	0.001996	0.0213908	1.0082802
C14orf101	-4.2469018	0.001996	0.0213908	1.0090815	SLC25A27	-4.4008207	0.001996	0.0213908	1.0231117
STAT5A	-4.2558478	0.001996	0.0213908	1.0185109	RPRM	-4.4008393	0.001996	0.0213908	1.0169744
MXRA5	-4.2558665	0.001996	0.0213908	1.0149159	ZADH2	-4.410524	0.001996	0.0213908	1.0197783

Gene Symbol	Score	Feature P	FDR (BH)	Fold Change	Gene Symbol	Score	Feature P	FDR (BH)	Fold Change
CCDC15	-4.410826	0.001996	0.0213908	1.0159557	ZNF611	-4.5420855	0.001996	0.0213908	1.0135181
PPP1CB	-4.4115159	0.001996	0.0213908	1.0031775	TOM1	-4.5472979	0.001996	0.0213908	1.0055809
HCP5	-4.4127236	0.001996	0.0213908	1.0101988	ADAM8	-4.548146	0.001996	0.0213908	1.0093296
BTN3A2	-4.4152334	0.001996	0.0213908	1.0380931	TLK2	-4.5491405	0.001996	0.0213908	1.0048973
ATP12A	-4.4236603	0.001996	0.0213908	1.0244473	BANF2	-4.5524944	0.001996	0.0213908	1.0119579
PDE1B	-4.4289423	0.001996	0.0213908	1.0318169	EXOC7	-4.5535491	0.001996	0.0213908	1.0073786
TPP1	-4.4349352	0.001996	0.0213908	1.0113121	COG4	-4.5556137	0.001996	0.0213908	1.0089371
PERP	-4.4351893	0.001996	0.0213908	1.0114704	APCDD1	-4.5568911	0.001996	0.0213908	1.0528608
SLC29A4	-4.4353636	0.001996	0.0213908	1.0093976	COQ9	-4.5672914	0.001996	0.0213908	1.0020409
CDYL2	-4.4364522	0.001996	0.0213908	1.0114691	RAD52	-4.5703486	0.001996	0.0213908	1.011019
DHPS	-4.4395815	0.001996	0.0213908	1.0071615	AB266802	-4.572911	0.001996	0.0213908	1.1868903
SLC9A8	-4.4431207	0.001996	0.0213908	1.0111979	TAS2R31	-4.5729532	0.001996	0.0213908	1.0200014
NAV2	-4.4451576	0.001996	0.0213908	1.0052175	MCC	-4.5755962	0.001996	0.0213908	1.0260686
KCNH5	-4.4470893	0.001996	0.0213908	1.0342819	GAL	-4.578279	0.001996	0.0213908	1.0331207
MYSM1	-4.4471005	0.001996	0.0213908	1.0072839	SPG11	-4.5829609	0.001996	0.0213908	1.0124861
ZNF167	-4.4497159	0.001996	0.0213908	1.0174622	NUDT12	-4.5837822	0.001996	0.0213908	1.015282
MUM1	-4.4525264	0.001996	0.0213908	1.0122598	ETFB	-4.5840825	0.001996	0.0213908	1.0064974
ARSG	-4.454671	0.001996	0.0213908	1.0153621	IFT172	-4.5842867	0.001996	0.0213908	1.0096257
SLC24A1	-4.4577081	0.001996	0.0213908	1.0150563	ZNF238	-4.5846562	0.001996	0.0213908	1.0082798
KIAA1161	-4.4602441	0.001996	0.0213908	1.0350728	CTH	-4.5866803	0.001996	0.0213908	1.0123518
AKR1A1	-4.4619172	0.001996	0.0213908	1.0041657	ZSCAN16	-4.5881065	0.001996	0.0213908	1.0062076
WDR27	-4.4634521	0.001996	0.0213908	1.0165749	MUTYH	-4.5900023	0.001996	0.0213908	1.0080144
CDS2	-4.4641023	0.001996	0.0213908	1.0021218	RHOU	-4.5925558	0.001996	0.0213908	1.0382546
CGGBP1	-4.4646965	0.001996	0.0213908	1.0068901	SAMD15	-4.5937644	0.001996	0.0213908	1.0208425
TAS2R1	-4.464879	0.001996	0.0213908	1.0167421	CTNNBIP1	-4.5978583	0.001996	0.0213908	1.0023033
ZNF334	-4.4654058	0.001996	0.0213908	1.0071571	CDH10	-4.5983671	0.001996	0.0213908	1.061313
WDTC1	-4.4656256	0.001996	0.0213908	1.0155273	TCEANC2	-4.6017699	0.001996	0.0213908	1.0112956
KDM6B	-4.4684643	0.001996	0.0213908	1.0169648	FFAR2	-4.6052002	0.001996	0.0213908	1.0106984
C3orf58	-4.4806813	0.001996	0.0213908	1.0318436	PCGF5	-4.6068659	0.001996	0.0213908	1.0183912
GPR39	-4.4807592	0.001996	0.0213908	1.0505816	SLC22A3	-4.6100122	0.001996	0.0213908	1.0491974
MED7	-4.4809873	0.001996	0.0213908	1.0113547	FN1	-4.613827	0.001996	0.0213908	1.0250147
ZNF123P	-4.4846274	0.001996	0.0213908	1.0095042	ZNF90	-4.6146033	0.001996	0.0213908	1.004447
VPS28	-4.485019	0.001996	0.0213908	1.0124571	BHLHB9	-4.6170955	0.001996	0.0213908	1.0115701
PCDHB14	-4.4853072	0.001996	0.0213908	1.018398	ZNF763	-4.619002	0.001996	0.0213908	1.0193611
SMG6	-4.4855426	0.001996	0.0213908	1.0053881	TCF7	-4.6209417	0.001996	0.0213908	1.0039862
MOBP	-4.4903434	0.001996	0.0213908	1.0463712	ZDHHC21	-4.6234451	0.001996	0.0213908	1.0101055
GBAP1	-4.4905845	0.001996	0.0213908	1.0326524	TRAPPC3	-4.6255686	0.001996	0.0213908	1.0079916
KCNE3	-4.4945046	0.001996	0.0213908	1.0220819	MAML3	-4.6263754	0.001996	0.0213908	1.0330292
AK7	-4.4966565	0.001996	0.0213908	1.0203518	PREX2	-4.6290284	0.001996	0.0213908	1.0112581
NDUFB5	-4.4990869	0.001996	0.0213908	1.0042705	EPB41L4A	-4.6367608	0.001996	0.0213908	1.027459
COL4A5	-4.50334	0.001996	0.0213908	1.0155673	SEC22C	-4.6416223	0.001996	0.0213908	1.0072459
ZNF236	-4.5042274	0.001996	0.0213908	1.0086376	RIC3	-4.6437483	0.001996	0.0213908	1.0092245
RNASE6	-4.5102186	0.001996	0.0213908	1.0297413	EML2	-4.6546666	0.001996	0.0213908	1.0134141
AKAP3	-4.5111888	0.001996	0.0213908	1.0226585	CST2	-4.6626813	0.001996	0.0213908	1.0574353
C7orf26	-4.5192795	0.001996	0.0213908	1.0035594	AGBL2	-4.6642187	0.001996	0.0213908	1.0135485
FRZB	-4.5236453	0.001996	0.0213908	1.0587343	ADAMTS3	-4.6672425	0.001996	0.0213908	1.0096122
PPAPDC2	-4.5249515	0.001996	0.0213908	1.0147918	LZTR1	-4.6679547	0.001996	0.0213908	1.0100443
STK36	-4.5253276	0.001996	0.0213908	1.0104678	TADA2A	-4.6692588	0.001996	0.0213908	1.0131856
PPP1R21	-4.5280386	0.001996	0.0213908	1.0117202	ARSE	-4.6694221	0.001996	0.0213908	1.0341354
PLCD1	-4.5363611	0.001996	0.0213908	1.009698	RFFL	-4.6722472	0.001996	0.0213908	1.0057515

Gene Symbol	Score	Feature P	FDR (BH)	Fold Change	Gene Symbol	Score	Feature P	FDR (BH)	Fold Change
SPG21	-4.6772564	0.001996	0.0213908	1.0022904	HOOK2	-4.8542256	0.001996	0.0213908	1.0038012
RMND5B	-4.682072	0.001996	0.0213908	1.0105635	HAS2	-4.8562143	0.001996	0.0213908	1.1180481
QARS	-4.6958081	0.001996	0.0213908	1.0035506	PROCA1	-4.86176	0.001996	0.0213908	1.005907
FLJ39653	-4.6978549	0.001996	0.0213908	1.0095763	EOMES	-4.8646707	0.001996	0.0213908	1.1073978
ZFP30	-4.6988054	0.001996	0.0213908	1.0129918	ADAD1	-4.8697401	0.001996	0.0213908	1.0290666
CXCR4	-4.7099569	0.001996	0.0213908	1.0517751	LYRM5	-4.8706263	0.001996	0.0213908	1.0172812
ARL2BP	-4.7107309	0.001996	0.0213908	1.0052526	AK097033	-4.8761179	0.001996	0.0213908	1.0207193
C11orf70	-4.7113681	0.001996	0.0213908	1.0182335	USP40	-4.8761749	0.001996	0.0213908	1.0153922
SYNJ1	-4.719678	0.001996	0.0213908	1.0206852	PPP1R3E	-4.8923137	0.001996	0.0213908	1.012851
METTL23	-4.7238109	0.001996	0.0213908	1.0099518	LGR5	-4.8969784	0.001996	0.0213908	1.0873193
FAN1	-4.7243002	0.001996	0.0213908	1.0042726	DUSP19	-4.9053515	0.001996	0.0213908	1.0440184
COQ5	-4.732583	0.001996	0.0213908	1.0063067	USP53	-4.9073962	0.001996	0.0213908	1.0108065
MYCBPAP	-4.7327471	0.001996	0.0213908	1.0214738	ALDH16A1	-4.9077391	0.001996	0.0213908	1.0042218
CARD6	-4.7395245	0.001996	0.0213908	1.0340172	ZNF329	-4.9113262	0.001996	0.0213908	1.0084776
DENND5A	-4.7403277	0.001996	0.0213908	1.0062076	KDM1B	-4.9139594	0.001996	0.0213908	1.0073021
SRR	-4.7434937	0.001996	0.0213908	1.0105849	TMEM116	-4.9150359	0.001996	0.0213908	1.0142249
CPNE4	-4.743621	0.001996	0.0213908	1.0106351	FGF20	-4.9201953	0.001996	0.0213908	1.0069283
B9D1	-4.7485476	0.001996	0.0213908	1.0108993	ZNF514	-4.9283002	0.001996	0.0213908	1.0188606
THBS2	-4.7605123	0.001996	0.0213908	1.0223397	TSPAN14	-4.9285999	0.001996	0.0213908	1.0086533
OAS3	-4.7618795	0.001996	0.0213908	1.0096341	IGF2R	-4.932157	0.001996	0.0213908	1.0040169
NIT1	-4.7652354	0.001996	0.0213908	1.0102736	CEACAM1	-4.9493116	0.001996	0.0213908	1.0096549
NUDT13	-4.7729971	0.001996	0.0213908	1.0286674	C1QTNF6	-4.9643211	0.001996	0.0213908	1.0185442
AKIP1	-4.7748749	0.001996	0.0213908	1.0093839	ENPP6	-4.9694112	0.001996	0.0213908	1.0182297
PI4KA	-4.7787739	0.001996	0.0213908	1.007004	PIGP	-4.9702118	0.001996	0.0213908	1.0210599
MDM1	-4.7819751	0.001996	0.0213908	1.0185371	HNRPLL	-4.9713921	0.001996	0.0213908	1.0060383
C14orf133	-4.7836994	0.001996	0.0213908	1.0096325	NDST2	-4.9741271	0.001996	0.0213908	1.0057143
STAP2	-4.7881175	0.001996	0.0213908	1.017974	PCDHB10	-4.9756101	0.001996	0.0213908	1.0254032
KIAA1383	-4.7889435	0.001996	0.0213908	1.0154163	NPRL3	-4.984006	0.001996	0.0213908	1.0066185
KIF5B	-4.7901227	0.001996	0.0213908	1.0026333	PPL	-4.9863059	0.001996	0.0213908	1.0037997
ARFGAP2	-4.7915214	0.001996	0.0213908	1.0112265	ZNF154	-4.9889304	0.001996	0.0213908	1.015638
C2orf42	-4.7954687	0.001996	0.0213908	1.0104258	KAL1	-5.0049557	0.001996	0.0213908	1.0107243
TRIM38	-4.7985559	0.001996	0.0213908	1.0675249	PNLIPRP3	-5.0083317	0.001996	0.0213908	1.0105715
SERPINB1	-4.8079699	0.001996	0.0213908	1.0183986	ZNF18	-5.0101324	0.001996	0.0213908	1.0119015
SMPD1	-4.8080799	0.001996	0.0213908	1.0239752	UFL1	-5.0219823	0.001996	0.0213908	1.0174858
KRT8	-4.812484	0.001996	0.0213908	1.0060244	AGAP8	-5.0341035	0.001996	0.0213908	1.007287
NEK9	-4.8145222	0.001996	0.0213908	1.0120651	HHLA1	-5.0358568	0.001996	0.0213908	1.0536203
RANBP10	-4.8170304	0.001996	0.0213908	1.004851	ZFYVE19	-5.0439232	0.001996	0.0213908	1.0093951
CREBL2	-4.8190746	0.001996	0.0213908	1.0086933	LOC729737	-5.0444232	0.001996	0.0213908	1.0091
GMPR	-4.8237568	0.001996	0.0213908	1.0911464	CDA	-5.0461915	0.001996	0.0213908	1.0631876
ZNF319	-4.8255686	0.001996	0.0213908	1.0111082	SAMD13	-5.0574514	0.001996	0.0213908	1.0295758
ARHGAP19	-4.8273328	0.001996	0.0213908	1.0062989	RIMBP2	-5.0624247	0.001996	0.0213908	1.0322536
TMEM62	-4.8277828	0.001996	0.0213908	1.0303286	PPP2R1A	-5.0629489	0.001996	0.0213908	1.0027174
COPS7A	-4.8292638	0.001996	0.0213908	1.0088004	TCFL5	-5.0659282	0.001996	0.0213908	1.0035371
CEP95	-4.8293639	0.001996	0.0213908	1.0073662	SDCCAG8	-5.0660175	0.001996	0.0213908	1.0133023
C12orf32	-4.8314607	0.001996	0.0213908	1.004152	RFESD	-5.0690527	0.001996	0.0213908	1.0425203
PCDHB15	-4.8330505	0.001996	0.0213908	1.0176964	YTHDC1	-5.0694397	0.001996	0.0213908	1.0084776
ZC3H6	-4.8370978	0.001996	0.0213908	1.0343041	GPRASP2	-5.0740356	0.001996	0.0213908	1.0133355
MSTO1	-4.8373797	0.001996	0.0213908	1.0046893	GPCPD1	-5.074161	0.001996	0.0213908	1.0306706
RBP1	-4.8423284	0.001996	0.0213908	1.0191574	SYT4	-5.0787285	0.001996	0.0213908	1.0143987
GEMIN8P4	-4.8512124	0.001996	0.0213908	1.0178483	CYP1B1	-5.0860927	0.001996	0.0213908	1.043076

Gene Symbol	Score	Feature P	FDR (BH)	Fold Change	Gene Symbol	Score	Feature P	FDR (BH)	Fold Change
TMEM136	-5.0921366	0.001996	0.0213908	1.0110164	ZFHX4	-5.3788923	0.001996	0.0213908	1.0345725
FPGT	-5.0984717	0.001996	0.0213908	1.028887	KLHDC1	-5.3844307	0.001996	0.0213908	1.0380547
ABHD11	-5.09922	0.001996	0.0213908	1.0118984	FAM160A2	-5.3981968	0.001996	0.0213908	1.0080945
DRG2	-5.1000453	0.001996	0.0213908	1.0035537	APOBEC3B	-5.4042199	0.001996	0.0213908	1.0223258
GPSM2	-5.1078541	0.001996	0.0213908	1.0146413	REC8	-5.4107682	0.001996	0.0213908	1.0082783
PEX6	-5.1090655	0.001996	0.0213908	1.0093685	PNPLA4	-5.4171241	0.001996	0.0213908	1.0139772
MCMDC2	-5.1092302	0.001996	0.0213908	1.0317315	HSD17B8	-5.4174196	0.001996	0.0213908	1.0161502
FAHD2B	-5.1099485	0.001996	0.0213908	1.0056999	ADCY5	-5.4180792	0.001996	0.0213908	1.0121851
GUSB	-5.1180958	0.001996	0.0213908	1.0121485	MID2	-5.4310826	0.001996	0.0213908	1.0217825
TAF7	-5.1269016	0.001996	0.0213908	1.00697	AHSA2	-5.4399824	0.001996	0.0213908	1.0151004
TMEM218	-5.1413151	0.001996	0.0213908	1.0196274	NBR1	-5.4407052	0.001996	0.0213908	1.0121747
TBC1D2	-5.1532316	0.001996	0.0213908	1.0117418	HNRNPH2	-5.444488	0.001996	0.0213908	1.0046656
CLSTN3	-5.1645324	0.001996	0.0213908	1.0117293	ELMO2	-5.4565653	0.001996	0.0213908	1.0081857
PTPN6	-5.1679292	0.001996	0.0213908	1.0109596	HS1BP3	-5.4882551	0.001996	0.0213908	1.0042022
VPS33B	-5.1684103	0.001996	0.0213908	1.0104607	SPATA6	-5.4911694	0.001996	0.0213908	1.0125199
PROX1	-5.1725436	0.001996	0.0213908	1.0395958	H1F0	-5.4952313	0.001996	0.0213908	1.0122601
EFHC1	-5.174051	0.001996	0.0213908	1.0105422	OPRK1	-5.4999066	0.001996	0.0213908	1.019502
PARP14	-5.17558	0.001996	0.0213908	1.0105194	SATB2	-5.5016916	0.001996	0.0213908	1.0286901
MAGI2	-5.1762763	0.001996	0.0213908	1.010886	CAPN1	-5.5102841	0.001996	0.0213908	1.0058476
MCEE	-5.1848197	0.001996	0.0213908	1.0100899	AP1G2	-5.5104565	0.001996	0.0213908	1.0130205
SENP7	-5.1850107	0.001996	0.0213908	1.0275093	R3HDM2	-5.5115249	0.001996	0.0213908	1.016695
MKNK1	-5.1918004	0.001996	0.0213908	1.0091249	CPXM1	-5.5127324	0.001996	0.0213908	1.0182301
FANCG	-5.1942241	0.001996	0.0213908	1.0081454	SIAE	-5.5218902	0.001996	0.0213908	1.0172075
RNF135	-5.2135789	0.001996	0.0213908	1.0125179	PGBD4	-5.5267291	0.001996	0.0213908	1.0141141
TBC1D9B	-5.2220827	0.001996	0.0213908	1.0015709	TLR5	-5.5323434	0.001996	0.0213908	1.0103357
PMF1	-5.2295818	0.001996	0.0213908	1.0009549	SRD5A3	-5.5335277	0.001996	0.0213908	1.0117739
PIGM	-5.233058	0.001996	0.0213908	1.011047	PCDHB1	-5.5359425	0.001996	0.0213908	1.0605676
CCNI	-5.2354383	0.001996	0.0213908	1.0022692	C4orf33	-5.5481222	0.001996	0.0213908	1.0207379
NS3BP	-5.2359986	0.001996	0.0213908	1.0073605	GRM4	-5.5481246	0.001996	0.0213908	1.0311708
COMMD8	-5.2390438	0.001996	0.0213908	1.0144937	APOBEC3G	-5.5547258	0.001996	0.0213908	1.0614988
CREB3L4	-5.2413853	0.001996	0.0213908	1.0170349	KATNAL1	-5.5611615	0.001996	0.0213908	1.0112428
BNIP3P1	-5.2451768	0.001996	0.0213908	1.0392967	SUN2	-5.5632299	0.001996	0.0213908	1.0134869
ITPKB	-5.248981	0.001996	0.0213908	1.0229628	ZNF518A	-5.5789652	0.001996	0.0213908	1.0114684
NMRAL1	-5.2492408	0.001996	0.0213908	1.0072554	PPP1R16A	-5.58915	0.001996	0.0213908	1.0082481
CAMK1D	-5.257156	0.001996	0.0213908	1.0151285	STRA6	-5.5972477	0.001996	0.0213908	1.015022
LRRTM1	-5.258899	0.001996	0.0213908	1.025266	CPEB4	-5.6005874	0.001996	0.0213908	1.010418
FBXW4P1	-5.2633575	0.001996	0.0213908	1.0064698	LPAR6	-5.6036369	0.001996	0.0213908	1.0715982
C14orf93	-5.2672501	0.001996	0.0213908	1.0073117	ARGLU1	-5.6050067	0.001996	0.0213908	1.0075909
SERAC1	-5.2818615	0.001996	0.0213908	1.0173053	HERC2P4	-5.6124903	0.001996	0.0213908	1.0080545
AKD1	-5.2820657	0.001996	0.0213908	1.0085687	C5	-5.6307231	0.001996	0.0213908	1.1057837
DCAF12	-5.2995159	0.001996	0.0213908	1.0035627	DCTN4	-5.6349525	0.001996	0.0213908	1.0055283
GRAP	-5.302618	0.001996	0.0213908	1.0186508	ARHGAP26	-5.6746948	0.001996	0.0213908	1.0083889
NBPF12	-5.3140816	0.001996	0.0213908	1.0053077	BTN3A1	-5.6883209	0.001996	0.0213908	1.027363
TNC	-5.3218874	0.001996	0.0213908	1.0410567	RCAN3	-5.6923149	0.001996	0.0213908	1.0057244
C20orf194	-5.3248367	0.001996	0.0213908	1.0114502	DOPEY2	-5.712081	0.001996	0.0213908	1.0178907
ZNF638	-5.3304555	0.001996	0.0213908	1.0073891	GUSBP11	-5.7148005	0.001996	0.0213908	1.006042
HBP1	-5.3654116	0.001996	0.0213908	1.0118801	RCBTB2	-5.7166644	0.001996	0.0213908	1.0112435
PQLC3	-5.3750308	0.001996	0.0213908	1.0069816	DKFZP686I15217	-5.7266578	0.001996	0.0213908	1.0109473
N4BP2L2	-5.3784205	0.001996	0.0213908	1.0033527	PMP22	-5.7390459	0.001996	0.0213908	1.0240351
APBB1	-5.3787165	0.001996	0.0213908	1.0057237	SUPT7L	-5.7483588	0.001996	0.0213908	1.0072957

Gene Symbol	Score	Feature P	FDR (BH)	Fold Change	Gene Symbol	Score	Feature P	FDR (BH)	Fold Change
CRYZL1	-5.7583099	0.001996	0.0213908	1.0125772	LTA4H	-6.2096408	0.001996	0.0213908	1.0023755
SLC16A9	-5.7621406	0.001996	0.0213908	1.0073555	C22orf40	-6.2188435	0.001996	0.0213908	1.0136813
RPP25L	-5.7762057	0.001996	0.0213908	1.0069534	OGDHL	-6.2435582	0.001996	0.0213908	1.0103209
IL23A	-5.778009	0.001996	0.0213908	1.0298833	NAGK	-6.2567458	0.001996	0.0213908	1.0139553
DMRT3	-5.7821332	0.001996	0.0213908	1.0094458	ENPP5	-6.2573689	0.001996	0.0213908	1.0117057
NECAP2	-5.7999738	0.001996	0.0213908	1.0058794	CLEC6A	-6.277395	0.001996	0.0213908	1.0310508
ADAMTS6	-5.8024918	0.001996	0.0213908	1.0263552	DUSP10	-6.2847652	0.001996	0.0213908	1.0323026
SLC10A7	-5.8082535	0.001996	0.0213908	1.0166965	EPG5	-6.2869049	0.001996	0.0213908	1.0125229
RETSAT	-5.8177157	0.001996	0.0213908	1.0074847	TEP1	-6.2968136	0.001996	0.0213908	1.0233379
LDB2	-5.8303147	0.001996	0.0213908	1.0204909	GBF1	-6.2977325	0.001996	0.0213908	1.00527
GABBR1	-5.8486527	0.001996	0.0213908	1.0076366	TTLL1	-6.3107859	0.001996	0.0213908	1.0133646
ZBTB26	-5.8502179	0.001996	0.0213908	1.0168768	LEPREL1	-6.3152329	0.001996	0.0213908	1.0288409
DOCK8	-5.8512302	0.001996	0.0213908	1.0172222	PINK1	-6.3207651	0.001996	0.0213908	1.0329763
TSPAN5	-5.8590589	0.001996	0.0213908	1.0081435	KIAA1107	-6.321009	0.001996	0.0213908	1.0399074
MIXL1	-5.8740661	0.001996	0.0213908	1.1246946	IGSF1	-6.32877	0.001996	0.0213908	1.0098029
POLL	-5.899571	0.001996	0.0213908	1.0162974	SGK494	-6.341087	0.001996	0.0213908	1.0124155
C15orf57	-5.9465688	0.001996	0.0213908	1.008121	PCSK9	-6.3530142	0.001996	0.0213908	1.0098845
NBPF10	-5.9515782	0.001996	0.0213908	1.0050467	ATXN1	-6.355711	0.001996	0.0213908	1.0267574
CDNF	-5.964275	0.001996	0.0213908	1.0257097	PARP12	-6.3695905	0.001996	0.0213908	1.0206462
CMKLR1	-5.9647618	0.001996	0.0213908	1.0543557	BBS10	-6.3787513	0.001996	0.0213908	1.0238258
SYNE1	-5.9656972	0.001996	0.0213908	1.010136	SLC22A15	-6.397113	0.001996	0.0213908	1.0225883
PTGR2	-5.9665455	0.001996	0.0213908	1.0108443	LSMD1	-6.4034304	0.001996	0.0213908	1.011214
TLN2	-5.968371	0.001996	0.0213908	1.013012	SEMA4G	-6.4208372	0.001996	0.0213908	1.0111831
COL6A1	-5.968718	0.001996	0.0213908	1.0145212	RAB19	-6.4599269	0.001996	0.0213908	1.0073259
CYP4V2	-5.9994252	0.001996	0.0213908	1.0325584	CCDC14	-6.4738275	0.001996	0.0213908	1.0078323
DDIT4	-6.0046819	0.001996	0.0213908	1.0304614	TROAP	-6.50564	0.001996	0.0213908	1.0104448
PTPN18	-6.0046891	0.001996	0.0213908	1.0068963	ZNRD1-AS1	-6.5200957	0.001996	0.0213908	1.0318545
PGM1	-6.0107409	0.001996	0.0213908	1.0121444	HELZ	-6.5263434	0.001996	0.0213908	1.0040928
VPS26B	-6.0209142	0.001996	0.0213908	1.0057304	KLHL24	-6.5270657	0.001996	0.0213908	1.0097981
MAML2	-6.0232128	0.001996	0.0213908	1.013374	SNX9	-6.5370678	0.001996	0.0213908	1.0083389
WDFY3	-6.036662	0.001996	0.0213908	1.0056093	FTO	-6.5630217	0.001996	0.0213908	1.0048053
AP4M1	-6.0437991	0.001996	0.0213908	1.0059149	NLRX1	-6.5693373	0.001996	0.0213908	1.0155203
SNRNP200	-6.053102	0.001996	0.0213908	1.0034278	SLC9A9	-6.5713641	0.001996	0.0213908	1.0915002
HDAC6	-6.0547109	0.001996	0.0213908	1.0111765	TP53BP1	-6.58435	0.001996	0.0213908	1.0073387
EYA1	-6.0575135	0.001996	0.0213908	1.0178322	PPOX	-6.6038875	0.001996	0.0213908	1.0177472
OXSM	-6.0580489	0.001996	0.0213908	1.0245953	KLHL9	-6.6112099	0.001996	0.0213908	1.0103998
PRKAG1	-6.0584701	0.001996	0.0213908	1.0078941	PMS2P4	-6.6133854	0.001996	0.0213908	1.0058011
MARCH3	-6.059689	0.001996	0.0213908	1.0097099	NBPF8	-6.6180398	0.001996	0.0213908	1.0052526
ALS2CR8	-6.0723321	0.001996	0.0213908	1.0423831	ENOSF1	-6.6208283	0.001996	0.0213908	1.0147079
ASCC1	-6.0819753	0.001996	0.0213908	1.0054338	GSDMD	-6.6318657	0.001996	0.0213908	1.0039931
CYP2C8	-6.0844083	0.001996	0.0213908	1.0379163	SEC31B	-6.6417835	0.001996	0.0213908	1.0171753
FBP1	-6.0863872	0.001996	0.0213908	1.0191153	BBS1	-6.654126	0.001996	0.0213908	1.0038918
MALAT1	-6.0878125	0.001996	0.0213908	1.005487	TRIM52	-6.6953697	0.001996	0.0213908	1.0091708
PMS2P6	-6.0998912	0.001996	0.0213908	1.0082616	NCAPD2	-6.7033504	0.001996	0.0213908	1.0044218
OR51T1	-6.110794	0.001996	0.0213908	1.0224434	COL6A2	-6.7221847	0.001996	0.0213908	1.0102154
CCNG2	-6.1284131	0.001996	0.0213908	1.0154356	FGF10	-6.7357912	0.001996	0.0213908	1.0220856
CTSL1	-6.1407509	0.001996	0.0213908	1.0096872	CPT1A	-6.7445011	0.001996	0.0213908	1.0461119
LPAR1	-6.1717765	0.001996	0.0213908	1.0185823	TBCK	-6.7596295	0.001996	0.0213908	1.0116935
PMS2P5	-6.1829235	0.001996	0.0213908	1.0074686	RNF14	-6.7640311	0.001996	0.0213908	1.0136365
MSH5	-6.1946535	0.001996	0.0213908	1.0226191	CTC1	-6.8026302	0.001996	0.0213908	1.0110192

Gene Symbol	Score	Feature P	FDR (BH)	Fold Change	Gene Symbol	Score	Feature P	FDR (BH)	Fold Change
ZNF780A	-6.8203534	0.001996	0.0213908	1.0198257	PCDHGC5	-7.60633	0.001996	0.0213908	1.0135791
LRRK2	-6.8251211	0.001996	0.0213908	1.0120889	RTKN	-7.6406832	0.001996	0.0213908	1.010845
BTBD8	-6.8379752	0.001996	0.0213908	1.039614	PAAF1	-7.704145	0.001996	0.0213908	1.0212825
RGL2	-6.8467386	0.001996	0.0213908	1.006915	OR5BB1P	-7.7092229	0.001996	0.0213908	1.0133493
H1FX	-6.8717564	0.001996	0.0213908	1.0066605	ELP4	-7.7127593	0.001996	0.0213908	1.0072173
CPNE1	-6.8789632	0.001996	0.0213908	1.0065941	GNAL	-7.7147281	0.001996	0.0213908	1.0144457
ATXN7L3B	-6.8805017	0.001996	0.0213908	1.0078618	PLAG1	-7.7226229	0.001996	0.0213908	1.0134185
TTC14	-6.894903	0.001996	0.0213908	1.0104663	ASB11	-7.7337011	0.001996	0.0213908	1.0050931
ZSCAN30	-6.9036443	0.001996	0.0213908	1.0286459	N6AMT1	-7.760891	0.001996	0.0213908	1.0141682
MKS1	-6.904772	0.001996	0.0213908	1.0118545	BEX4	-7.780978	0.001996	0.0213908	1.0094665
DPAGT1	-6.9067276	0.001996	0.0213908	1.0042365	PDZD2	-7.7910886	0.001996	0.0213908	1.0125668
GTF3C3	-6.9201383	0.001996	0.0213908	1.0076056	UBE3B	-7.7999708	0.001996	0.0213908	1.0140684
KDM5D	-6.9364615	0.001996	0.0213908	1.011044	HSPA1L	-7.8002439	0.001996	0.0213908	1.0202218
DTNBP1	-6.9393123	0.001996	0.0213908	1.0073761	TRMT1L	-7.8203208	0.001996	0.0213908	1.0118037
MBNL3	-6.9482239	0.001996	0.0213908	1.0330621	FAM47C	-7.830081	0.001996	0.0213908	1.0084473
NARFL	-6.9710759	0.001996	0.0213908	1.008163	SMARCA2	-7.8654215	0.001996	0.0213908	1.030897
ZNF738	-6.9815044	0.001996	0.0213908	1.0116053	CNOT3	-7.8675605	0.001996	0.0213908	1.0014691
ATP6V0D1	-6.9975344	0.001996	0.0213908	1.007703	FBXW4	-7.8678944	0.001996	0.0213908	1.0158653
OR2T8	-7.0279945	0.001996	0.0213908	1.0219167	VPS11	-7.875959	0.001996	0.0213908	1.0085609
CAMKK2	-7.0388473	0.001996	0.0213908	1.0105632	PRSS3P2	-7.8833193	0.001996	0.0213908	1.0374144
APOBEC3D	-7.0581189	0.001996	0.0213908	1.021927	ENTPD5	-7.8852634	0.001996	0.0213908	1.0140382
KLHDC9	-7.063413	0.001996	0.0213908	1.0173316	SLC16A13	-7.8919061	0.001996	0.0213908	1.025727
PREX1	-7.1037629	0.001996	0.0213908	1.0283352	CAPRIN2	-7.9082943	0.001996	0.0213908	1.0165459
PTGR1	-7.1192104	0.001996	0.0213908	1.0106408	LMO1	-7.9100107	0.001996	0.0213908	1.0253746
SLC25A35	-7.1308651	0.001996	0.0213908	1.0166699	C20orf94	-7.9270821	0.001996	0.0213908	1.0108004
NCR1	-7.1381442	0.001996	0.0213908	1.0108386	PPT2-EGFL8	-7.9337182	0.001996	0.0213908	1.007765
TIAM1	-7.1588596	0.001996	0.0213908	1.0090368	PLA2G16	-7.9615979	0.001996	0.0213908	1.0088071
APBB3	-7.1624921	0.001996	0.0213908	1.0196872	SLC16A12	-7.9810232	0.001996	0.0213908	1.0512863
SRGAP1	-7.2323208	0.001996	0.0213908	1.0141602	PAFAH2	-7.9851788	0.001996	0.0213908	1.0152099
MGST2	-7.2508129	0.001996	0.0213908	1.0366003	ZNF827	-7.9936053	0.001996	0.0213908	1.0140477
CXorf22	-7.2911331	0.001996	0.0213908	1.0423064	FOXP4	-8.0965315	0.001996	0.0213908	1.0077353
PMS2L2	-7.2935853	0.001996	0.0213908	1.0076842	NBPF1	-8.0993942	0.001996	0.0213908	1.0052265
MED12	-7.3179864	0.001996	0.0213908	1.0119546	CHTF8	-8.1109178	0.001996	0.0213908	1.0082099
TDRKH	-7.3208918	0.001996	0.0213908	1.0069643	ITSN2	-8.1400592	0.001996	0.0213908	1.0084864
AB067525	-7.3303437	0.001996	0.0213908	1.0072393	ZSWIM5	-8.1827985	0.001996	0.0213908	1.0137577
SV2A	-7.3455087	0.001996	0.0213908	1.0053008	C1orf56	-8.2110879	0.001996	0.0213908	1.011313
CYP2B7P1	-7.3670052	0.001996	0.0213908	1.014175	DDX26B	-8.2123131	0.001996	0.0213908	1.0143506
C5orf54	-7.4146723	0.001996	0.0213908	1.0298981	GAD1	-8.2337551	0.001996	0.0213908	1.0848196
TUBB2B	-7.4150767	0.001996	0.0213908	1.0065717	MDM4	-8.2997959	0.001996	0.0213908	1.011044
CST1	-7.4175501	0.001996	0.0213908	1.1314613	GPRASP1	-8.3228972	0.001996	0.0213908	1.0183566
STRADA	-7.426592	0.001996	0.0213908	1.0121332	COMMD7	-8.3433356	0.001996	0.0213908	1.011247
ATF6B	-7.4366202	0.001996	0.0213908	1.0100357	FBXO25	-8.3956263	0.001996	0.0213908	1.0147133
ZMAT1	-7.4411535	0.001996	0.0213908	1.0465816	MARCH11	-8.4016406	0.001996	0.0213908	1.0119423
HSDL1	-7.4522162	0.001996	0.0213908	1.0048042	CXorf24	-8.4119368	0.001996	0.0213908	1.0132279
KCNT2	-7.4795759	0.001996	0.0213908	1.0105633	ADCK1	-8.4682679	0.001996	0.0213908	1.0119605
KIF6	-7.5191915	0.001996	0.0213908	1.0175677	TIGD4	-8.4707371	0.001996	0.0213908	1.0175841
NCSTN	-7.5210694	0.001996	0.0213908	1.0087905	ZNF608	-8.473945	0.001996	0.0213908	1.0138703
KLF10	-7.532847	0.001996	0.0213908	1.0136684	HERC3	-8.5316734	0.001996	0.0213908	1.0222669
RALYL	-7.5503483	0.001996	0.0213908	1.0384504	SRSF7	-8.5384209	0.001996	0.0213908	1.0040691
AFF1	-7.6042106	0.001996	0.0213908	1.0053923	CNPY4	-8.5457915	0.001996	0.0213908	1.0151007

Gene Symbol	Score	Feature P	FDR (BH)	Fold Change
IQGAP3	-8.5855723	0.001996	0.0213908	1.0163604
C11orf71	-8.603748	0.001996	0.0213908	1.0264958
FAM100B	-8.6802277	0.001996	0.0213908	1.0151502
PPAPDC1B	-8.6882102	0.001996	0.0213908	1.0078017
ZNF70	-8.7305134	0.001996	0.0213908	1.0140972
DTX3L	-8.7426248	0.001996	0.0213908	1.02818
MSH5-SAPCD1	-8.7523786	0.001996	0.0213908	1.0176554
HERC2P2	-8.8056669	0.001996	0.0213908	1.0088492
INTS3	-8.8665774	0.001996	0.0213908	1.0053616
CLVS2	-8.8750339	0.001996	0.0213908	1.036194
BRD8	-8.8859292	0.001996	0.0213908	1.007403
TMX4	-8.8912818	0.001996	0.0213908	1.0019127
PARP15	-8.9081506	0.001996	0.0213908	1.0239857
RABGGTA	-8.9672209	0.001996	0.0213908	1.0047702
TCP11L2	-9.0927091	0.001996	0.0213908	1.0558479
DRD1	-9.1245135	0.001996	0.0213908	1.0344994
VPS36	-9.1479002	0.001996	0.0213908	1.0120461
RAB7L1	-9.1546481	0.001996	0.0213908	1.0149167
LMBR1L	-9.1766946	0.001996	0.0213908	1.011401
ARHGEF2	-9.2464331	0.001996	0.0213908	1.0116702
C21orf59	-9.3698631	0.001996	0.0213908	1.0026706
MTL5	-9.379902	0.001996	0.0213908	1.0174982
TTLL4	-9.3944922	0.001996	0.0213908	1.0016988
MUC3B	-9.4368042	0.001996	0.0213908	1.0131157
KLF8	-9.4489356	0.001996	0.0213908	1.0155101
ANKRD20A11P	-9.481308	0.001996	0.0213908	1.0236418
CALCOCO1	-9.5782684	0.001996	0.0213908	1.0112989
BNIP3	-9.6010714	0.001996	0.0213908	1.0200455
VPS52	-9.7167898	0.001996	0.0213908	1.0089596
DNAJC28	-9.7592289	0.001996	0.0213908	1.0308906
SLC38A7	-9.8729415	0.001996	0.0213908	1.0083526
SLC16A14	-9.9345222	0.001996	0.0213908	1.0272934
FAM122C	-10.187996	0.001996	0.0213908	1.0357442
LINC00526	-10.213373	0.001996	0.0213908	1.0086617
STAT2	-10.547114	0.001996	0.0213908	1.0206233
CCDC50	-10.891381	0.001996	0.0213908	1.0116598
HEMK1	-11.066724	0.001996	0.0213908	1.0162138
CXCR7	-11.251905	0.001996	0.0213908	1.0320491
ARRDC3	-11.506191	0.001996	0.0213908	1.0467913
WDSUB1	-11.518339	0.001996	0.0213908	1.0193503
TUG1	-11.786437	0.001996	0.0213908	1.0029582
SURF1	-11.90916	0.001996	0.0213908	1.005738
ORAI3	-11.974893	0.001996	0.0213908	1.0160472
MCCC1	-12.552318	0.001996	0.0213908	1.0081205
NEK8	-13.070066	0.001996	0.0213908	1.0092931
KIAA0895	-13.277734	0.001996	0.0213908	1.0256696
CRTC3	-13.495518	0.001996	0.0213908	1.0219474
PNPO	-14.319965	0.001996	0.0213908	1.0168687
GALT	-14.383633	0.001996	0.0213908	1.0107884
LIN7A	-14.743146	0.001996	0.0213908	1.016246
NSUN3	-15.969391	0.001996	0.0213908	1.010991
CCDC122	-17.135958	0.001996	0.0213908	1.0196309
APOBEC3F	-19.348266	0.001996	0.0213908	1.0393252